A SEMI-EMPIRICAL ASSESSMENT OF PLUNGE POOL SCOUR: TWO-DIMENSIONAL APPLICATION OF ANNANDALE'S ERODIBILITY INDEX METHOD ON FOUR DAMS IN BRITISH COLUMBIA, CANADA

by

Amanda J. Rock

ProQuest LLC.
789 East Eisenhower Parkway
P.O. Box 1346
Ann Arbor, MI 48106 - 1346

A thesis submitted to the Faculty and the Board of Trustees of the Colorado School of Mines in partial fulfillment of the requirements for the degree of Master of Science (Geological Engineering).

Golden, Colorado

Date _____

Signed: _____
Amanda J. Rock

Signed: _____
Dr. Jerry D. Higgins
Thesis Advisor

Golden, Colorado

Date _____

Signed: _____
Dr. Paul Santi
Professor and Head
Department of Geology & Geological Engineering

ABSTRACT

Rock scour downstream of dam foundations and spillways has become a significant dam safety concern in recent years. As design flood estimates increase and older infrastructure is expected to pass larger amounts of water, downstream river beds and plunge pools are subjected to progressively greater stream power from rapidly flowing water. A need exists to quantify the erosive capacity of the flowing water and the erodibility of earth materials to evaluate potential scour in these susceptible areas. Annandale's Erodibility Index Method, widely considered a state of the art scour prediction method, offers an approach to quantify scour depth by comparing the erosive capacity of flowing water and the ability of rock to resist it.

This study assesses the accuracy of Annandale's Erodibility Index Method for estimating rock scour depth in plunge pools. The success by which the method may be implemented is dependent on the accuracy of methods to quantify the rate of energy dissipation of plunging jets (applied stream power) and the ability to estimate the capacity of rock to resist the power of the flowing water. The stream power of plunging jets is quantified by making use of published research, while the ability of rock to resist scour is computed using a geo-mechanical index, known as the Erodibility Index.

The Erodibility Index that was used to estimate the scour resistance of the various stratigraphic layers downstream of four BC Hydro dam spillways located in British Columbia, Canada relies on in-situ rock parameters consisting of UCS strength values, RQD values, joint spacing, aperture, alteration, roughness, and orientation. The jet stream power was calculated using continuous daily discharge records and spillway geometries at each of the dams, and published research on stream power quantification. The spillway types included one long spillway chute with a free overfall and a number of flip bucket-type energy dissipaters.

Comparison between the numerically generated scour profiles and a series of plunge pool surveys at each of the dams provided a means of determining accuracy. Scour depths and the distances between the end of the spillways and the points of maximum scour were matched. The study revealed that correlations between calculated and observed scour profiles improved with the quality of geologic information and with the certainty by which the stream power of jets and their decay could be quantified.

The geologic information at two of the dams, Revelstoke and Seven Mile Dams, was incomplete and resulted in a generalized characterization of the scour resistance of the plunge pool rock. At these dams it was not possible to spatially characterize changes in scour resistance of the rock in the plunge

pool. The geologic information at Peace Canyon and W.A.C. Bennett Dams was more informative and allowed quantification of the spatial distribution of plunge pool scour resistance in each case.

The research further identified that jet theory associated with flip buckets provides good estimates of stream power and its decay, but that hydraulic theory used to quantify the energy dissipation in long spillway chutes may be incomplete at this point in time. The combined inadequacy of geologic data and the insufficiency of hydraulic theory related to long spillway chutes resulted in the comparison between surveyed and calculated scour depths at Revelstoke Dam being particularly poor. Contrasting this result, it was found that better understanding of flip bucket hydraulics and more informative geologic information resulted in very good correlations between calculated and surveyed scour profiles at Peace Canyon and W.A.C. Bennett Dams. The comparison provided more pleasing results at Seven Mile Dam than at Revelstoke Dam, in spite of the relatively poor geologic information in the plunge pool area of Seven Mile Dam. The improved correlation at Seven Mile Dam may be attributed to the fact that it has a flip bucket spillway, which resulted in better quantification of jet stream power and its decay.

In summary the analysis results indicate a strong correlation between surveyed and modeled plunge pool depth and invert location at dam sites where both the hydraulics and geology are well understood. It is concluded from this research that Annandale's Erodibility Index Method is an accurate method for estimating plunge pool depth when geologic information is available and spillway and plunge pool hydraulics are well-understood. A lack of information or understanding of the spatial distribution of materials generally results in less accurate predictions.

Although this research project was not directed towards determining the rate of scour of rock, a good correlation was found between cumulative energy (the product of stream power and duration) and scour depth. This preliminary result provides encouragement for future research into using the Erodibility Index Method to quantify the rate of scour in rock.

The analysis would benefit from more robust rock parameter datasets that would allow for the inclusion of a Monte Carlo simulation within the model. Additionally, a larger dataset of dams including those with various spillway structure types and geologic environments would be valuable moving forward.

TABLE OF CONTENTS

LIST OF FIGURES

LIST OF TABLES

LIST OF SYMBOLS

A	Area of plunging jet footprint
a_1	Coefficient value for calculating mean dynamic pressure coefficient
$a_{2...5}$	Coefficient values for calculating fluctuating dynamic pressure coefficient ($Y/D_j < 14$)
b_1	Coefficient value for calculating mean dynamic pressure coefficient
$b_{2..3}$	Coefficient values for calculating fluctuating dynamic pressure ($Y/D_j \geq 14$)
C_p	Mean dynamic pressure coefficient
C'_p	Fluctuating dynamic pressure coefficient
C_{pr}	Radial mean dynamic pressure coefficient
C'_{pr}	Radial fluctuating dynamic pressure coefficient
C_r	Coefficient of relative density
C_{sp}	Average stream power decay coefficient
d	Depth of tailwater drawdown
D_{50}	Median soil grain size
D_i	Initial plunging jet diameter
D_j	Diameter of core of a round jet
D_{out}	Diameter of outer layer of jet
D_p	Average dynamic pressure coefficient
f	Friction factor
Fr_i	Froude Number at jet issuance
g	Acceleration due to gravity
H	Vertical distance through which a plunging jet falls
h_v	Plunging jet kinetic energy
J	Actual length of plunging jet
J_a	Joint wall alteration number
J_n	Joint set number
J_p	Length of jet core
J_r	Joint wall roughness
J_s	Orientation and shape number
J_r	Joint wall roughness
K	Erodibility index (EI)
K_2	Coefficient allowing for the effects of air resistance
K_b	Block size number

K_d	Interparticle or interblock shear strength number
K_j	Empirically determined factor = 6.3 for most jets
L_b	Jet breakup length
L_j	Jet trajectory length
M_s	Mass strength number
P	Stream Powers
$P(E)$	Probability of rock removal
P_c	Critical rock erosion stream power threshold
P_{jet}	Total jet stream power
p_{rms}	Root mean square of pressure
Q	Total jet discharge
q	Unit discharge
r	Radial distance from submerged jet centerline
r_{max}	Maximum radial extension of turbulent shear layer
RQD	Rock Quality Designation
T_u	Turbulence intensity
UCS	Unconfined compressive strength of rock
v'	Axial velocity fluctuations
V	Mean jet velocity
V_i	Initial plunging jet velocity
V_j	Jet velocity at water surface of plunge pool
w	Tailrace width (ft)
x	Horizontal distance over which a plunging jet falls
Z	Vertical distance through which a plunging jet falls
α	Kinetic energy correction factor
β	Total bucket deflection angle (^{o}) (Pfister, 2014)
δ	Equivalent deflector angle (^{o})
γ	Unit weight of water
Θ	Spillway flip bucket / ski-jump angle
φ	Spillway/chute face angle (^{o}); Friction Angle (^{o})
φ_{Tu}	Turbulence intensity factor
ρ	Mass density of water
ρ_r	Mass density of rock
ξ	Angle of jet impingement with plunge pool

ACKNOWLEDGEMENTS

I would like to thank Faizal Yusuf and BC Hydro for their willingness to share their data on the four dam sites assessed over the course of this research project. In addition, I would like to thank Dr. Hank Falvey, who contributed greatly to my understanding of jet hydraulics and energy dissipation, and my colleague Robert Humphries, whose moral support and thought provoking questions throughout this process have been a tremendous boon.

CHAPTER 1

INTRODUCTION

Rock scour downstream of dam foundations and spillways is a significant dam safety concern. As design floods increase and older infrastructure is modified to pass larger amounts of water, downstream river beds and plunge pools are subjected to progressively larger shear stresses from rapidly flowing water. Excessive scour due to plunging jets or high velocity flow in plunge pools, specifically, can undermine foundations, compromise the stability of riverbanks, and lead to eventual catastrophic dam failure.

Traditionally most of the geological investigation of dam sites is focused on the dam foundation, abutments, and the upstream reservoir area. Experience has shown that the investigation of scour potential downstream of dam spillways is very important; rock quality in this area can have a significant impact on long term dam stability. For example, in the case of Kariba Dam along the border of Zambia and Zimbabwe, scour proceeded to excavate a plunge pool more than 90 meters deep, nearly as tall as the dam itself (Bollaert et al., 2012).

Recent publications show a shift in hydraulic research toward quantifying and predicting scour potential, especially in plunge pools (Annandale, 1995, 2006; Bollaert, 2002, 2004; Bollaert & Schleiss, 2005). Scour potential, however, is of interest anywhere man-made structures interfere with nature, such as at bridge piers and abutments and along embankments (Richardson, 1996; Keaton, 2013). Advances in the understanding of jet hydraulics and plunge pool energy dissipation since the 1970s have also contributed to more accurate scour predictions. Many scour assessments currently rely heavily on model scale studies, which can be costly to construct and do not necessarily accurately replicate the scour processes occurring at the prototype scale (Schleiss, 2002). Understanding the science of energy dissipation in both the atmosphere and the plunge pool can help more accurately predict scour and aid in the selection of the most effective energy dissipaters and rock reinforcement during spillway design.

CHAPTER 2

THESIS STATEMENT

This thesis evaluates Annandale's Erodibility Index Method (EIM) (1995, 2006) for estimating rock scour depth in plunge pools by applying the methodology to four BC Hydro dams located in British Columbia, Canada. The four dams include Peace Canyon Dam, Seven Mile Dam, W.A.C. Bennett Dam, and Revelstoke Dam and represent different plunge pool geologic environments; relatively flat lying sedimentary units with minor structural alteration at Peace Canyon and W.A.C. Bennett Dams and intruded granitic dykes and contact and regionally metamorphosed sediments at Seven Mile and Revelstoke Dams.

Results from analyses based on spillway discharge data, plunge pool geology and rock strength, and density of geologic data are compared to existing plunge pool surveys to evaluate the methodology. This analysis differs from Monfette's (2004) previous research on the same BC Hydro dam sites in five ways:

- by accounting for geologic variability within a plunge pool,
- by applying scour along a two-dimensional profile,
- by applying Ervine & Falvey's (1987), Bollaert's (2002), and Castillo's (2006) research on fluctuating and mean dynamic pressure coefficients to calculate energy decay within a plunge pool,
- by accounting for progressive plunge pool scour from a series of discharge events, and
- by assessing the importance of the density of the available geologic data.

This approach allowed for spatial variability of geologic parameters and cumulative scour development from a series of spillway discharge events. Different discharges over the spillway result in different jet trajectories, trajectory lengths, breakup lengths, impingement angles, and degree of jet spread. As a result, the higher stream power values are applied to different parts of the plunge pool depending on discharge and the exposure of different erodible materials over time. Weak underlying shale layers, for example, may be protected from erosion by a stronger overlying sandstone unit. Once the stronger unit has been removed, erosion of the shale becomes possible at lower stream power values.

In engineering practice, detailed geologic data are not always available. The dam sites assessed in this study represent areas with both reasonable geologic data, collected from drilling programs within the plunge pool or adjacent areas and surficial mapping, as well as sites with limited geologic data that require some interpretation to conduct the analysis. The variety in data density at the dam sites within this

study will provide some insight into the influence of the amount of available information on the accuracy of the results.

CHAPTER 3

PREVIOUS RESEARCH

This research represents the second application of Annandale's Erodibility Index Method to the four BC Hydro dams in question. In 2004, Monfette completed a Master's of Science thesis at the University of British Columbia in Vancouver, BC on the same four BC Hydro dams assessed in this analysis. The focus of her work was on the comparison of traditional empirical methods for predicting scour with the EIM, and assessing the accuracy of the EIM by comparing calculated scour depths with existing plunge pool surveys.

Monfette calculated the average erodibility index for the materials in the plunge pool at each dam site and used discharge data to calculate the stream power of the plunging jets. The plunge pool at each location was characterized in terms of 'Low', 'Mean', and 'High' erodibility index values to provide the likely range of material erodibility. In her analysis, 'Mean' erodibility index values are considered representative of the bulk of the plunge pool bedrock (Monfette, 2004).

The erosive capacity of water along the jet centerline trajectory was calculated using computational methods developed by Ervine et al. (1997), Ervine and Falvey (1987), Lewis (1996) and Bohrer (1998) as shown in Figure 3.1. Ervine and Falvey's (1987) research focused on turbulent circular jets issuing horizontally, plunging through the atmosphere, and diffusing into a pool. The 1987 research led to plunging jet velocity calculations based on an estimated 8^{o} inner core decay and the assumption of linear velocity decay with depth (Monfette, 2004). The influence of jet development on the velocity profile was accounted for by using the Bohrer et al. (1998) empirical dimensional analysis approach. Lewis's (1996) dimensional equation technique (DET) was then applied to factor air drag into the developed jet velocity profile equation.

For each discharge event Monfette calculated the stream power distribution in the plunge pool. The stream power profile and the erodibility index value of the plunge pool material were then plotted together. The point of intersection represented the maximum scour depth associated with the spillway discharge (Figure 3.2). Calculated maximum scour depths were then compared to existing plunge pool surveys of the four dams to assess the accuracy of the methodology.

The results of Monfette's analysis are shown in Figure 3.3. According to the analysis, Annandale's Erodibility Index Method consistently underestimated the eroded plunge pool elevation, with a standard error value of 53 ft, or +/- 26.5 ft. Monfette concluded that the inability to account for geologic

Computational Step	Equation	Source
1. Estimate the flow depth at the exit of the spillway bucket (jet thickness), do.	$d_o = y\cos\theta$ * $E = y + \frac{q^2}{2gy^2}$	Bernoulli Equation
2. Calculate the jet velocity at the exit of the spillway bucket, Vo.	$V_o = q/y$	
3. Determine the jet breakup length, Lb. The jet breakup length is the fall distance before the free jet loses its coherence and becomes a conglomeration of discrete water particles. The breakup length marks the limit between undeveloped jet and developed jet.	$C^2 = \frac{1}{\left(\frac{2L_b}{d_o F_o^2}+1\right)\left(\sqrt{\frac{2L_b}{d_o F_o^2}+1}-1\right)^2}$ ** $C = 1.14 \cdot Tu \cdot F_o^2$ $F_o = V_o/\sqrt{gd_o}$	Ervine et al., 1997
4. Compute the jet velocity at impact with the plunge pool surface, Vi.	Undeveloped jet $V_i = \sqrt{V_o^2 + 2gH_d}$	Ervine et al., 1997
	Developed jet $V_i = \sqrt{V_o^2 + 2gH_d} - RF$ $RF = \sqrt{3C_d(\rho_a/\rho_w)(H_d/\Phi)V_o^2}$	Lewis et al., 1996
5. Estimate the jet thickness at impact with the plunge pool surface, di.	*** $d_i = d_o\sqrt{\frac{V_o}{V_i}}$	Ervine et al., 1997
6. Estimate the mean air concentration of the jet at impact, Ci.	$C_i = \frac{B_i}{1+B_i}$ where $B_i = 0.2\sqrt{\frac{H_d}{d_o}}$	Ervine and Falvey, 1987
7. Determine the underwater velocity at all points along the jet centreline trajectory, V.	Undeveloped jet $V = 4V_i d_i/L$ $V = V_i$ for $L \le 4d_i$	Ervine and Falvey, 1987
	Undeveloped jet $\frac{V}{V_i} = 0.0675\left[\left(1-C_i\right)\left(\frac{V_i^2}{gL}\right)\right] + 0.1903$ $V = V_i$ for $\left[\left(1-C_i\right)\left(\frac{V_i^2}{gL}\right)\right] \ge \frac{1-0.1903}{0.0675}$ Developed jet $\ln\left(\frac{V}{V_i}\right) = 0.638\ln\left[\left(1-C_i\right)\left(\frac{V_i^2}{gL}\right)\right] - 1.848$ $V = V_i$ for $\ln\left[\left(1-C_i\right)\left(\frac{V_i^2}{gL}\right)\right] \ge \frac{1.848}{0.638}$	Bohrer et al., 1998

Notes.
* Assumed energy loss on spillway surface of 5% for Peace Canyon and Seven Mile and 10% for Portage Mountain and Revelstoke.
** Estimated turbulence intensity (Tu) of 5% for flip bucket jets.
*** Calculated from gravitational considerations only.

Figure 3.1 Computational methods for calculating the linear velocity profile along the jet centerline (from Monfette, 2004). See Monfette (2004) for an explanation of variables.

heterogeneity throughout the plunge pool area and the application of spillway discharges as discreet, independent events contributed to the lack of agreement between observed rock scour and modeled scour maximum rock depths (Monfette, 2004). In addition, Monfette's research indicated that an improved method of calculating stream power decay with depth was necessary to improve the analysis results (Monfette, 2004).

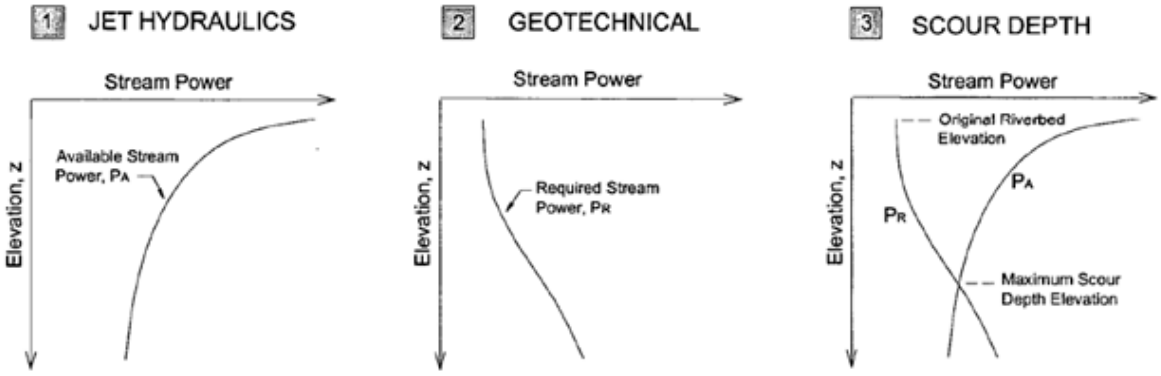

Figure 3.2 Conceptual approach of the Erodibility Index Method in the assessment of plunge pool scour (modified from Monfette, 2004).

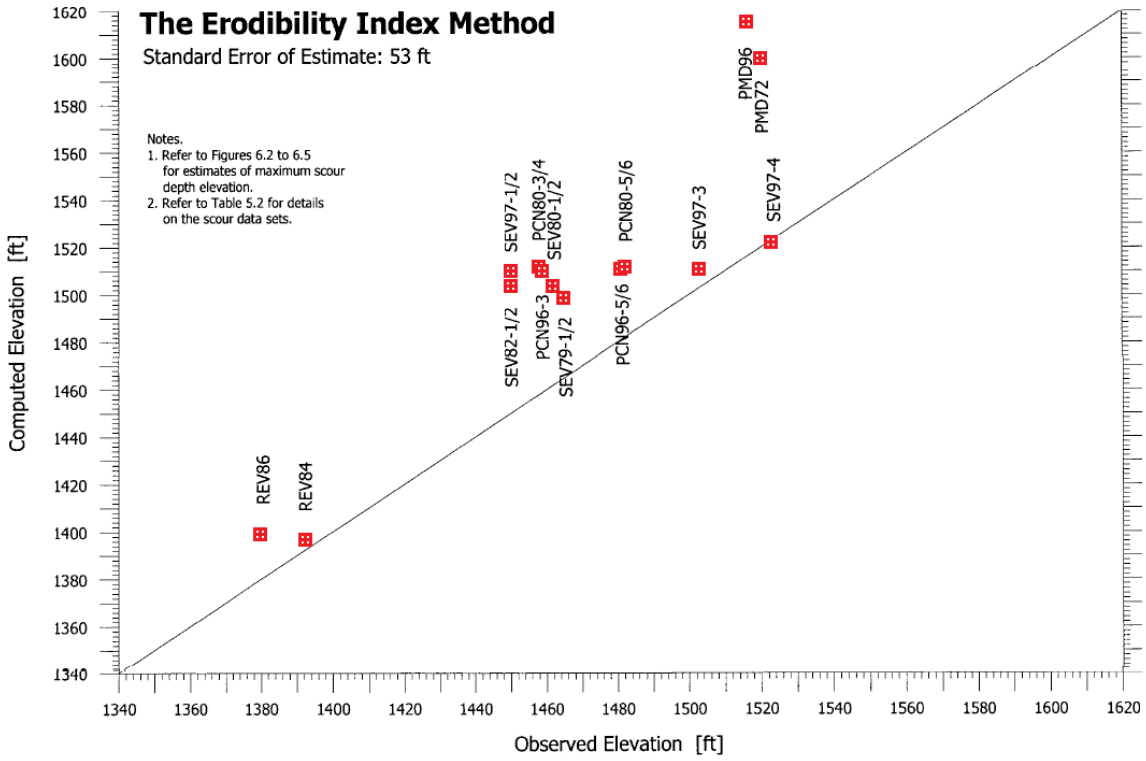

Figure 3.3 The Erodibility Index Method versus predicted plunge pool floor elevation results (Monfette, 2004).

CHAPTER 4

BACKGROUND

Assessing scour in rock and other earth materials, especially in the context of the complex plunge pool environment, is an emerging science in the hydraulic and hydrology fields. Even most research into scour depths at bridge piers and abutments only dates back to the latter half of the 20th century (Richardson, 1996). Most of the scour methodologies developed prior to the mid 1990's dealt with only specific hydrologic cases and were not applicable to a wide range of material characteristics (Annandale, 2006). Equations traditionally used to estimate scour in plunge pools include Veronese's 1937 equation, Yildiz and Uzucek's 1994 modification of Veronese's equation, and Mason and Arumugam's 1985 equation (USBR, 2012). These relationships are all empirically developed to estimate scour depth based almost entirely on the characteristics of the plunging jet. Only Mason and Arumugam's 1985 equation attempts to account for the characteristics of the rock material by including the median grain size of the foundation material in the calculation (USBR, 2012). In reality, multiple material characteristics play a role in the erosive resistance of earth materials to water.

More recently, research by Annandale (1995, 2006) led to the development of a semi-empirical method for assessing scour in a wide variety of earth materials, ranging from cohesive sediment and clastic materials to rock. Bollaert (2004), and Bollaert & Schleiss (2005) have also developed the Comprehensive Scour Model (CSM) for scour assessment in plunge pools. This methodology focuses on the mechanics of failure, including crack propagation due to pressure fluctuations within rock joints and block uplift (Bollaert 2002, 2004; Bollaert & Schleiss, 2005). Bollaert's approach addresses plunge pool erosion of rock only, whereas Annandale's methodology can be applied to a wider range of material types in a variety of flow scenarios.

To assess plunge pool scour, both the erosive capacity of the water and the erosive resistance of the rock material must be quantified. The erosive capacity of the water can be represented by the rate of energy dissipation of the plunging jet over the jet impact area, or the stream power of the jet. Similarly, the resistance to erosion of the rock material can be represented by the amount of stream power that the material is capable of resisting over the applied area.

4.1 The Erosive Power of Plunging Jets

The erosive capacity of water due to plunging jets depends on both the characteristics of the free falling jet and energy dissipation within the plunge pool, as shown in Figure 4.1. Quantifying the erosive capacity of water must therefore be broken down into two parts:

1. The Falling Jet
2. The Plunge Pool

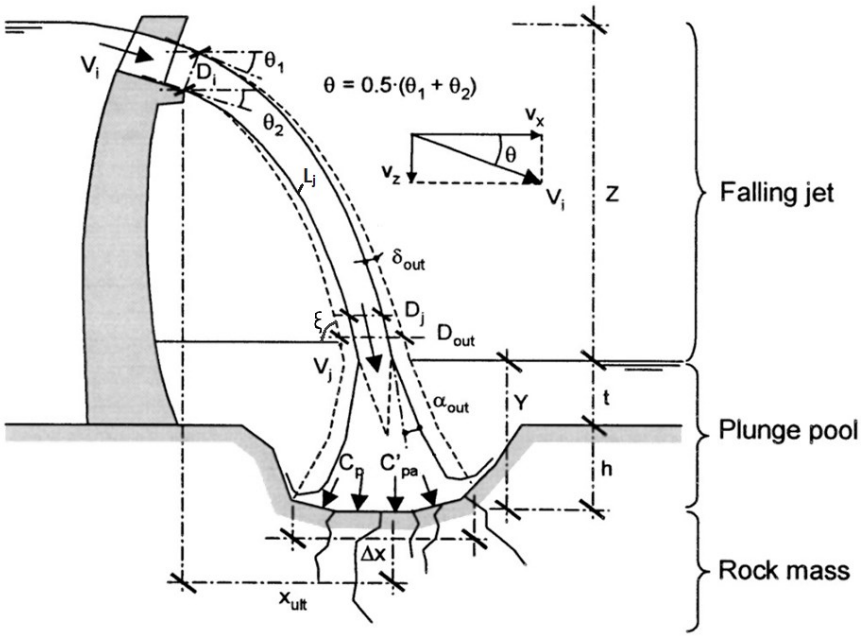

Figure 4.1 Sketch of main parameters of free overfall jet plunging into pool and breaking up rock mass (Bollaert & Schleiss, 2005).

4.1.1 The Falling Jet

During discharge events water flowing over the spillway becomes airborne before impinging onto the surface of the plunge pool. For all intents and purposes the initial jet at the top of the spillway is considered a solid mass of water with minimal air entrainment. As the jet follows its trajectory, both along the spillway face in the case of ski-jump spillways and through the air, two important processes happen, as shown in Figure 4.2: 1) the jet is subjected to gravity and the solid water core of the jet contracts and 2) the jet begins to entrain air at its outer boundary, which leads to internal turbulence and jet breakup (Bollaert, 2002; Ervine & Falvey, 1987).

Characterizing the airborne portion of the jet requires knowledge of the initial flow over the spillway and the amount of dispersion that occurs during the fall. The issuance velocity can be deduced

from spillway discharge measurements and specific energy concepts (Henderson, 1966). The turbulence of the free falling jet entrains air.

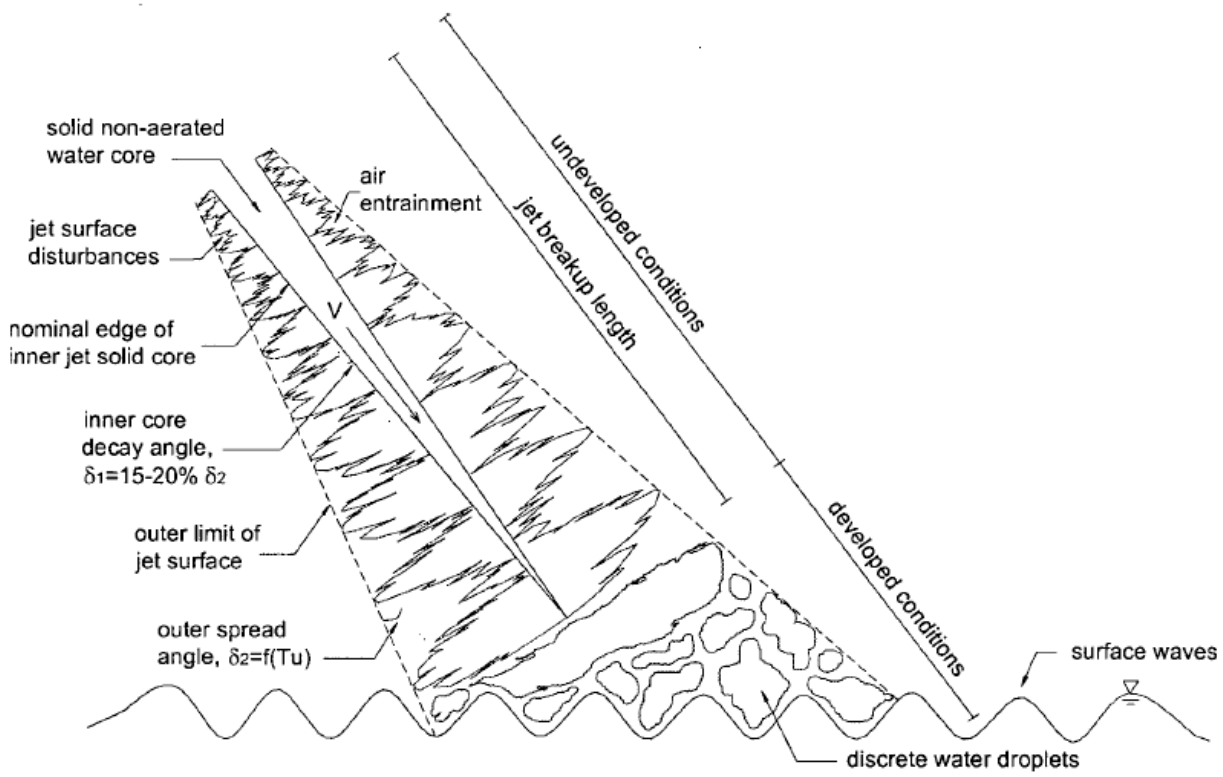

Figure 4.2 Schematic diagram of turbulent breakup of a free falling jet (Ervine et al., 1997).

The degree of internal turbulence experienced by the plunging jet is a function of the jet issuance conditions and is represented by the initial turbulence intensity, T_u (Ervine & Falvey, 1987; Ervine et al., 1997). This variable is defined as the ratio of the root-mean-square of the axial velocity fluctuations , *v'*, to the mean velocity of the jet ,*V*, as shown in Equation 4.1 (Bollaert, 2002). The initial turbulence intensity reflects the amount of air entrainment experienced by the jet. Free overfall jets only experience mixing during free fall, minimizing the degree of turbulence intensity. Ski jump outlet jets experience mixing during both flow down the spillway face and while airborne, which results in higher turbulence intensities. Jets emerging from valve outlets are already turbulent in nature, thus increasing the value of T_u in this case. The value of this parameter can also be calculated based on the friction factor, *f*, at the base of the spillway.

$$T_u = \frac{\sqrt{(v')^2}}{V} = \frac{v'}{V} = 0.25\sqrt{f} \qquad (4.1)$$

Table 4.1 Typical Values of Issuance Turbulence Intensity, T_u, at Various Outlet Structure Types.

Type of Outlet Structure	Turbulence Intensity T_u
Free overfall	0.00 – 0.03
Ski jump outlet	0.03 – 0.05
Valve	0.03 – 0.08

(Bollaert, 2002)

The plunging jet geometry is also dependent on the issuance velocity, V_i, the issuance jet thickness, D_i, and the average issuance angle, α_j, Froude Number and discharge depth from the terminal structure angle, θ, shown in Figure 4.1 (Pfister, 2014). These values can be used with physics-based equations to calculate the horizontal and vertical distances to impingement, x and z respectively, and the jet trajectory length, L_j, using Equations 4.2 and 4.3 (Wahl, 2008, Pfister, 2014):

$$z = x\tan\theta - \frac{x^2}{4h_v(\cos\theta)^2} \tag{4.2}$$

$$L_j = \int_0^x \sqrt{1 + \left[\tan\theta - \frac{2x}{4h_v(\cos\theta)^2}\right]^2} \cdot dx \tag{4.3}$$

Here, the x and z values are based on a coordinate system where the jet outlet represents the origin, x increases in the direction of the plunge pool, and z decreases as the jet loses elevation. The variable h_v is the kinetic energy of the jet, equal to $V_i^2/2g$. The value of x when z equals the difference in elevation between the flip bucket lip and the tailwater level indicates the horizontal distance from the base of the spillway to the center of the jet at impact with the plunge pool.

The jet character changes as the inner core of the jet contracts with distance. As long as the core exists, the jet is considered undeveloped and is composed of both an intact core and discrete water droplets in the outer fringe. A jet becomes fully developed when the solid core has completely contracted. Fully developed jets are composed almost entirely of discrete clumps of water. If the fall distance is large enough, the erosive capacity of the jet is limited because air drag causes the drops to slow to terminal velocity (Annandale, 2006). Various jet breakup length equations exist for different jet types and issuance conditions. Falvey (1990) developed equations for circular jets issuing from free over falls, Castillo (2006, 2007) developed an equation for rectangular jets issuing from free over falls, and most recently Pfister et al.(2014) has developed an equation for rectangular ski-jump generated jets, which his research indicated have much shorter breakup lengths than other types of energy dissipaters. Any one of these equations may be more or less appropriate for a given scenario and care should be taken when selecting the breakup length equation, as this parameter can have a significant impact on energy dissipation within the plunge pool. Pfister et al.'s rectangular ski-jump generated jet breakup length equation and Castillo's

(2006, 2007) equations were selected for this analysis based on the jet type and issuance conditions of the four dams assessed here. Peace Canyon Dam, Seven Mile Dam, and W.A.C. Bennett Dam spillway structures terminate at flip bucket type energy dissipaters, which are best represented by Pfister's (2014) jet breakup length equation, and Revelstoke Dam spillway terminates at a horizontal free overfall at the end of a long chute, which is best represented by Castillo's (2006, 2007) jet breakup length equation.

The breakup length, L_b, is calculated using Equation 4.4 (Pfister, 2014) for Peace Canyon, Seven Mile, and W.A.C. Bennett Dams. Fr_i is the Froude Number at jet issuance and equal to $V / \sqrt{(g \cdot D_i)}$. The variables φ and δ represent the angle of the spillway or chute face and the equivalent deflector angle, respectively, as defined by Pfister (2014).

$$L_b = \frac{76 \cdot D_i \cdot (1+\sin(\varphi))}{Fr_i \cdot (1+\tan(\delta))^4} \tag{4.4}$$

The breakup length, L_b, is calculated using Equation 4.5 (Castillo, 2006, 2007) for Revelstoke Dam.

$$L_b = 0.85 \frac{D_i \cdot Fr_i^2}{(1.07 T_u Fr_i^2)^{0.82}} \tag{4.5}$$

When the breakup length is less than the trajectory length (from 4.3) the jet is fully developed upon impingement with the plunge pool. When the breakup length is greater than the trajectory length the jet is undeveloped and a portion of the jet core still exists upon impingement. Many spillways are designed to maximize the jet trajectory length through the air by modifying the issuance angle to allow as much jet breakup as possible. The reduced erosive capacity of fully developed jets can improve plunge pool performance and limit erosion.

The footprint over which the plunging jet is applied is defined by the maximum outer diameter of the jet at impact (Ervine et al., 1997). The decay of the inner core of the jet occurs at an angle 15-20% of the angle of outer jet spread for circular jets, which is function of the jet turbulence intensity.

$$D_{out} = D_i + 2 \cdot 0.38(T_u L_j) \tag{4.6}$$

The diameter of the solid core of an undeveloped round jet at impact is described by Equation 4.7 (Ervine et al., 1997):

$$D_j = D_i \sqrt{\frac{V_i}{V_j}} \tag{4.7}$$

Where V_j is the impact velocity, defined by $\sqrt{(Vi^2+2gH)}$, where H is the difference between the Energy Grade Line (EGL) at the base of the spillway and the elevation of the tailwater level.

And the angle of impingement of the jet with the plunge pool, ξ, from horizontal, is a function of the kinetic energy of the jet, h_v, issuance thickness, D_i, issuance angle, Θ, and horizontal jet length, x, as outlined in Equation 4.8. The angle of impingement affects energy dissipation within the plunge pool. A low impingement angle results in greater energy dissipation at shallower depths.

$$\xi = arctan\left[tan\theta - \frac{x}{2(h_v)(cos\theta)^2}\right](-1) \tag{4.8}$$

The stream power of plunging jets, P_{jet}, is calculated based on the total jet discharge, Q, the difference between the Energy Grade Line at the base of the spillway and the tailwater level, H, and unit weight of water, γ.

$$P_{jet} = \gamma QH \tag{4.9}$$

The stream power per unit area can then be calculated by dividing the total stream power of the jet by the jet's footprint, area A, where it impacts at the surface of the tailwater (Equation 4.10):

$$p_{jet} = \frac{\gamma QH}{A} \tag{4.10}$$

The area, A, over which the jet impacts is based from the outer jet diameter, d_{out}, from Equation 4.6, and the distance along the jet trajectory, L_j (4.3). In the event that the jet becomes fully developed before impinging on the water surface, the use of the jet core diameter would be zero and the calculations would indicate that no energy is imparted to the plunge pool. Impact of the jet with the plunge pool does impart some energy regardless of the development of the jet, so the use of the jet core diameter is not logical for this analysis.

4.1.2 The Plunge Pool

Further energy dissipation occurs when the falling jet impacts the relatively stationary plunge pool. As it progresses downward it experiences energy dissipation in both the vertical direction and the horizontal direction. As outlined in Section 4.1.2.1 below, research by Ervine & Falvey (1987), Ervine et al. (1997), Bollaert (2002), and Castillo (2006) address the vertical dissipation of energy with depth. The horizontal dissipation of energy with depth, while not as thoroughly researched, has been addressed by Bollaert (2002) and is presented in Section 4.1.2.2

4.1.2.1 Vertical Energy Dissipation

The energy dissipation with depth is more complicated than a simple linear decay. Ervine & Falvey (1987) and Ervine et al. (1997) found that the outer turbulent zone of the jet expands at a different angle than that at which the inner core contracts. Figure 4.3 shows how the expansion and contraction angles change depending on the condition of the jet (ie. almost laminar, smooth turbulent, or rough turbulent).

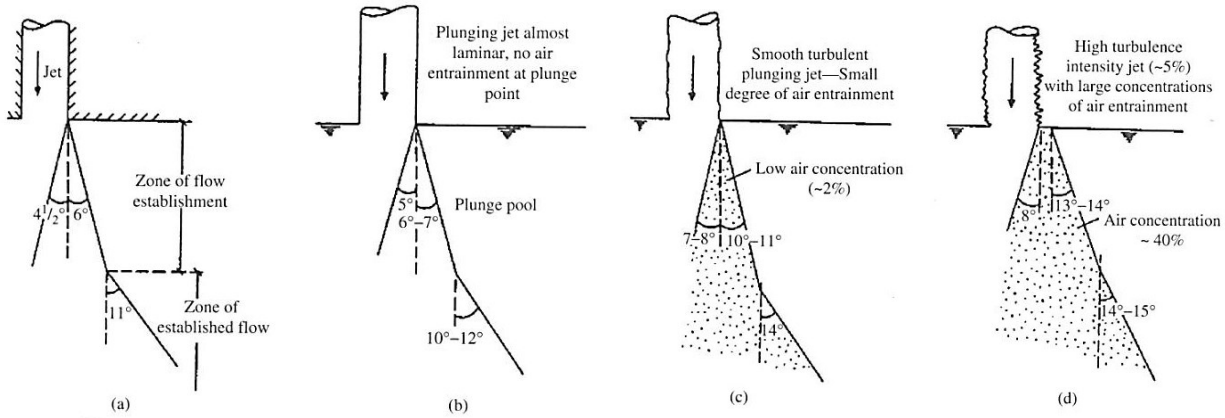

Figure 4.3 Diffusion of round jets in a plunge pool. (a) submerged jet, (b) almost laminar plunging jet, (c) smooth turbulent plunging jet, and(d) highly turbulent plunging jet. (Ervine & Falvey, 1987).

Once submerged, the jet expands with depth until it reaches the rock-water interface. At this point the water can no longer progress forward and instead spreads out along the interface, forming wall jets, pictured in Figure 4.4. These hydraulic features carry some of the energy away from the impingement zone. The amount of energy, however, is greatly reduced, with the impingement zone experiencing the most severe hydrodynamic action (Beltaos & Rajaratnam, 1973; 1974).

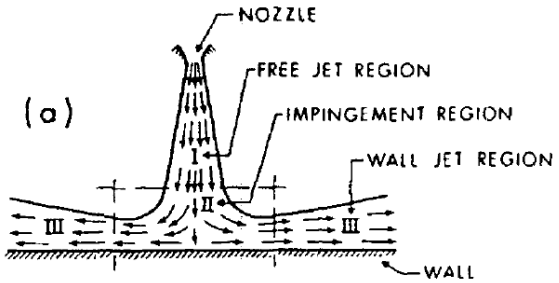

Figure 4.4 Two-dimensional jet diffusion and impingement on a flat surface, showing regions of different flow regimes (Beltaos & Rajaratnam, 1973).

Energy dissipation within the plunge pool is accounted for by incorporating both the mean pressure at depth as well as the amplitude of the pressure fluctuations about the mean. Ervine & Falvey's (1987), Bollaert's (2002), and Castillo's (2006) research into pressure fluctuations show that in an open, flat bottomed plunge pool the vertical pressure component can be broken down into the mean pressure and the dynamic pressure. As illustrated in Figure 4.5, the dynamic pressure represents the relatively constant average pressure experienced in the plunge pool and the fluctuating pressure represents the amplitude of the pressure changes about the mean over time.

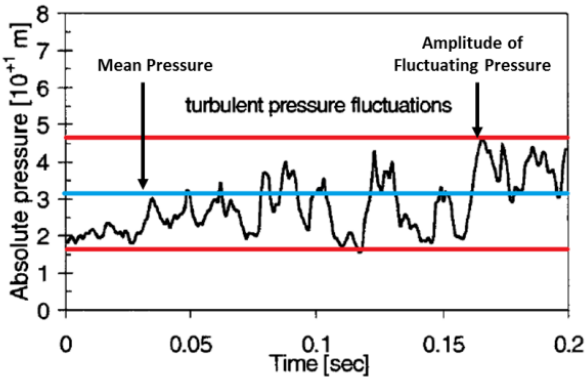

Figure 4.5 Mean and dynamic pressures at the bottom of an open, flat bottomed plunge pool (modified from Bollaert, 2002).

The researchers have developed coefficients to account for the magnitude of the dynamic and fluctuating pressures and their decay with dimensionless plunge pool depth, represented by the ratio Y/D_j (plunge pool depth, Y, to the jet diameter at plunge pool impingement D_j) (Bollaert, 2002). The coefficients represent the portion of the total pressure that exists at a given depth and range from zero to roughly 1.0 for the mean dynamic pressure component and from zero to approximately 0.3 for the fluctuating component. The two components include the average dynamic pressure coefficient, C_p, and the fluctuating dynamic pressure coefficient, C'_p.

Figure 4.6 shows the summary of the research on the mean dynamic pressure coefficient, separating out rectangular and circular jets by the degree of jet aeration. As shown in the plot, for dimensionless depths of less than 4, C_p remains constant. This region is referred to as the zone of flow establishment and indicates the depth at which the jet core begins to disintegrate (Castillo, 2006). At this point the mean dynamic pressure begins to decay and energy loss begins within the plunge pool. Note that Castillo's plot shows the line of best fit for data based on the ratio of fall height H to jet breakup length, L_b. For ski jump spillways the fall height is replaced with the head difference between the EGL and the tailwater level to account for head loss due to friction along the spillway face.

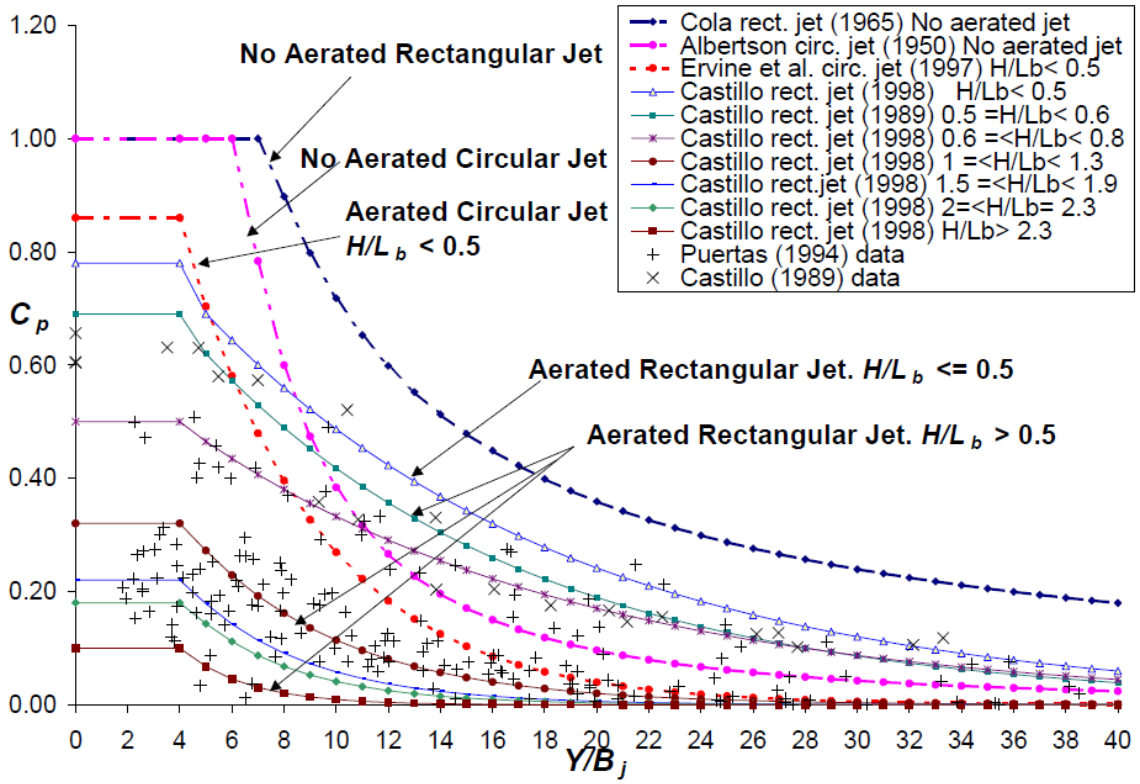

Figure 4.6 Summary of studies on the non-dimensional mean dynamic pressure coefficient C_p as a function of Y/D. Distinction is made between circular and rectangular jets, and between impinging and submerged jets (Castillo, 2006; 2007).

Castillo's research indicates that the average dynamic pressure coefficient, C_p, can be defined in terms of dimensionless plunge pool depth and jet breakup length (Castillo, 2006; 2007):

$$C_p = \alpha_1 e^{-b_1(\frac{Y}{D})} \qquad (4.12)$$

Where α_1 and b_1 are parameters defined by Castillo for various jet breakup length ratios. Table 4.2 shows these parameters, their associated jet breakup length ratios, and values of C_p in the zone of flow establishment ($Y/D<4$), where C_p remains constant. Equation 4.12 can be used to calculate C_p for dimensionless depths greater than 4.

Figure 4.7 shows the fluctuating dynamic pressure coefficient with dimensionless plunge pool depth based on Castillo's (2006) research. As shown, the fluctuating dynamic pressure coefficient is higher for jets with higher turbulence intensities. For all turbulence intensities, C'_p starts low, increases, reaches its peak value at a dimensionless depth of approximately 6, and then begins to decay with depth.

The magnitude of the fluctuating dynamic pressure is much lower than that of the mean dynamic pressure, reaching a maximum at approximately $C'_p = 0.32$ for high turbulence intensities.

Table 4.2 Parameters of the exponential law of the mean dynamic pressure coefficients in function of the different jet break-up length.

H/L_b	a_1	b_1	C_p (Y/D) < 4
< 0.5	0.98	0.070	0.78
0.5-0.6	0.92	0.079	0.69
0.6-0.8	0.65	0.067	0.50
1.0-1.3	0.65	0.174	0.32
1.5-1.9	0.55	0.225	0.22
2.0-2.3	0.50	0.250	0.18
>2.3	0.50	0.400	0.10

(Castillo, 2006; 2007)

The fluctuating dynamic pressure coefficient, C'_p, is defined for rectangular jets by Castillo (2006) in Equations 4.13 and 4.14, depending on the dimensionless plunge pool depth. Castillo's data for rectangular jets corresponds well with Bollaert's (2002) similar work with round jets, although Bollaert's research does not distinguish between different breakup lengths.

$$C'_p = a_2\left(\frac{Y}{D_j}\right)^3 + a_3\left(\frac{Y}{D_j}\right)^2 + a_4\left(\frac{Y}{D_j}\right) + a_5 \qquad \text{if } Y/D<14 \qquad (4.13)$$

$$C'_p = b_2\left(\frac{Y}{D_j}\right)^{b_3} \qquad \text{if } Y/D \geq 14 \qquad (4.14)$$

Where a_2, a_3, a_4, a_5, and b_2 and b_3 are coefficient values for calculating the fluctuating dynamic pressure and are dependent on the degree of jet development, H/L_b, as shown in Table 4.3.

Table 4.3 Coefficient values for calculating the fluctuating dynamic pressure coefficient of rectangular jets for different breakup lengths.

Polynomial Fit For *Y/D < 14*					
H/L_b	a_2	a_3	a_4	a_5	**Type of Jet**
≤1.4	0.0003	-0.0104	0.0900	0.083	Compact – Developed-Disintegrated
1.5-2	0.0003	-0.0094	0.0745	0.050	Developed-Disintegrated
>2	0.0002	-0.0061	0.0475	0.010	Developed-Disintegrated
Potential Fit For *Y/D ≥ 14*					
H/L_b		b_2	b_3		**Type of Jet**
≤1.4		5.30	-1.405		Compact – Developed-Disintegrated
1.5-2		3.14	-1.422		Developed-Disintegrated
>2		1.50	-1.500		Developed-Disintegrated

(Castillo, 2006)

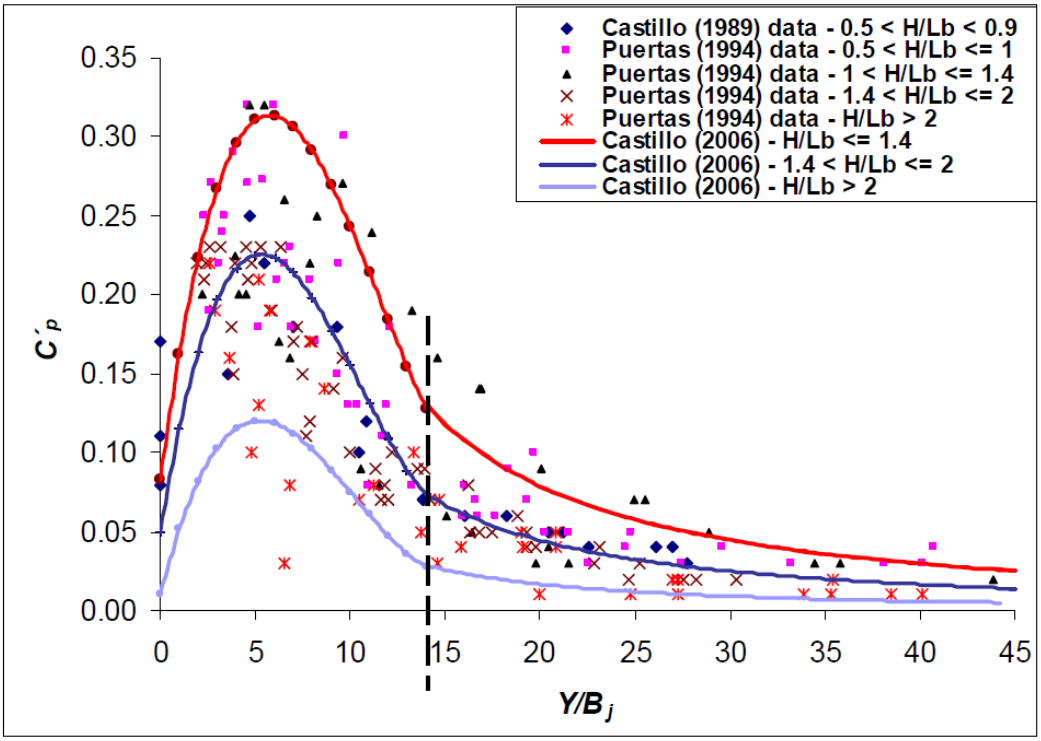

Figure 4.7 Non dimensional fluctuating mean dynamic pressure with plunge pool depth for rectangular jets (Castillo, 2006), showing distinction between different breakup lengths.

4.1.2.2 Horizontal Energy Dissipation

Horizontal energy dissipation occurs as the frayed fringes of the jet mix with the stationary water at the jet-plunge pool boundary. Additionally, the wall jets (discussed briefly in Section 4.1.2.1) transfer energy laterally outward at the contact with the plunge pool bottom.

Bollaert (2002) addressed the issue of horizontal energy dissipation away from the jet centerline by applying sensors radially outward from the jet's point of impingement on the plunge pool bottom during his experimentation. The sensor readings during jet impingement allowed him to determine the radial distribution of the surface pressures for a 72 mm diameter jet. Bollaert's research showed that pressure sensors located further away from the jet center experienced reduced pressure signals, as expected. Figure 4.8 shows the reduction between pressures recorded at 75 mm from the jet centerline (sensor a^{ii}) and 150 mm from the jet centerline (sensor a^{iv}). The first plot in the figures shows a significant decrease in pressure with distance from the center due to the influence of jet core impact. When present, the core produces higher pressures than the frayed outer zone of the jet. The second plot shows higher variability closer to the jet centerline, but only a slightly larger mean pressure than the sensor located further away.

The radial distribution of the mean dynamic pressure and the fluctuating dynamic pressure are important quantities to approximate the lateral extent of erosion within the plunge pool. In a similar manner to the way vertical energy dissipation is represented by the dimensionless plunge pool depth, the horizontal energy dissipation due to the radial distribution of the jet is represented by dimensionless radial distance. This parameter is defined as the ratio of the radial distance from the jet centerline, r, to the maximum radial extension of the zone influenced by the turbulent shear layer of the impacting jet, r_{max}, defined as shown in Equation 4.15:

$$r_{max} = 0.5D_j + 0.25Y \tag{4.15}$$

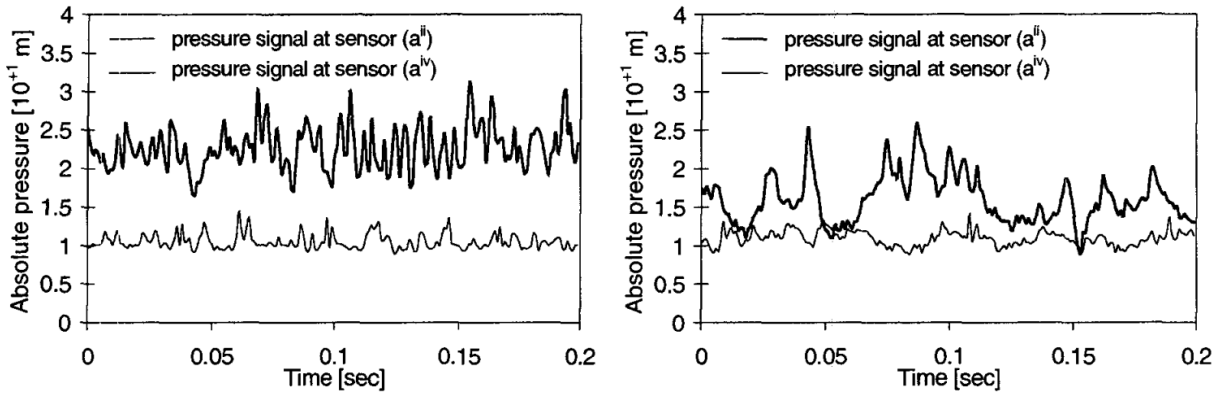

Figure 4.8 Pressure signal measured at sensor (a^{ii}), located at 75 mm of radial distance from the rock joint, and at sensor (a^{iv}), located at 150 mm radial distance from the rock joint; a) core jet impact; b) developed jet impact (Bollaert, 2002).

As defined previously, D_j represents the jet diameter at impact with the plunge pool and Y represents the depth below the surface of the plunge pool. The addition of the product $0.25Y$ to the radius at impingement accounts for the jet spread with depth, generally 13-14° or a ratio of 1:4 (0.25) (Bollaert, 2002).

As illustrated in Figure 4.8, the change in pressure with distance from the centerline varies depending on the development of the jet. Figure 4.9 shows the distribution of mean and fluctuating dynamic pressure coefficients with dimensionless distance away from the jet centerline.

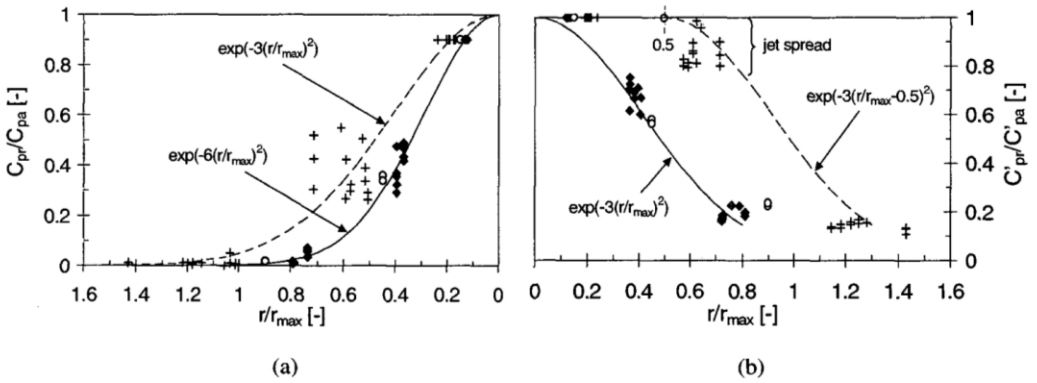

Figure 4.9 Radial distribution of the non-dimensional dynamic pressure coefficients at the plunge pool bottom: a) mean dynamic pressure coefficients C_p; b) root-mean square pressure coefficient C'_p. The reference distance r_{max} is defined as the maximum radial extension of the zone that is subjected to the turbulent shear layer of the impacting *jet* $r_{max} = 0.5D_j + 0.25Y$ (Bollaert, 2002).

The ratios, shown along the y-axis represent the proportion of the average and fluctuating dynamic pressure coefficients that can be applied with distance, where C_{pr} and C'_{pr} are the mean and fluctuating dynamic pressure coefficients, respectively. C_{pa} here is the equivalent of C_p. The ratios for the mean portion of the pressure distribution are expressed in Equations 4.16 for developed jets and Equation 4.17 for undeveloped depths (Bollaert, 2002):

$$\frac{C_{pr}}{C_p} = e^{-3\left(\frac{r}{r_{max}}\right)^2} \quad \text{for developed jets and all } r \text{ values} \qquad (4.16)$$

$$\frac{C_{pr}}{C_p} = e^{-6\left(\frac{r}{r_{max}}\right)^2} \quad \text{for undeveloped jets and all } r \text{ values} \qquad (4.17)$$

The ratios for the fluctuating portion of the pressure distribution are expressed in Equations 4.18 for developed jets and Equations 4.19 and 4.20 for undeveloped depths, depending on the value of r (Bollaert, 2002):

$$\frac{C'_{pr}}{C'_p} = e^{-3\left(\frac{r}{r_{max}}\right)^2} \quad \text{for developed jets and all } r \text{ values} \qquad (4.18)$$

$$\frac{C'_{pr}}{C'_p} = e^{-3\left(\frac{r}{r_{max}}-0.5\right)^2} \quad \text{for undeveloped jets and } r > 0.5r_{max} \qquad (4.19)$$

$$\frac{C'_{pr}}{C'_p} = 1 \quad \text{for undeveloped jets and } r \leq 0.5r_{max} \qquad (4.20)$$

4.1.2.3 Total Energy Dissipation

The combination of the mean and fluctuating dynamic pressure coefficients results in a non-linear energy decay with depth, dependent on the jet turbulence intensity, impact velocity, break up length, and trajectory length. The mean and fluctuating dynamic pressure coefficients can be combined with the radial mean and fluctuating dynamic pressure coefficient ratios to calculate the total dynamic pressure at a dimensionless depth within the plunge pool. In a similar manner, the coefficients can also be combined to calculate the total stream power, P_{total}, at a dimensionless depth (Y/D_j), as shown in Equation 4.21, modified from Annandale (2006) to account for the lateral dissipation of energy with distance from the jet centerline:

$$P_{total}\left(\frac{Y}{D_{out}},\frac{r}{r_{max}}\right) = p_{jet}\left[\left(C_p\left(\frac{Y}{D_{out}}\right)\frac{C_{pr}}{C_p}\left(\frac{r}{r_{max}}\right)\right)+\left(C'_p\left(\frac{Y}{D_{out}}\right)\frac{C'_{pr}}{C'_p}\left(\frac{r}{r_{max}}\right)\right)\right] \quad (4.21)$$

Where p_{jet} is the calculated stream power at impingement, defined by the discharge, drop height, and cross sectional area from Equation 4.10. Equation 4.21 can be used to calculate the total stream power as a function of depth within the plunge pool and lateral distance from the jet centerline by recalculating the mean and fluctuating dynamic pressure coefficients and radial mean and fluctuating dynamic pressure coefficient ratios for the appropriate dimensionless plunge pool depth.

4.2 The Rock Mass

In the early 1990's Annandale, among other researchers, began assessing the erodibility of earth materials in the context of Kirsten's (1982) geomechanical index on excavatability. The goal of all of the researchers was to develop a relationship between key rock parameters and the ease of their removal by hydraulic forces. Annandale's methodology, in particular, focused on finding a balance between the geologic engineering properties of the earth material and the hydraulic flow conditions such that one was not weighted higher in importance than the other (Annandale, 1995). The methodology is based on over 150 field observations, including 137 spillway observations from dams in Kansas and Arkansas, as well as scour data from four dams in South Africa and Bartlett Dam in Arizona. The methodology addresses scour of essentially all rock and soil types, ranging from loose sands, clays and silts to strong granite and gneiss rock formations. Figure 4.10 shows the relative magnitude of stream power in rivers, around bridge piers, and downstream of overtopping dams as well as the resistance of the various earth materials.

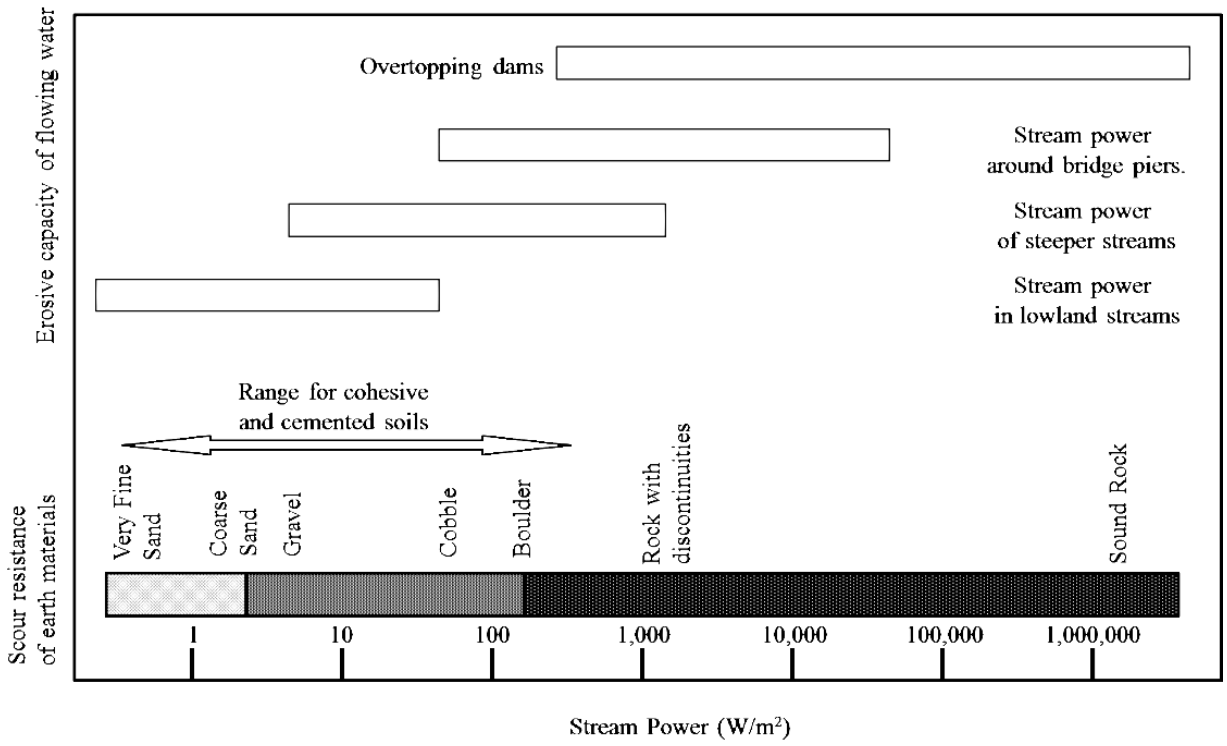

Figure 4.10 Schematic illustration of the relative magnitude of stream power and the resistance to scour offered by earth materials. This figure is qualitative and should not be used for analysis and design (Annandale, 2006).

Annandale's Erodibility Index Method, originally published in 1995, determined that the erodibility of earth materials was dependent on the material strength, block or particle size, discontinuity conditions and orientations, as outlined in Equation 4.22, below:

$$K = M_s \cdot K_b \cdot K_d \cdot J_s \qquad (4.22)$$

Where:

K = Erodibility index value

M_s = Mass strength number

K_b = block size number

K_d = discontinuity/bond shear strength number

J_s = relative ground structure number

This relationship is applicable to both soil and rock materials. For rock materials the resistance to erosion increases in materials with strong chemical bonds within the rock's crystal structure. The presence of fractures and/or imperfections in the rock mass, however, reduce the overall ability to resist erosion, which results in a lower K value than rock with no fractures or imperfections (Annandale, 2006).

As a result, for rock, both intact and rock mass parameters are used to quantify the erosive resistance of the material. For soil materials the resistance to erosion increases in materials with larger grain sizes or cohesion.

Figure 4.11 shows the distribution of the data from Annandale's (1995) analysis and the derived scour threshold for various stream powers. Threshold stream power necessary to initiate erosion is related to the erodibility index (K) value from Equation 4.26 and Figure 4.11, with K along the x-axis and the associated stream power along the y-axis, in kW/m^2. The dashed line represents the threshold value, with the square points (pink) representing tested samples that did not experience scour and the diamonds (blue) representing tested samples that did experience scour.

The threshold stream power necessary to initiate erosion (P_c) can then be calculated from the erodibility index K value as follows in Equations 4.23 and 4.24 (Annandale, 1995, 2006):

$$P_c = 0.48(K)^{0.44} \quad \text{for } K \leq 0.1 \tag{4.23}$$

$$P_c = K^{0.75} \quad \text{for } K > 0.1 \tag{4.24}$$

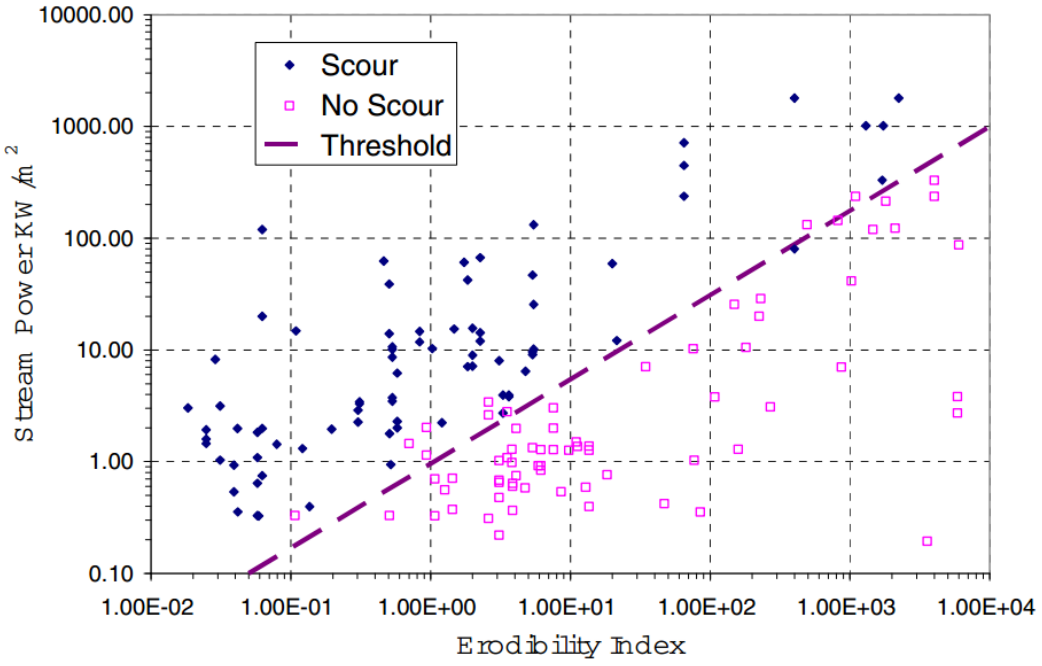

Figure 4.11 Erosion threshold relating stream power and erodibility index (Annandale 1995, 2006).

The threshold identified in Figure 4.11 represents a solid boundary at which erosion initiates. In reality, however, the threshold is better represented by a region. When a data point falls within the threshold region there is uncertainty as to whether or not the material will erode (Wibowo et al., 2005). Wibowo et al.'s(2005) research developed a logistic regression to assess the probability of scour based on the stream power experienced by the bed and the erosive resistance of the bed material, from Annandale's erodibility index. Based on Annandale's original dataset and binary logistic regression, Wibowo produced a series of threshold lines, each associated with a different probability of failure. The 50% probability line corresponded well with Annandale's original erosion threshold. Wibowo et al.'s (2005) logistic regression is expressed as:

$$P(E) = \frac{1}{1+e^{-(-1.859-7.029\ln K+9.798\ln P_{tot})}} \tag{4.25}$$

Where *P(E)* is the probability of failure, *K* is the erodibility index, and P_{tot} is the stream power experienced by the rock. The rock erodibility parameters used in Equation 4.22 to quantify the erodibility index *K* value can be calculated using the relationships developed in the following sections.

Mass Strength Number (M_s)

For rock, the mass strength number is based on Unconfined Compressive Strength (UCS) values from intact rock samples (MPa) (Annandale, 2006). Higher rock strengths indicate higher resistance to rock scour, per Equations 4.26 and 4.27:

$$M_s = C_r \cdot 0.78 \cdot UCS^{1.05} \qquad \text{When } UCS \leq 10 \text{ MPa} \tag{4.26}$$

$$M_s = C_r \cdot UCS \qquad \text{When } UCS > 10 \text{ MPa} \tag{4.27}$$

C_r is a coefficient of relative density (Equation 4.27), defined in terms of acceleration due to gravity (g in m/s^2) and the mass density of the rock (ρ in kg/m^3). The numeric term in the denominator normalizes C_r to a reference unit weight of rock (in N/m^3).

$$C_r = \frac{g*\rho_r}{27 \times 10^3} \tag{4.28}$$

M_s can also be estimated from field observations, as shown in Appendix A, Table A.1. For soils, the M_s value is a function of a cohesive material's stiffness and a non-cohesive material's density. Values range from 0.02 to 0.41 and can be estimated from vane shear strength for cohesive soils and from SPT blow count for non-cohesive soils.

Block Size Number (K_b)

K_b is a function of joint spacing and the number of joint sets in a rock mass, as shown in Equation 4.29. Joint spacing is estimated based on Rock Quality Designation[1] (RQD) values and joint sets are established from Kirsten's (1982) joint set number (J_n), shown in Appendix A, Table A.2. More intact rock, with fewer joint sets, results in larger rock blocks, which are more difficult to remove.

$$K_b = \frac{RQD}{Jn} \tag{4.29}$$

Block size number for cohesive soils is assumed equal to unity. For non-cohesive soils, K_b is calculated from the characteristic particle diameter, D_{50}, (in m), as shown in Equation 4.30:

$$K_b = 1000 D_{50}^3 \tag{4.30}$$

Discontinuity/Bond Shear Strength Number (K_d)

K_d represents the relative resistance offered by discontinuities in rock. It is calculated from the joint wall roughness (J_r) and joint wall alteration number (J_a) (Kirsten, 1982), as shown in Equation 4.31.

$$K_d = \frac{Jr}{Ja} \tag{4.31}$$

Joint roughness contributes to rock stability due to the higher frictional resistance experienced along discontinuities. Joint infill or alteration detracts from the stability, as these features reduce the frictional resistance. Tables for estimating joint wall roughness and joint wall alteration number are shown in Appendix A, Table A.3 and Table A.4.

For granular soils K_d is estimated based on the residual friction angle via Equation 4.32:

$$K_d = \tan(\varphi) \tag{4.32}$$

Relative Ground Structure Number (J_s)

J_s is a function of 1) the orientation of least favorable discontinuities within the rock, that is, discontinuities that are most easily eroded due to their orientation relative to flow direction and 2) the shape of the material units. Values for this parameter are shown in Appendix A, Table A.5. Adverse joint

[1] RQD can also be estimated based on the equation $RQD = 105 - (10/D)$ where D is the mean block diameter in meters (Annandale, 2006).

orientations result in higher pressures within the joints themselves, which increase the likelihood of rock removal. Favorable joint orientations prevent pressure buildup within joints. Figure 4.12 shows favorable and unfavorable joint discontinuity orientations, based on flow direction. For soils, this parameter is set equal to unity.

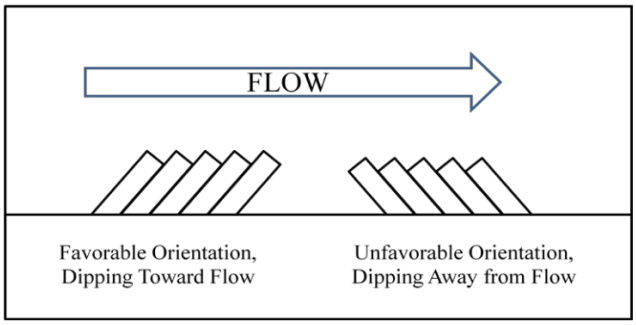

Figure 4.12 Favorability of discontinuity orientation, based on flow direction (USBR, 2012).

CHAPTER 5

DAM SITE DESCRIPTIONS

Four dam sites were selected for this analysis, based on the availability of data to both a) characterize plunge pool materials and spillway discharge and b) validate modeling based on existing plunge pool surveys. The four dams include Peace Canyon Dam, Seven Mile Dam, Revelstoke Dam, and W.A.C. Bennett Dam and are located across British Columbia as shown in Figure 5.1. All dams are owned and operated by BC Hydro, public energy utility.

Figure 5.1 Dam site locations in British Columbia, Canada.

The following sections provide general dam and spillway characteristics as well as the geologic environment in which the facilities are located.

5.1 Peace Canyon Dam

Peace Canyon Dam is located in north central British Columbia on the Peace River about 92 miles upstream from where the Peace River crosses the British Columbia-Alberta border, as shown in Figure 5.1. The dam is one of the two dams constructed on the Peace River near Hudson's Hope, B.C. The W.A.C. Bennett Dam, discussed further in Section 5.4, is the second dam in the area and is located

upstream of Peace Canyon Dam. Outflow from Williston Lake, retained by W.A.C. Bennett Dam, is the inflow to Peace Canyon Dam. Completed in 1980, the dam is a concrete gravity structure and retains Dinosaur Reservoir, which extends 14 miles upstream of the structure. The dam itself, pictured in Figure 5.2, is 1,130 ft long and 200 ft tall.

Figure 5.2 Peace Canyon Dam, showing the six-gated overflow spillway on the left (river right) and the powerhouse on the right (river left).

Peace Canyon Dam is a run-of-the-river dam. Dinosaur Reservoir has a surface area of 2,200 acres and a storage volume of 175,000 acre-feet when the pool is at Maximum Normal Reservoir Level (El. 1,650 ft). Maximum Flood Reservoir Level is at elevation 1,655 ft. The spillway is located on the river-right side of the dam the power intake section is located on the left, as depicted in Figure 5.2. The power intake portion of the dam consists of four units and has a maximum sustainable generating capacity of 700 MW (BCH Report No. H1742).

Site Geology

The Peace River Valley is located in the foothills of the northern Rocky Mountains, a 35 mile wide transitional zone where the high altitude Rocky Mountains to the west meet the low-lying, interior plains to the east. The Peace River itself flows generally east through a glacial trough, at right angles to the regional structural trend of the bedrock geology. Glacial infill of the Peace River valley upstream of the present day Peace Canyon Dam resulted in the river's diversion and subsequent down-cutting through sedimentary bedrock along the new path, forming the 14-mile long, 700-foot deep canyon. Peace Canyon Dam is located at the downstream end of the river-cut canyon (BCH Report No. H1742).

Surficial deposits in the area are largely glacial till deposited in the late Pleistocene. The region has undergone three periods of glaciation, including regional glaciation and more localized alpine

glaciation. Deposits in the area tend to be discontinuous periglacial or interglacial basal river sands and gravels, glacial till, and lake deposits. Post glaciation debris flow and alluvial fan deposits are also present in the area (BCH Report No. H1742).

Spillway Characteristics

The Peace Canyon spillway is located on the river-right side of the dam and is a gated six-bay ogee-shaped overflow spillway with flip buckets at the toe. Spillway bays are equipped with radial 50 feet wide by 41.5 feet high gates. Bays are numbered one through six, beginning at the powerhouse and proceeding in the river-right direction. The spillway is split into two chutes to provide lateral flow control, one consisting of spillway bays one and two and the other consisting of spillway bays three through six. Typical sections of the spillway are provided in Figure 5.3 and Figure 5.4. The spillway crest level is at elevation 1,612 ft and the top of the radial gates is elevation 1,652 ft, when completely closed. The spillway profile consists of an ogee-shaped crest, followed by a long convex circular section that merges with the dam back slope, at 0.7647 H: 1.0 V, which then merges into a 55 ft flip bucket radius. Spillway bays one and two have a flip bucket lip angle of 30 degrees from horizontal and bays three through six have an angle of 20 degrees (BCH Report No. H1742).

The design spillway capacity, based on the probable maximum flood (PMF) release from the upstream W.A.C. Bennett Dam, is 363,000 cfs (BCH Report No. H1742). Spillway gates can be operated independently and at variable gate heights to safely pass the discharge based on the spillway gate rating curves. Spillway bays three and four are the primary gates used for water discharge because they are centered on the plunge pool area, minimizing the risk to the stability of the powerhouse and river bank (BCH Report No. H1742). Spillway operating procedure dictates the gate opening and closing order to minimize damage to the plunge pool, downstream river bank, and powerhouse. Gate opening and closing orders are as follows:

- Opening: 3, 4, 6, 5, 1, 2
- Closing: 2, 1, 6, 5, 4, 3

The order is largely based the proximity of the various bays to the powerhouse. To reduce damage, bays five and six are preferred to bays one and two. Additionally, bays one and two require greater flow to initiate flip action and propel water away from the structures due to the higher flip bucket release angle (BCH Report No. H1742). A summary of spillway characteristics is provided in Table 5.1.

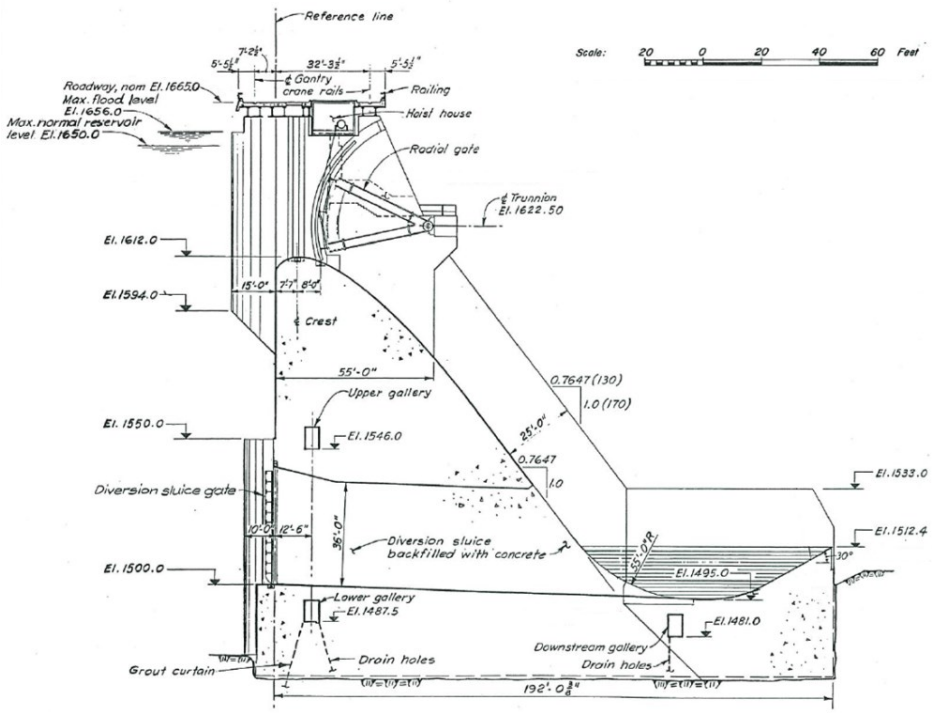

TYPICAL SECTION THROUGH SPILLWAY BAYS 1 AND 2

Figure 5.3 Cross Section of Spillway Bays 1 & 2.

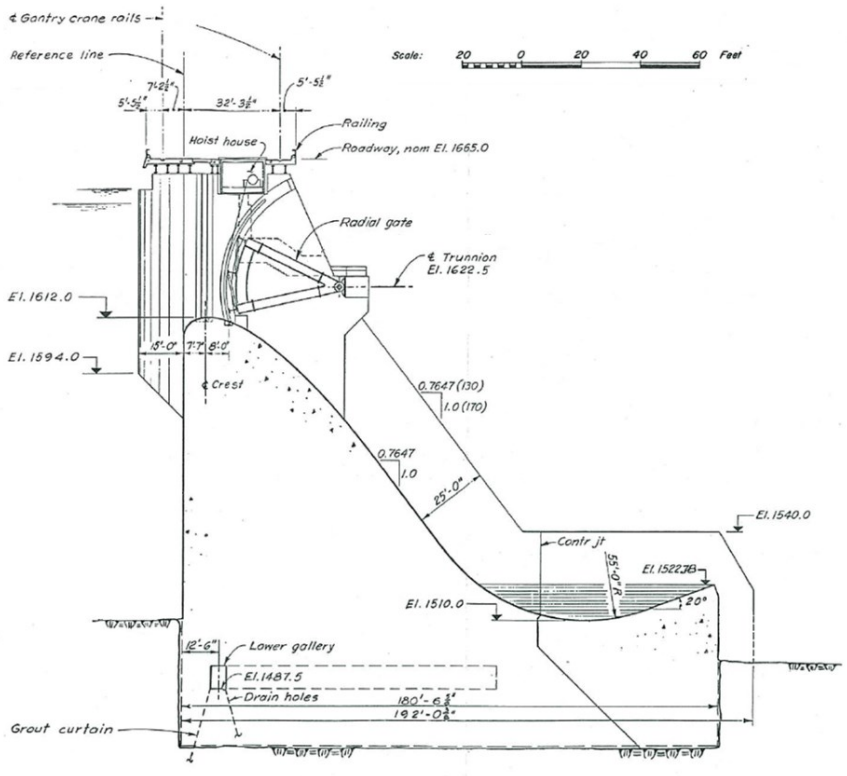

TYPICAL SECTION THROUGH SPILLWAY BAYS 3 TO 6

Figure 5.4 Cross Section of Spillway Bays 3 through 6.

Table 5.1 Peace Canyon Dam Key Spillway Characteristics

General	
Type of Spillway	Gated Overflow Spillway
Total Spillway Width	440 ft across spillway blocks S1 – S7
Overall Spillway Length	240 ft (Bays 1-2) 220 ft (Bays 3-6)
Headworks	
Number of Overflow Bays	6
Pier Width	10 ft
Ogee Crest Elevation	El. 1,612 ft
Gates	6 Radial Gates
Gates Dimension	50 ft wide x 41.5 ft high
Terminal Structure	
Energy Dissipation	Flip Buckets
Bucket Radius	55 ft
Bucket Invert Elevation	El. 1,495 ft (Bays 1-2) El. 1,510 ft (Bays 3-6)
Bucket Lip Angle	30^o (Bays 1-2) 20^o (Bays 3-6)
Bucket Lip Elevation	El. 1,512.37 ft (Bays 1-2) El. 1,522.77 ft (Bays 3-6)
Bucket Width	116 ft (Bays 1-2 combined) 234 ft (Bays 3-6 combined)
Hydraulics	
Normal Conditions	
Maximum Normal Reservoir Level	El. 1,650 ft
Tailwater level with Three Units Rated Discharge	El. 1,518 ft
Flood Conditions	
Inflow Design Flood[1]	330,200 cfs
Maximum Flood Level[1]	El. 1,652.4 ft
Maximum Tailwater Level[2]	El. 1,532 ft

Notes: (Monfette, 2004); [1](BCH Report No. OMSPCN, 2003); [2] Monfette's estimate from current tailwater rating curve (BCH Drawing No. 1007-C14-D4954)

5.2 Seven Mile Dam

Seven Mile Dam is a concrete gravity structure in the Kootenay region of southwestern British Columbia on the Pend d'Oreille River, 6 miles upstream from its confluence with the Columbia River near the Canada-U.S. border, as shown in Figure 5.1. When filled to the maximum normal reservoir level, the dam retains 85,000 acre-ft of water, which covers a ten square mile area. The dam has been designed as a run-of-the-river dam, with outflows equaling inflows and relatively little change in reservoir head. The dam is a 1,138 ft long structure with a straight axis and a maximum height from the bottom of the

drainage sump to the deck of 262.5 ft. The axis consists of a 350 ft long north gravity section on the right, a 336 ft long power intake section, a 322 ft long spillway section, and a 130 ft long south gravity section on the left (BCH Report No.1743; BCH Report No. PSE-362). Figure 5.5 shows the dam configuration looking upstream. Reservoir filling was completed in November 1979 and power generation began in 1980.

Figure 5.5 Seven Mile Dam – photograph of upstream view of the concrete gravity structure.

Site Geology

Bedrock in the area consists of meta-sedimentary, volcanic, and intrusive rocks ranging from Tertiary to Lower Cambrian age. This sequence is in contact with the Waneta Fault to the north and with volcanic rocks to the south. The non-calcareous meta-sedimentary rocks in the area exhibit strong foliations that generally dip to the south. On site and extending to the west, Tertiary aged leucocratic granites have been intruded into the Pend d'Oreille Sequence consisting of argillite, silty argillite, siltstone and minor limestone (BCH Report No. PSE-362). Rocks of the Pend d'Oreille Sequence can be found along the valley walls, extending approximately 5 miles upstream of the dam to well downstream. The dam site itself is underlain by the Pend d'Oreille Sequence and the Tertiary leucocratic granite intrusions. Tertiary granites on site consist of sills of various size, dykes, or irregular masses and are pictured just downstream of the right abutment in Figure 5.5 (BCH Report No. 1743). The region has a complex history of structural deformation, with evidence for low grade metamorphism, contact metamorphism, folding, shearing, and faulting. Tight fold axes are generally oriented roughly east-west across the region. Thrust faulting and faulting along bedding associated with folding are common. Structural features are cross-cut by the younger Tertiary granites.

The glacially modified Pend d'Oreille River valley is a glacial trough with moderately steep slopes at elevations above 4,000 ft (BCH Report No. 1743). Shallower slopes in the river valley are covered with glacial till and outwash deposits in areas. Two prominent glacial till and outwash terraces are present within the valley at approximately 1,700 ft and 1,900 ft elevation (BCH Report No. 1743). Local buried channels have been identified, resulting in sometimes deep alluvial deposits within the valley. The reservoir shoreline has experienced some sliding and sloughing, primarily in terrace deposits. No deep-seated movements have been observed (BCH Report No. 1743).

Spillway Characteristics

The ogee-shaped spillway is controlled by five 50-ft wide vertical lift gates with flip buckets at the toe. The spillway crest level is at 1,679 ft elevation. The top of the gates, when closed, are at elevation 1,733 ft. The spillway geometry is split into two sections separated by a training wall. Section one consists of spillway bays one and two. This section is comprised of an ogee-shaped crest that merges with the dam back slope of 0.8H:1V, which in turn merges into a 60 ft radius and a 75-ft long downward sloping section which terminates in a 60 ft radius flip bucket with an exit angle of 30°. Section two consists of bays three, four, and five. The geometry of section two is similar to section one, but excludes the 75 ft long downward sloping section. Spillway cross sections are shown in Figure 5.6. The split chute design was adopted to address concerns about jet impingement on the powerhouse structure and to minimize construction costs.

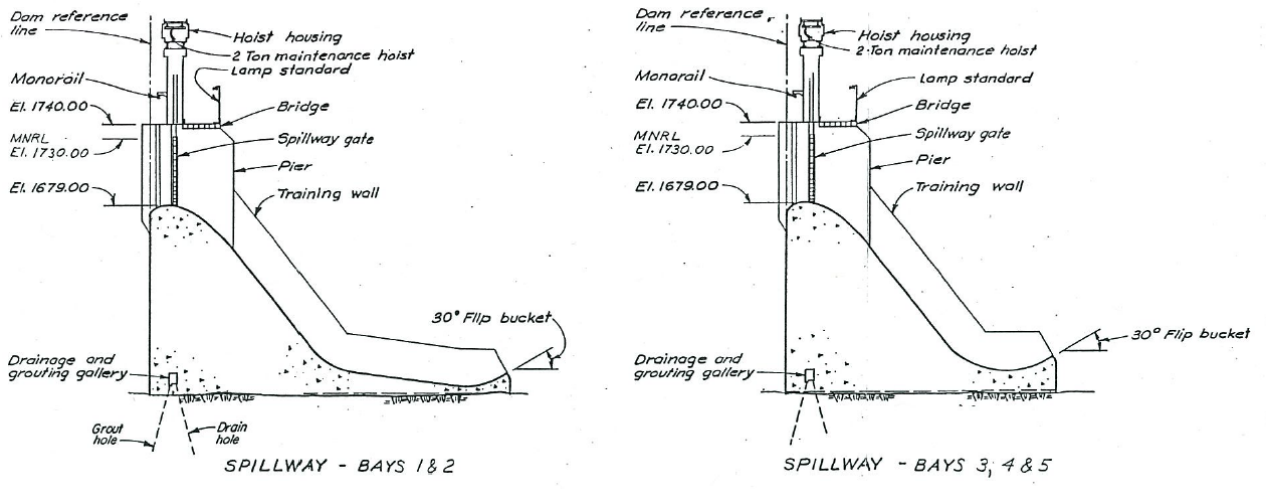

Figure 5.6 Seven Mile Dam spillway cross sections (BCH Report No. H1743).

The bucket lip elevations for sections one and two are 1,555.54 ft and 1,565.54 ft respectively (BCH Report No. H1743). The spillway facilities were built to safely pass the inflow design flood of

370,000 cubic feet per second (cfs) with no damage to the dam, spillway, or intake structure. Table 5.2 gives values for key spillway characteristics (Monfette, 2004).

Spillway gate operation varies based on the flow the structure must pass. Gates one and two are used exclusively for flows up to 17,400 cfs. Spillway gates one through four are used under normal conditions. Efforts to minimize the impact of discharge on the left bank downstream of the dam preclude the use of gate 5 unless there is danger to the dam or other spillway gates (BCH S.O.O 4P-36, 1997).

Table 5.2 Seven Mile Dam Key Spillway Characteristics

General	
Type of Spillway	Gated Overflow Spillway
Total Spillway Width	322 ft
Overall Spillway Length	330 ft (Bays 1-2)
	250 ft (Bays 3-5)
Headworks	
Number of Overflow Bays	5
Pier Width	12 ft
Ogee Crest Elevation	El. 1,679 ft
Gates	5 Vertical Lift Gates
Gates Dimension	50 ft wide x 54.42 ft high
Terminal Structure	
Energy Dissipation	Flip Buckets
Bucket Radius	60 ft
Bucket Invert Elevation	El. 1,545 ft (Bays 1-2)
	El. 1,555 ft (Bays 3-5)
Bucket Lip Angle	30^{o} (Bays 1-5)
Bucket Lip Elevation	El. 1,555.54 ft (Bays 1-2)
	El. 1,565.54 ft (Bays 3-5)
Bucket Width	115.5 ft (Bays 1-2 combined)
	177.5 ft (Bays 3-5 combined)
Hydraulics	
Normal Conditions	
Maximum Normal Reservoir Level	El. 1,730 ft
Tailwater level with Three Units Rated Discharge	El. 1,523 ft
Flood Conditions	
Inflow Design Flood	376,900 cfs
Maximum Flood Level	El. 1,732 ft
Maximum Tailwater Level[1]	El. 1,556 ft

Notes: (Monfette, 2004); [1] Monfette's estimate from current tailwater rating curve (BCH Drawing No. 224-C14-B1740)

5.3 Revelstoke Dam

Revelstoke Dam is located along the Columbia River in southeastern British Columbia three miles north of the city of Revelstoke. The general location is shown in Figure 5.1. The Revelstoke Hydropower Project is located between the upstream Mica Hydropower Project and the downstream Keenleyside Project. The project's concrete gravity dam is placed in the steep-sided, north-south oriented portion of the Columbia River valley between the Selkirk and Monashee Mountain Ranges (BCH Report No. H1864). The structure, shown in Figure 5.7, retains Lake Revelstoke, which consists of 4.3 million acre-ft at Maximum Normal Reservoir Level (Elev. 1,880 ft). The primary dam consists of a 1,550 ft long concrete gravity dam that is 575 ft tall at its highest point. An earthfill embankment is also present along the river-right bank, as shown on the left side of Figure 5.7. This portion of the dam is 3,800 ft long and extends 260 ft above the ground surface. The spillway is visible on the river-right side of the concrete gravity structure. The spillway consists of two gated overflow bays and two intermediate gated outlets, which are rarely operated. All gates empty to a long chute, which transports water well downstream of the dam. The powerhouse associated with the project consists of five hydropower units with a generating capacity of 2,480 MW of power, with provisions to install one additional unit (BCH L.O.O. No. 3PO3-47, 2000).

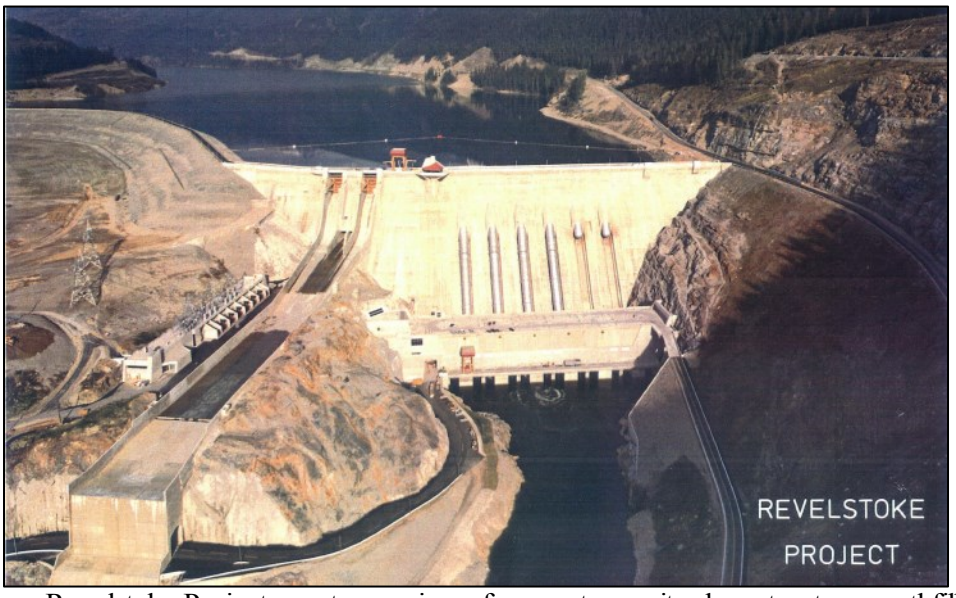

Figure 5.7 Revelstoke Project– upstream view of concrete gravity dam structure, earthfill embankment structure (river right, photo left) and spillway chute (river right, photo left).

Site Geology

Regionally, the Revelstoke Project is located within the Columbia River Fault Zone. To the west of the zone lies the Monashee Complex and to the east likes the Selkirk Allochthon. Both complexes consist of metamorphic rocks primarily of sedimentary origin (BCH Report No. H1864). The Monashee Complex to the west represents a Precambrian succession of mixed gneisses and meta-sediments, which have undergone multiple deformation events. Rocks within the Complex range from 2.7 billion year old to 700 million year old gneiss (BCH Report No. H1864). The Clachnacudainn Slice of the Selkirk Allachthon borders the Columbia River Fault Zone on the east and consists of granodioritic plutonic rocks and metasediments. Movement along the Columbia River Fault Zone from 160 to 45 million year ago resulted in the formation of a 0.6 mile thick mylonite zone and intense brittle fracturing and gouging within the dam site.

The project itself sits within the glacially eroded Columbia River Valley. Surficial deposits in the valley consist of remnants of early valley fill, glacial till and outwash, and postglacial deposits (BCH Report No. H1864). The most extensive deposits within the Revelstoke Project area include late glacial and post-glacial outwash and lacustrine deposits, dominantly silt, sand, and gravel (BCH Report No. H1864). The reservoir banks are lined with active landslides, historic landslide deposits, and generally landslide-susceptible materials.

Spillway Characteristics

The headworks of the spillway are located at the transition between the concrete to the earthfill dams. The headworks consist of two radial gate overflow bays and two low level outlets. The radial overflow bays are gated by 45 ft wide by 59 ft tall radial gates located at the ogee-shaped spillway crest at elevation 1,825ft. The low level outlets are gated by 17.5 ft wide by 25 ft high radial release gates located at elevation 1,700ft. Water discharges into a 975 ft long chute, where it is transported to the terminal horizontal free overfall structure and pre-excavated plunge pool at the river-right bank downstream of the dam (BCH Report No. H1864). As shown in Figure 5.8, the chute is initially steep, following the face of the dam at a slope of 1.0 V:0.76 H from the spillway crest, then grading to a gentler slope of 1.0 V:0.1715 H at the beginning of the chute at elevation 1,690ft, where the low level outlets discharge down the center of the spillway, for 300 ft. The chute then shallows to a slope of 0.002 and continues for another 472 ft, expanding from 120 ft wide where the 0.002 slope begins to 150 ft wide at the horizontal free overfall terminal structure located at elevation 1,620 ft that projects water into the pre-excavated plunge pool of elevation 1,425 ft (BCH Report No. H1864). Table 5.3 shows pertinent spillway characteristics.

When in operation, spillway gates are opened and closed at the same time and maintained at the same level to promote stable hydraulic conditions within the spillway chute (BCH L.O.O. 3PO3-47, 2000). Discharge records also indicate the exclusive use of either overflow bays or the low level outlet works; the two are not used simultaneously.

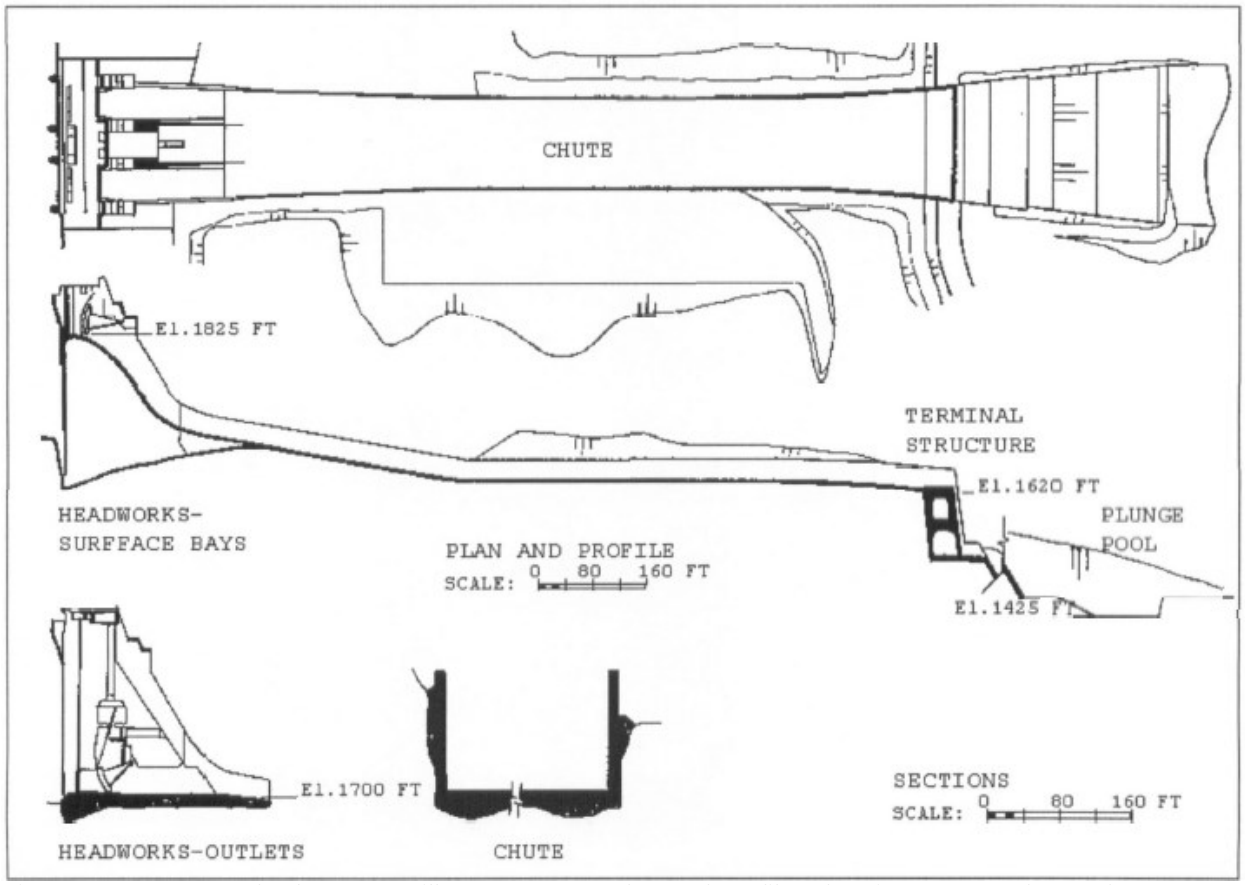

Figure 5.8 Revelstoke Dam spillway structure plan and profile, showing crest, outlet, and pre-excavated plunge pool elevations (Monfette, 2004); low level outlet gates shown in lower left of figure

5.4 W.A.C. Bennett Dam

W.A.C. Bennett Dam is located 14 miles upstream of Peace Canyon Dam on the Peace River. This facility is located at the head of Peace River Canyon. The dam is one of the largest earth embankment dams in the world, extending 6,700 ft across Peace River Canyon and rising 600 ft from the foundation. Water is released either to the G.M. Shrum Generating Station or through the long chute spillway, pictured along the river-right of the dam in Figure 5.9. The dam retains Williston Lake, a 684 square mile reservoir when at Maximum Normal Reservoir Level (El. 2,205 ft), containing 60.2 million acre-ft of water.

The G.M. Shrum Generating Station consists of 10 hydropower units that are capable of producing 2,730 MW of power. The generating station came online in September of 1968 and was generating at full capacity by February 1980.

Table 5.3 Revelstoke Dam Key Spillway Characteristics

General	
Type of Spillway	Long Chute Spillway
Total Spillway Width	224 ft across spillway blocks S1 – S3
Overall Spillway Length	1,300 ft
Headworks	
Radial Overflow Bays	
Number of Bays	2
Pier Width	N/A
Ogee Crest Elevation	El. 1,825 ft
Gates	2 Radial Gates
Gates Dimension	45 ft wide x 59 ft high
Low Level Outlets	
Number of Outlets	2
Pier Width	10 ft
Sill Elevation	El. 1,700 ft
Gates	2 Outlet Sector Gates
Gate Dimensions	17.5 ft wide x 25 ft. high
Terminal Structure	
Energy Dissipation	Horizontal Free Overfall
Bucket Radius	0^o
Bucket Invert Elevation	El. 1,620 ft
Bucket Lip Angle	0^o
Bucket Lip Elevation	El. 1,620 ft
Bucket Width	150 ft
Hydraulics	
Normal Conditions	
Maximum Normal Reservoir Level	El. 1,880 ft
Tailwater level with Four Units Rated Discharge	El. 1,459 ft
Flood Conditions	
Inflow Design Flood	251,000 cfs
Maximum Flood Level	El. 1,884 ft
Maximum Tailwater Level[1]	El. 1,481 ft

Notes: (Monfette, 2004); [1] Monfette's estimate from BCH Drawing of spillway profile (BCH Drawing No. 212-C21-U11/U47/U48).

Figure 5.9 W.A.C. Bennett Embankment Dam, showing orientation of dam, spillway, and G.M. Shrum Generating Station (energeticcity.ca).

Site Geology

The W.A.C. Bennett Dam and surrounding facilities have been constructed in a glacial trough carved through Meso- and Cenozoic sedimentary sandstones, siltstone, and shale. Peace Canyon, and now Williston Lake, extends easterly roughly perpendicular to the regional structural trend of the bedrock. Rocks on site are of the Cadomin/Dunlevy and Gething Formations. The lower Cadomin/Dunlevy Formation makes up the majority of the foundation rock and consists dominantly of strong quartz sandstones, with some softer shale layers subject to slaking, and sporadic coal seams ranging from less than an inch to several feet in thickness. Sedimentary rocks in this region have been subjected to folding and faulting, however no large scale structural features are located in the immediate vicinity of the damsite. The overlying Gething Formation consists of massive and interbedded shale with thin sandstone beds, but is located higher on the Peace River Canyon walls and not beneath the dam foundation or plunge pool (Domage & Campbell, 1963).

Surficial deposits on site are primarily glacial deposits, sourced from the three identified glaciations to which the area was subjected. Included among these are periglacial and interglacial river sand and gravel deposits, glacial tills, and glacio-lacustrine and fluvial units deposited during glacier retreat (BCH Report No. H1756, 1988). Glacial kame deposits and kettles have also been noted on terraces around the reservoir area. Post-glacial river deposits, alluvial fans, and landslide deposits are the youngest noted surficial materials on site.

Spillway Characteristics

The W.A.C. Bennett spillway headworks consists of three radial discharge bays at the ogee crest (El. 2,145), each 50 ft wide and 61 ft tall, and nine gated sluices. Sluices are also incorporated into the headworks at elevation 2,105 ft in groups of three below each overflow bay, but are considered out of service. The primary purpose of the sluices was to provide additional discharge in the event that the power plant is un-operational. Radial gates and sluice gates discharge to a 2,240 ft long trapezoidal channel with a typical width of 100 ft. Chute walls are 57 ft high. The spillway ends at a spoon shaped concrete flip bucket that sits approximately 300 ft below reservoir level. The terminal structure has a flip bucket angled at 30 degrees. A summary of key spillway characteristics is provided in Table 5.4. The combined discharge is 325,000 cfs for the radial gates, when the reservoir is at elevation 2,215 ft (BCH Report No. H1756, 1988). A plan and profile of the spillway is provided in Figure 5.10.

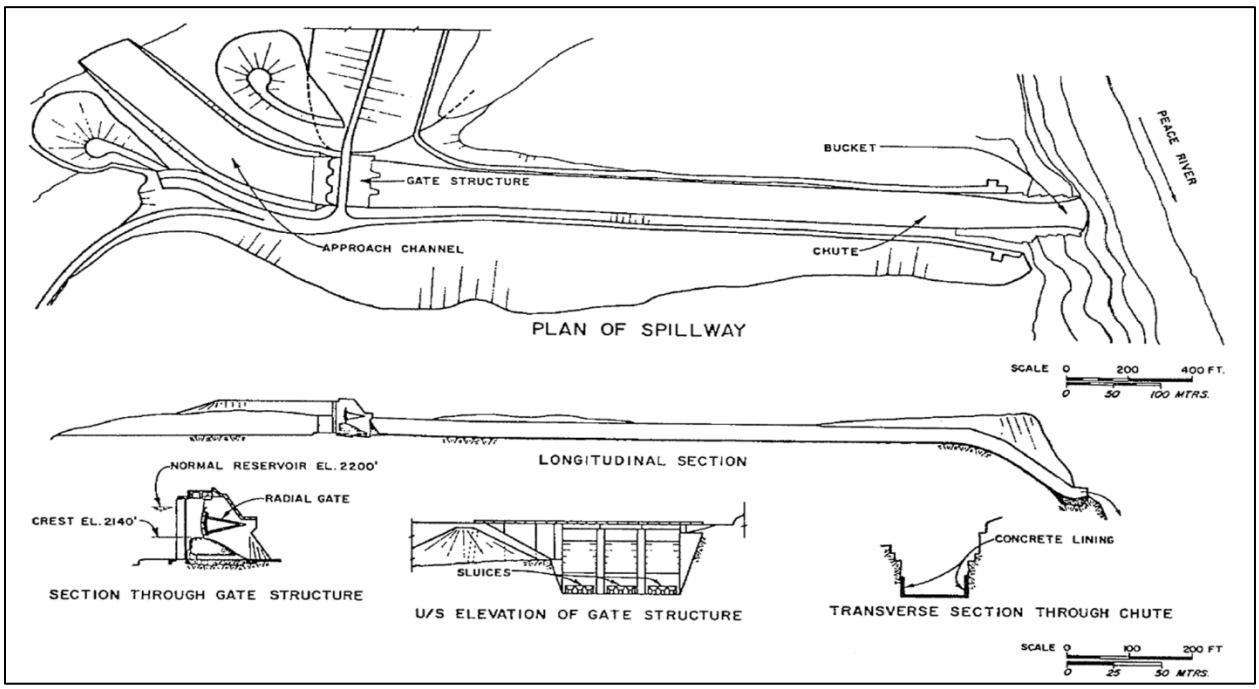

Figure 5.10 W.A.C. Bennett Spillway generalized plan and profile (BCH Report No. H2224, 1967)

Table 5.4 W.A.C. Bennett Dam Key Spillway Characteristics

General	
Type of Spillway	Long Chute Spillway
Total Spillway Width	205 ft across headworks
Overall Spillway Length[1]	2,400 ft
Headworks	
Radial Gates	
Number of Bays	3
Pier Width	15 ft
Ogee Crest Elevation	El. 2,145 ft
Gates	3 Radial Gates
Gates Dimension	50 ft wide x 61 ft high
Sluices	
Number of Sluices	9
Pier Width	8 ft
Sill Elevation	El. 2,105 ft
Gates	9 Vertical Lift Gates
Gate Dimensions	6 ft wide x 8 ft. high
Terminal Structure	
Energy Dissipation	Asymmetrical Flip Bucket
Bucket Radius	Variable
Bucket Invert Elevation	El. 1,876 ft
Bucket Lip Angle	30°
Bucket Lip Elevation	El. 1,890 ft
Bucket Width	135 ft (lip length)
Hydraulics	
Normal Conditions	
Maximum Normal Reservoir Level	El. 2,205 ft
Tailwater level with Ten Units Rated Discharge[1]	El. 1,655 ft
Flood Conditions	
Inflow Design Flood[2]	273,053 cfs
Maximum Flood Level[2]	El. 2,208.8ft
Maximum Tailwater Level[3]	El. 1,664 ft

Notes: (Monfette, 2004); [1] Estimate from Monfette, 2004; [2] from BCH Report No. E835, 2012; [3] estimate from BCH Drawing of spillway profile (BCH Drawing No. 1006-C14-U812, 1006-C21-U16/U32);

CHAPTER 6

METHODOLOGY

The methodology employed here is focused on calculating the deepest extent and location of plunge pool scour from spillway geometry and flow data, with an emphasis on accounting for changes in the erosive resistance of the rock material within the plunge pool. To achieve this, the data outlined in Table 6.1 were required for each of the four dams investigated.

Table 6.1 Required data for plunge pool scour analysis.

Hydrology Parameters	Geology Parameters	Spillway Geometry Parameters	Plunge Pool Geometry
• Spillway discharge hydrograph • Reservoir elevation • Tailwater elevation • Spillway gate rating curves	• Plunge pool geologic maps • UCS strength values • RQD values • No. of joint sets • Joint properties; wall roughness, separation • Joint set orientations	• Spillway crest height • Spillway profile • Spillway width • Gate height	• Initial river bed geometry • Plunge pool surveys over time

A numerical model was developed to approximate the location of jet impact with the plunge pool and the energy dissipation that occurs with depth as the jet moves through the water. The general methodology for this analysis consisted of six parts:

- Numerical model creation,
- Generation of hydraulic model inputs,
- Plunge pool cross section selection,
- Creation of the cross section geomechanical models,
- Numerical modeling of the plunge pool,
- Conduction of sensitivity analyses, and
- Comparison of modeled and existing cross sections

6.1 Numerical Modeling Approach and Model Creation

The numerical model developed for this analysis, named *EIM_ProfileCalc*, is based on the jet hydraulic theory and Erodibility Index Method outlined in Section 4. Input parameters into the model include general spillway characteristics:

- Full dam name and abbreviation

- Spillway terminal structure type,
- Elevation of flip bucket lip,
- Angle of flip bucket lip,
- Radius of flip bucket lip,
- Spillway face slope angle,
- Length of modeled spillway

Rock erodibility information:

- Length of modeled plunge pool profile,
- Minimum elevation of modeled plunge pool profile, and
- 1 ft x 1 ft array of erodibility index *K* values for modeled plunge pool profile

And hydraulic information for each day of record:

- Date of record
- Jet velocity at issuance,
- Jet diameter at issuance,
- Froude number at issuance,
- EGL elevation at issuance,
- Manning's roughness at issuance, and
- Tailwater elevation.

EIM_ProfileCalc reads in the spillway and rock erodibility information for the dam site and the daily hydraulic information and immediately generates an output file that records important jet hydraulic parameters for each day of record.

Spillway information is entered directly into the program and does not change over the course of model operation. The extent and minimum elevation of the modeled profile, however, must be larger than the anticipated location of the plunge pool invert. If scour exceeds the lateral or vertical extent of the modeled profile, the profile dimensions must be modified in the program for successful operation.

Erodibility index information is entered as a comma delimited '.csv' grid. Row one of the table contains the distance downstream from the flip bucket lip or terminal structure. Column one contains the range of elevation from the flip bucket to the minimum modeled elevation. All other cells contain the

erodibility index *K* values representative of the rock material at that location. Figure 6.1 shows an example of an abbreviated input erodibility index Array.

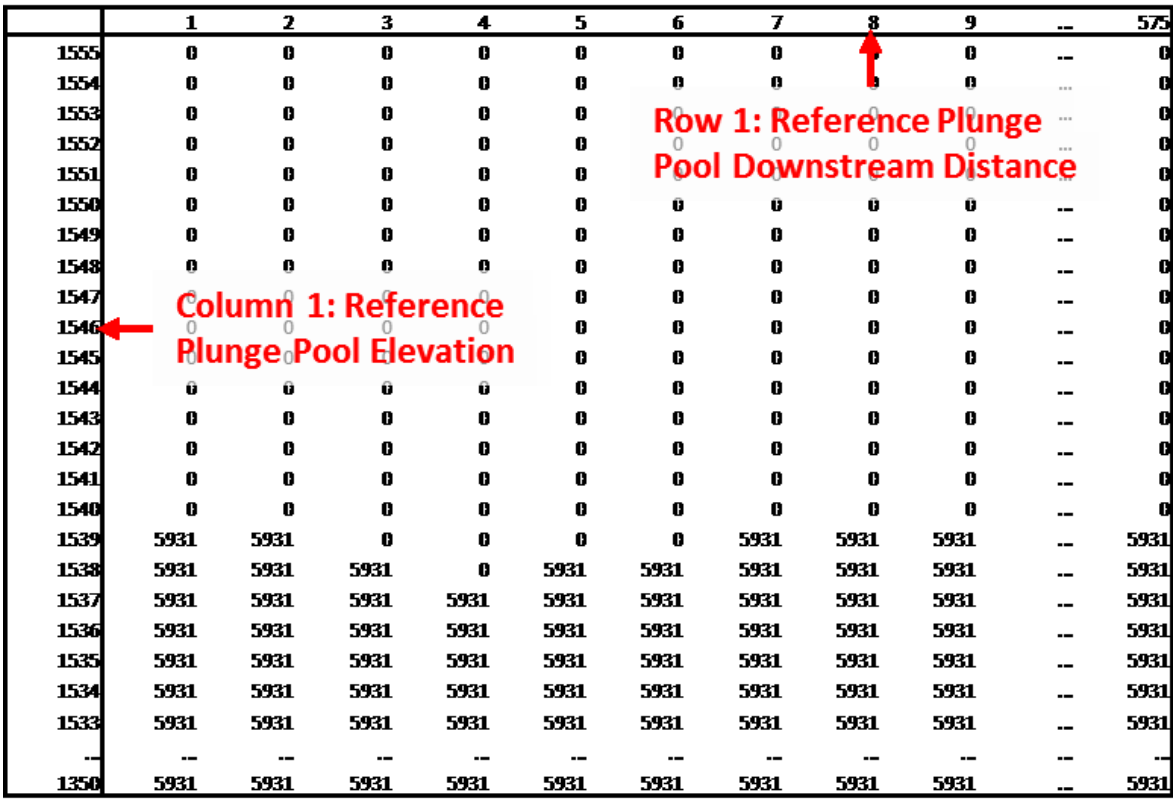

	1	2	3	4	5	6	7	8	9	...	575
1555	0	0	0	0	0	0	0	0	0	...	0
1554	0	0	0	0	0	0	0	0	0	...	0
1553	0	0	0	0	0	0	0	0	0	...	0
1552	0	0	0	0	0	0	0	0	0	...	0
1551	0	0	0	0	0	0	0	0	0	...	0
1550	0	0	0	0	0	0	0	0	0	...	0
1549	0	0	0	0	0	0	0	0	0	...	0
1548	0	0	0	0	0	0	0	0	0	...	0
1547	0	0	0	0	0	0	0	0	0	...	0
1546	0	0	0	0	0	0	0	0	0	...	0
1545	0	0	0	0	0	0	0	0	0	...	0
1544	0	0	0	0	0	0	0	0	0	...	0
1543	0	0	0	0	0	0	0	0	0	...	0
1542	0	0	0	0	0	0	0	0	0	...	0
1541	0	0	0	0	0	0	0	0	0	...	0
1540	0	0	0	0	0	0	0	0	0	...	0
1539	5931	5931	0	0	0	0	5931	5931	5931	...	5931
1538	5931	5931	5931	0	5931	5931	5931	5931	5931	...	5931
1537	5931	5931	5931	5931	5931	5931	5931	5931	5931	...	5931
1536	5931	5931	5931	5931	5931	5931	5931	5931	5931	...	5931
1535	5931	5931	5931	5931	5931	5931	5931	5931	5931	...	5931
1534	5931	5931	5931	5931	5931	5931	5931	5931	5931	...	5931
1533	5931	5931	5931	5931	5931	5931	5931	5931	5931	...	5931
...	...	...	...	...	...	...	...	...	...	...	...
1350	5931	5931	5931	5931	5931	5931	5931	5931	5931	...	5931

Figure 6.1 Input erodibility index array example format

Daily hydraulic information may consist of a continuous series or discrete points; the model does not require a continuous data series. Points *must*, however, be in chronological order if a series of points is used. The input daily hydraulic information file, also in '.csv' format, consists of six columns. Row one of the file contains the data type. Each subsequent row contains the values for each recorded data point, as shown in Figure 6.2. The 'Date' value must be formatted with dashes only and flow depth, velocity, EGL, and tailwater elevation must be in English units.

The model uses the velocity and flow depth at jet issuance, taken at the flip bucket or ski-jump lip, and calculates the jet trajectory, point of impingement with the tailwater, turbulence intensity and break up length and diameter of the jet at impingement, as outlined in the equations in Section 4.1.1. The stream power of the jet at plunge pool impingement is calculated based on the total discharge from the spillway gates upstream of the profile, the jet footprint, and the elevation difference between the EGL and tailwater elevations.

Date	Flow Depth (ft)	Velocity (ft/s)	Energy Grade Line Elev. (ft)	Froude Number	Manning's Roughness	Tailwater Elev. (ft)
IN_DATE	IN_DI	IN_VI	IN_EGL	IN_FR	IN_N	IN_TW
1979-11-7	1.88	55.2	1637.53	21.16	0.0157	1526
1979-11-8	3.53	70.65	1670.96	19.74	0.0161	1526
1979-11-9	3.45	70.25	1669.99	19.85	0.0161	1526
1979-11-10	3.53	70.65	1670.98	19.74	0.0161	1526
1979-11-11	3.36	69.78	1668.84	19.99	0.016	1526
1979-11-12	3.35	69.75	1668.77	20	0.016	1526
1979-11-13	3.37	69.84	1669	19.97	0.016	1526
1979-11-14	3.27	69.31	1667.73	20.12	0.016	1526
1979-11-15	3.18	68.78	1666.47	20.26	0.016	1526
1979-11-16	3.2	68.88	1666.71	20.23	0.016	1526
1979-11-17	3.33	69.63	1668.5	20.03	0.016	1526
1979-11-18	3.16	68.65	1666.14	20.29	0.016	1526
1979-11-19	3.2	68.92	1666.8	20.22	0.016	1526
1979-11-20	3.23	69.06	1667.12	20.18	0.016	1526
1979-11-21	3.18	68.79	1666.49	20.25	0.016	1526
1979-11-22	2.86	66.69	1661.59	20.7	0.0159	1526
1979-11-23	2.66	65.1	1657.97	20.97	0.0159	1526
2013-7-7	1.96	8.41	1586.65	3.16	0.0158	1521

Figure 6.2 Input hydraulic information table example format

Once the jet becomes submerged in the plunge pool the energy dissipation with depth and distance from the jet centerline is calculated based on the hydraulic formulae outlined in Section 4.1.2. The average and fluctuating dynamic pressure coefficients are calculated at one foot intervals, measured vertically downward from the tailwater surface and populate a one-dimensional array with the same number of elements as the height of the plunge pool profile. The average and fluctuating radial dynamic pressure coefficients are also calculated at one foot intervals and populate a two-dimensional array with the same dimensions as the input erodibility index array. The four coefficient values and the jet stream power at impingement are then combined using Equation 4.21 to calculate the stream power for each one foot by one foot cell to develop a stream power array for the profile area.

The stream power and erodibility index values for each square foot are then combined using Wibowo et al.'s (2005) regression analysis, Equation 4.25, to assess the probability of material removal at each array cell. Probability values range from 0.0 to 1.0, with 0.0 representing a 0% likelihood of rock removal and 1.0 represented a 100% likelihood of rock removal. Array cells with values greater than or equal to 0.50 are assumed to be removed by the power of the jet.

The original erodibility index input profile, which contains the erodibility index value for each cell is then modified such that cells with a probability of removal greater than 50% are 'removed'. These EI values are replaced with a value of 0.0 to signify their removal.

This process was repeated for each date of discharge over the spillway. The modified input EI profile that reflects areas where rock material has been removed becomes the EI array for the next daily discharge, resulting in cumulative plunge pool scour over time.

The procedure can be repeated for any desired time frame and produces output profile matrices and figures for all modeled dates. The comparison between the calculated profile and existing profiles can then be conducted to assess accuracy of the calculated scour depth. The program code itself, with annotations, is attached in Appendix B.

6.2 Hydraulic Model Input

The hydraulic input for the model were derived from gate discharge and height opening values at each spillway crest using the US Bureau of Reclamation's PROFILE Water Surface Profile Program for Prismatic Channels Version 1.10 (not dated). PROFILE is based on calculations and programming from the Bureau of Reclamation's Engineering Monograph No. 42 (Falvey, 1990). The software uses the Standard Step Method to compute the subcritical or supercritical water surface profile for a user-defined channel shape and slope. The program is capable of accounting for air entrainment, which produces more realistic velocity and flow depth values at the downstream end of the spillway, and provides Manning's Roughness values at the spillway flip bucket lip that can be used to calculate the flow turbulence intensity. Input discharge values for PROILE and reservoir and tailwater levels were generally determined using different methods based on data availability for the various dam sites due to changes in data collection, record keeping methods, and spillway geometry. An initial Manning's roughness of 0.012, representative of finished concrete, was applied to all four sites.

Flow characteristics calculated by PROFILE are based on simplified spillway profiles for each dam site and are described in more detail below.

Peace Canyon Dam

Individual spillway bay discharge data were available for major discharge events from April 1980 through the present. Statistics on the pre-April 1980 spills were also available from Monfette (2004) including the number of days of operation for each spillway bay, maximum daily average values for each bay, and the maximum sustained discharge for each bay for one week and one month time periods.

To simplify the analysis, the PROFILE models developed for the two Peace Canyon cross sections were based on the spillway section half-width; flow was modeled through one spillway bay, assuming no lateral flow expansion downstream of the spillway piers when training walls are not present at the spillway section boundaries. Input discharge values are the average discharge through Bays 3 and 4 and through Bays 5 and 6 for each day of record and the associated gate height for that discharge value based on the Peace Canyon Dam spillway discharge rating curve.

Seven Mile Dam

Individual spillway bay discharge data were available for major discharge events through 2002. From 2003 to present, spillway bay discharge data was back calculated using reservoir elevation, recorded gate height opening, and the Seven Mile Dam spillway rating curves.

The PROFILE model for Seven Mile spillway was based on the spillway half-width of the section housing Bays 1 and 2. Input discharge values are the average discharge through gates one and two for each day of record. The input gate height is that associated with the average flow and the daily average reservoir level, based on the Seven Mile spillway rating curve.

Revelstoke Project

Spillway discharge data, differentiated between the upper radial gates and the low level outlet gates was available from 1984 through 2013. No data was available for 1983, when the spillway became operational and began passing flows. Discharge through the two outlet types was assumed to be evenly distributed between both radial gates or through both low level outlets, depending on the outlet type used. Flow was not observed to occur simultaneously through upper and lower outlet types. The gate or outlet heights were those associated with the average discharge and reservoir level.

Two PROFILE models were developed for Revelstoke spillway due to the complex spillway geometry and the presence of the low level outlet gates along the center of the spillway. The models are based on the spillway half-width and exhibit lateral flow expansion downstream of the radial gate training walls, as shown in Figure 6.3.

For the case of discharge through the low level outlets (Figure 6.3, Top), flow proceeds downstream to the end of the training walls that separate the overflow and low level outlets. Flow is then assumed to expand outward from the edge of the training wall until it reaches the outer walls of the spillway chute. The expansion angle has been calculated based on relationships between the upstream channel width, flow depth, and Froude Number for abrupt flow expansion (Rouse, 1950). Rouse (1950)

presents surface contours of flow downstream of a sudden expansion for Froude Numbers 1, 2, 4, and 8. Because flow through either type of spillway outlet is anticipated to be highly supercritical, the contours associated with the highest Froude Number (Fr=8) were used to estimate the expansion angle. For the case of discharge through the radial overflow bays expansion occurs from the training wall to the spillway centerline, where it continues downstream to the spillway terminal structure. The expansion angle is calculated in the same manner, where the upstream width used in the calculation is twice the distance between the spillway wall and the training wall. Output velocity and flow depth values are then applied to the entire spillway width.

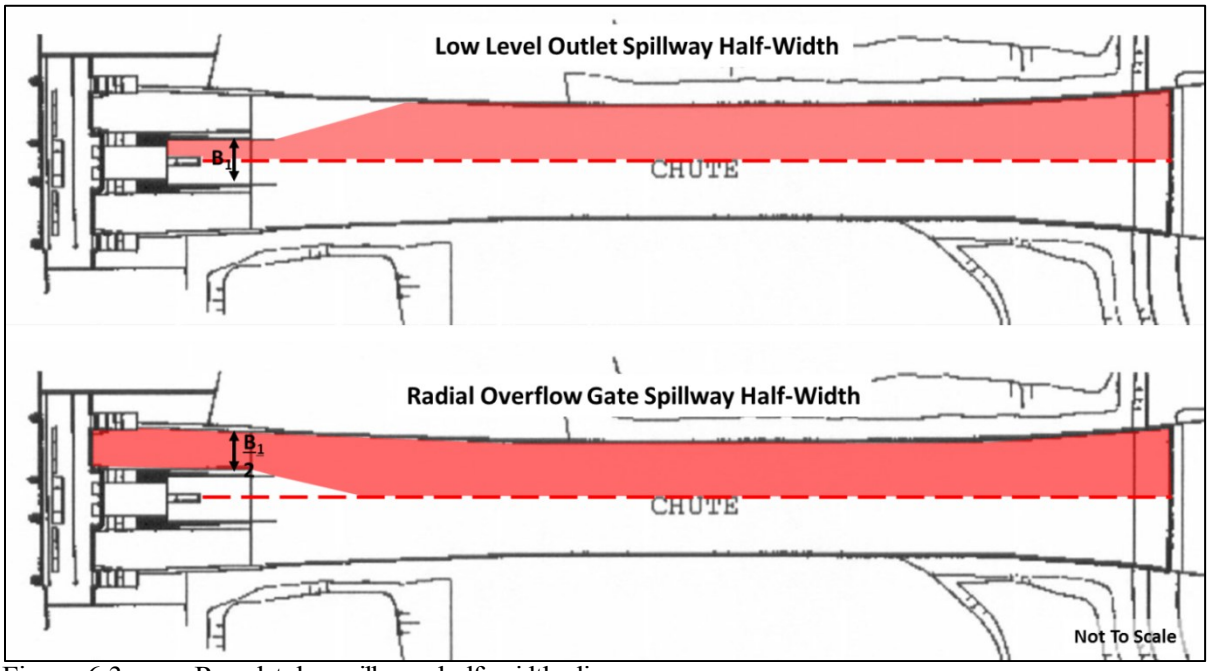

Figure 6.3 Revelstoke spillway half-width diagram

W.A.C. Bennett Dam

Daily discharge data through the W.A.C. Bennett spillway was provided by BC Hydro for the entire period of spillway operation. To simplify the calculations, the total discharge was assumed to be equally distributed between the three spillway bays to estimate gate height thickness during each spill event on record, even though spillway operational procedure require a center gate to outer gate opening ratio of 0.7:1.0.

The PROFILE model for W.A.C. Bennett spillway models the total spillway width and length. The input discharge for this model is the total discharge through the spillway. The input gate height is that for one gate passing one third of the total spillway discharge. The discharge is assumed to pass through

one 150 ft wide 'gate' that is the total width of all three spillway gates. The width of the profile downstream of the spillway piers will equal the entire spillway width.

6.3 Cross Section Selection

The locations of the cross sections were selected based on the hydraulic conditions at each spillway and the availability of geologic data to adequately characterize the plunge pool area. Cross sections were selected at the locations shown in Table 6.2 for each dam site. Section locations are also pictured in Figure 6.4.

Table 6.2 Dam cross section numbers and locations.

Dam Site	No. of Cross Sections	Location of Sections	Section Name
Seven Mile Dam	1	Along the centerline of Spillway Bays (SB) 1 & 2	SEV-12
Peace Canyon Dam	2	Along centerline of SB 3 & 4 Along centerline of SB 5 & 6	PCN-34 PCN-56
Revelstoke Dam	1	Aligned with plunge pool invert	REV-1
W.A.C. Bennett Dam	1	Aligned with plunge pool invert	WAC-C

Peace Canyon Dam was selected to host multiple cross sections. The two spillway sections downstream of Peace Canyon Dam experience different hydraulic flows, with Bays 3 and 4 generally passing larger amounts of each discharge event. In addition, the plunge pool downstream of spillway gates three and four is likely defined by the 'hinge zone' described in detail in Section 7.1.3. This important geologic feature is also located downstream of spillway gates five and six, but downstream of the primary area of jet impact. This second section downstream of Bay 5 and 6 served as an additional reference point for this investigation.

Each existing plunge pool survey was digitized using ArGIS Version 10.2 software and the topography along the profiles was plotted. Figures showing the topography and tables summarizing the location and elevation of the plunge pool inverts along the modeled profile lines for each of the four dam sites are provided in Section 7. Digitized surveys themselves are shown in Appendix C.

6.4 Geomechanical Model

Geomechanical models for each plunge pool cross section were created based on borehole and calyx hole data, foundation investigation and design reports, surficial mapping of the plunge pool and/or nearby foundation material, and regional geologic information.

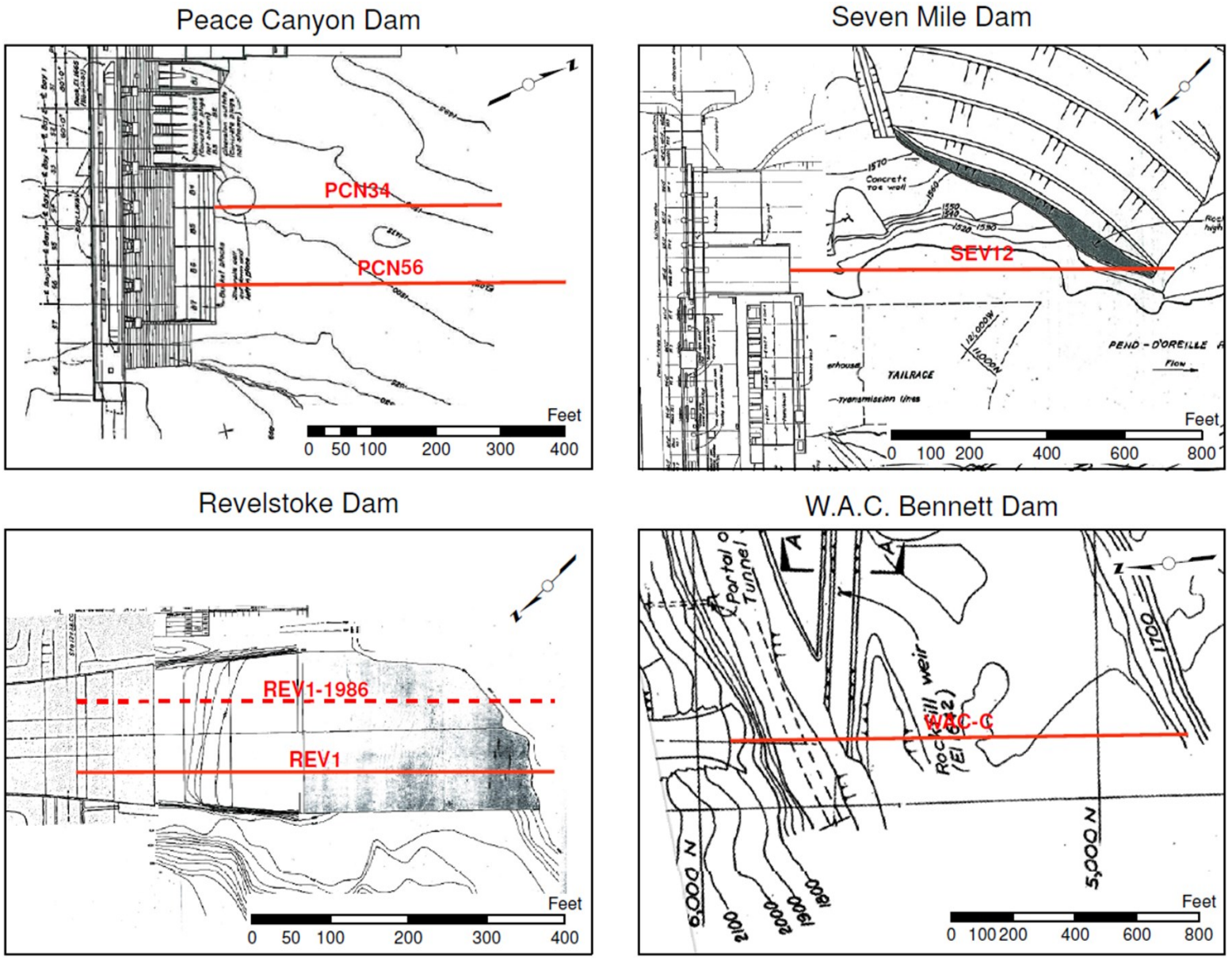

Figure 6.4 Modeled cross section locations. Note: REV-1-1986 shows the section through the plunge pool invert at that date.

Engineering geologic (EG) zones were developed for rock with similar engineering characteristics. Higher density geologic data naturally led to greater subdivision of materials into EG zones. The Seven Mile and Revelstoke plunge pools had limited information on the distribution of geologic materials, resulting in limited zonation of each plunge pool. Peace Canyon and W.A.C. Bennett plunge pools exhibited higher density of information on the spatial distribution of materials, thus more EG zones were used to describe the plunge pool along each cross section.

Once zones were identified, Annandale's Erodibility Index Method was used to assess the critical stream power threshold for each zone, based on Equation 4.21, for each model. Erodibility index values were assessed based on average rock parameters across an EG zone as well as the best and worst expected parameters for use in the sensitivity analysis. 'High' and 'Low' erodibility indices were based on parameter values one standard deviation away from the mean, when enough data was available to generate a distribution. For cases where limited data were available, the maximum and minimum data values were used to represent the 'High' and 'Low' EI values, respectively. To account for radial flow away from the jet at the rock-water interface, the Relative Ground Structure Number, J_s, was modified slightly. J_s values were calculated considering flow in the upstream as well as downstream direction and the minimum value was selected for use in the model.

The critical stream power values and initial plunge pool bathymetry were then used to create a one foot by one foot array along each plunge pool profile. The highest elevation of each array was defined as the location of the flip bucket lip. The lowest elevation extended below the deepest extent of surveyed scour. Profile length was dependent on the lateral extent of existing scour along each profile. A summary of the profile extents is provided in Table 6.3. Each array cell was then assigned an appropriate erodibility index value, based on the EG zone in which the cell was located. Areas within the profile above the existing bathymetry were assigned an erodibility index value of zero.

Table 6.3 Modeled Profile Extents

Dam Site	Profile	Minimum Elevation (ft)	Maximum Elevation (ft)	Length (ft)	Model EI Array Dimensions
Peace Canyon Dam	PCN-34	1400	1523	450	125 x 451
	PCN-56	1400	1523	550	125 x 551
Seven Mile Dam	SEV-12	1200	1555	575	357 x 576
Revelstoke Dam	REV-1	1150	1621	615	473 x 616
W.A.C. Bennett Dam	WAC-C	1350	1889	1,125	541 x 1126

Note: Model input array dimensions include the number of feet between the maximum and minimum elevations, the length, plus an additional reference row denoting feet downstream and an additional reference column denoting elevation.

6.5 Sensitivity Analysis

A sensitivity analysis to determine the range of scour hole depths that can be expected based on minimum and maximum erodibility index values has also been included in this assessment. 'Low' erodibility index values represent the worst case scenario, when the lowest of each EIM input parameter are combined to provide the highest estimate of scour and the greatest expected plunge pool depth. 'High' erodibility index values represent the best possible scenario, when the best of each EIM input parameter are combined to provide lowest estimate of scour and the least expected plunge pool depth.

6.6 Comparison of Numerically Generated Profile and Existing Profile

Once numerical modeling was completed, the modeled maximum plunge pool depths and locations were quantitatively and qualitatively compared with the values from existing plunge pool surveys. In some cases, the invert elevation has been shown to remain the same or increase over time, rather than decrease. This is likely due to infilling of the plunge pool with sediment and eroded material, which can migrate throughout the plunge pool and tailrace area. To account for this, surveyed invert elevations that reflected infilling were adjusted such that the deeper of the current survey or previous survey depth was used.

Differences between the profiles were assessed by calculating the coefficient of determination, or the R^2 value, for the maximum scour depth and location along the profile, using Equation 6.1. An R^2 value closer to 1.0 indicates a strong linear relationship between the two data sets. As the value decreases the relationship is considered less statistically significant. An R^2 line with a slope near one-to-one and a y-intercept near zero indicates that modeled erosion is not only proportional, but also to scale. The threshold R^2 value will be determined based on the number of modeled data points, using Equation 6.1, where s_x^2 is the variance of the surveyed plunge pool depths and s_y^2 is the variance of the modeled plunge pool depths.

$$R^2 = \frac{s_{yx}^2}{s_y^2} \tag{6.1}$$

It is important to consider the natural variation common in geologic environments, which results in overall lower R^2 values than other more uniform data sets.

An analysis of the residuals was also conducted to assess the distribution and location of areas of higher error. The standard error of estimate, s_{yx}, was calculated for each type of dam site as well as for the overall dataset using a modified form of the equation, based on the assumption that the 'predicted values', usually the result of calculating a line of best fit, are equal to the surveyed plunge pool depths using Equation 6.2 (Kachigan, 1991):

$$s_{yx} = \sqrt{\frac{\sum(y_i - x_i)^2}{n-2}} \quad (6.2)$$

Where y_i is the modeled plunge pool depth, x_i is the target, surveyed plunge pool depth, and n is the total number of data points. This variation of the standard error of estimate equation is based on the assumption that the modeled and surveyed plunge pool depth should be related in a one-to-one relationship; That is, $y = x$, rather than the conventional $y = mx + b$ linear relationship identified for general linear regression lines.

CHAPTER 7

ANALYSIS

Outlined in the subsequent sections is the data analysis for each of the four dams assessed in this study. The analysis includes the compilation of existing plunge pool surveys, plunge pool invert data, discharge, reservoir, and tailwater data, geomechanical model creation, and the generation of sensitivity analysis values. Output from the model is shown and explained in Sections 8 and 9 of this paper.

7.1 Peace Canyon Dam

Rock scour at Peace Canyon Dam was assessed from October 1979 through June 2007, the date of the most recent plunge pool survey.

7.1.1 Plunge Pool Topography

Existing plunge pool surveys were used to assess the development of scour over time for each facility. The number of surveys and density of survey points varied between dam sites and over time for the same dam site. Nine plunge pool surveys were available for Peace Canyon Dam, from October 1979 through June 2007. In two cases for PCN-34 and three cases for PCN-56, no discharge occurred between plunge pool surveys. When multiple surveys occur between discharge events, the more recent survey was used. As a result, the surveys from April 1983 and July 1987 were not used for PCN-34 and the surveys from April 1983, October 1985, and July 1987 were not used for PCN-56. Profiles of each survey used in the analysis for both PCN-34 and PCN-56 were constructed to assess the location and elevation of the plunge pool invert. Each survey was plotted with the initial 1979 survey and the Normal Tailwater Level (El. 1,518 ft) to provide a frame of reference and to show the degree of plunge pool development over time. Profiles for PCN-34 are provided in Figure 7.1 and Figure 7.2. Dashed lines along the profiles indicate areas of less certainty where interpretation was required to complete the profiles.

Profiles for PCN-56 are provided in Figure 7.3 (page 56) and Figure 7.4 (page 57). As shown, for both sections the majority of scour occurred during the initial spill events in late 1979 and early 1980. Scour along profile PCN56 proceeds much further downstream than expected for a plunge pool that develops solely from an impinging jet. Based on the plunge pool topography from Appendix C, it is likely that the majority of downstream erosion has occurred as a result of both scour along planes of weakness as well as from the erosion of the hinge zone (Section 7.1.3) by jet action from spillway bays three and four. As a result, plunge pool invert depths and locations used for PCN-56 in this analysis have been taken from the upstream portion of the plunge pool that is the result of scour from the impinging jets

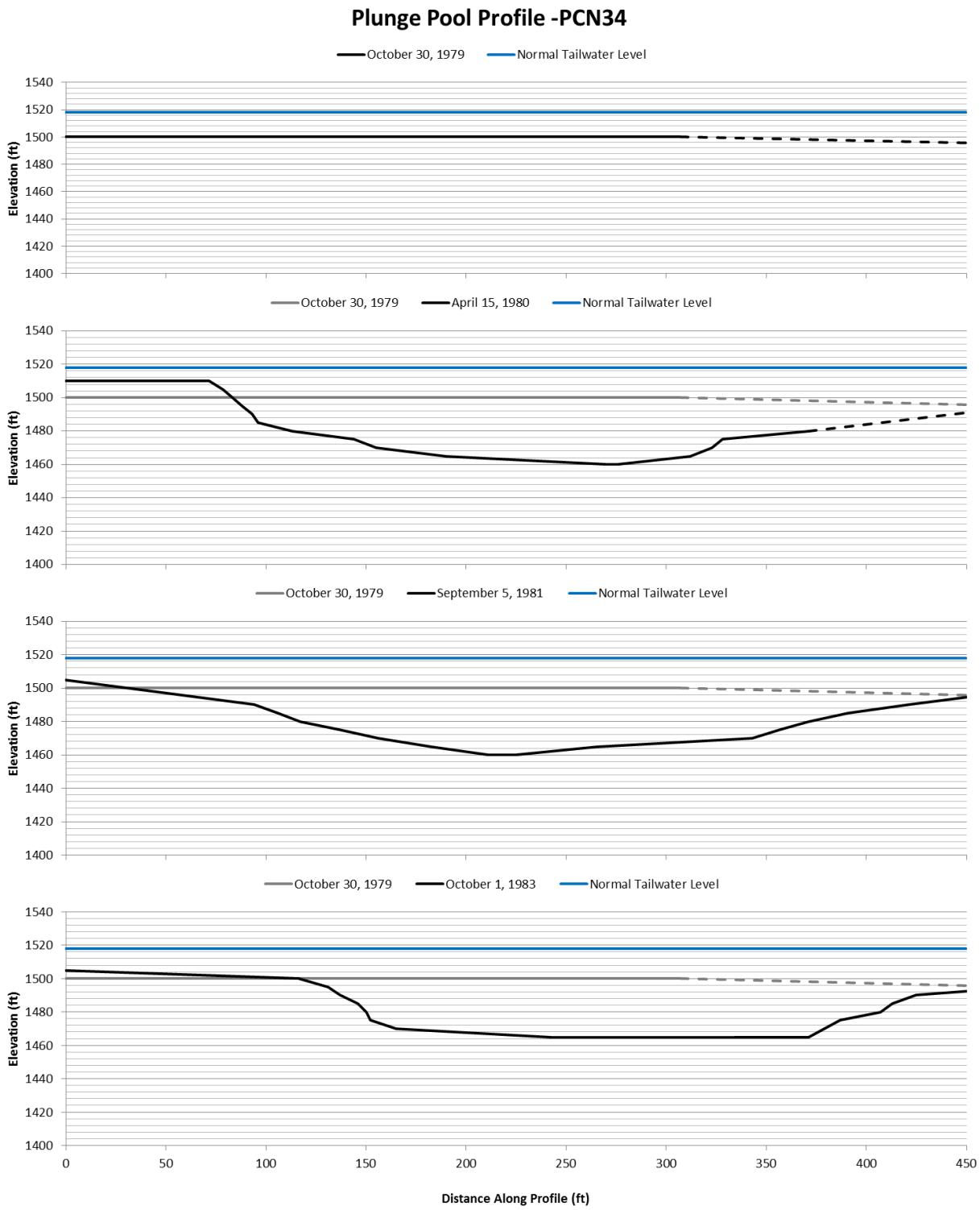

Figure 7.1 PCN-34 plunge pool survey profiles, 1979 through 1983

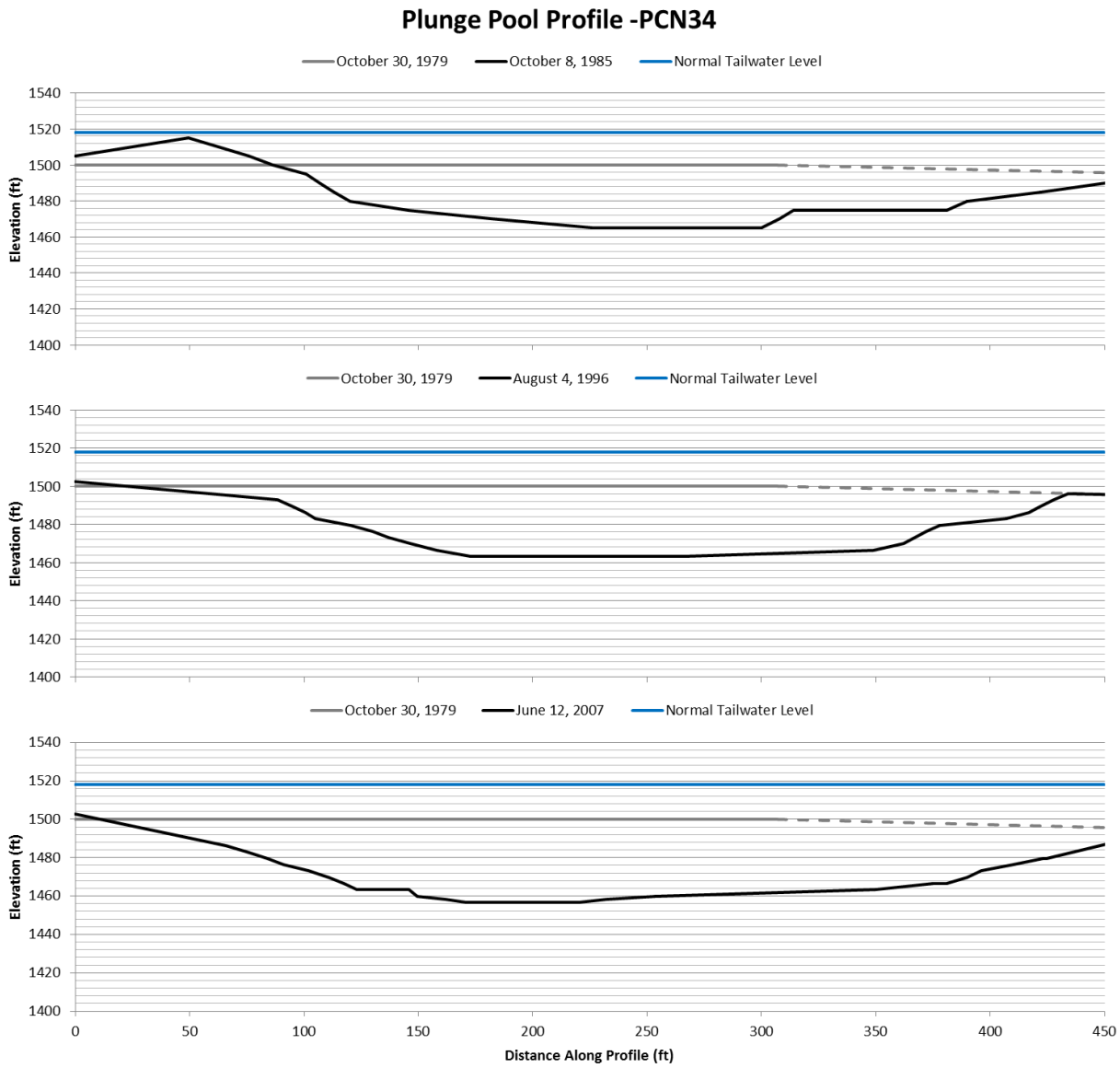

Figure 7.2 PCN-34 plunge pool profiles, 1985 through 2007

originating from Bays 5 and 6. Erosion more than 300 ft downstream of the spillway is assumed not to be the result of these impinging jets alone, but has been created by flow emanating from PCN-34. Table 7.1 (page 57) shows the date of each survey, the elevation of the plunge pool invert along section, the location of the invert, and the length of the invert for PCN-34 and PCN-56. The values reported in Table 7.1 serve as the basis of comparison for the model. Full surveys of the Peace Canyon plunge pool can be found in Appendix C.

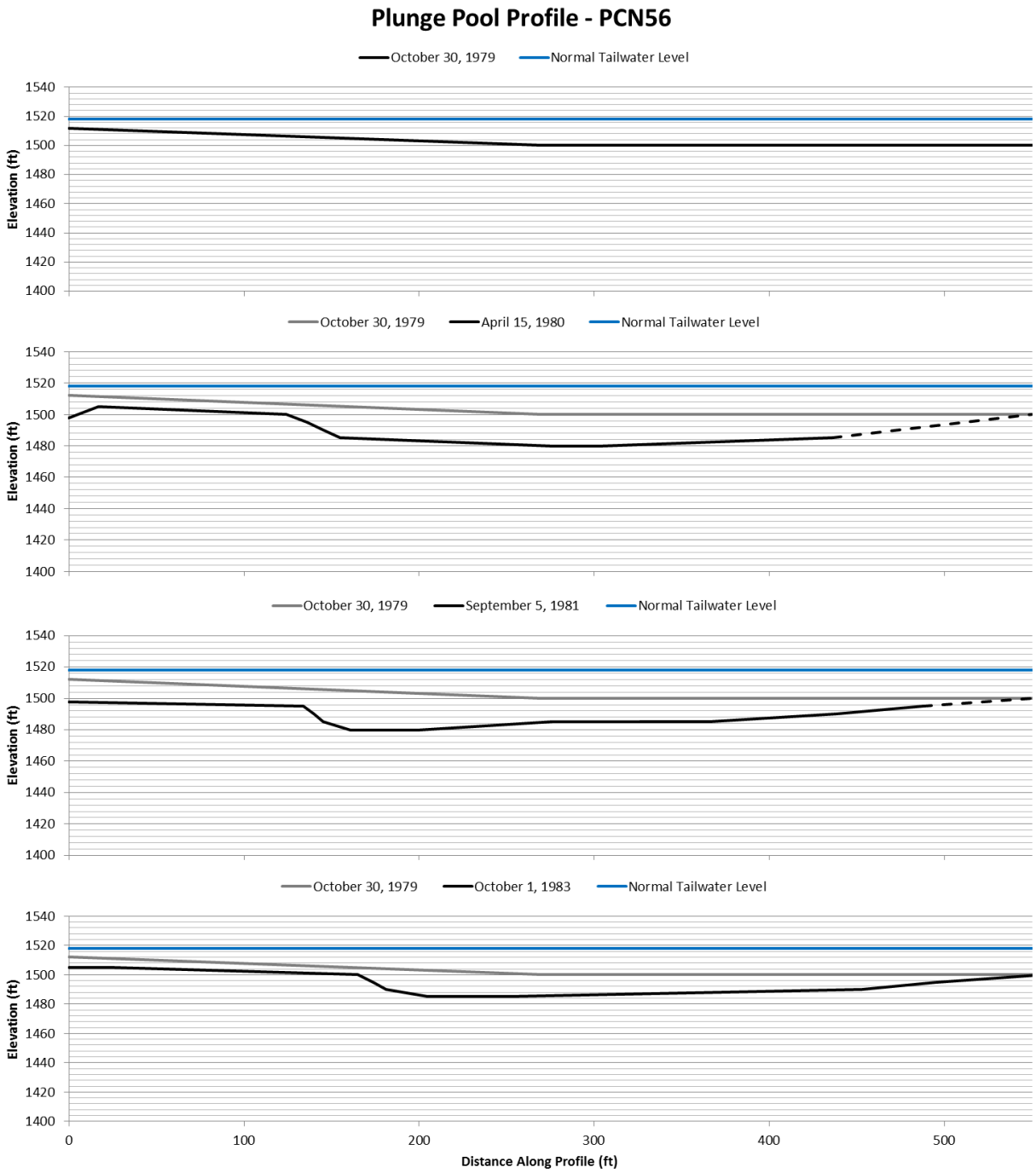

Figure 7.3 PCN-56 plunge pool survey profiles, 1979 through 1983

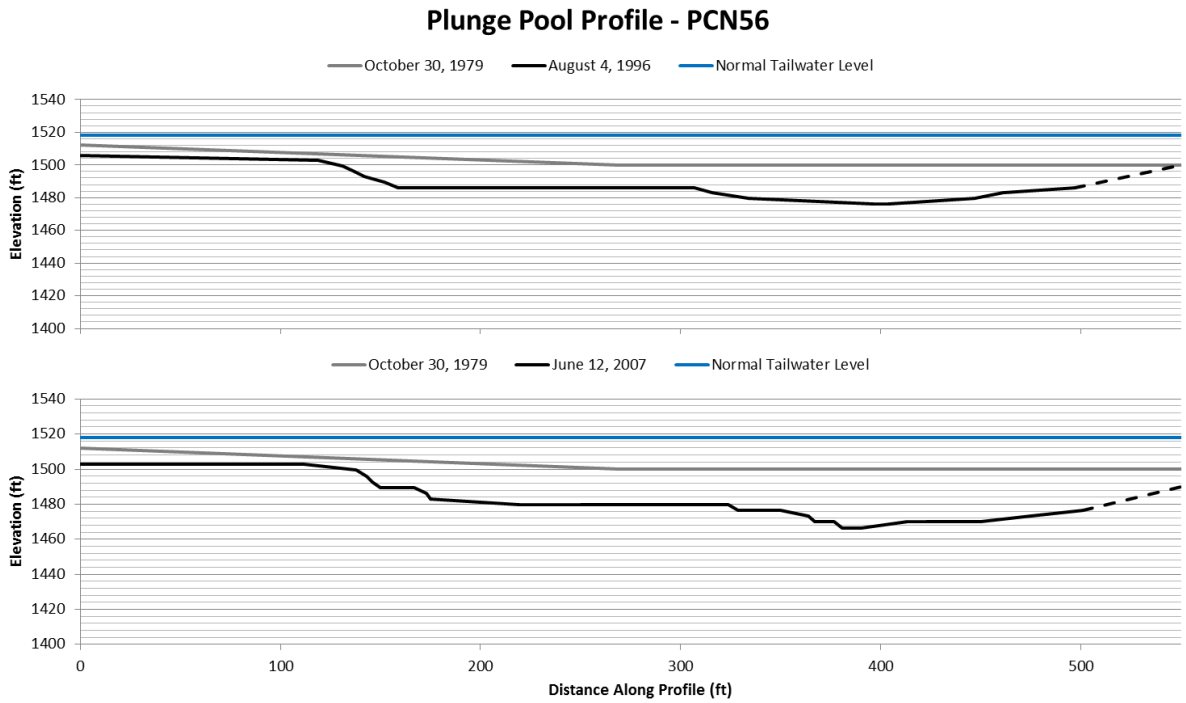

Figure 7.4 PCN-56 plunge pool survey profiles, 1996 through 2007

Profiles for both PCN-34 and PCN-56 show the development of broad, flat bottomed plunge pools over time. The plunge pool is noticeably deeper downstream of spillway bays three and four, although both exhibit the same characteristic shape.

Table 7.1 Peace Canyon Dam summary of plunge pool survey invert location and elevation for profile PCN-34 and PCN-56

Survey Date	PCN-34			PCN-56[5]		
	Invert Center[1] (ft)	Invert Length[2] (ft)	Elevation (ft)	Invert Center[1] (ft)	Invert Length (ft)	Elevation (ft)
October 30, 1979[3]	-	-	1500	-	-	1505
April 15, 1980	273	6	1460	229	145	1483
September 5, 1981	218	14	1460	180	38	1480
October 1, 1983	353	37	1465	229	47	1485
October 8, 1985[4]	263	74	1465	-	-	-
August 4, 1996	220	93	1463	233	148	1486
June 12, 2007	196	49	1457	260	80	1480

Note: [1]Invert center location is the distance downstream of the spillway flip bucket lip; [2]Invert length is the distance from the upstream end to downstream end of the deepest portion of the plunge pool; [3]Topography of Oct. 30, 1979 survey did not display an invert; [4]No discharge was reported through spillway bays 5 and 6 for the period between the Oct. 1, 1983 and Oct. 8, 1985 surveys; [5] PCN-56 invert center, length, and elevation values taken from the upstream (<300 ft) portion of the plunge pool.

7.1.2 Hydraulic Model Input

The Peace Canyon Dam Spillway has been in operation since October 28th, 1979, but has only passed discharge on eight occasions, as shown in Figure 7.5 (page 60). Prior to commissioning of the powerhouse and generating units in April 1980, 100% of discharge from Dinosaur Reservoir was passed through the spillway gates. Limited records of this event exist in the form of the total spillway discharge hydrograph (Monfette, 2004), but no individual spillway gate opening or discharge records were available. After commissioning of the hydropower unit, spills occurred in 1980, 1981, 1983, 1996, 2002, and 2012. Statistical information on the duration and magnitude of flows is provided in Table 7.2. The Peace Canyon Dam spillway rating curves were used to calculate the gate height opening for each day of recorded discharge, based on the mean reservoir level.

As outlined in Section 6, daily discharge and gate height data were used with the USBR's PROFILE to generate jet issuance conditions at the spillway base. Table 7.3 provides summary statistics of the issuance velocity (V_i), flow depth (D_i), and turbulence intensity (T_u) for spillway bays three and four and spillway bays five and six of Peace Canyon Dam.

Table 7.2 Peace Canyon Dam major spill event statistics

Year	1979[1]	1980-Pre[1]	1980-Post	1981	1983	1984	1996	2002	2012
Period of Spill	10/28-12/31	1/1-4/1	4/11-5/1	7/23-8/6	7/1-7/20	10/9-10/16	6/23-8/18	7/7-7/30	5/8-7/28
Days of Discharge									
Spillway	65	90	10	12	15	6	55	22	25
Bay 3	62	76	2	12	15	6	55	22	25
Bay 4	64	78	5	7	15	6	54	22	20
Bay 5	52	48	7	0	12	0	40	3	1
Bay 6	54	51	3	2	12	0	41	3	1
Maximum Average Daily Discharge (cfs)									
Spillway	56,000	60,000	37,000	48,000	45,000	14,000	115,000	63,000	64,000
Bay 3	15,500	27,500	12,000	21,000	15,000	7,000	47,000	26,000	25,000
Bay 4	15,500	27,500	17,000	21,000	15,000	7,000	31,000	25,000	25,000
Bay 5	14,000	18,000	17,000	-	12,000	-	23,000	13,000	11,000
Bay 6	6,000	18,000	14,000	16,000	12,000	-	23,000	13,000	11,000

Note: [1]1979 and Jan-Apr 1980 spillway discharge events inferred from digitized total spillway discharge hydrograph (Monfette, 2004); No individual bay information available apart from provided statistics; From BCH Flocal database, 2014.

Table 7.3 Peace Canyon Dam Jet Issuance Summary Statistics

	Bays 3 & 4 (PCN-34)			Bays 5 & 6 (PCN-56)		
	V_i (ft/s)	D_i (ft)	T_u (%)	V_i (ft/s)	D_i (ft)	T_u (%)
Count	142	142	142	169	169	169
Minimum	47.91	1.32	3.2	36.38	1.10	3.4
Average	68.94	4.14	3.6	66.18	2.93	3.7
Maximum	79.01	8.08	4.0	74.88	5.14	4.1
St. Deviation	8.40	2.28	0.25	7.75	0.93	0.17

7.1.3 Geomechanical Models

The geomechanical characterization of the Peace Canyon Dam plunge pool area was based on data from 2,869 feet of logged core, foundation excavation mapping, strength testing programs, and design reports on Peace Canyon Dam. This facility had the highest density of geologic information of any of the dam sites assessed in this investigation.

Geology

The plunge pool geology at Peace Canyon Dam is largely dominated by the interbedded silty shale and shaley siltstone units of the Cretaceous Gates Formation. These units are mostly massive and exhibit little or no lamination, except in localized areas. Contacts between interbeds within the foundation shale member are gradational in nature. The bottom three to four feet of the foundation shale grades to siltstone, then becomes the resistant 30-foot thick sandstone layer at an elevation of approximately 1,415 to 1,420 ft. In general, the bedding of all layers strikes 60 to 80 degrees east of north and dips 2 degrees to the northwest, in the upstream direction (BCH Report No. 966). Stratigraphic columns of the units within the upper hundred feet of the plunge pool area are provided for PCN-34 and PCN-56 in Figure 7.6. Elevation values are taken at the downstream toe of the spillway along the respective profiles.

The shale and silty shale units of the Gates Formation have relatively low clay content in this area and are dominantly composed of rock flour cemented with silica and calcite. They are generally hard to medium hard and tend to ravel at the surface. The basal sandstone unit is characterized as competent, hard, and is composed of medium to coarse sand. This unit is sparsely fractured and massive in nature (BCH Report No. H1742). Limited drilling has been conducted into the basal sandstone.

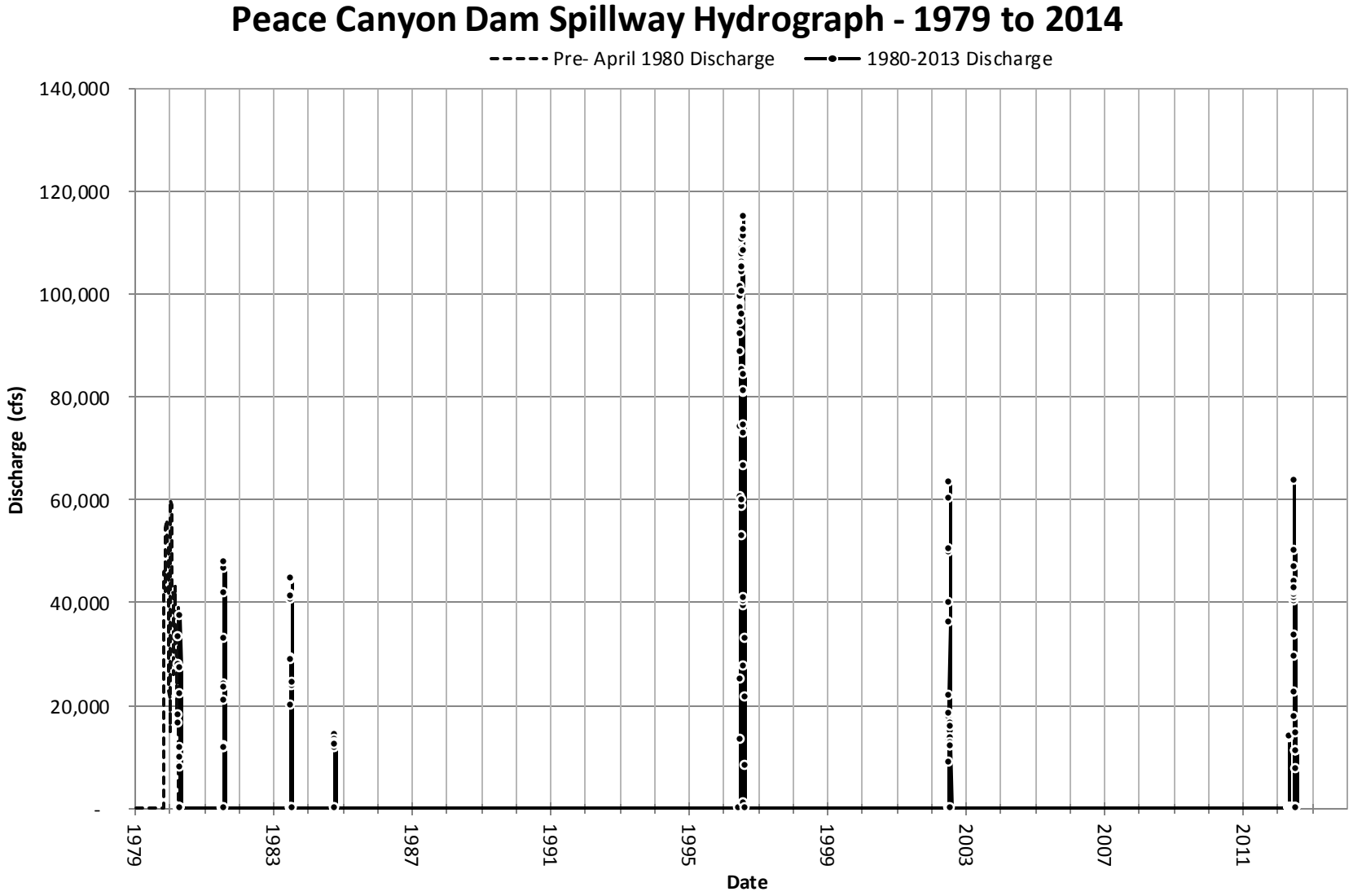

Figure 7.5 Peace Canyon Dam Spillway Hydrograph through 2013; points indicate daily average discharge values.

Unconfined Compressive Strength testing was conducted on multiple samples at Peace Canyon Dam based on testing programs by Ripley and Associates in 1961, Ripley, Klohn & Leonoff Ltd. in 1967, and International Power and Engineering Consultants Ltd. in 1970. Values from these programs, as well as design summaries of other investigations (BCH Report No. H1742), were used to calculate the typical, high and low expected UCS strength values for the various rock types present within the plunge pool. UCS strength values for each lithology were applied to all instances of that lithology within the stratigraphic column. UCS values from samples soaked for seven days were used when available, as these values were considered more representative of field conditions; where unavailable, UCS values from air dried samples were used.

Table 7.4 summarizes the UCS strength values for the various rock types in the stratigraphic column. The rock's hardness is not reduced by the more highly fractured nature of the rock within the hinge zone (BCH Report 822), therefore the UCS values in Table 7.4 are applied to both General and hinge zone areas within the plunge pool.

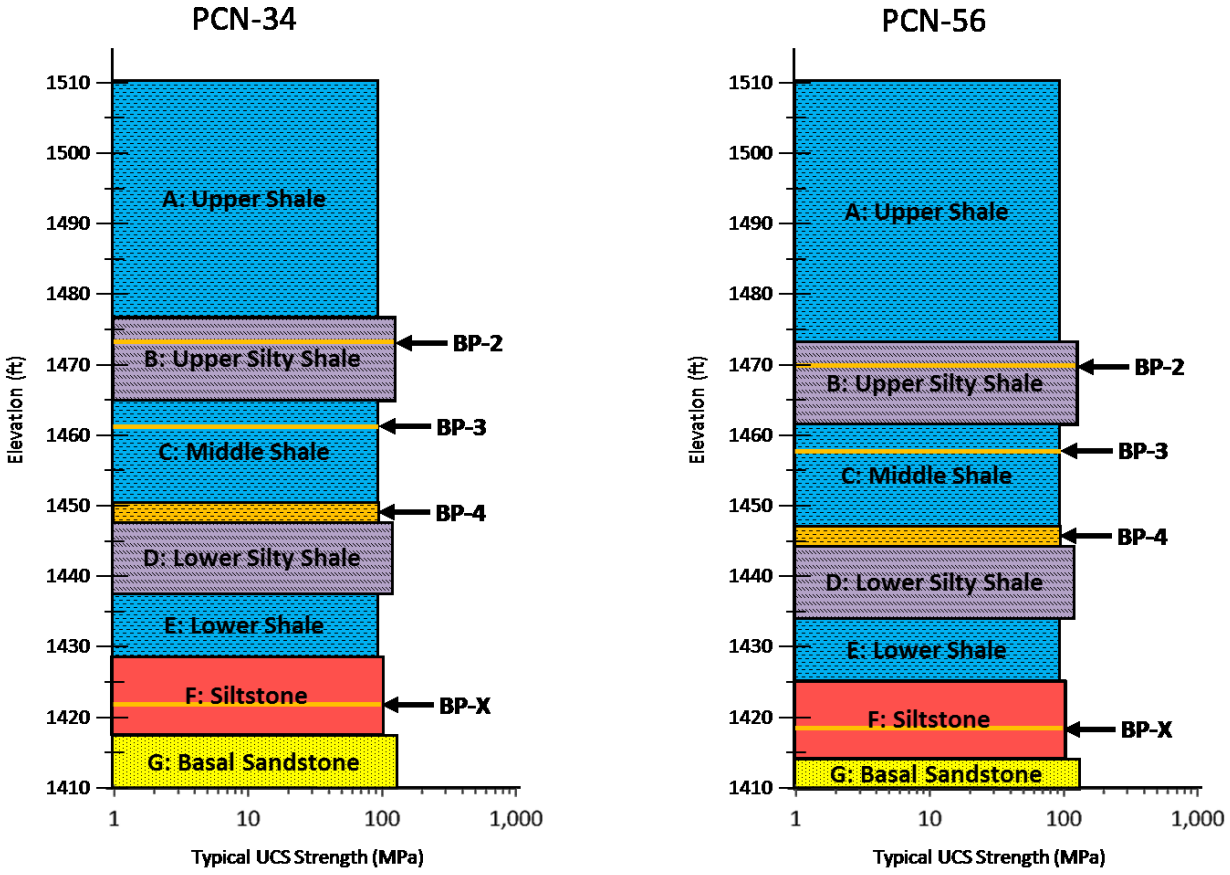

Figure 7.6 Peace Canyon Dam stratigraphic columns, showing approximate locations of notable bedding planes (elev. taken at spillway downstream toe along respective profiles)

Table 7.4 Peace Canyon Dam UCS rock strength (MPa) for lithologic units

Lithology	UCS Strength (MPa)		
	Low	Mean	High
Silty Shale/Shaley Silt	60	120	184
Shale	17	103	185
Siltstone	69	104	139
Sandstone	76	133	221

Note: Siltstone and sandstone strength values based on dry UCS tests; Silty Shale/Shaley Silt and Shale strength values based on soaked UCS tests.

Table 7.5 shows the RQD values for the various units, both within and outside of the hinge zone. The presence of the hinge zone does not cause a notable decrease in RQD, with the exception of the upper shale unit, which is nearer the surface and more prone to stress release fractures. Upper and lower RQD values represent the RQD values a distance of one standard deviation away from the mean RQD value. RQD values are also provided for BP-4.

Table 7.5 Peace Canyon Dam RQD values for stratigraphic units

Unit	RQD Value (%)					
	General			Hinge Zone		
	Lower	Mean	Upper	Lower	Mean	Upper
Upper Shale	56	80	100	50	76	100
Upper Silty Shale[1]	56	80	100	50	76	100
Middle Shale	56	80	100	50	76	100
BP-4	44	73	100	58	72	86
Lower Silty Shale	72	90	100	78	91	100
Lower Shale	73	90	100	73	89	100
Siltstone	65	87	100	65	85	100
Basal Sandstone	71	88	100	75	90	100

Note: Values from BCH Hydro Doc. No. 15472-03 & No. 15472-09; 1977/1978 borehole series CH, CHQ, STH, TS, & PS; [1]Upper Silty Shale RQD values assumed equal to Upper Shale RQD values.

Relaxation joints coincident with bedding planes are present in the upper 30 to 50 feet of the Upper Shale and Silty Shale units below the river bed. These joints are more prominent in the center of the river bed and tend to become less noticeable near the abutments (BCH Report No. 822). Five major relaxation joints along bedding planes were noted during exploration. These planes tended to show noticeable separation, with silt or sand infilling up to two inches. The approximate elevations and descriptions of these major planes are provided in Bedding planes BP3 and BP4 were noted in the majority of logs from the CH, CHQ, STH, PS, and TS borehole series from 1977 and 1978 spillway grouting exploration programs (BCH Doc. No. 15472-03 & No. 15472-09). Only bedding plane BP4 was large enough to be considered in this model. Other bedding planes consisted of distinct planes, rather than a zone of weaker, more fractured material. The joint spacing for bedding planes and relaxation joints open

sub-parallel to bedding planes was determined from the borehole logs for materials both within and outside of the more highly fractured hinge zone (discussed further in this section) and are provided in Table 7.7 (page 64). 'Low' values represent lower quality areas with higher fracture density and 'High' values represent the higher quality areas, with lower fracture density.

Bedding planes BP 3 and BP 4 were noted in the majority of the logs from the CH, CHQ, STH, PS and TS borehole series from 1977 and 1978 spillway grouting exploration programs (BCH Doc. No. 15472-03 & No. 15472-09). Only bedding plane BP 4 was large enough to be considered in this model. Other bedding planes consisted of distinct planes, rather than a zone of weaker, more fractured material. The joint spacing for bedding planes and relaxation joints open sub-parallel to bedding planes was determined from the borehole logs for materials both within and outside of the more highly fractured hinge zone (discussed further in this section) and are provided in Table 7.7. 'Low' values represent lower quality areas with higher fracture density and 'High' values represent the higher quality areas, with lower fracture density.

Table 7.6 Prominent bedding planes within the Peace Canyon plunge pool area and associated depths.

Plane	Approx. Elevation (ft)	Description
BP 2	1,476	Most prominent bedding plane; up to two inches of soft, decomposed shale infilling
BP 3	1,465	Occurs immediately above a 2- to 3-inch thick ripple-marked sandstone bed which is continuous throughout the intake and spillway areas; varies from a tight contact to a half-inch infilled or fractured separation; dominantly planar, with ripple-marks adding secondary roughness
BP 4	1,453	Zone of discontinuous bedding separations occurring about 11.5 feet below BP 3. The zone averages about 3 feet in thickness in the spillway area, with up to four distinct bedding planes present within the zone. Individual cracks commonly terminate abruptly, split or curve upward and end in overlying shale. Bedding separations are not continuous and frequently step vertically from one level to another within the zone
BP X	1,425	Hairline fracture located about 5 feet above the contact with the basal sandstone

Modified from BCH Report No. 966

Prominent subvertical jointing also occurs throughout the upper shale and silty shale units. The primary set, J1, strikes 30 to 40 degrees north of east and has a spacing of roughly 10 ft to 30 ft down to the elevation of the BP-2 plane, based on mapped portions of the spillway foundation (BCH Report No. 966 Appendix A). Joints are usually tight and not persistent, terminating into bedding plane fractures (BCH Report No. 9/85). This joint set is present and more closely spaced around BP 3 and in roughly the upper half of the Middle Shale between BP 3 and BP 4, with a spacing of 5 ft to 15 ft. Very few joints are

found below this level, as reflected in the borehole logs as well as RQD values. This set occurs sporadically within the basal sandstone unit, with larger variations in orientation. All joints found in this unit are tight and few extend for significant lengths (BCH Report No. 822). Most high angle joints logged are planar and slightly rough in nature (BCH Doc. No. 15472-09).

A secondary subvertical joint set, J2, is also present in the area, striking 60 to 70 degrees west of north. Few fractures of this set were mapped within the spillway foundation. They appear to occur sporadically in individual shale beds and at depth within the basal sandstone. J2 joints terminate very near where they initiate, either into other fractures or into bedding planes with depth (BCH Report No. 966).

Table 7.7 Peace Canyon Dam bedding/relaxation joint spacing by stratigraphic unit

Unit	Bedding/Relaxation Joint Spacing (ft)					
	General			Hinge Zone		
	Low	Mean	High	Low	Mean	High
Upper Shale[1]	1.0	5.8	14.8	1.2	3.0	6.9
Upper Silty Shale[1]	1.0	5.8	14.8	1.2	3.0	6.9
Middle Shale	1.0	5.8	14.8	1.2	3.0	6.9
Lower Silty Shale	3.1	7.9	11.3	2.6	6.0	11.9
Lower Shale	1.7	7.0	11.5	1.1	7.9	12.6
Siltstone	2.2	7.0	15.7	1.2	4.9	10.8
Basal Sandstone	-	-	-	-	-	-

Note: [1]Upper Shale and Silty Shale values are assumed equal to Middle Shale values, as these units were not logged within the boreholes; [2]Few or no bedding/relaxation joints were logged within the basal sandstone unit, therefore no spacing is provided here.

A more highly fractured zone is present immediately downstream of spillway bays two, three and four, trending along the strike of J1 in the downstream direction. This "hinge zone" is composed of the same N30E to N40E trending subvertical joint set present throughout the plunge pool, but with much closer fracture spacing; tight, closed joints spaced from one to three feet and open joints – up to four inches – of the same orientation spaced five to 15 ft apart. Many individual fractures are traceable for 100 ft or more along strike (BCH Report No. 9/85). No shearing or offset of bedding has been observed in this area and the high fracture density is likely due to more regional rock flexure. The swarm of fractures is approximately 100 ft wide beneath the spillway foundation and likely extends downstream through the plunge pool. An eroded channel was also identified in this area beneath spillway bay one prior to dam construction. Both features trend downstream toward the plunge pool area, however there is no subsurface information to confirm their extent beyond the spillway foundation footprint. Figure 7.7 on page 66 shows the location of the hinge zone beneath the spillway foundation and select cross sections. The figure illustrates the relatively flat, laterally continuous nature of the bedrock and the approximate depths of the prominent bedding planes described in Table 7.6.

The mean Joint Roughness Value, Jr, was determined based on the most often occurring shape and roughness of all discontinuities logged for each unit. The 'High' and 'Low' values here represent the upper and lower bounds of shape and roughness, excluding outliers. These values are provided in Table 7.8.

Table 7.8 Peace Canyon Dam Joint Roughness Number for stratigraphic units

Unit	Joint Character and Roughness Number					
	General			Hinge Zone		
	Low	Mean	High	Low	Mean	High
Upper Shale	C/SM 1.5	PL/SR 1.5	IR/R 3.0	PL/SM 1.0	PL/SR 1.25	IR/R 3.0
Upper Silty Shale	C/SM 1.5	PL/SR 1.5	IR/R 3.0	PL/SM 1.0	PL/SR 1.25	IR/R 3.0
Middle Shale	C/SM 1.5	PL/SR 1.5	IR/R 3.0	PL/SM 1.0	PL/SR 1.25	IR/R 3.0
Lower Siltstone	PL/SR 1.25	PL/R 1.5	IR/R 3.0	PL/SR 1.25	PL/R 1.5	IR/R 3.0
Lower Shale	PL/SM 1.0	PL/R 1.5	PL/R 1.5	C/SR 1.25	PL/SR 1.25	PL/R 1.5
Siltstone	PL/SR 1.25	PL/R 1.5	IR/R 3.0	C/SR 1.25	PL/R 1.5	IR/VR 4.0
Basal Sandstone	PL/SM 1.0	PL/R 1.5	PL/VR 1.75	PL/SM 1.0	PL/SR 1.25	PL/R 1.5

Note: C-curved, PL-planar, IR-irregular, SM-smooth, SR-slightly rough, R-rough, VR-very rough

Erodibility Index and Critical Stream Power Values

Seven geomechanical zones were identified based on the similarity of material properties from Tables 7.6 through 7.8. The EI and critical stream power values are provided in Table 7.9 (page 67). The distribution of the geomechanical zones is shown in Figure 7.8 (page 69) and Figure 7.9 (page 69). 'Low' values for each zone represent the minimum 'Low' value expected, 'High' values represent the maximum 'High' value expected, and 'Mean' values represent the average value expected for the contributing stratigraphic units.

7.2 Seven Mile Dam

Plunge pool scour for Seven Mile Dam was assessed from October 1979 through December 2011, the date of the most recent available plunge pool survey.

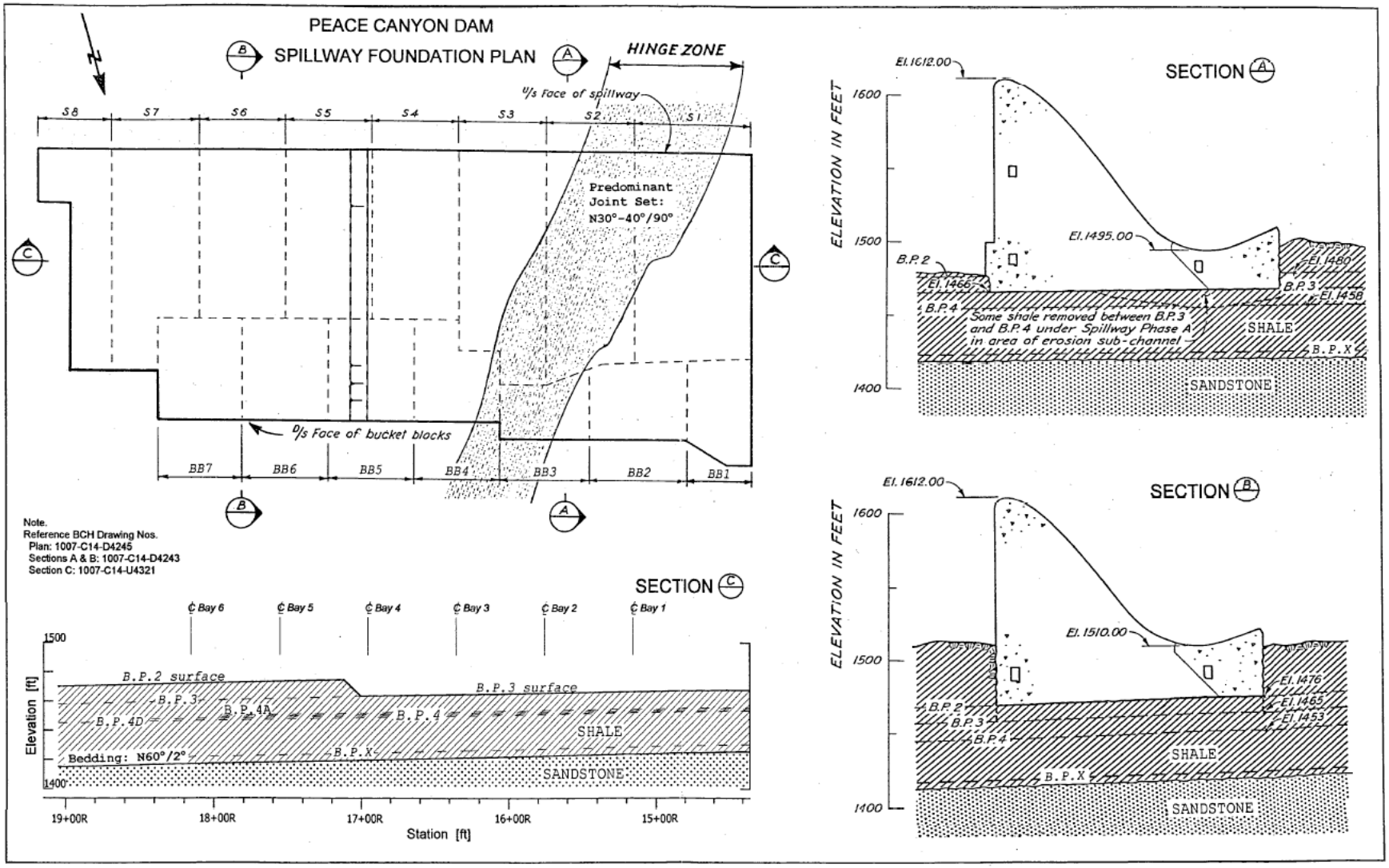

Figure 7.7 Peace Canyon Dam spillway foundation geology (BCH Drawing No. 1007-C14-D4245 (Plan), 1007-C14-D4243 (Sections A&B), 1007-C14-U4321 (Section C))

Table 7.9a Peace Canyon Dam erodibility index tables for geomechanical zones

Zone	**Zone A**			**Zone B**			**Zone C**			**Zone D**		
Contributing Stratigraphic Units	General Upper Shale General Upper Silty Shale General Middle Shale			General BP 4			General Lower Silty Shale General Lower Shale General Siltstone Hinge Zone Siltstone			General Basal Sandstone Hinge Zone Basal Sandstone		
Parameters	**Low**	**Mean**	**High**	**Low**	**Mean**	**High**	**Low**	**Mean**	**High**	**Low**	**Mean**	**High**
UCS (MPa)	17	109	186	17	103	186	17	108	186	76	133	221
RQD (%)	56	80	100	44	73	100	65	88	100	71	89	100
ρ (kg/m^3)	2579	2592	2619	2579	2579	2579	2579	2645	2691	2611	2611	2611
C_r	0.94	0.94	0.95	0.94	0.94	0.94	0.94	0.96	0.98	0.95	0.95	0.95
J_r	1.5	1.5	3.0	1.5	1.5	3.0	1.0	1.5	4.0	1.00	1.5	1.8
J_n	3.34	2.73	2.73	3.34	2.73	2.73	2.73	2.73	2.73	2.73	2.24	1.83
J_a	3.00	1.00	1.00	4.00	2.00	1.00	2.00	1.00	0.75	1.00	0.75	0.75
M_s	*16.3*	*102.5*	*176.5*	*16.3*	*96.7*	*173.8*	*16.3*	*103.7*	*181.4*	*71.9*	*126.3*	*209.3*
K_b	*16.8*	*29.3*	*36.6*	*13.2*	*26.7*	*36.6*	*23.8*	*32.2*	*36.6*	*26.0*	*39.7*	*54.6*
K_d	*0.5*	*1.5*	*3.0*	*0.4*	*0.8*	*3.0*	*0.5*	*1.5*	*5.3*	*1.0*	*2.0*	*2.3*
J_s	*0.61*	*0.76*	*0.78*	*0.61*	*0.68*	*0.71*	*0.62*	*0.71*	*0.78*	*0.78*	*0.78*	*0.78*
EI (*K*)	**83.4**	**3409**	**15130**	**49.1**	**1319**	**13562**	**120**	**3571**	**27637**	**1459**	**7826**	**20813**
P_c (kW/m^2)	**27.6**	**446**	**1364**	**18.6**	**219**	**1257**	**36.3**	**462**	**2143**	**236.0**	**832**	**1733**

Table 7.9b (continued) Peace Canyon Dam erodibility index tables for geomechanical zones

Zone	**Zone E**			**Zone F**			**Zone G**		
Contributing Stratigraphic Units	Hinge Zone Upper Shale Hinge Zone Upper Silty Shale Hinge Zone Middle Shale Hinge Zone BP 4			Hinge Zone Lower Silty Shale			Hinge Zone Lower Shale		
Parameters	**Low**	**Mean**	**High**	**Low**	**Mean**	**High**	**Low**	**Mean**	**High**
UCS (MPa)	17	107	186	60	120	184	17	103	186
RQD (%)	50	75	100	78	91	100	73	89	100
ρ (kg/m^3)	2579	2589	2619	2619	2619	2619	2579	2579	2579
C_r	0.94	0.94	0.95	0.95	0.95	0.95	0.94	0.94	0.94
J_r	1.0	1.3	3.0	1.3	1.5	3.0	1.3	1.3	1.5
J_n	3.34	2.73	2.73	3.34	2.73	2.73	3.34	2.73	2.73
J_a	8.00	4.00	2.00	3.00	2.00	0.75	3.00	2.00	0.75
M_s	*16.3*	*101.1*	*176.5*	*57.1*	*114.3*	*175.2*	*16.3*	*96.7*	*173.8*
K_b	*15.0*	*27.5*	*36.6*	*23.4*	*33.3*	*36.6*	*21.9*	*32.6*	*36.6*
K_d	*0.1*	*0.3*	*1.5*	*0.4*	*0.8*	*4.0*	*0.4*	*0.6*	*2.0*
J_s	*0.78*	*0.78*	*0.78*	*0.78*	*0.78*	*0.78*	*0.68*	*0.78*	*0.78*
EI (*K*)	**23.8**	**677**	**7565**	**433**	**2229**	**20021**	**101**	**1537**	**9933**
P_c (kW/m^2)	**10.8**	**133**	**811**	**95.0**	**324**	**1683**	**31.9**	**245**	**995**

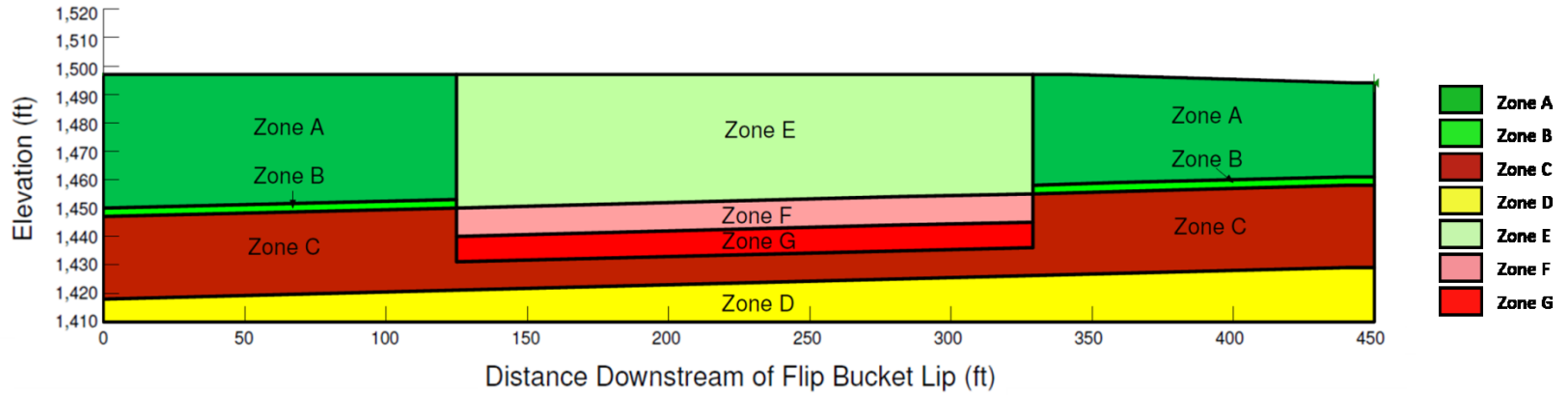

Figure 7.8 Peace Canyon Dam Profile PCN-34 geomechanical model

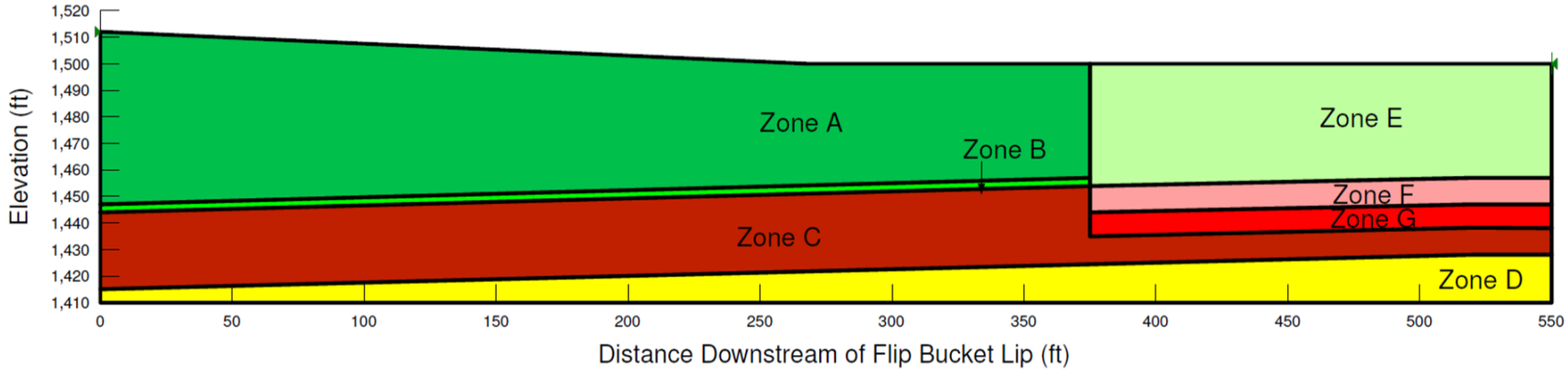

Figure 7.9 Peace Canyon Dam Profile PCN-56 geomechanical model (see Figure 7.8 for key)

7.2.1 Plunge Pool Topography

Eight surveys of the Seven Mile Dam plunge pool and tailrace area were conducted between October 1979 and December 2011. An additional survey conducted over the summer of 2014 was not available for this analysis. Surveys were generally taken following large discharge events, although the Seven Mile Dam spillway operates on an annual basis. Topographic profiles along SEV-12 are provided in Figure 7.10 (page 72) and Figure 7.11 (page 73). Dashed lines along the profiles indicate areas of less certainty where interpretation was required to complete the profiles. Table 7.10 also shows the invert location, length, and elevation for each survey, which are used as the basis for model comparison. Full plunge pool and tailrace surveys can be found in Appendix C.

Surveys indicate that significant scour occurred between the December 1979 and August 1982 surveys, during large discharges associated with spillway use prior to the commissioning of the generators. Plunge pool development at this location has proceeded more vertically downward than laterally downstream, likely due to geologic environment in which the plunge pool is located.

Table 7.10 Seven Mile Dam summary of plunge pool survey invert location and elevation for profile SEV-12

Survey Date	Invert Center[1] (ft)	Invert Length[2] (ft)	Elevation (ft)
October 30, 1979	250	1	1498
December 14, 1979	318	22	1475
August, 1982	389	1	1450
September 20, 1984	381	72	1460
October 15, 1986	398.5	29	1450
October 1, 1988	370	1	1447
November 18, 1997	391.5	57	1457
December 9, 2011	356	1	1449

Note: [1]Invert center location is the distance downstream of the spillway flip bucket lip; [2]Invert length is the distance from the upstream end to downstream end of the deepest portion of the plunge pool.

7.2.2 Hydraulic Model Input

The Seven Mile Dam Spillway has been in operation since November 1979 and operates on an annual basis, as shown in the historic spillway hydrograph in Figure 7.12 (page 74). Prior to 1984 records for spillway bays one and two were summed and spillway bays three and four were reported individually. For this reason, the individual bay discharge values for bays one and two for this time period are assumed to be equally divided between the two bays. Although daily gate height information was available for Seven Mile Dam spillway between 1984 and 2014, some gate height data was altered such that the individual spillway bay discharges deduced from these values summed to +/- 10% of the total discharge

reported passing through all bays on the day of record. Statistical data for the eight largest discharge events are provided in Table 7.11.

As outlined in Section 6, daily discharge and gate height data were used with the USBR's PROFILE to generate jet issuance conditions at the spillway base. Table 7.12 provides summary statistics of the velocity (V_i), flow depth (D_i), and turbulence intensity (T_u) for spillway bays one and two at Seven Mile Dam.

Table 7.11 Seven Mile Dam major spill event statistics

Year	**1981**	**1982**	**1983**	**1986**	**1996**	**1997**	**2011**	**2012**
Period of Spill	1/28-10/22	3/11-11/20	3/11-11/4	2/27-11/28	1/12-8/18	2/1-7/18	4/4-7/22	3/31-8/1
Days of Discharge								
Spillway	114	135	146	105	174	116	93	113
Bays 1&2	114	135	146	94/28	174/151	116/87	93/74	112/99
Bay 3	39	40	20	23	120	80	70	81
Bay 4	39	40	20	0	87	73	57	72
Maximum Average Daily Discharge (cfs)								
Spillway	76,000	100,000	82,000	77,000	97,000	112,000	91,000	95,000
Bays 1&2	49,000	69,000	49,000	60,000	33,000/31,000	36,000/37,500	37,000/30,000	31,500/28,000
Bay 3	18,000	16,500	16,500	18,000	30,500	31,000	28,000	31,500
Bay 4	18,000	16,500	16,500	0	17,000	11,000	11,500	31,500

Note: Values separated by a slash indicate the value for bay 1 followed by the value for bay 2, where data was available; From BCH Flocal database.

Table 7.12 Seven Mile Dam Jet Issuance Summary Statistics

	Bays 1 & 2 (SEV-12)		
	V_i (ft/s)	D_i (ft)	T_u (%)
Count	2,068	2,068	2,068
Minimum	4.37	1.20	3.2
Average	55.90	2.61	3.7
Maximum	82.80	7.57	4.1
St. Deviation	18.83	1.42	0.23

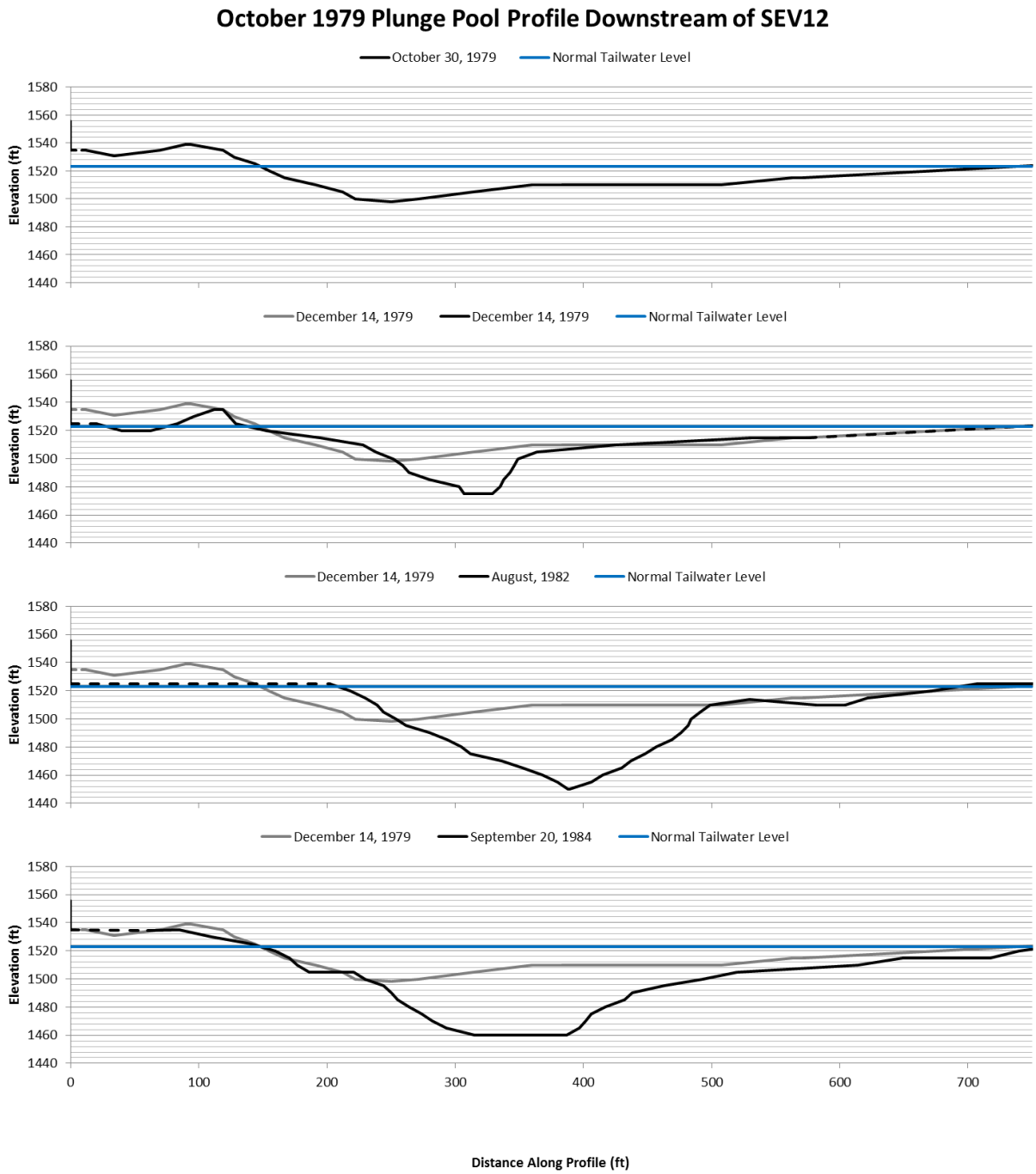

Figure 7.10 SEV-12 plunge pool survey profiles, 1979 through 1984

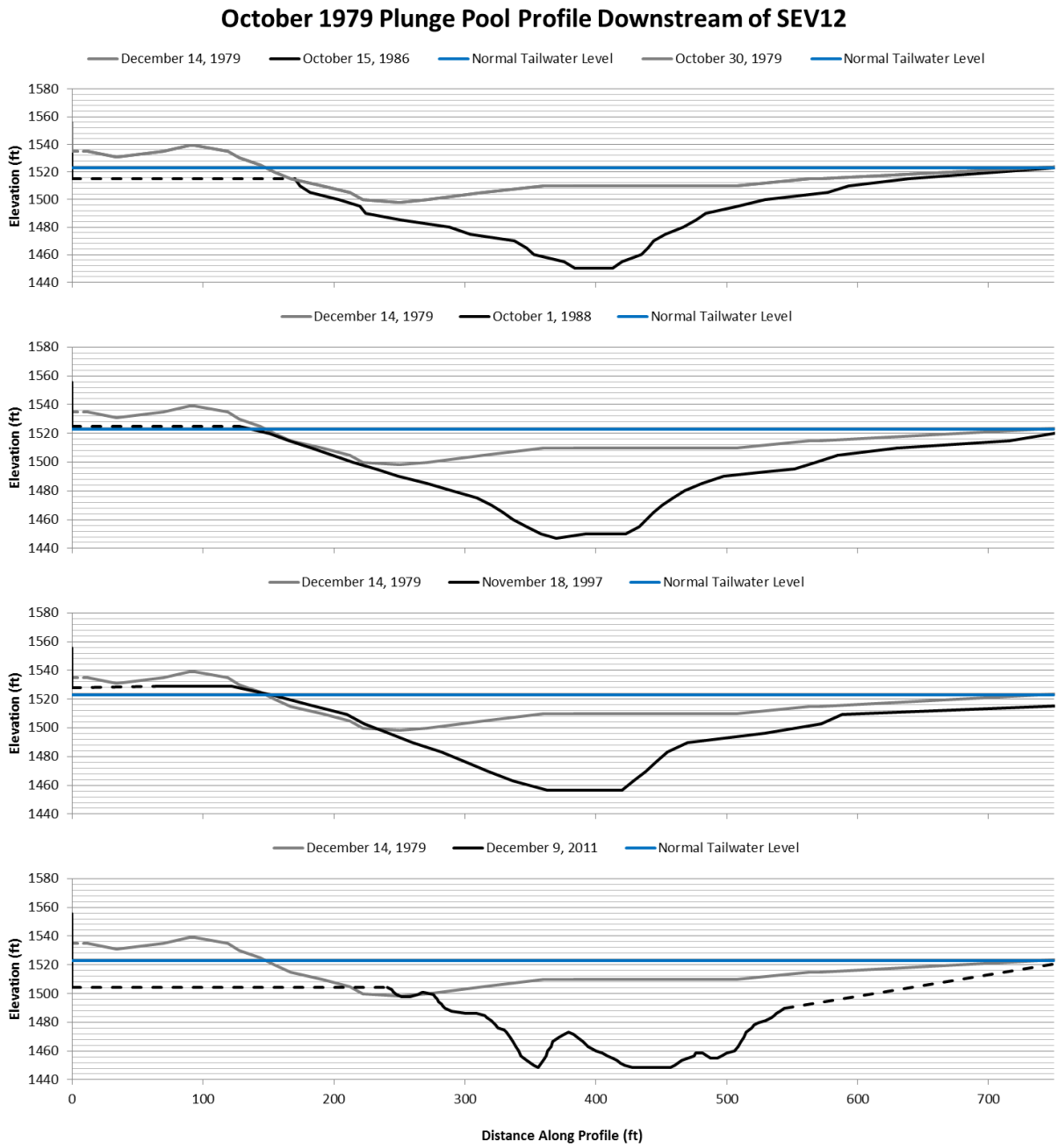

Figure 7.11 SEV-12 plunge pool survey profiles, 1986 through 2011

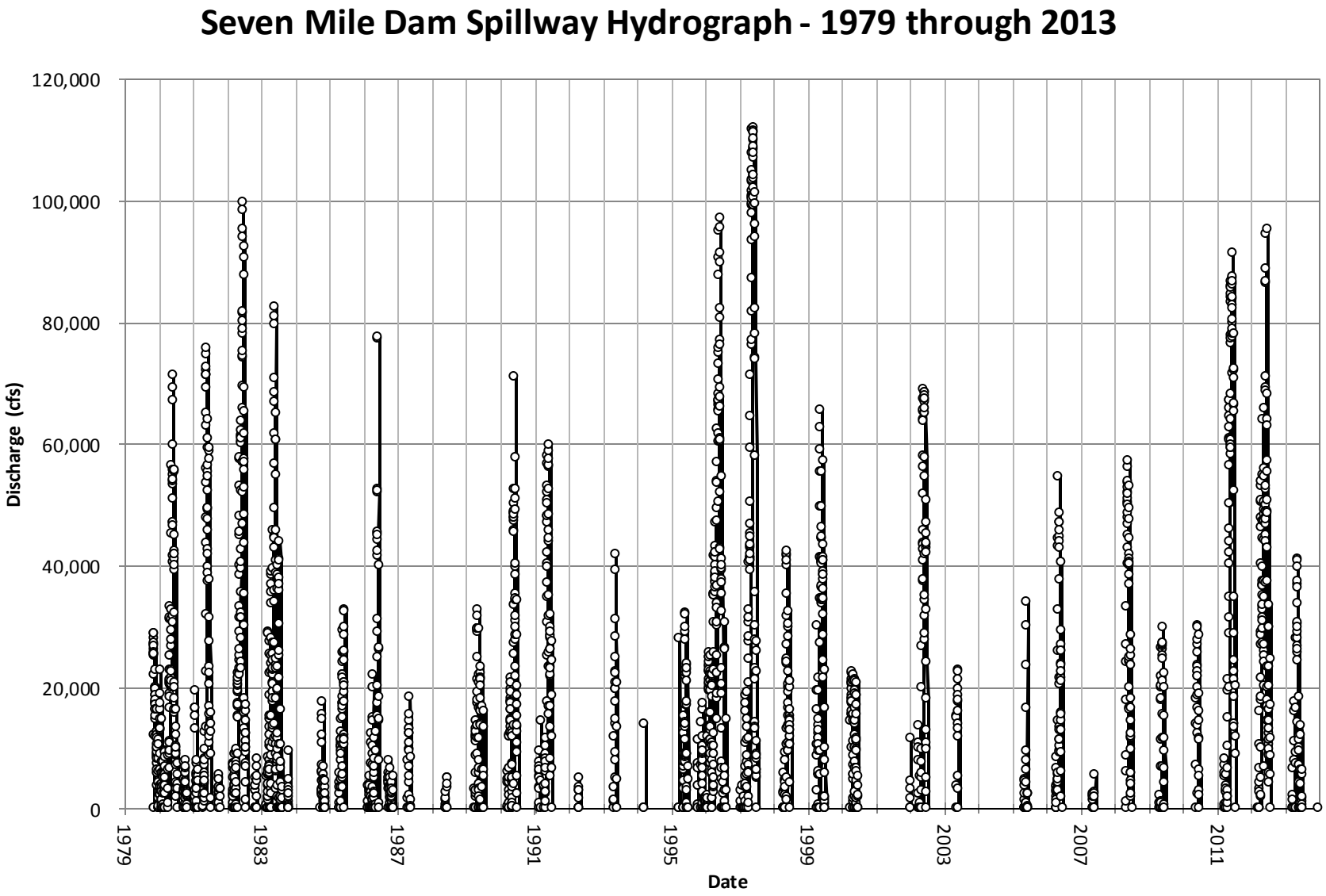

Figure 7.12 Seven Mile Dam Spillway Hydrograph through 2013; points indicate daily average discharge values.

7.2.3 Geomechanical Model

The geomechanical characterization of the Seven Mile Dam plunge pool area was largely based on data from the Seven Mile Project Design Report (BCH Report No. H1743, 1989) and the Dam Safety Improvements Working Dam Foundation Summary (BCH Report No. PSE401, 2002). A complete list of resources can be found in the References section of this report. This facility had very good rock quality information in the area beneath the spillway foundation and along the river-left bank near the plunge pool area. No mapping of the area immediately downstream of the spillway blocks was conducted, however, and the distribution of rock materials within the plunge pool is currently unknown.

Geology

Three rock types were identified in the plunge pool area for Seven Mile Dam: granite, massive argillite, and rehealed argillite. A fourth type, phyllitic argillite, is present on site but is located at higher elevations above the other units and not within the plunge pool area. Material properties for the three plunge pool rock types – including UCS strength, RQD, joint orientation, aperture, roughness, and infilling – were compiled in the Dam Safety Improvements Working Dam Foundation Summary (BCH Report No. PSE401, 2002), which serves as the basis for the analysis of profile SEV-12.

Geologic mapping of the spillway and plunge pool was only completed for portions above the normal tailwater level. Due to variability in topography and the location of the footprint of the dam foundation, the 1989 geologic map could not be reliably georeferenced with regard to the 1999-2000 geologic map. Figure 7.13 (page 78) and Figure 7.14 (page 79) show the plunge pool and adjacent portions of the 1989 and 1999-2000 geologic maps.

The dam and spillway are founded on a large southeasterly dipping sill of granite that has intruded into the older argillite of the area. This sill is approximately 500 ft thick and extends 50 ft to 100 ft downstream of the spillway flip buckets. The large sill is accompanied by smaller granitic intrusions that are present downstream of the dam within the existing stream bed, along the left abutment, and downstream of the existing plunge pool focus hole (BCH Report No. PSE362). The granite on site is composed of euhedral grains of orthoclase and plagioclase in a very fine grained quartz-feldspar matrix. Joints within this unit are generally randomly oriented. Some fractures have been healed with calcite and quartz infilling (BCH Report No. PSE362). Fracture spacing ranges from several inches near the granite-argillite contact to tens of feet within the massive granite (BCH Report No. PSE401).

The argillite within the plunge pool area is fine grained and grey-black to black in color. Hardness varies, depending on whether the unit is present in its rehealed, phyllitic, or massive form. Mapping and core logging conducted during the 1999-2000 Auxiliary Spillway Investigation indicate the spatial distribution of the different argillite forms is complex and variable (BCH Report No. PSE401).

Rehealed argillite (rA) is moderately hard, graphitic, and has a chaotic fabric. This unit is slightly foliated in zones and contains multiple shear zones healed with calcite and/or quartz infilling of one to two millimeters. Jointing is primarily along the foliation but random joints are also present (BCH Report No. PSE362).

Massive argillite (A) is present to a limited extent on the left abutment, within and downstream of the plunge pool focusing hole. This unit is composed of rehealed argillite fragments that range in size from a few millimeters to a few centimeters. Massive argillite is very hard and lacks foliation. This unit also includes healed shear features and calcite/quartz healed fractures that are one to two millimeters wide. Random joints are present throughout this unit (BCH Report No. PSE362).

Due to the complex spatial variability and lack of plunge pool mapping, profile SEV-12 is assumed to consist of massive argillite and granite (BCH Report No. PSE362). While it is likely that other rock types are present within the plunge pool, the orientation of plunge pool development – which is roughly along strike of the foliation and granite-argillite contact – supports the hypothesis that these units make up a large portion of the plunge pool profile. The range of UCS strength values for the plunge pool materials are provided in Table 7.13.

Table 7.13 Seven Mile Dam UCS rock strength (MPa) for rock type

Rock Type	UCS Strength (Mpa)		
	Low	Mean	High
Left Bank/Spillway Granite[1]	100	163	252
Phyllitic Argillite	90	135	175
Rehealed Argillite	40	40	50
Massive Argillite[1]	60	122	252

Note: [1]Granite and massive argillite values calculated from the river-left bank and spillway portion of the dam foundation, based on ; From Thurber and AMEC testing programs (BCH Report No. PSE401, 2002)

Left bank/spillway granite and massive argillite RQD values were calculated from nine borehole logs from 1973-2000 located within the spillway foundation footprint and the left bank. 'High' and 'Low' values are represented by the mean plus or minus the standard deviation for each unit. Phyllitic and rehealed argillite RQD values are representative values, as determined by BCH Report No. PSE401. RQD values are notable larger for the left bank/spillway granite, and fairly uniform between the phyllitic and

massive argillite, as shown in Table 7.14. Rehealed argillite represents a much more highly fractured and less competent material.

Table 7.14 Seven Mile Dam RQD values for rock types

Unit	RQD (%)		
	Low	Mean	High
Left Bank/Spillway Granite	64	87	100
Phyllitic Argillite	25	57	80
Rehealed Argillite	10	30	60
Massive Argillite	25	60	75

Note: Granite and Massive Argillite RQD values calculated from 9 boreholes logs in the spillway and left bank area (all logged argillite assumed massive argillite) (BCH Report No. PSE401, 2002)

All rock types were subject to at least three 'joint sets' or preferentially oriented random joints: exfoliation joints, foliation joints, and random joints. General joint spacing by rock type is provided in Table 7.15. Exfoliation joints are the most predominant joint, striking roughly parallel to the river channel and dipping moderate to steeply towards the northwest and southeast. These joints are continuous across the dam width, with weathering penetrating to depths of up to 25 ft (BCH Report No. PSE401).

Table 7.15 Seven Mile Dam joint spacing by rock type

Unit	Joint Spacing (in)		
	Low	Mean	High
Left Bank/Spillway Granite	3	8	30
Phyllitic Argillite	3	10	12
Rehealed Argillite	1	3	8
Massive Argillite	1	4	12

The argillite unit found on the river-left bank exhibits foliation joints spaced between 0.8 and 8 inches. Foliation joints are fresh to slightly weathered and are generally smooth and planar. The majority of the foliation joints dip into the south bank at approximately 30 degrees. Others, found within the rehealed argillite, are randomly oriented (BCH Report No. PSE401). The rehealed argillite experienced a much higher degree of jointing than other units, described by site geologists as 'sugar cubing.'

Two to three weak joint sets were observed in the massive granite, although joints here are generally randomly oriented (BCH Report No. PSE401). The random joints are generally spaced from 4 to 12 inches near the surface to 12 to 40 inches at depth. Some moderate to highly weathered zones exhibit much smaller joint spacing – between 0.8 and 4 inches (BCH Report No. PSE401).

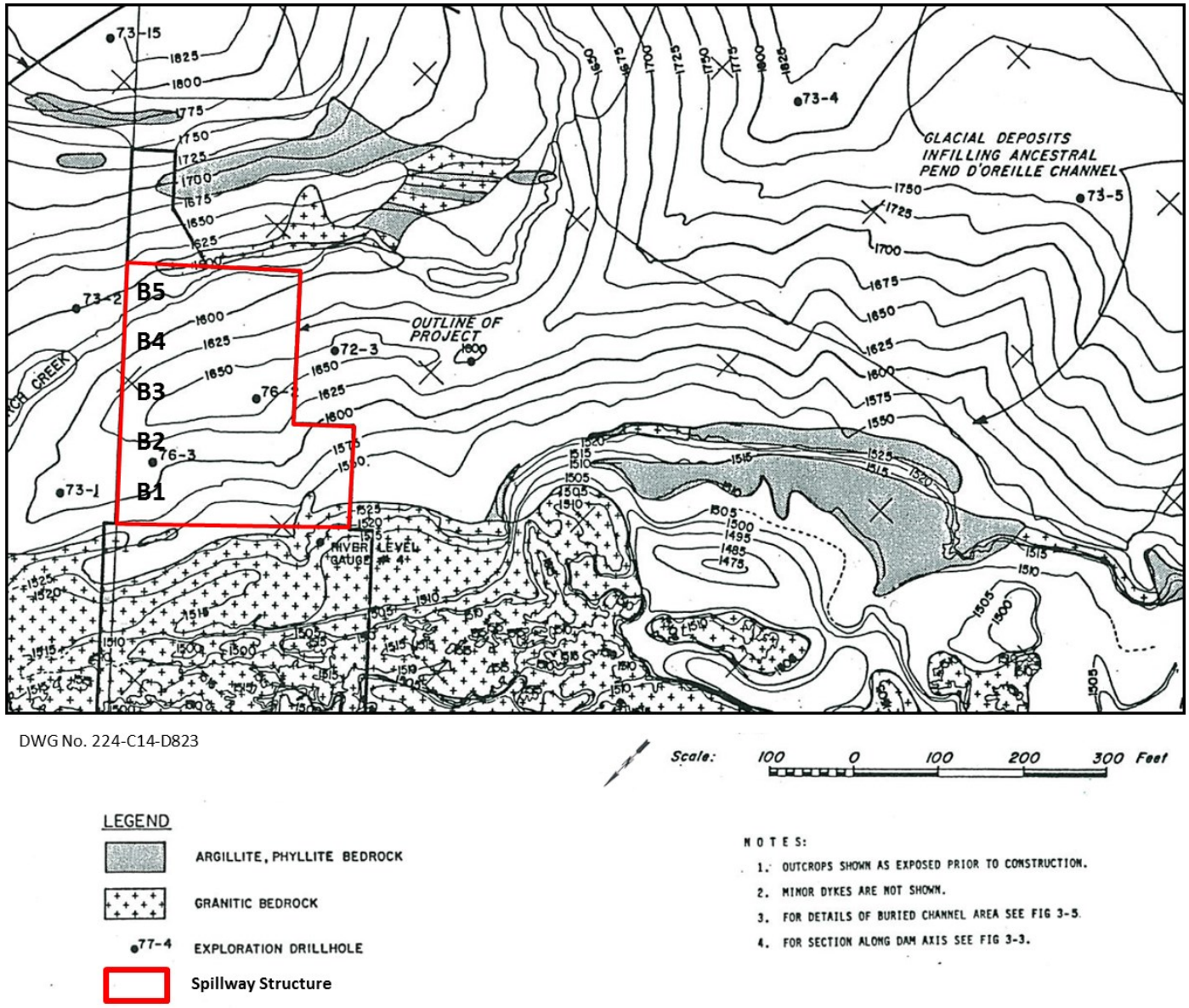

Figure 7.13 Seven Mile Dam plunge pool and adjacent area geology from BCH Report No. H1743, 1989

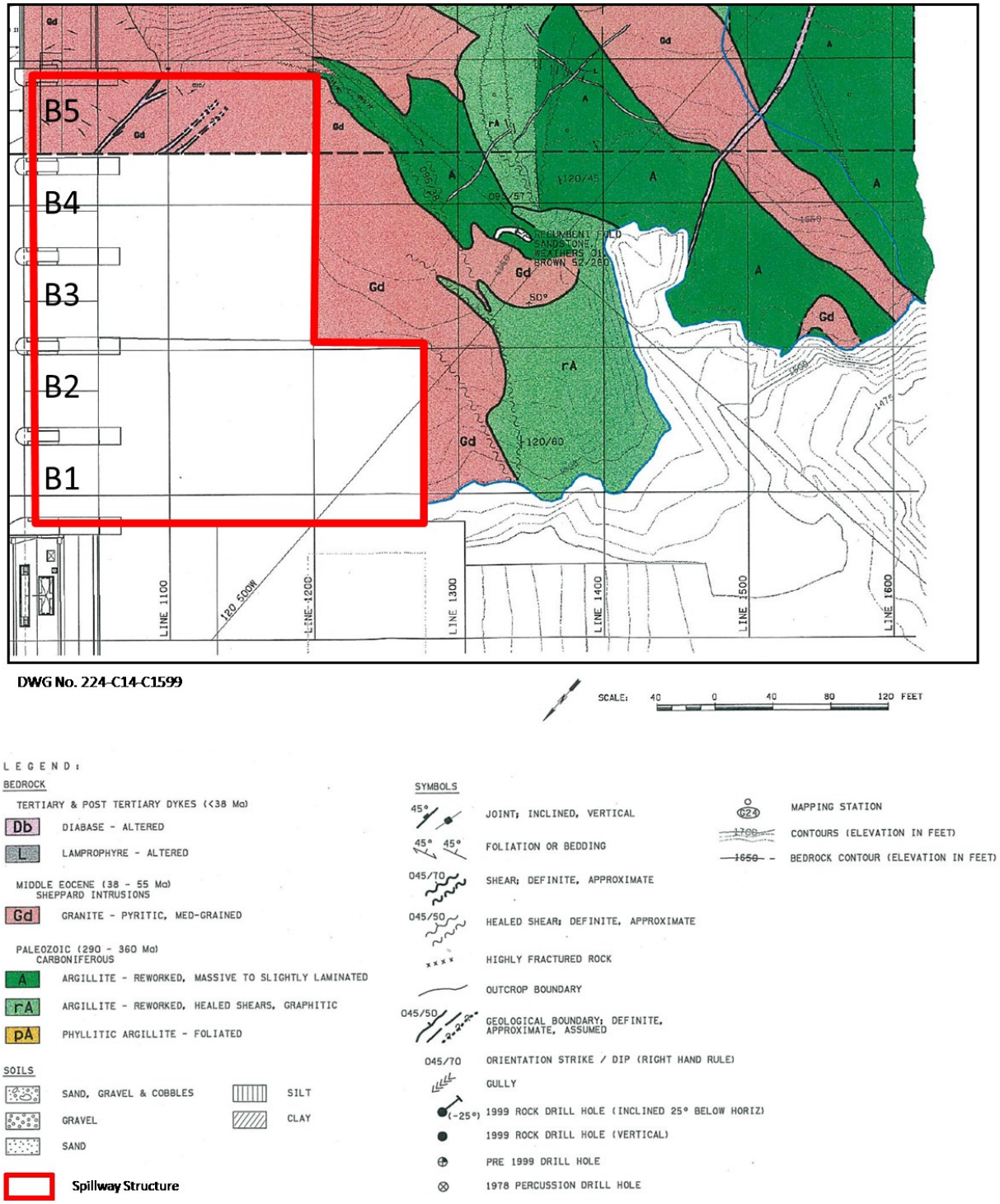

Figure 7.14 Seven Mile Dam plunge pool and adjacent area geology from BCH Report No. PSE401, 2002

Joints are generally planar and smooth for most materials on sight. Very little variability is present within or between materials, as shown in Table 7.16. Some slickensides were noted along shear zones within the granite and argillite, however slickensides are not characteristic of the majority of joints. Joints were generally subjected to limited alteration. In some cases graphitic or chloritic coating was present along joint planes in the massive and rehealed argillite units.

Erodibility Index and Critical Stream Power Values

Due to the complex spatial variability and lack of plunge pool mapping, profile SEV-12 is assumed to consist entirely of a mix of granite and massive argillite, the intermediate argillite form that has been noted within close proximity to the plunge pool invert (BCH Report No. PSE362). While it is likely that other rock types are present within the plunge pool, the orientation of plunge pool development – which is roughly along strike of the foliation and granite-argillite contact – supports the hypothesis that these units make up a large portion of the plunge pool profile, potentially along a weaker argillite-granite contact. The 'Low,' 'Mean,' and 'High' input EI values for the model were calculated as the average of the 'Low' granite and massive argillite parameters, the average of the 'Mean' granite and massive argillite input parameters, and the average of the 'High' granite and massive argillite input parameters, respectively.

Table 7.16 Seven Mile Dam Joint Roughness Number for rock types

Unit	Joint Roughness		
	Low	**Mean**	**High**
Left Bank/Spillway Granite	SM/PL 1	SM/PL-W 1.5	SM/W 2
Phyllitic Argillite	SM/PL 1	SR/PL 1.25	R/PL 1.5
Rehealed Argillite	SM/PL 1	IR/PL 1.5	SM/W 2
Massive Argillite	SM/PL 1	SM/PL-R 1.5	PL/SM/DISC 1.5

Note: W-wavy, PL-planar, IR-irregular, SM-smooth, SR-slightly rough, R-rough, DISC-discontinuous (BCH Report No. PSE401, 2002).

Although massive argillite and granite were presumed to be the dominant materials within the plunge pool, erodibility index values were generated for the other materials on site to assess the variability that may be expected between geologic materials. The plunge pool profile SEV-12 is shown in Figure 7.15, with the October 1979 pre-spill topography. Erodibility index values and critical stream power values are reported for the Seven Mile plunge pool in Table 7.17 (page 82).

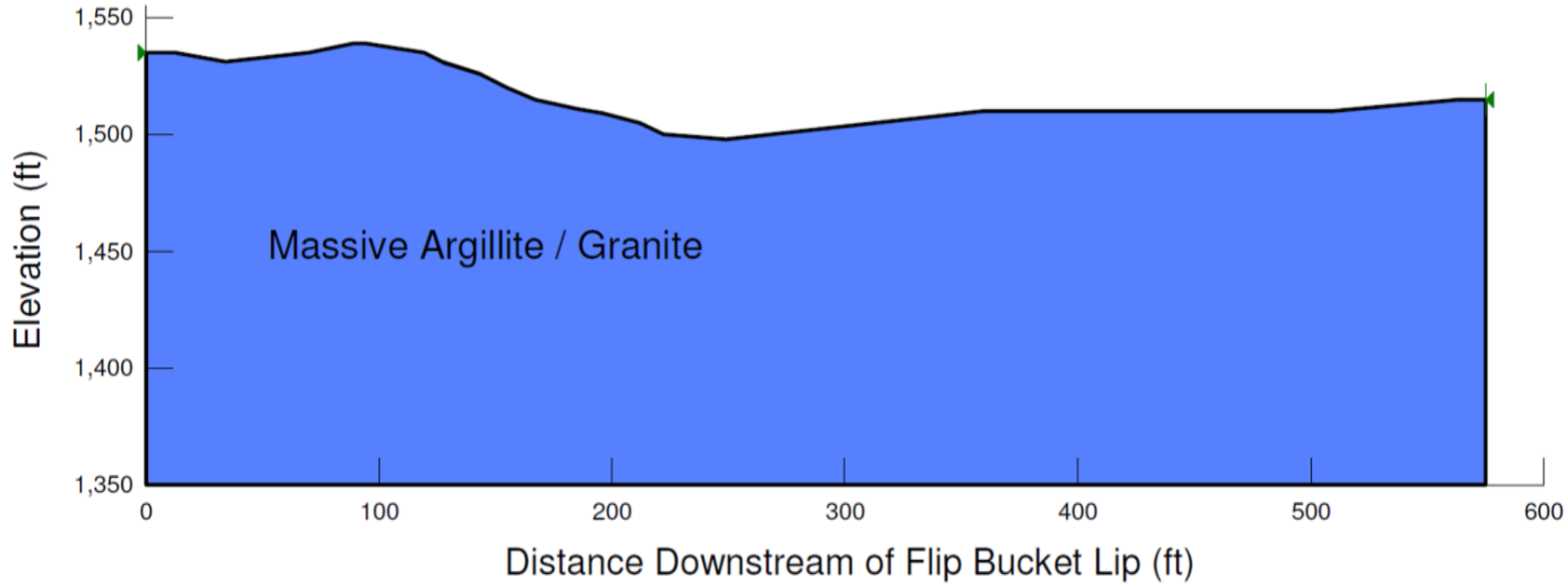

Figure 7.15 Seven Mile Dam Profile SEV-12 geomechanical model

Table 7.17 Seven Mile Dam Erodibility Index and critical stream power values by rock type

Para-meters	Granite			Rehealed Argillite			Massive Argillite			Phyllitic Argillite			Massive Arg. / Granite[1]		
	Low	**Mean**	**High**	**Low**	**Mean**	**High**	**Low**	**Mean**	**High**	**Low**	**Mean**	**High**	**Low**	**Mean**	**High**
UCS (Mpa)	100	163	252	40	40	50	60	122	252	90	135	175	68	142.5	252
RQD (%)	65	87	100	10	30	60	25	56	86	25	70	80	45	72	93
ρ (kg/m^3)	2146	2595	2675	2707	2747	2803	2707	2747	2803	2707	2747	2803	2427	2671	2739
C_r	0.78	0.94	0.97	0.98	1.00	1.02	0.98	1.00	1.02	0.98	1.00	1.02	0.88	0.97	1.00
J_r	1.0	1.5	2.0	1.0	1.5	2.0	1.0	1.50	2.0	1.0	1.25	1.5	1.0	1.50	2.0
J_n	3.34	2.73	2.73	5.00	3.34	3.34	2.73	2.73	2.73	2.73	2.73	2.73	3.04	2.73	2.73
J_a	2.0	2.0	1.0	4.0	2.5	0.75	4.0	1.75	1.25	4.0	2.0	1.0	3.0	1.9	1.1
M_s	*78.0*	*153.7*	*244.9*	*39.3*	*39.9*	*50.9*	*59.0*	*99.8*	*203.7*	*88.5*	*134.7*	*178.2*	*59.5*	*138.3*	*250.8*
K_b	*14.7*	*31.9*	*26.9*	*2.0*	*9.0*	*18.0*	*9.2*	*20.9*	*27.5*	*9.2*	*25.6*	*29.3*	*14.7*	*26.4*	*34.1*
K_d	*0.5*	*0.8*	*2.0*	*0.3*	*0.6*	*2.7*	*0.3*	*0.9*	*1.6*	*0.3*	*0.6*	*1.5*	*0.3*	*0.8*	*1.8*
J_s	*0.49*	*0.54*	*0.57*	*0.46*	*0.49*	*0.53*	*0.46*	*0.53*	*0.53*	*0.46*	*0.49*	*0.53*	*0.48*	*0.54*	*0.55*
EI (*K*)	**326**	**1984**	**10228**	**9.1**	**105**	**1293**	**62.2**	**1155**	**5979**	**93.2**	**1058**	**4152**	**138**	**1561**	**8353**
P_c (kW/m^2)	**76.7**	**297**	**839**	**5.2**	**32.9**	**216**	**22.1**	**198**	**680**	**30.0**	**186**	**517**	**40.30**	**248**	**874**

Note: [1]Massive Arg. / Granite Low, Mean and High values calculated as the average of granite and massive argillite 'Low' values, average of granite and massive argillite 'Mean' values, and average of granite and massive argillite 'High' values, respectively.

7.3 Revelstoke Dam

Plunge pool scour for Revelstoke Dam was assessed from January 1984 through July 2002, the date of the most recent plunge pool survey.

7.3.1 Plunge Pool Topography

Five surveys of the Revelstoke Dam plunge pool and tailrace area were conducted between May 1984 and July 2002. Topographic profiles along REV-1 are provided in Figure 7.16 (page 84), including the as-excavated plunge pool in 1979. Dashed lines along the profiles indicate areas of less certainty where interpretation was required to complete the profiles. Figure 7.16 also shows the invert location, length, and elevation for each survey, which were used as the basis for model comparison. Full plunge pool and tailrace surveys can be found in Appendix C. In addition to the surveys located along REV-1, an additional profile through the deepest point of the plunge pool invert from the August 1986 survey is also provided to show the lowest elevation of plunge pool scour. This survey is also found in Table 7.18, as the August 11, 1986 (Invert) and in Figure 7.16 as the dashed profile line along with the solid REV-1 1986 profile line.

Surveys indicate that significant scour occurred prior to the May 1984 and August 1986 surveys. Plunge pool development at this location has proceeded both vertically downward and laterally downstream. The focus hole has changed location within the plunge pool over time, likely due to geologic variability.

Table 7.18 Revelstoke Dam summary of plunge pool survey invert location and elevation for profile REV-1

Survey Date	Invert Center[1] (ft)	Invert Length[2] (ft)	Elevation (ft)
1979 –As Excavated	232	103	1425
May 15, 1984	330	88	1395
August 11, 1986	413	10	1405
August 11, 1986 (Invert)	378	48	1385
September 22, 1991	237	23	1410
July 24, 2002	308	1	1408

Note: [1]Invert center location is the distance downstream of the spillway flip bucket lip; [2]Invert length is the distance from the upstream end to downstream end of the deepest portion of the plunge pool.

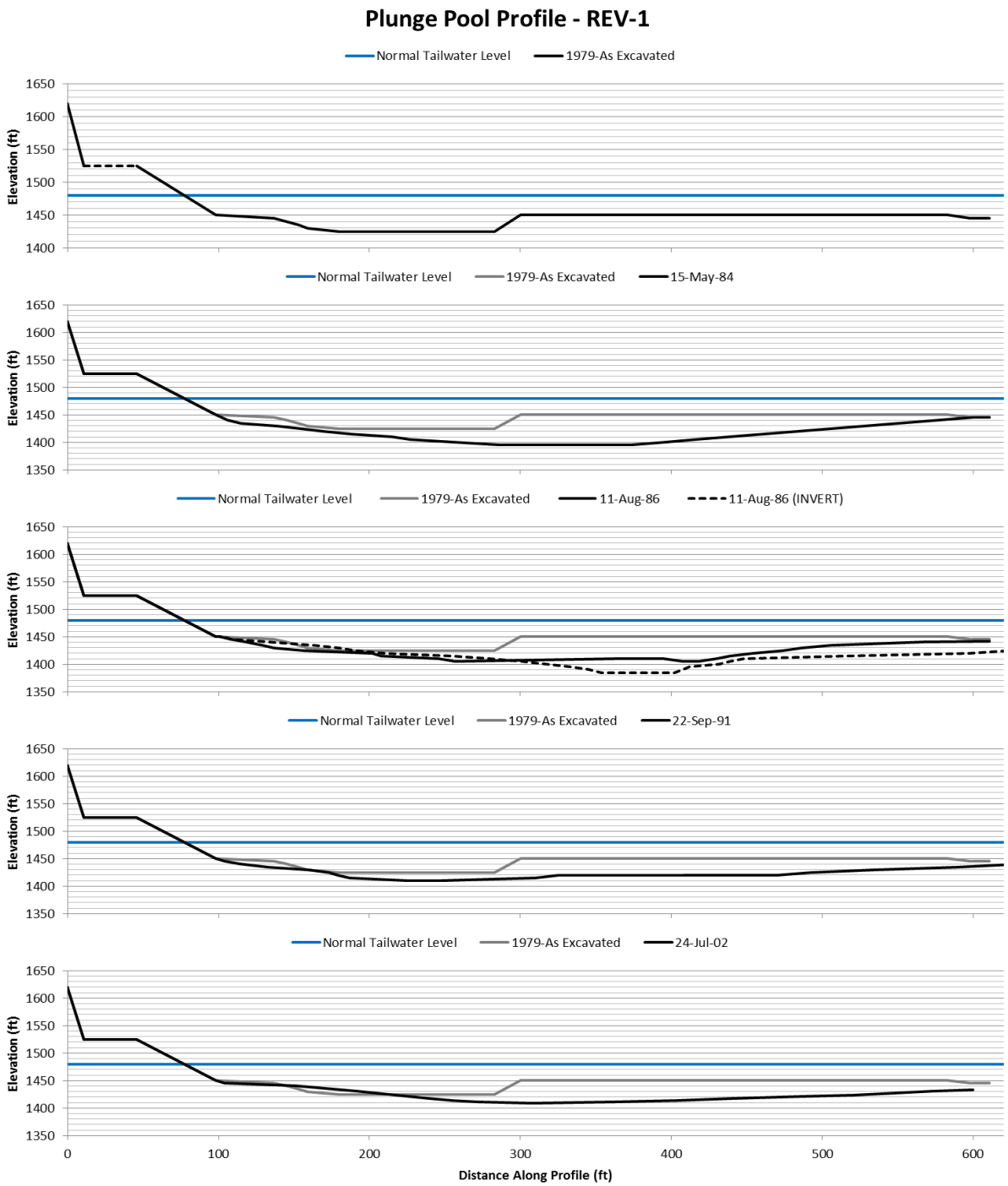

Figure 7.16 REV-1 plunge pool survey profiles, 1979 through 2002

7.3.2 Hydraulic Model Input

The Revelstoke Spillway has been in operation since October 1983. The initial discharge event, which began October 1, 1983 and continued through September 14, 1984, was passed exclusively through

the low level outlets. After 1984 these outlets were used on only one other occasion for spillway testing over a four day period in 1986. During the five other periods of spillway operation – in 1985, 1990, 1991, 1997, and 2012 – discharge was passed through the radial bays. The largest discharge event experienced by Revelstoke occurred in 1991, reached 35,500 cfs through the two radial bays, and cause partial slope failure within the plunge pool. Figure 7.17 (page 86) shows the spillway hydrograph for the life of the facility and statistical data on each of the major events is provided in Table 7.19. No data was available for 1983.

As outlined in Section 6, daily discharge and gate height data were used with the USBR's PROFILE to generate jet issuance conditions at the spillway base. Table 7.20 (page 85) provides summary statistics of the velocity (V_i), flow depth (D_i), and turbulence intensity (T_u) for the entire spillway at Revelstoke Dam.

Table 7.19 Revelstoke Project major spill event statistics

Year	**1983**[1]	**1984**	**1985**	**1986**	**1990**	**1991**	**1997**	**2012**
Period of Spill	10/1-12/31	1/1-9/14	2/14-6/13	7/25-7/28	6/14-6/18	8/9-8/25	10/2-10/5	5/17-7/30
Total Days of Discharge								
Spillway	~90	125	8	4	5	12	4	30
Outlets 1 & 2	~90	125	0	4	0	0	0	0
Surface Bays 1 & 2	0	0	8	0	5	12	4	30
Maximum Average Daily Discharge (cfs)								
Spillway	NA	30,500	31,000	11,000	17,000	35,500	18,000	30,000
Outlets 1 & 2	NA	15,250	15,500	5,500	-	-	-	-
Surface Bays 1 & 2	-	-	-	-	8,500	17,750	9,000	15,000

Note: [1]1983 discharge data unavailable; From BCH Flocal database.

Table 7.20 Revelstoke Dam Jet Issuance Summary Statistics

	Total Spillway		
	V_i (ft/s)	D_i (ft)	T_u (%)
Count	170	170	170
Minimum	17.21	0.83	3.5
Average	40.50	2.68	3.7
Maximum	60.62	3.90	4.3
St. Deviation	9.80	0.71	0.16

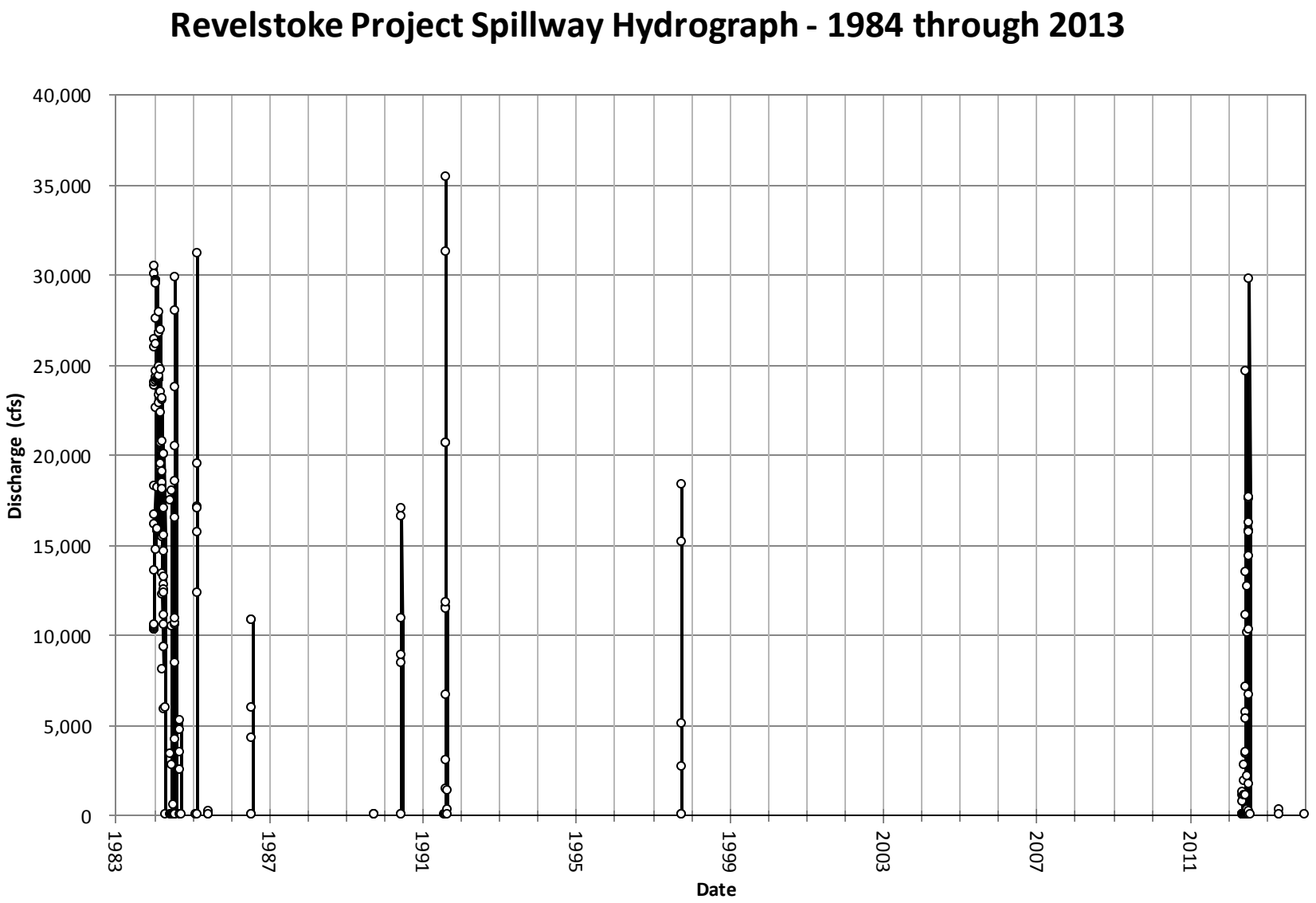

Figure 7.17 Revelstoke Project Spillway hydrograph through 2013; points indicate daily average discharge values.

7.3.3 Geomechanical Models

The geomechanical characterization of the Revelstoke Project plunge pool is largely based on borehole data from 1973-1976 exploratory programs and mapping of the excavated plunge pool invert in 1982 as well as the 1991 post-plunge pool failure drilling program. Exploration programs from the 1970's provide information on both rock and overburden within the plunge pool. The 1991 boreholes extended only to bedrock, providing information on overburden alone. Plunge pool invert mapping outlined the spatial distribution of the various rock units along the invert boundaries. Geologic mapping of the plunge pool invert was also used to characterize fracture orientation and spacing, which were not elaborated on the visual borehole logs used for this analysis. Although some information used is not in the immediate vicinity of the plunge pool invert, the proximity is considered near enough and conditions similar enough for use in this analysis.

Geology

The Revelstoke plunge pool is located in the metamorphic Monashee Complex rock that has been extensively affected by historic activity along the Columbia River Fault (BCH Report No. H1864). Bedrock is located at elevation 1,530ft, approximately, and is covered by glacial till and outwash deposits from as many as three glaciations. Overburden material is composed of sand to gravel sized sediment with boulders and cobbles. Depth to bedrock is variable within the plunge pool; the thickness of overburden material varies over small distances and ranges from approximately 10ft to 116ft, based on boreholes from 1973-1976 exploration programs: 73-8, 73-9, 74-2, 75-18, 75-20, 75-21, and 76-32 (BCH Doc. No. RW-9304-08, 1992). During initial excavation of the plunge pool overburden material was removed from the invert area down to elevation 1,425ft. Mapping of the excavation sidewalls showed complex distribution of the geologic units, with numerous fractures and shears causing offsetting. The most widespread geologic units are the quartzite gneiss and mica/biotite gneiss. Pure and impure quartzite, schist, and limited pegmatite and marble were also identified. Geologic maps of the east and west invert walls are shown in Figure 7.18 (page 91). The various types of discontinuities on site are identified in the figure by color. These features will be discussed further later on in this section. Geologic units are noted with abbreviations.

Rock strength varies between the materials and a sampling of the laboratory UCS tests conducted on site was used to assess their strength. Table 7.21 provides a summary of the rock strength values by rock type.

Table 7.21 Revelstoke Dam UCS rock strength (MPa) for lithologic units

Lithology	UCS Strength (MPa)		
	Low	Mean	High
Quartzite	27	46	66
Impure Quartzite/Quartzite Gneiss	43	69	101
Biotite/Mica Gneiss[1]	28	47	71
Schist	43	49	58

Note: [1]Biotite/Mica Gneiss values from biotite gneiss and basic gneiss tests (5 tests); (BCH Report No. Z0671, 1972).

Plunge pool materials are extensively fractured due to activity along the Columbia River Fault. The degree of faulting and alteration of the metamorphic materials is evident in the rock RQD values from the 1970's exploratory boreholes. Table 7.22 provides a summary of RQD values from boreholes 75-18, 75-20, 75-21, and 76-32 located in the plunge pool. RQD values were grouped based on lithology across all four boreholes. The 'Mean' value represents the average value, the 'High' value represents the RQD one standard deviation above the mean, and the 'Low' value represents the RQD one standard deviation below the mean. 82% of RQD data available was collected on the quartzite gneiss; 96 of the 117 recorded RQD values. 12% of the RQD data was for quartzite (14 values). The last 6% of data was split between the biotite/mica gneiss, schist, and marble. As a result, the RQD values used for the schist was approximated as ranging from a 'Low' RQD value of 5% (the minimum value allowable for the Rock Mass Rating (RMR) system) to a 'High' RQD value of 19%, a value the same distance from the mean value of 12% as the 'Low' value for schist. There was generally no increase in RQD values with depth, indicating that the high degree of fracturing is not the product of surface weathering processes and relaxation alone.

Table 7.22 Revelstoke Dam RQD values for lithologic units

Lithology	RQD (%)		
	Low	Mean	High
Quartzite	11	40	69
Impure Quartzite/Quartzite Gneiss	8	30	52
Biotite/Mica Gneiss[1]	40	51	62
Schist	5	12	15

Note: Based on logged boreholes (BCH Doc. No. RW-9304-08, 1992)

During geologic mapping of the plunge pool inverts five different discontinuity sets were identified from 177 mapped discontinuities. Mapping did not differentiate between fractures, shears, and faults, however field notes and geologic investigation reports indicate that a large number of the discontinuities display offset, slickensides, or are gouge-filled. The five discontinuity sets were differentiated based both on their relationship to local foliation direction and degree of dip. The joint set orientations and the numbers of mapped discontinuities are provided in Table 7.23. Orientations are based

on strike and dip measurements taken along the excavated invert walls. Measurements were input into RocScience Dips Software v6.006 (2012), where the mean orientation was calculated for each discontinuity type. Two steeply dipping sets were identified from the data, with Steep-1 occurring more frequently than Steep-2.

Table 7.23 Revelstoke Dam plunge pool discontinuity sets

Discontinuities	Orientation		Number
	Strike[1]	Dip	
Foliation	061	22	58
Foliation-Parallel	047	41	54
Foliation-Normal	174	42	34
Steep-1	066	85	23
Steep-2	162	81	7

Note: [1]Strike based on right-hand rule. (BCH Doc. No. RW-9304-08, 1992)

Apparent joint spacing was also estimated from plunge pool invert mapping. One horizontal transect was taken across each mapped wall and two additional vertical transects were taken – one along the west wall and one along the north wall – for six total transects that represent all three dimensions. Apparent spacing values for the five discontinuity sets and for all discontinuities combined are provided in Table 7.24. The degree of fracturing described in the text and the orientation of the foliation/foliation-parallel, foliation-normal, and steep-1 joint sets suggest that rock blocks formed by the discontinuities have equal length-to-width-to-height ratios.

Table 7.24 Revelstoke Dam discontinuity apparent spacing

Lithology	Spacing (ft)		
	Low	Mean	High
Foliation	4.5	47.4	86.4
Foliation-Parallel	0.5	19.7	48.8
Foliation-Normal	1.0	20.6	42.7
Steep-1	2.9	28.1	53.2
Steep-2[1]	-	39.9	-
Total	0.5	10.5	21.0

Note: based on plunge pool invert mapping; one horizontal transect running along each wall and two transects vertically downward along north and west walls; [1]Only one space value available for Step-2 joint set (BCH Doc. No. RW-9304-08, 1992)

Joint condition and roughness values were unavailable in the graphic borehole logs used for this analysis. As a result, joint condition and roughness values were inferred from plunge pool invert mapping and descriptions of the rockmass in geologic and design reports. Numerous mapped discontinuities from 1982 invert mapping exhibit 1/8in to 4in separation and are gouge-filled fractures and shears. This degree of infilling occurs in all discontinuity types but is most common in the foliation-parallel and foliation-

normal joint sets. Offset, accompanied by slickensides on fracture surfaces, is apparent on many of the foliation-parallel joint and shears, likely due not only to intense fracturing but also to weakness along foliation planes (BCH Doc. No. RW-9304-08, 1992). Foliation-parallel discontinuities are also commonly coated in graphite or subject to chloratization. Due to the presence of slickensides, gouge, and the degree of fracturing, joint shapes across all discontinuity sets and assumed to be planar to wavy. Shearing with visible offset is more common in the biotite/mica gneiss portion of the mapped invert walls, likely due to strong mica and biotite cleavage along foliation. As a result biotite/mica gneiss joint character and roughness values are inferred to be lower than those for quartzite and quartzite gneiss. Schist values are anticipated to be even lower due to low core recovery in this unit and its soft, fissile nature (BCH Report No. RO-0958-12, 1957). Joint roughness and alteration values are provided in Table 7.25 and Table 7.26.

Table 7.25 Revelstoke Dam Joint Roughness Number for rock types

Unit	Joint Roughness		
	Low	Mean	High
Quartzite	SM/PL 1	SM/PL-W 1.5	SM/W 2
Impure Quartzite/Quartzite Gneiss	SM/PL 1	SM/PL-W 1.25	SM/W 2
Biotite/Mica Gneiss[1]	SL/PL 0.75	SL/PL 1	SM/PL 1.5
Schist	SL/PL 0.75	SL/PL 1	SM/PL 1.5

Note: W-wavy, PL-planar, IR-irregular, SL-slickensided, SM-smooth, SR-slightly rough, R-rough; (BCH Doc. No. RW-9304-08, 1992; BCH Report No. RO-0958-12, 1957)

Table 7.26 Revelstoke Dam Joint Alteration Number for rock types

Unit	Joint Separation/Alteration		
	Low	Mean	High
Quartzite	13	8	3
Impure Quartzite/Quartzite Gneiss	13	8	3
Biotite/Mica Gneiss[1]	18	8	3
Schist	18	10	6

Note: (BCH Doc. No. RW-9304-08, 1992; BCH Report No. RO-0958-12, 1957)

Erodibility Index and Critical Stream Power Values

Although the quartzite, quartzite gneiss, and biotite/mica gneiss displayed some variability in rock strength and RQD values, the erodibility index values for the three units were very similar. For this reason, as well as complex spatial distribution of materials, the three units have been combined into one gneiss/quartzite unit for this analysis, as shown in Figure 7.19 (page 92). The schist unit has significantly lower erodibility index values.

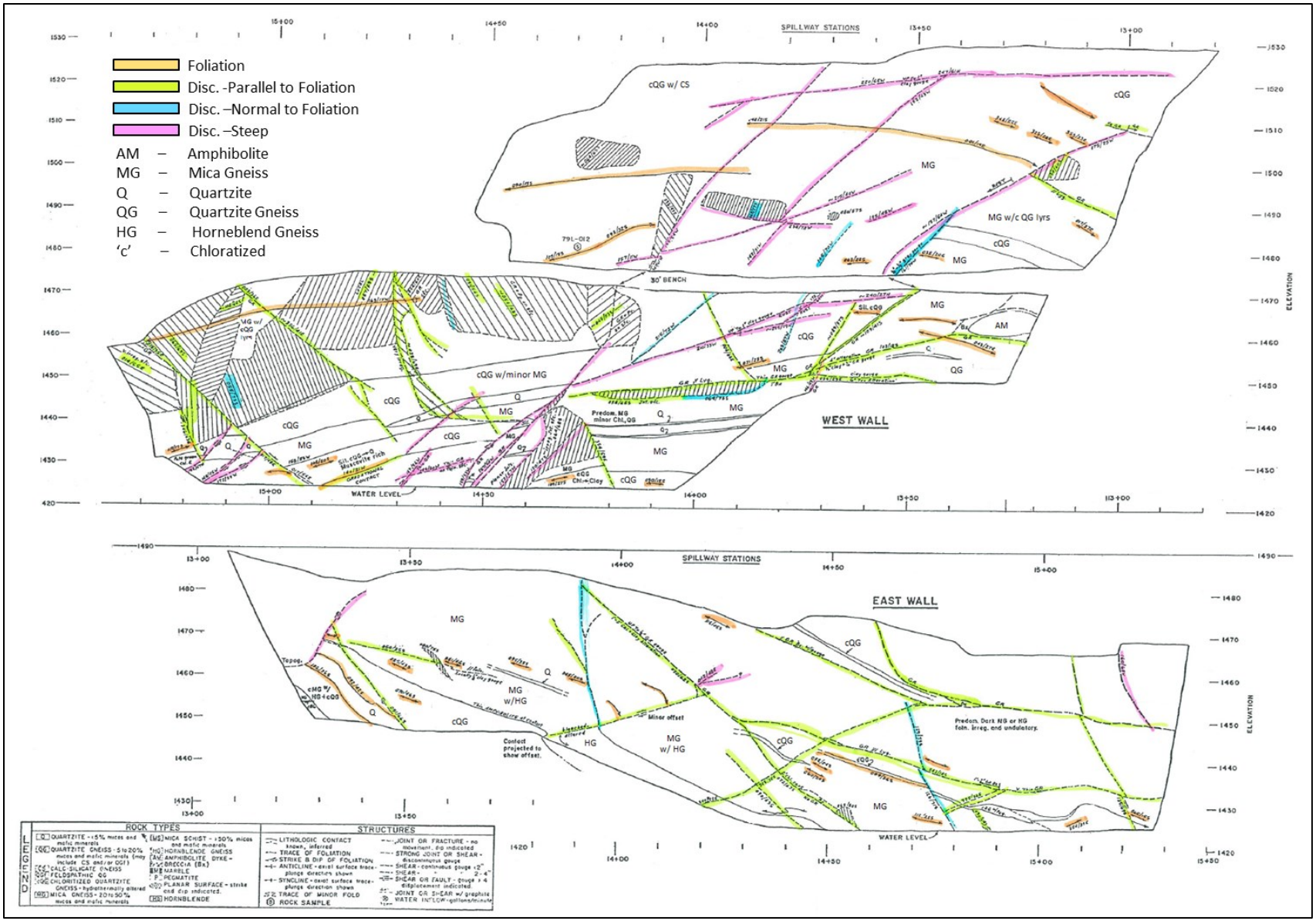

Figure 7.18 Revelstoke plunge pool invert mapping - east and west walls (modified from BCH Doc. No. RW-9304-08, 1992)

Table 7.27 Revelstoke Dam erodibility index and critical stream power values by rock type

Parameters	Gneiss/Quartzite			Schist		
	Low	Mean	High	Low	Mean	High
UCS (MPa)	35	57	80	43	49	58
RQD (%)	20	40	69	5	12	15
ρ (kg/m^3)	2750	2750	2750	2750	2750	2750
C_r	1.00	1.00	1.00	1.00	1.00	1.00
J_r	0.9	1.33	2.0	0.75	1.0	1.5
J_n	5.00	3.34	2.24	5.00	3.34	2.24
J_a	14.67	6.00	3.00	18.00	10.00	6.00
M_s	*35.0*	*57.0*	*79.9*	*43.0*	*49.0*	*58.0*
K_b	*3.9*	*12.1*	*30.8*	*1.0*	*3.6*	*6.7*
K_d	*0.1*	*0.2*	*0.7*	*0.0*	*0.1*	*0.3*
J_s	*0.49*	*1.14*	*1.5*	*0.49*	*1.14*	*1.50*
EI (*K*)	**4.2**	**174**	**2462**	**0.9**	**20**	**146**
P_c (kW/m^2)	**2.9**	**48**	**350**	**0.9**	**9**	**42**

The Revelstoke plunge pool was modeled as gneiss/quartzite-only due to the volume of quartzite, quartzite gneiss, and biotite/mica gneiss present in the plunge pool borings and from invert mapping compared to the schist. In addition, a lack of detailed information on the spatial distribution of the units with depth limited the complexity of the model. Cross section REV-1 is shown in Figure 7.19 (page 93). The upstream portion of the cross section identified as 'Concrete' represents the portion of the cross section under the concrete apron below the spillway terminal structure. This portion of the model has been assigned an EI value of 100,000 kW/m2 to indicate that erosion of this material does not occur.

7.4 W.A.C. Bennett Dam

Plunge pool scour for W.A.C. Bennett Dam was assessed from June 1968 through October 2002, the date of the most recent plunge pool survey.

7.4.1 Plunge Pool Topography

Although this facility has been in operation the longest, there were only three plunge pool surveys available for the tailrace and plunge pool area for W.A.C. Bennett Dam. Surveys are conducted in 1973, 1996, and 2002. Portions of the 1973 survey and riverbank topography were used to estimate the initial riverbed level in June 1972, prior to significant spills. Plunge pool topographic profiles along WAC-C are provided in Figure 7.16 (page 84). Dashed lines along the profiles indicate areas of less certainty where interpretation was required to complete the profiles. A summary of the location, length, and elevation of

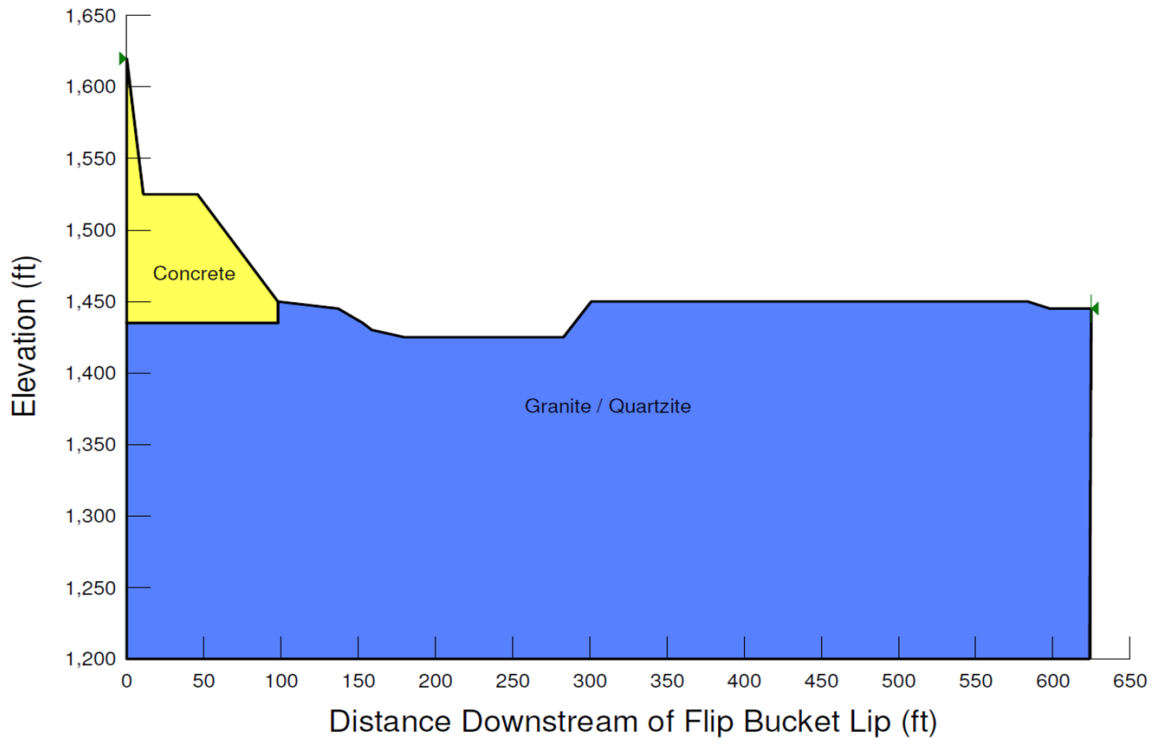

Figure 7.19 Revelstoke Dam Profile REV-1 geomechanical model

the plunge pool from each survey is provided in Table 7.28. Information from Table 7.28 serves as the basis for model comparison. Complete plunge pool surveys can be found in Appendix C.

The majority of scour in the W.A.C. Bennett Plunge pool occurred as a result of the 1972 spill event, when 90 ft of rock was removed from the plunge pool invert. An additional 14 ft of scour also occurred between 1973 and 1996. Some plunge pool infilling is evident after this period, when the invert rose 15 ft and returned to its 1973 level.

Table 7.28 W.A.C. Bennett Dam summary of plunge pool survey invert location and elevation for profile WAC-C

Survey Date	Invert Center[1] (ft)	Invert Length[2] (ft)	Elevation (ft)
June 13, 1972[3]	-	-	1621
May 19, 1973	713	17	1530
August 4, 1996	761	1	1516
October 1, 2002	640	1	1531

Note: [1]Invert center location is the distance downstream of the spillway flip bucket lip; [2]Invert length is the distance from the upstream end to downstream end of the deepest portion of the plunge pool; [3]June 1972 values inferred from denoted contours on May 1973 survey.

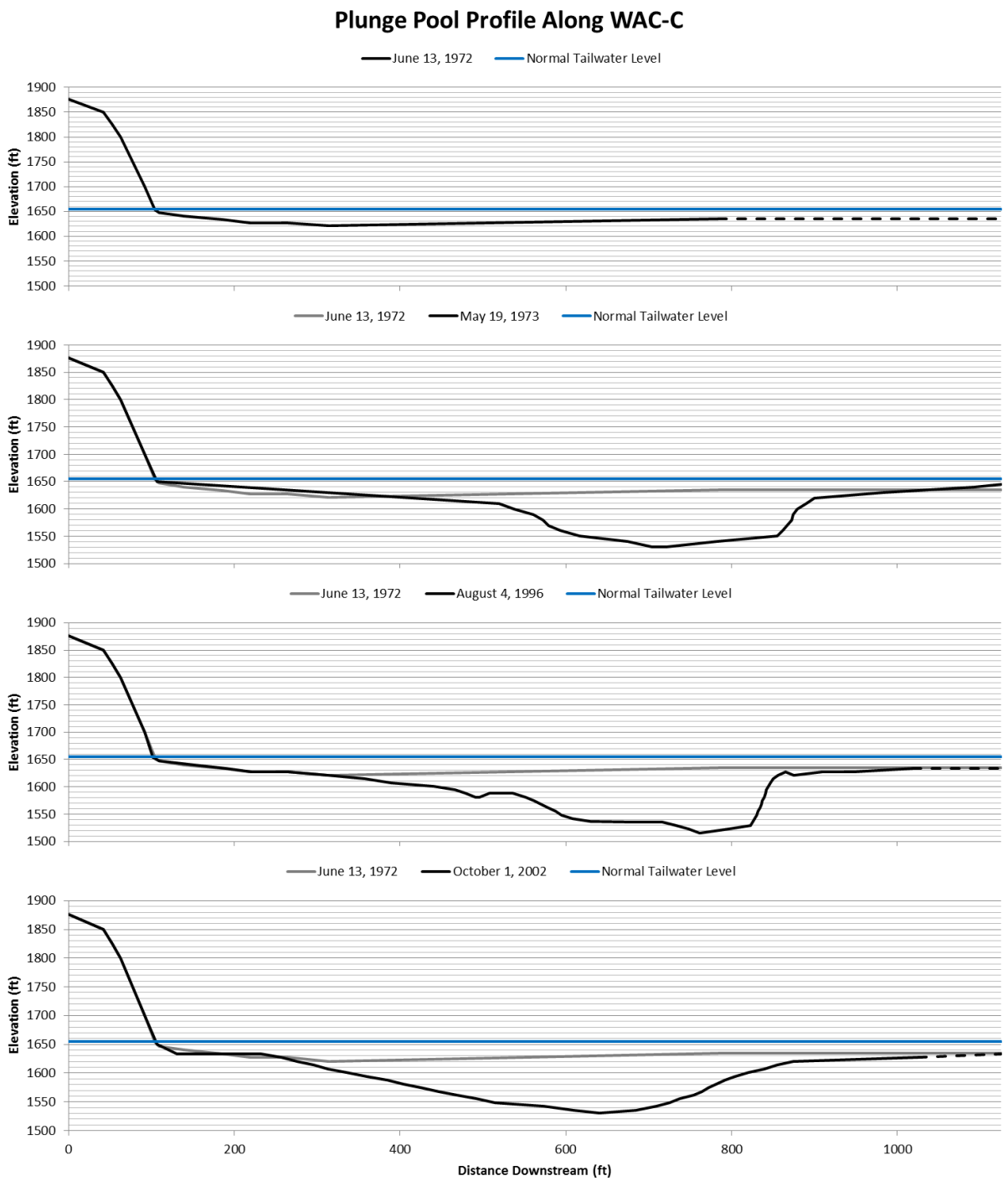

Figure 7.20 WAC-C plunge pool survey profiles, 1972 through 2011

7.4.2 Hydraulic Model Input

The W.A.C. Bennett spillway has been in operation since August 1968, but has only passed flows on nine occasions between 1968 and 2013: during 1972, 1974, 1976, 1981, 1983, 1984, 1996, 2002, and 2012. The longest duration of spill and highest daily average discharge occurred during the initial spill event in 1972. No spill event has achieved the duration or discharge since that time. The spillway hydrograph for 1968 through 2013 is provided in Figure 7.21 and a summary of discharge event statistics is provided in Table 7.29.

Table 7.29 W.A.C. Bennett Dam major spill event statistics

Year	**1972**	**1974**	**1976**	**1981**	**1983**	**1984**	**1996**	**2002**	**2012**
Period of Spill	6/13-9/14	7/23-8/29	7/7-8/27	7/24-8/5	5/10-8/23	3/1-10/15	6/24-8/17	7/8-7/29	6/26-8/2
Total Days of Discharge									
Spillway	85	36	36	13	68	25	55	22	26
Bay 1 - 3	85	36	36	13	68	25	55	22	26
Maximum Average Daily Discharge (cfs)									
Spillway	167,250	25,000	36,000	45,000	79,500	23,000	122,000	54,500	56,500
Bay 1 - 3	55,750	8,250	12,000	15,000	26,500	8,000	41,000	18,000	19,000

As outlined in Section 6, daily discharge and gate height data were used with the USBR's PROFILE to generate jet issuance conditions at the spillway base. Table 7.30 provides summary statistics of the velocity (V_i), flow depth (D_i), and turbulence intensity (T_u) for the entire spillway at W.A.C. Bennett Dam.

Table 7.30 W.A.C. Bennett Dam Jet Issuance Summary Statistics

	Total Spillway		
	V_i (ft/s)	**D_i (ft)**	**T_u (%)**
Count	344	344	344
Minimum	51.64	0.97	3.2
Average	90.32	2.73	3.7
Maximum	129.87	7.75	4.2
St. Deviation	17.77	1.51	0.24

7.4.3 Geomechanical Model

The geomechanical model developed for the W.A.C. Bennett plunge pool is based primarily off of geological and design reports on the general site area. No borehole information was available for the

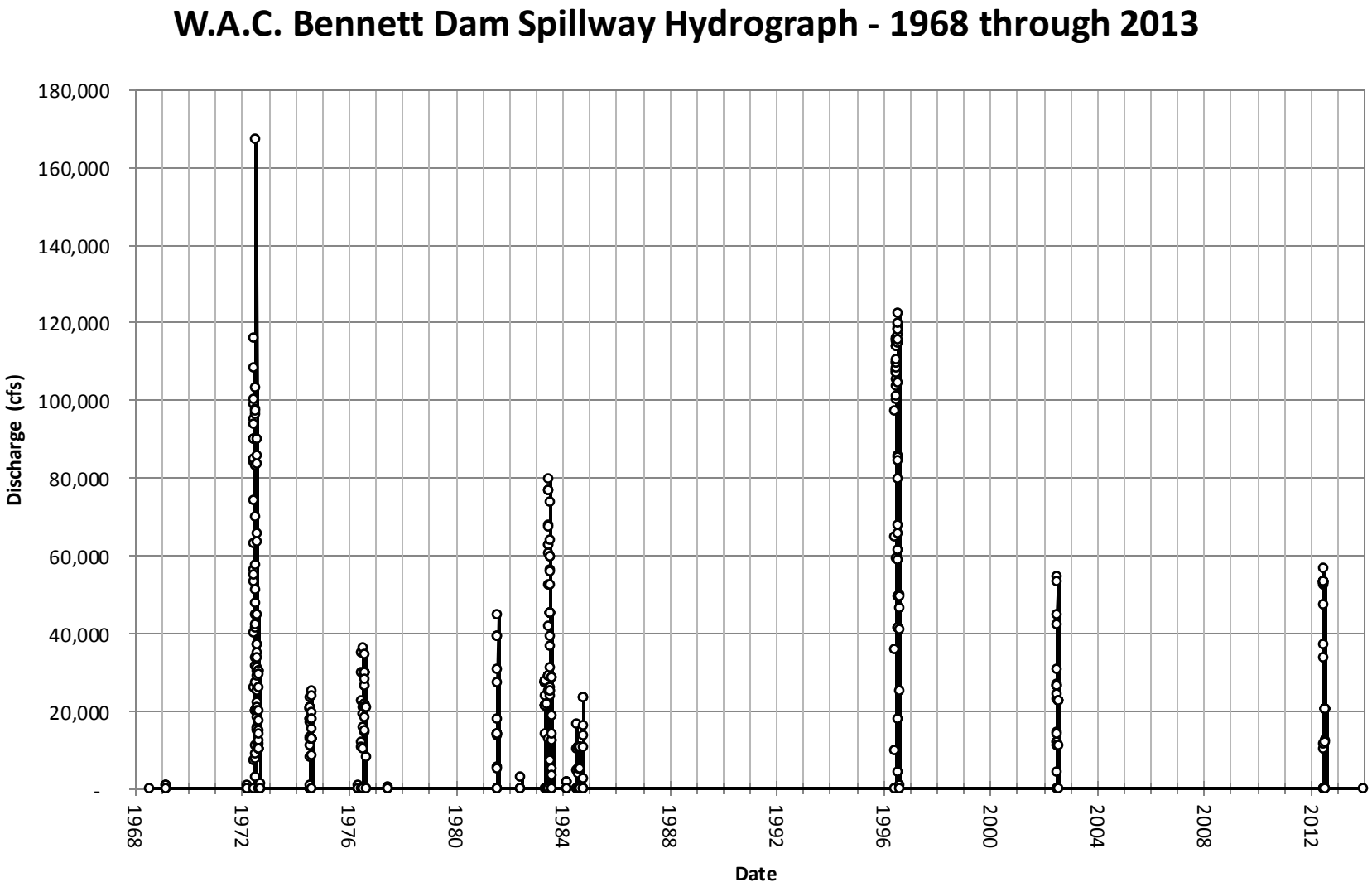

Figure 7.21 W.A.C. Bennett Spillway hydrograph through 2013; points indicate daily average discharge values

plunge pool or the immediate vicinity and stratigraphy for this area was extrapolated from an upstream borehole, based on site-wide dip and dip direction of the sedimentary units. UCS strength testing from samples near the dam foundation and abutments were considered representative of the plunge pool as well. This dam site has the least amount of geologic information available of any of the sites assessed in this study.

Geology

The W.A.C. Bennett plunge pool is located within the Peace River channel near the top of the Cadomin/Dunlevy Formation, at the base of the transition from this formation upward into the more shale-rich Gething Formation. Rock of the Cadomin/Dunlevy Formation is primarily massive sandstone with some interbedded shale layers and sporadic coal seams. In the upper 200 ft of the formation, where the plunge pool is located in the stratigraphic column, coal seams up to one foot in thickness are common. Figure 7.22 shows a section through the same portion of the stratigraphic column in which the plunge pool is located, although taken approximately 2,000 ft away. The column is representative of the type of stratigraphy expected at the top of the Cadomin/Dunlevy Formation where it transitions to Gething Formation; individual beds noted may or may not be present within the plunge pool itself. As shown in the figure, the rock grades from overburden and river gravel down to more competent shaley sandstone and massive sandstone with depth.

Rock strength for sandstone and shale materials were developed from testing of materials near the dam axis (Site 3A) as well as the nearby Sites 2 and 3, located upstream of the current dam axis, that were investigated prior to selection of what is now the W.A.C. Bennett Dam location. Rock strengths are similar across all three sites and the rock material properties of the Cadomin/Dunlevy Formation are continuous regionally. UCS strength values for sandstone and shale cores tested in the lab are provided in Table 7.31. Shale units on site are susceptible to slaking and weathering once exposed to water. Shale UCS strength values were therefore based on tests on saturated core samples due to the location of the rock beneath the water table. Sandstone saturated and dry tests resulted in very similar values and were not differentiated for this analysis.

Table 7.31 W.A.C. Bennett Dam UCS rock strength (MPa) for lithologic units

Lithology	UCS Strength (MPa)		
	Low	Mean	High
Sandstone	97	122	163
Shale	19	69	148

Note: Sandstone values from 7 tests, dry & saturated; shale values from 2 tests, dry & saturated, and shale UCS range provided in BCH Report 1765 (BCH Report No. 1756, 1988; BCH Report No. 31, 1959; BCH Report No. 105, 1959).

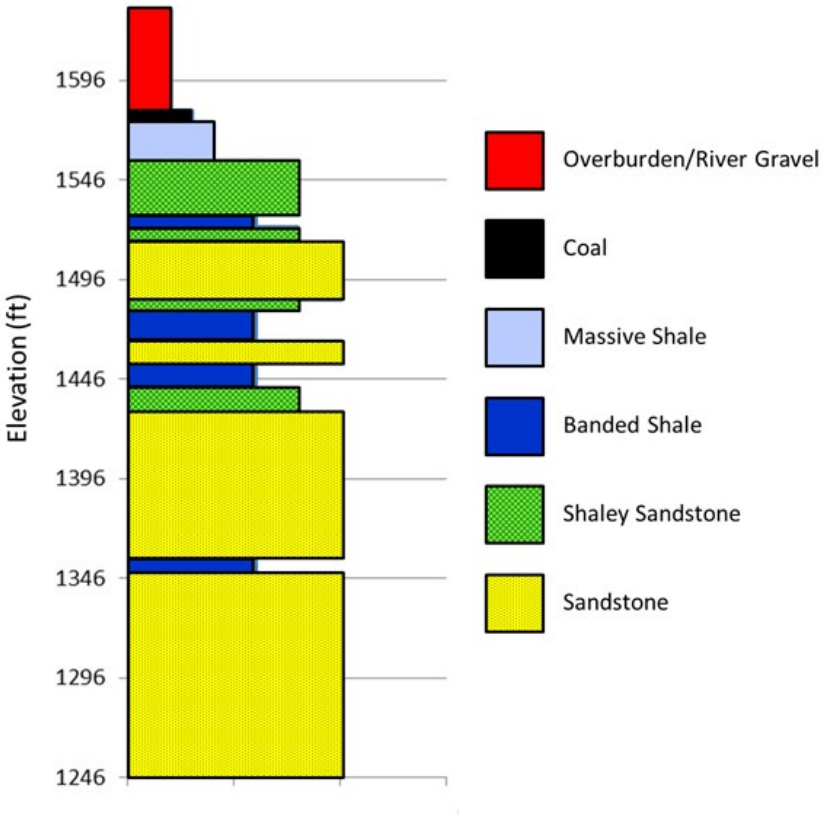

Figure 7.22 Stratigraphic column of the upper Cadomin/Dunlevy Formation from DH-8, depths adjusted to plunge pool level based on distance from pool and regional strike and dip (BCH Report No. N300 Vol. 3, 1959)

The W.A.C. Bennett dam site lacks any complex structural elements. The sedimentary rocks on site dip 5° to 15° toward the southwest, downstream of and roughly perpendicular to the dam axis. Jointing within both units is limited to subvertical relaxation joints in the canyon walls and bedding-parallel relaxation joints the valley to depths of approximately 100 ft below ground level. Joints along bedding planes do occur occasionally in the sandstone but are more common in the shale units, especially near coal seams, which may be highly fractured locally. Both units are generally described as very competent (BCH Report No. N300 Vol. 2, 1959). RQD values for the sandstone and shale units were inferred from descriptions of the rock and the reinforcement (or lack thereof) required in nearby water diversion tunnels and are provided in Table 7.32.

Table 7.32 W.A.C. Bennett Dam inferred RQD values for lithologic units

Lithology	RQD (%)		
	Low	Mean	High
Sandstone	90	95	100
Shale	70	85	90

Note: Values inferred from rock descriptions and not taken from borehole logs (BCH Report No. 1756, 1988; BCH Report No. N300 Vol.2, 1959; Dolmage & Campbell, 1963).

Fracture shape and roughness was also inferred from the text, although the topic was not discussed at length. The lack of faulting in the area and widely spaced fractures were interpreted to result in planar to undulating fractures, likely slightly rough to rough in the sandstone and smooth to slightly rough in the shale, since these features generally occur along bedding planes. Some sandstone fractures are likely irregular and very rough, as geologists noted conchoidal fracture of the sandstone occurred as well as breaks along existing bedding. Some slickensided surfaces were noted within coal seams and along shale contacts with coal seams. While isolated coal beds do exist in the Cadomin/Dunlevy Formation, they are much less common than in the overlying shaley Gething Formation. Joint roughness values are provided in Table 7.33

Table 7.33 W.A.C. Bennett Dam inferred joint roughness for lithologic units

Lithology	Joint Character and Roughness		
	Low	Mean	High
Sandstone	C/SR 2.5	IR/ R 3.5	IR/VR 4.0
Shale	PL/SM 1.0	PL-IR/SR 2.0	IR/R 3.0

Note: C-curved, PL-planar, IR-irregular, SL-slickensided, SM-smooth, SR-slightly rough, R-rough, VR-very rough ; Values inferred from rock descriptions and not taken from borehole logs (BCH Report No. 1756, 1988; BCH Report No. N300 Vol.2, 1959; Dolmage & Campbell, 1963).

Where fractures do exist, the rock mass is expected to break into elongated slabs due to the propensity of the material to fracture along low angle bedding planes, with few vertical fractures. Joint structure numbers for both units are anticipated to be in the range of 0.79 to 1.09, representative of elongated rock blocks inclined at a low angle.

In addition to bedrock, River gravels are also present near the surface in the river channel. Gravel, cobble, and boulder deposits are estimated to be approximately 30ft thick in the bedrock-cut channel based on borehole logs taken at the upstream, more shallow gradient Sites 2 and 3 (BCH Report No. N330, Vol. 2, 1959).The friction of angle of the gravel, cobbles, and boulders is approximated as 45^{o}, an appropriate value for poorly graded gravel with few fines (Meyerhoff, 1956). Median (D_{50}) grain sizes of the riverbed material were estimated as six inches, 12 inches, and 24 inches for the low, mean, and high cases based on the relatively high energy fluvial environment. Photographs of the river during low flow suggest a fairly uniform bed height across the channel without deep pools (BCH Report No. N330, Vol. 2, 1959).

Erodibility Index and Critical Stream Power Values

The W.A.C. Bennett plunge pool geomechanical model was broken into three zones based primarily on lithology. The top layer of the plunge pool model consists of river gravels, to depths of 30 ft below ground surface. Below the river gravels and down to elevation 1,522 ft (approximate) material is expected to consist of massive and banded shale with some weathered and more highly fractured shaley sandstone. These shallow materials are expected to have a lower erodibility index both because of the weaker nature of the shale as well as the more fractured nature of the sandstones that may be present. Beyond this depth the plunge pool is modeled as competent Cadomin/Dunlevy Formation sandstone. Input parameters, calculated erodibility index values, and associated critical stream power values are provided in Table 7.34. The geomechanical model of section WAC-C is also provided in Figure 7.23 (page 102).

Table 7.34 W.A.C. Bennett Dam erodibility index tables for geomechanical zones

Rock Parameters	**Sandstone**			**Shale/ Fractured Sandstone**			**Soil Parameters**	**Overburden - River Gravel**		
	Low	**Mean**	**High**	**Low**	**Mean**	**High**		**Low**	**Mean**	**High**
UCS (MPa)	97	122	163	19	69	148	D_{50} (in)	6	12	24
RQD (%)	90	95	100	70	85	95	ϕ (°)	45	45	45
ρ (kg/m^3)	2750	2750	2750	2750	2750	2750				
C_r	1.0	1.0	1.0	1.0	1.0	1.0				
J_r	2.5	3.5	4.0	1.0	2.0	3.0				
J_n	2.24	1.83	1.50	2.73	1.83	1.83				
J_a	1.0	0.75	0.75	2.5	1.75	1.0				
M_s	*96.9*	*121.9*	*162.9*	*19.0*	*68.9*	*147.9*	*M_s*	*0.41*	*0.41*	*0.41*
K_b	*40.2*	*51.9*	*66.7*	*25.6*	*46.4*	*51.9*	*K_b*	*3.5*	*28.3*	*226.5*
K_d	*2.5*	*4.7*	*5.3*	*0.4*	*1.1*	*3.0*	*K_d*	*1.00*	*1.00*	*1.00*
J_s	*1.00*	*1.15*	*1.25*	*1.00*	*1.15*	*1.25*	*J_s*	*1.00*	*1.00*	*1.00*
EI (*K*)	**9735**	**33961**	**72384**	**194.7**	**4209**	**28787**	**EI (*K*)**	**1.5**	**11.6**	**92.9**
P_c (kW/m^2)	**980.1**	**2502**	**4413**	**52.1**	**523**	**2210**	**P_c (kW/m^2)**	**1.3**	**6.3**	**29.9**

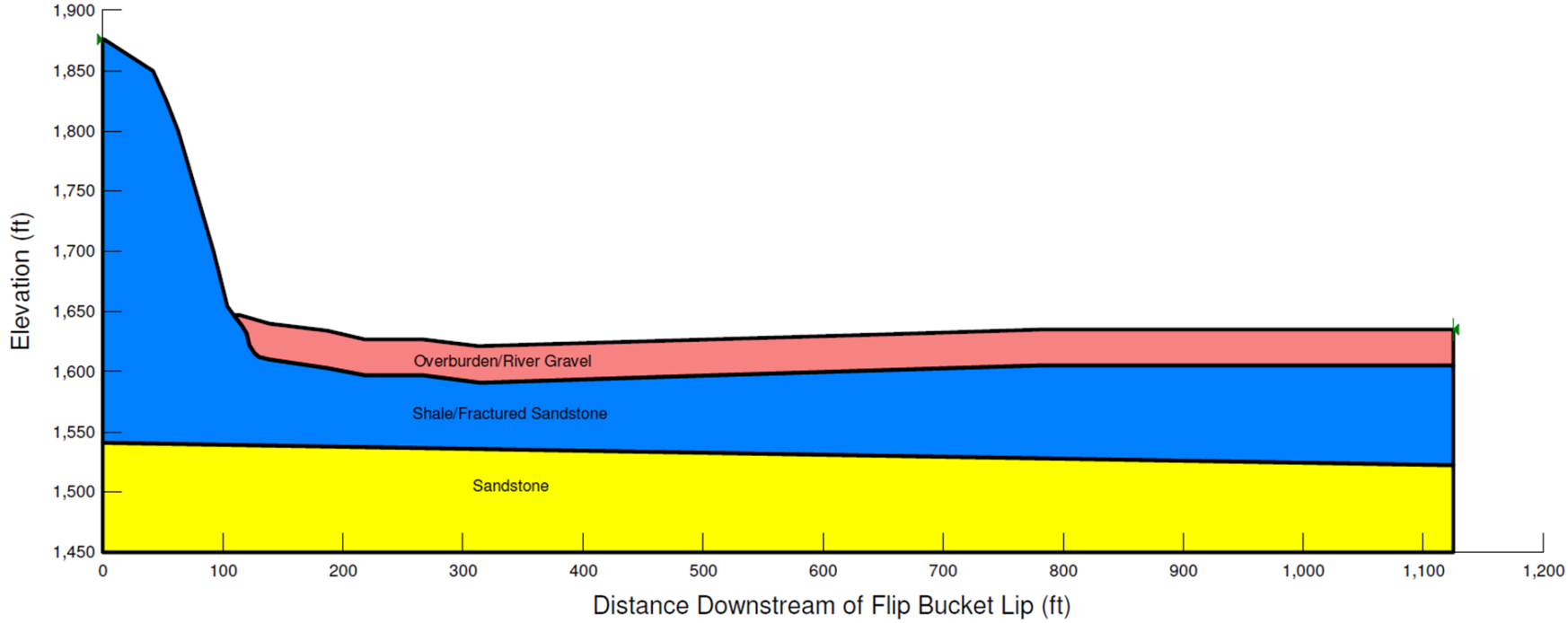

Figure 7.23 W.A.C. Bennett Dam Profile WAC-C geomechanical model

CHAPTER 8

RESULTS

Results for depth and downstream invert distance for the four dam sites assessed are presented below, produced from the *EIM_ProfileCalc* program developed for this analysis. Tabulated data for each day of record assessed, modeled depths and invert locations for the 'Low', 'Mean', and 'High' erodibility cases for each dam site are provided in Appendix D. Profiles developed by the program for each survey date are provided in Appendix E. Profiles show only material removed due to direct impact from the jet and do not account for rock removal from separation cells, undercutting and collapse of overhanging materials, or other methods of rock removal.

8.1 Plunge Pool Depth

Modeled results of plunge pool depth and the corresponding surveyed depths for each dam site are presented in Table 8.1. Surveyed plunge pool depths used for comparison were adjusted for infilling with sediment by assuming that only plunge pool deepening occurred over time. As a result, the deeper of the current and previous surveyed plunge pool depths over the series of survey data for each dam was used for comparison. In the table both surveyed and modeled depth were calculated by subtracting the deepest point of scour from a base elevation representing pre-spillway operation plunge pool conditions. Differences were calculated such that negative values indicate shallower modeled plunge pool depth than surveyed depth. Positive difference values indicate deeper modeled plunge pool depth than surveyed depth. In some cases characterized by 'Low' erodibility index profiles scour progressed past the lowest modeled elevation of the plunge pool. The scour depth for these cases is recorded as the maximum depth of the profile and a "+" symbol to indicate scour progression below this depth. Values including the "+" symbol represent a minimum depth or difference value and may be greater.

'Mean' and 'High' modeled and surveyed depths were fit to a one-to-one linear regression line. Goodness of fit of the line was assessed based on both the coefficient of determination (R^2 value) and the standard error of the estimate. 'Low' modeled depth values were not fit to linear regressions due to the number of uncertain values that exceeded the limits of the modeled profiles in the cases of the Seven Mile and Revelstoke Dams.

Table 8.2 provides a summary of the results of the plunge pool depth statistics for all combined dam sites, only dam sites with flip bucket type energy dissipaters, dam sites with sedimentary plunge pools (PCN and WAC), and dam sites with metamorphic plunge pools (SEV and REV).

Table 8.1 Model plunge pool depth results and comparison with surveyed depths

	Survey Date	Adjusted Survey Depth[2] (ft)	Modeled Depth[3] (ft)			Difference Survey vs. Modeled[4] (ft)		
			Low	Mean	High	Low	Mean	High
PCN-34	10/30/1979							
	4/15/1980	40	49	37	4	9	-3	-36
	9/5/1981	40	49	37	4	9	-3	-36
	10/1/1983	40	49	37	4	9	-3	-36
	10/8/1985	40	49	37	4	9	-3	-36
	8/4/1996	40	74	46	19	34	6	-21
	6/12/2007	43	74	46	19	31	3	-24
PCN-56	10/30/1979							
	4/15/1980	22	67	11	0	45	-11	-22
	9/5/1981	27	67	11	0	40	-16	-27
	10/1/1983	27	67	11	0	40	-16	-27
	8/4/1996	27	83	17	0	56	-10	-27
	6/12/2007	27	84	20	0	57	-7	-27
SEV-12	10/30/1979							
	12/14/1979	24	125	38	0	101	14	-24
	8/1982	49	200+	89	45	151+	40	-4
	9/20/1984	49	200+	89	45	151+	40	-4
	10/15/1986	49	200+	89	45	151+	40	-4
	10/1/1988	52	200+	89	45	148+	37	-7
	11/18/1997	52	200+	89	45	148+	37	-7
	12/9/2011	52	200+	89	45	148+	37	-7
REV-1	1979							
	5/15/1984	30	400+	200	69	370+	170	39
	8/11/1986[1]	40	400+	200	69	360+	160	29
	9/22/1991	40	400+	200	69	360+	160	29
	7/24/2002	40	400+	200	69	360+	160	29
WAC-C	6/13/1972							
	5/19/1973	91	228	126	94	137	35	3
	8/4/1996	105	228	126	94	123	21	-11
	10/1/2002	105	228	126	94	123	21	-11

Note: [1]Deepest surveyed point of the 1986 Revelstoke plunge pool survey, not along profile line; [2]Adjusts for plunge pool sediment infilling by assuming the deeper of the current and previous plunge pool depths over the series of survey dates for each dam; [3]Numbers followed by a "+" indicate scour progression below the modeled profile level and the value represents the lowest modeled profile level; [4]Positive values indicate deeper modeled than surveyed scour and negative values indicate shallower modeled than surveyed scour.

Table 8.2 Modeled depth vs. surveyed depth goodness of fit statistics

Dam Sites	R^2 *		Standard Error (ft)	
	Mean	High	Mean	High
All Dam Sites	n/a	0.47	71.6	24.8
Flip Bucket	0.62	0.53	25.2	23.0
Sedimentary Dam Sites (PCN & WAC)	0.88	0.51	15.7	27.8
Metamorphic Dam Sites (SEV & REV)	n/a	n/a	112.9	23.1

Note: * R^2 value representative of one-to-one relationship between modeled and surveyed values, not necessarily the statistical line of best fit; "n/a" values for R^2 indicate no degree of one-to-one relationship was attainable.

Plots of the modeled versus surveyed depth values were generated for 'Mean' modeled depths, 'High' modeled depths, and valid 'Low' modeled depths for each dam site. These plots are shown in Figure 8.1, A through D. For reference the one-to-one ideal relationship between the two values is also shown in these figures. Results are plotted with the surveyed values on the x-axis and the modeled values on the y-axis. The combined results for all dam sites are shown in Figure 8.2, and results for only dam sites with flip bucket type energy dissipaters – i.e. Peace Canyon, Seven Mile, and W.A.C. Bennett Dams – are shown in Figure 8.3.

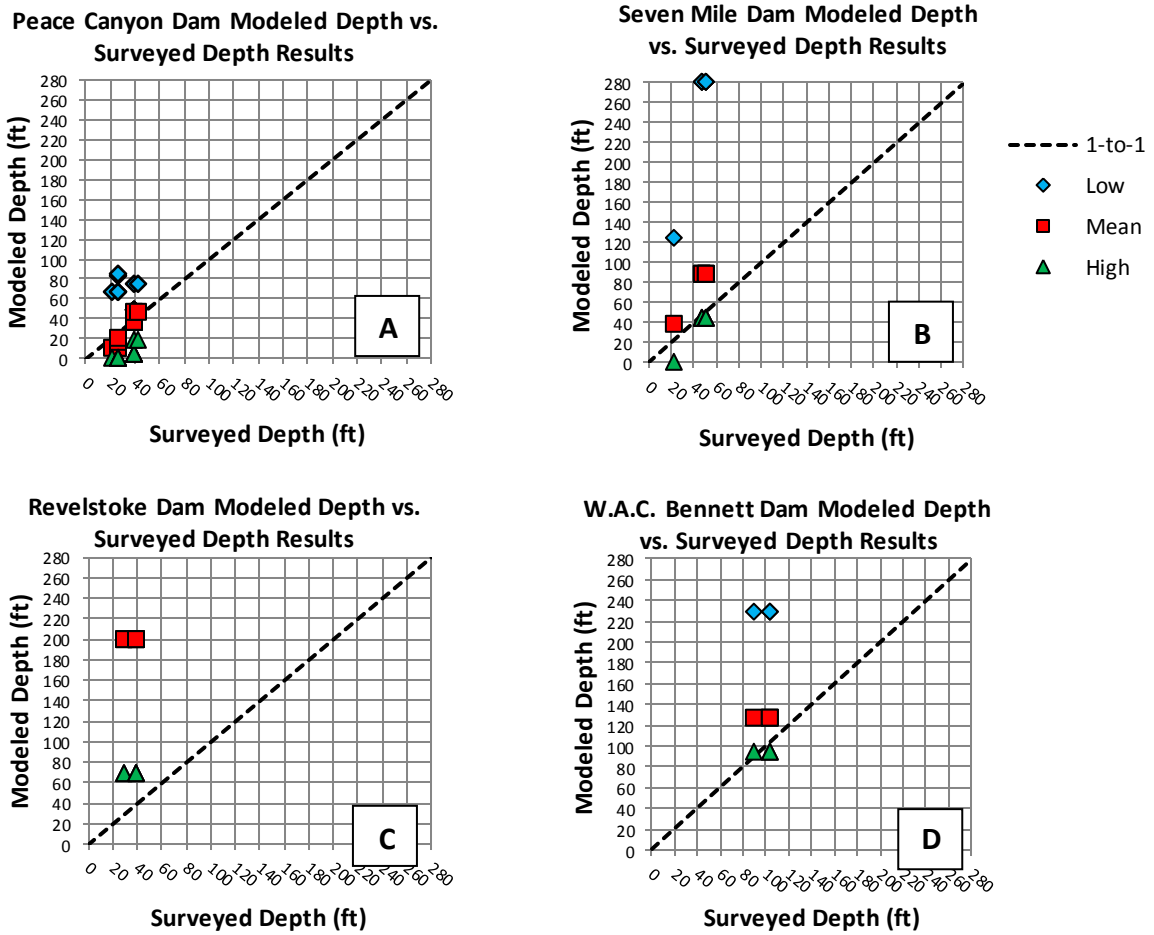

Figure 8.1 Modeled depth vs. surveyed depth results for all dam sites (individual)

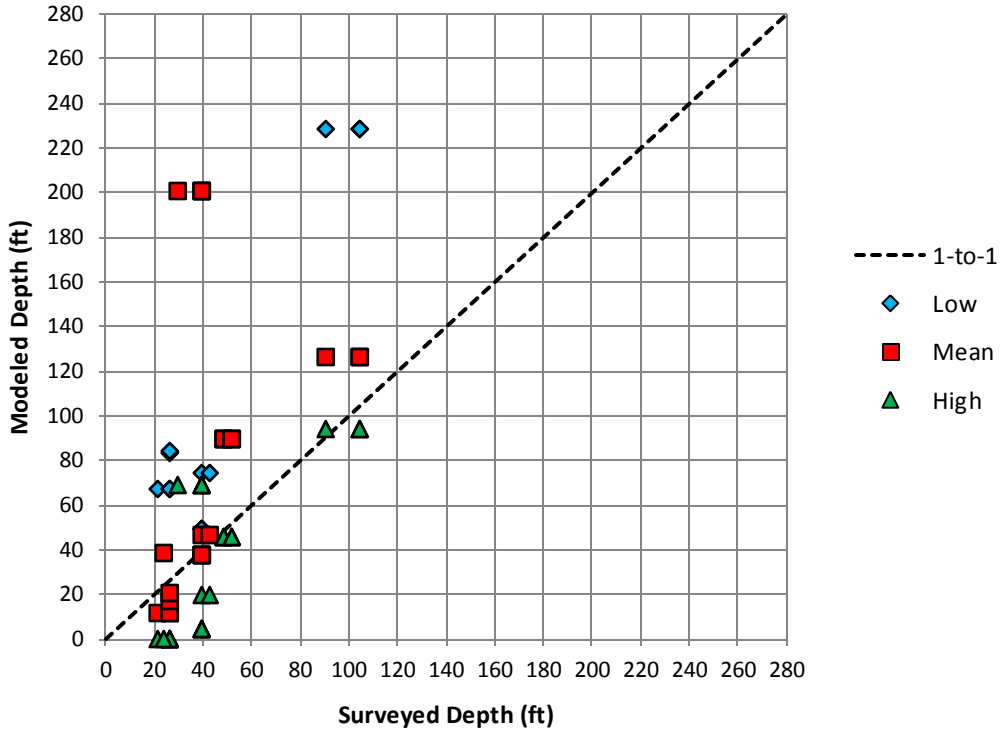

Figure 8.2 Modeled depth vs. surveyed depth results for all dam sites (combined)

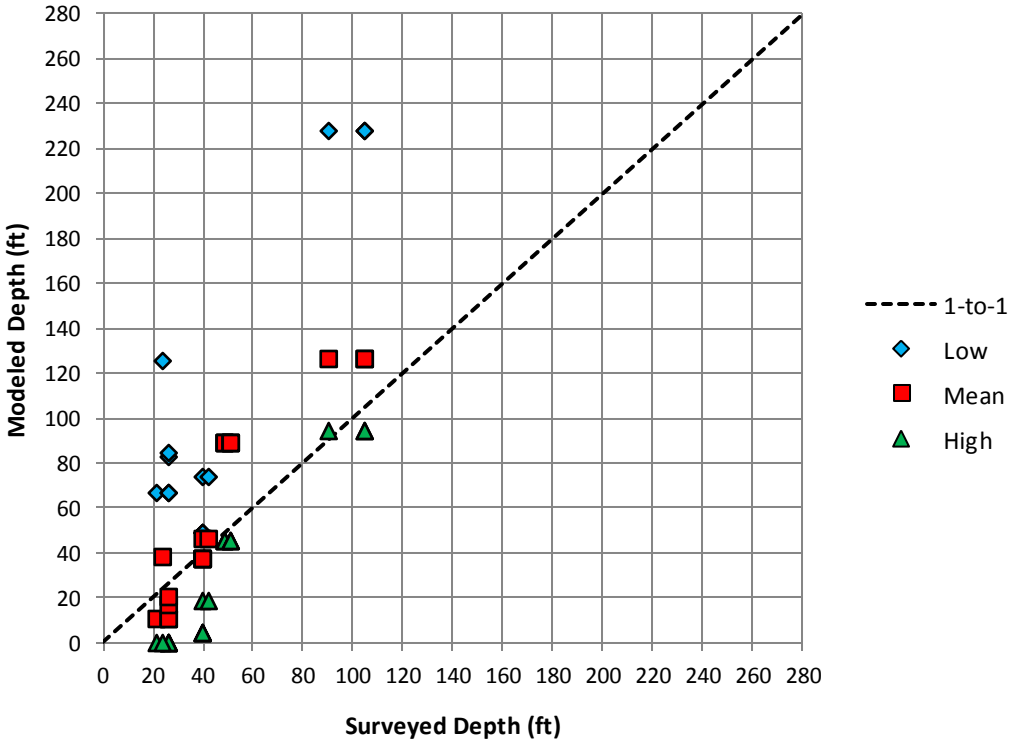

Figure 8.3 Modeled depth vs. surveyed depth results for dam sites with flip bucket energy dissipaters (combined)

8.2 Plunge Pool Invert Distance Downstream of Spillway

Modeled results of plunge pool invert distance downstream of the spillway and the corresponding surveyed distances for each dam site are presented in Table 8.3 (page 108). In the table both surveyed and modeled distances were measured downstream of the flip bucket or free overfall lip for each dam site. Differences between modeled and surveyed values were calculated such that negative values indicate that the modeled plunge pool invert is nearer to the spillway than the surveyed invert. Positive difference values indicate that modeled plunge pool invert is farther from the spillway than the surveyed invert. In some cases, characterized by 'Low' erodibility index profiles, scour progressed past the lowest modeled elevation of the plunge pool. The scour distance for these cases is not recorded in the table, as an accurate representation was not achievable.

'Mean' and 'High' modeled and surveyed distance values were fit to a one-to-one linear regression line. Goodness of fit of the line was assessed based on both the coefficient of determination (R^2 value) and the standard error of the estimate. 'Low' modeled distance values were not fit to linear regressions due to the number of uncertain values where scour exceeded the limits of the modeled profiles in the cases of the Seven Mile and Revelstoke Dams.

Table 8.4 (page 109) provides a summary of result statistics for all dam sites, dam sites with flip bucket type energy dissipaters, dam sites with sedimentary plunge pools (PCN and WAC), and dam sites with metamorphic plunge pools (SEV and REV) for 'Mean' and 'High' erodibility index values.

Plots of the modeled versus surveyed invert distance downstream of the spillway were generated for 'Mean' modeled distances, 'High' modeled distances, and valid 'Low' modeled distances for each dam site. These plots are shown in Figure 8.4, A through D (page 109). For reference the one-to-one ideal relationship between the two values is also shown in the figures.

The combined results for all dam sites are shown in Figure 8.5 (page 110), and combined results for dam sites with flip bucket type energy dissipaters – ie. Peace Canyon, Seven Mile, and W.A.C. Bennett Dams – are shown in Figure 8.6 (page 110).

Table 8.3 Model plunge pool invert distance downstream of spillway results and comparison with surveyed distances

	Survey Date	Survey Distance (ft)	Modeled Distance[2] (ft)			Difference Survey vs. Modeled[3] (ft)		
			Low	Mean	High	Low	Mean	High
PCN-34	10/30/1979							
	4/15/1980	273	283	256	183	10	-18	-90
	9/5/1981	218	283	256	183	65	38	-35
	10/1/1983	353	283	256	183	-70	-97	-170
	10/8/1985	263	283	256	183	20	-8	-80
	8/4/1996	220	309	269	223	90	50	3
	6/12/2007	196	308	269	223	113	74	27
PCN-56	10/30/1979							
	4/15/1980	229	296	171	n/a[4]	67	-58	n/a[4]
	9/5/1981	180	296	171	n/a[4]	116	-10	n/a[4]
	10/1/1983	229	296	171	n/a[4]	67	-58	n/a[4]
	8/4/1996	233	330	187	n/a[4]	97	-47	n/a[4]
	6/12/2007	260	319	196	n/a[4]	59	-65	n/a[4]
SEV-12	10/30/1979							
	12/14/1979	318	339	245	249	21	-74	-69
	8/1982	389	n/a	356	305	n/a	-34	-85
	9/20/1984	381	n/a	356	305	n/a	-26	-77
	10/15/1986	399	n/a	356	305	n/a	-43	-94
	10/1/1988	370	n/a	356	305	n/a	-15	-66
	11/18/1997	392	n/a	356	305	n/a	-36	-87
	12/9/2011	356	n/a	356	305	n/a	-1	-52
REV-1	1979							
	5/15/1984	330	n/a	292	225	n/a	-39	-106
	8/11/1986[1]	378	n/a	292	225	n/a	-87	-154
	9/22/1991	237	n/a	292	225	n/a	55	-12
	7/24/2002	308	n/a	292	225	n/a	-17	-84
WAC-C	6/13/1972							
	5/19/1973	713	924	843	835	211	130	122
	8/4/1996	761	924	843	835	163	82	74
	10/1/2002	640	924	843	835	284	203	195

Note: [1]Deepest surveyed point of the 1986 Revelstoke plunge pool survey, not along profile line; [2]Cases where scour proceeded beyond the extent of the profile are represented by "n/a"; [3]Positive values indicate deeper modeled than surveyed scour and negative values indicate shallower modeled than surveyed scour; [4]no scour occurred.

Table 8.4 Modeled distance downstream of invert vs. surveyed distance downstream of invert statistical relationships

Dam Sites	R^{2*}		Standard Error (ft)	
	Mean	High	Mean	High
All Dam Sites	0.87	0.79	72.0	100.2
Flip-Bucket	0.89	0.82	75.1	99.8
Sedimentary Dam Sites (PCN & WAC)	0.89	0.86	89.7	111.0
Metamorphic Dam Sites (SEV & REV)	n/a	n/a	50.3	96.0

Note: * R^2 value representative of one-to-one relationship between modeled and surveyed values, not necessarily the statistical line of best fit; "n/a" values for R^2 indicate no degree of one-to-one relationship was attainable.

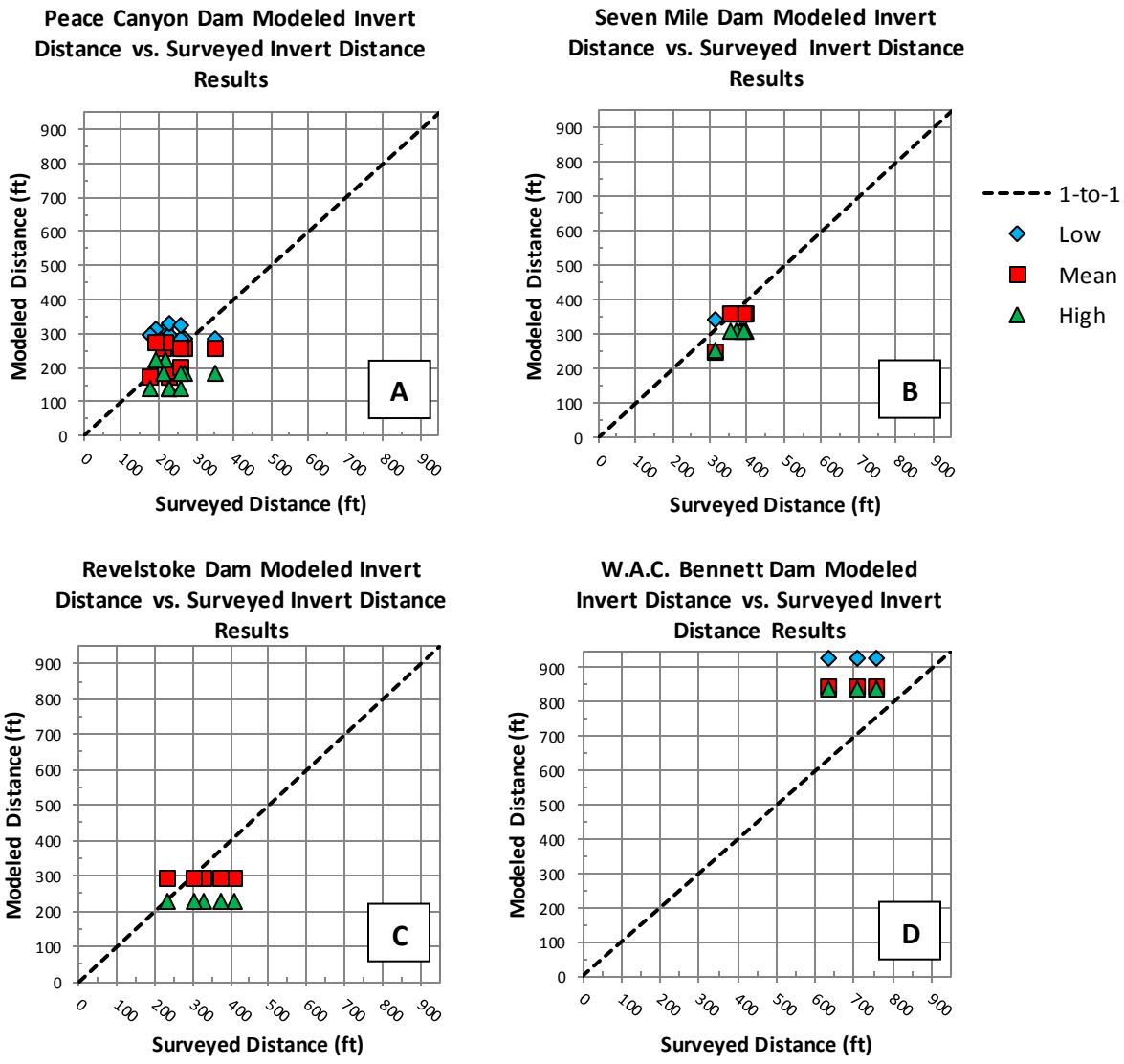

Figure 8.4 Modeled distance downstream of invert vs. surveyed distance downstream of invert results for all dam sites (individual)

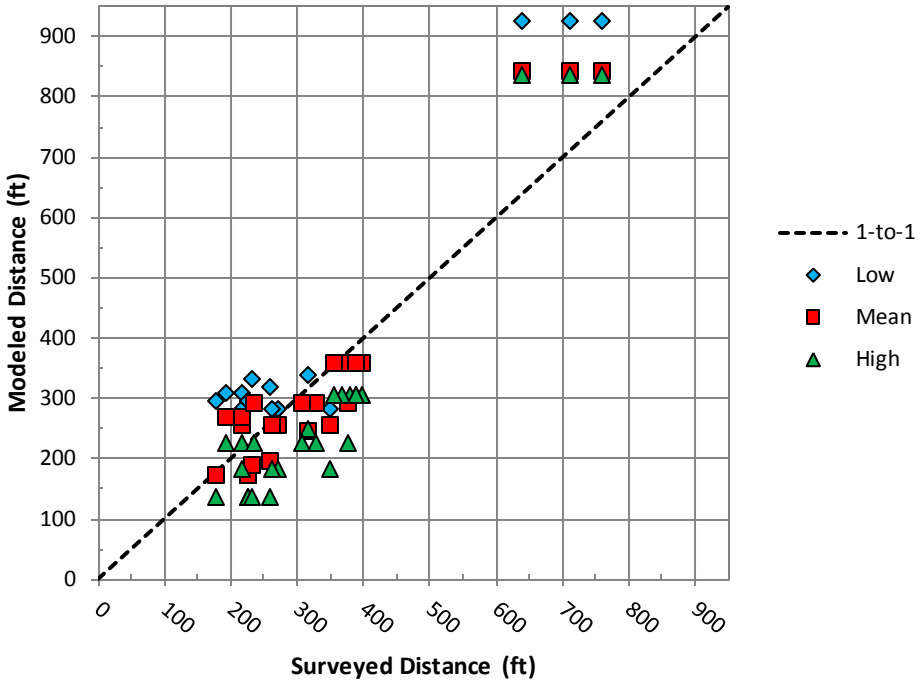

Figure 8.5 Modeled distance downstream of invert vs. surveyed distance downstream of invert results for all dam sites (combined)

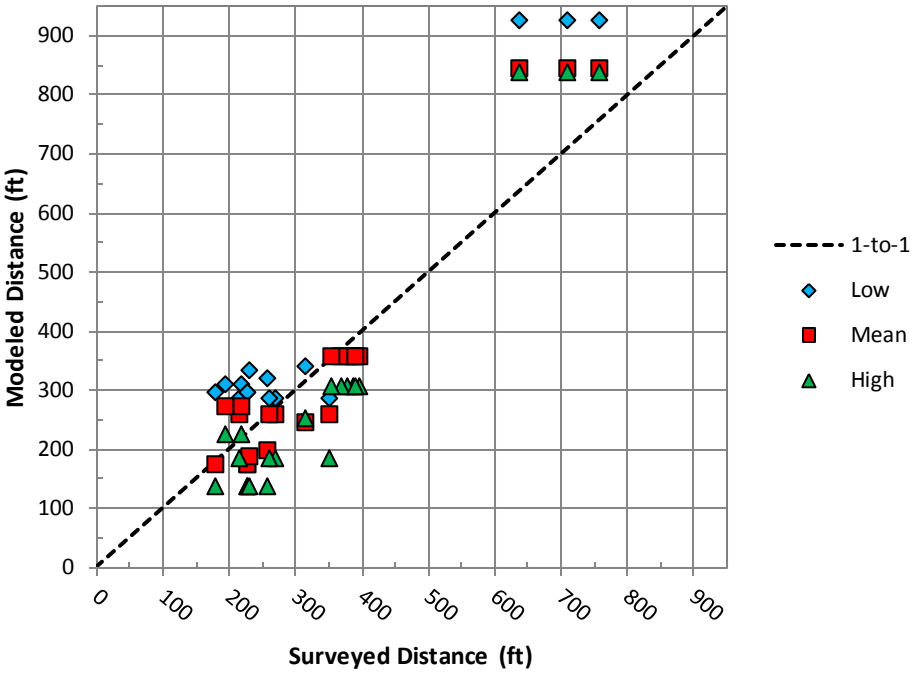

Figure 8.6 Modeled distance downstream of invert vs. surveyed distance downstream of invert results for dam sites with flip bucket energy dissipaters (combined)

8.3 Cumulative Energy vs. Depth

In addition to comparisons of surveyed versus modeled depth, relationships between the cumulative energy imparted to the plunge pool and the surveyed depth, modeled depth, and difference in depth were also assessed. Table 8.5 shows the cumulative energy (in mega joules) imparted to the plunge pool by the jets for each survey date. Cumulative energy is calculated as the integral, over time, of the product of stream power and duration.

Table 8.5 Cumulative energy imparted to plunge pool by survey date

	Survey Date	Cumulative Energy (MJ)
PCN-34	10/30/1979	-
	4/15/1980	9.27×10^{7}
	9/5/1981	2.80×10^{8}
	10/1/1983	4.48×10^{8}
	10/8/1985	4.86×10^{8}
	8/4/1996	2.72×10^{9}
	6/12/2007	3.38×10^{9}
PCN-56	10/30/1979	-
	4/15/1980	5.55×10^{7}
	9/5/1981	1.20×10^{8}
	10/1/1983	2.13×10^{8}
	8/4/1996	9.04×10^{8}
	6/12/2007	1.06×10^{9}
SEV-12	10/30/1979	-
	12/14/1979	7.33×10^{8}
	8/1982	8.11×10^{9}
	9/20/1984	1.09×10^{10}
	10/15/1986	1.27×10^{10}
	10/1/1988	1.28×10^{10}
	11/18/1997	2.68×10^{10}
	12/9/2011	3.76×10^{10}
REV-1	1979	-
	5/15/1984	3.19×10^{9}
	8/11/1986[1]	3.75×10^{9}
	9/22/1991	3.75×10^{9}
	7/24/2002	4.08×10^{9}
WAC-C	6/13/1972	-
	5/19/1973	1.06×10^{10}
	8/4/1996	3.37×10^{10}
	10/1/2002	3.69×10^{10}

Plots of the surveyed depth, modeled depth, and difference between surveyed and modeled depth versus cumulative energy for the 'Mean' and 'High' cases and the associated best fit lines are provided in Figure 8.7, Figure 8.8, and Figure 8.9 for all dam sites. Tabulated data for the goodness of fit of the trendlines, including standard error and R^2 values, are provided in Table 8.6. Note that plotted distances have been converted to meters to correspond with the units of cumulative energy; distances in Table 8.6 are provided in both feet and meters.

Similar plots for dam sites with flip bucket energy dissipaters are provided in Figure 8.10, Figure 8.11, and Figure 8.12 (pages 113-114). Tabulated data for the goodness of fit of the trend lines is provided in Table 8.7 (page 114).

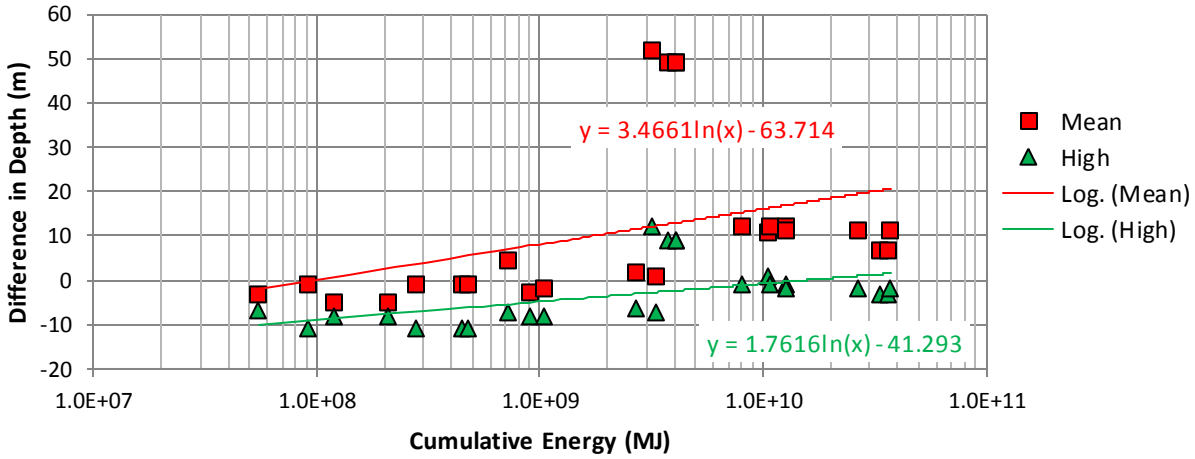

Figure 8.7 Cumulative energy vs. differences between surveyed and modeled depth (in meters) for all dam sites.

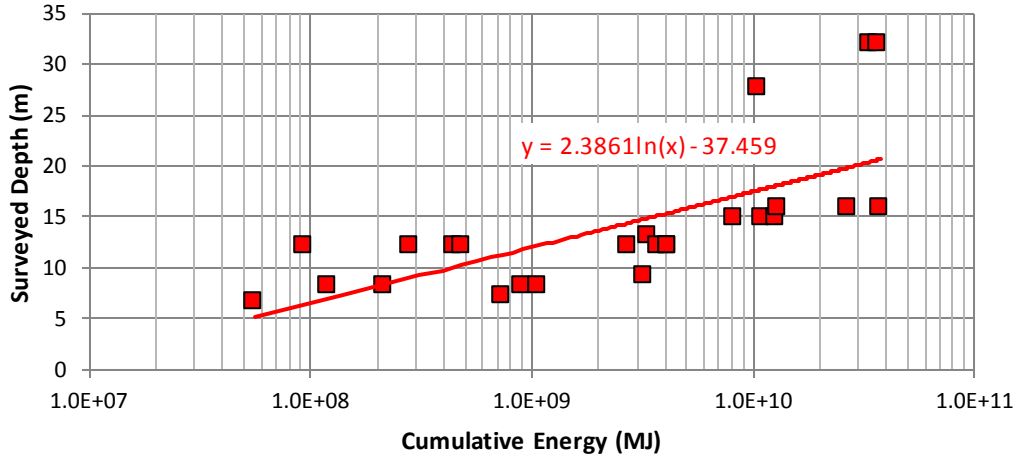

Figure 8.8 Cumulative energy vs. surveyed plunge pool depth (in meters) for all dam sites.

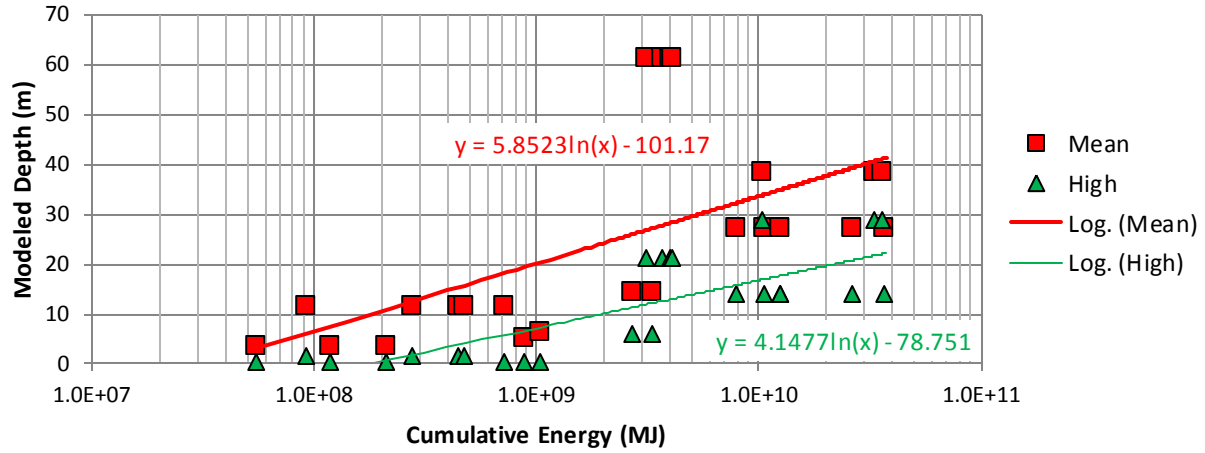

Figure 8.9 Cumulative energy vs. modeled plunge pool depth (in meters) for all dam sites.

Table 8.6 Cumulative Energy goodness of fit statistics for all dam sites.

Cumulative Energy vs.	R^2		Standard Error ft (m)	
	Mean	High	Mean	High
Depth Difference	0.14	0.26	56.2 (17.1)	19.4 (5.9)
Surveyed Depth	0.47	n/a	16.8 (5.1)	n/a
Modeled Depth	0.35	0.63	52.5 (16.0)	21.0 (6.4)

Note: R^2 and standard error values correspond to equations provided in Figure 8.7, Figure 8.8, and Figure 8.9; [1]Surveyed depth is the same between 'Mean' and 'High' cases and is therefore only provided once.

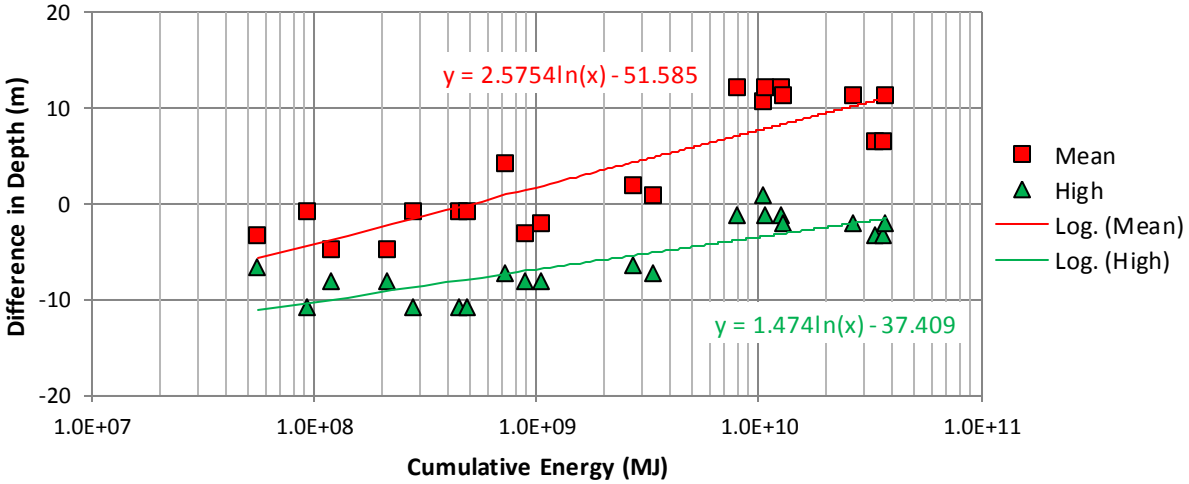

Figure 8.10 Cumulative energy vs. differences between surveyed and modeled depth (in meters) for dam sites with flip bucket type energy dissipaters.

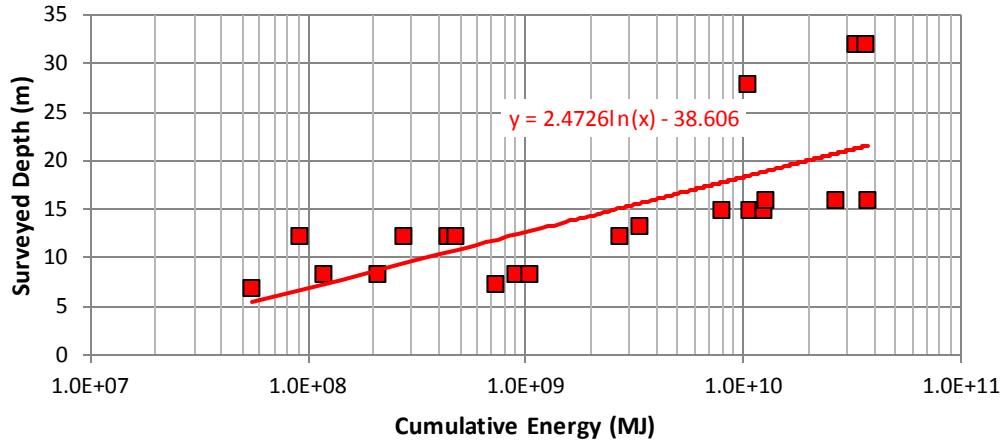

Figure 8.11 Cumulative energy vs. surveyed plunge pool depth (in meters) for dam sites with flip bucket type energy dissipaters.

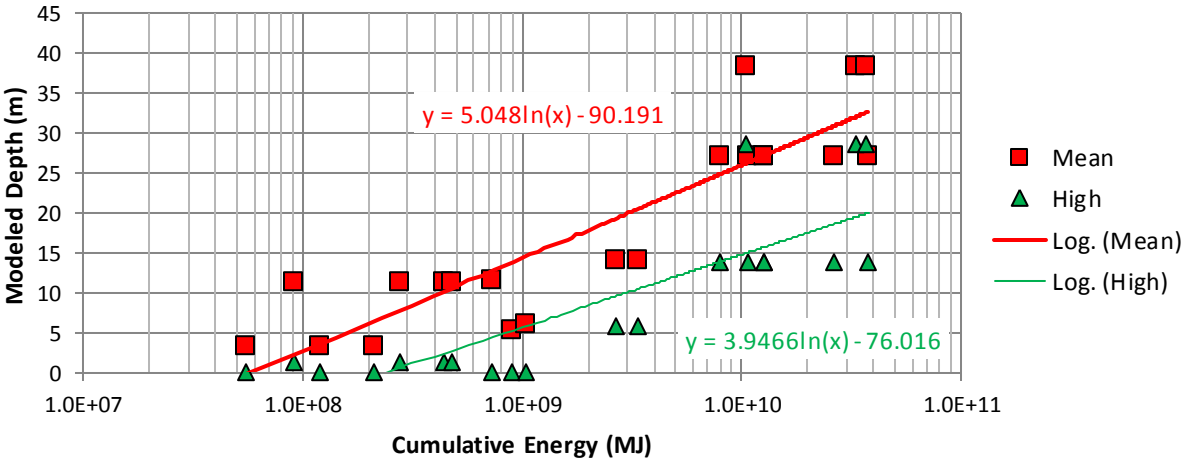

Figure 8.12 Cumulative energy vs. modeled plunge pool depth (in meters) for dam sites with flip bucket type energy dissipaters.

Table 8.7 Cumulative Energy goodness of fit statistics for dam sites with flip bucket type energy dissipaters.

Cumulative Energy vs.	R^2		Standard Error ft (m)	
	Mean	High	Mean	High
Depth Difference	0.74	0.67	11.0 (3.4)	7.4 (2.3)
Surveyed Depth[1]	0.52	n/a	17.3 (5.3)	n/a
Modeled Depth	0.79	0.70	18.5 (5.7)	18.6 (5.7)

Note: R^2 and standard error values correspond to equations provided in Figure 8.10, Figure 8.11 and Figure 8.12; [1]Surveyed depth is the same between 'Mean' and 'High' cases and is therefore only provided once.

CHAPTER 9

DISCUSSION

In what follows, the results outlined in Chapter 8 and limitations and potential sources of error within the analysis are discussed to assess the significance of the results.

9.1 Plunge Pool Depth and Downstream Distance of Invert

Satisfactory comparison between modeled and surveyed scour profiles depends on the availability and quality of geologic information and the ability to representatively quantify the temporal and spatial distribution of the stream power of plunging jets. Scour occurs when the stream power of a jet is greater than the ability of rock to resist it, as determined from the Erodibility Index scour threshold developed by Annandale (1995). Superior knowledge of the spatial distribution of the ability of earth material to resist scour combined with superior knowledge of the spatial and temporal distribution of jet stream power provides greater ability to accurately predict scour of rock. This research contributed to this understanding by not only mapping scour resistance of rock in two dimensions, but by also quantifying the stream power of jets and its decay in two dimensions. This allowed modeling scour profiles in two dimensions by comparing the scour resistance of rock to the stream power of the jet in spatial context.

The data that was available for the four case studies included regular plunge pool surveys, geologic information in the vicinity of the plunge pools (rarely within the plunge pools themselves), plans of the spillways and records of flow releases through the spillways. Satisfactory implementation of the Erodibility Index Method (Annandale, 1995; 2006) to quantify the scour resistance of rock requires representative records of rock mass strength (UCS); RQD and the number of joint sets (persistence); joint aperture, roughness and gouge; and the joint orientation and shape of rock blocks (Annandale 1995, 2006). Although geologic records exist for the case studies, they are fairly old and incomplete; not containing the most critical information. Significant amounts of judgment were required to map and extrapolate the geologic profiles representing scour resistance; more judgment was required in some cases than in others. In the cases of Peace Canyon and W.A.C. Bennett Dams the available geologic information could be used to develop two-dimensional maps of scour resistance in the vertical dimension. This was not possible in the cases of Seven Mile and Revelstoke Dams due to the lack of adequate geologic data.

The second set of information required to estimate scour relates to jet stream power and its decay, which was quantified by making use of hydraulic theory. The research project analyzed two types of spillways, viz. three flip buckets and one channel spillway with a free overfall at its end. Recent published

research about energy dissipation of flip buckets (Pfister, 2014) proved very useful to quantify jet stream power and its decay at Peace Canyon, W.A.C. Bennett and Seven Mile Dams. By contrast, this research revealed that the ability to quantify the energy dissipation of flowing water in long channel spillways and the ability to quantify the dissipation of jet energy emanating from such spillways and falling over long distances may be lacking.

Figure 9.1 and Figure 9.2 compares simulated and actual scour at Peace Canyon Dam Bays 3 and 4, and Bays 5 and 6 respectively. It is noted that the maximum scour depth is correctly modeled in the case of Bays 3 and 4, but that the lateral extent of the scour is not. The reason for this is that the model developed during this research project does not allow for slope failure, neither does it simulate the effect of flows escaping from the plunge pool nor for deposition and abrasion by rock previously scoured.

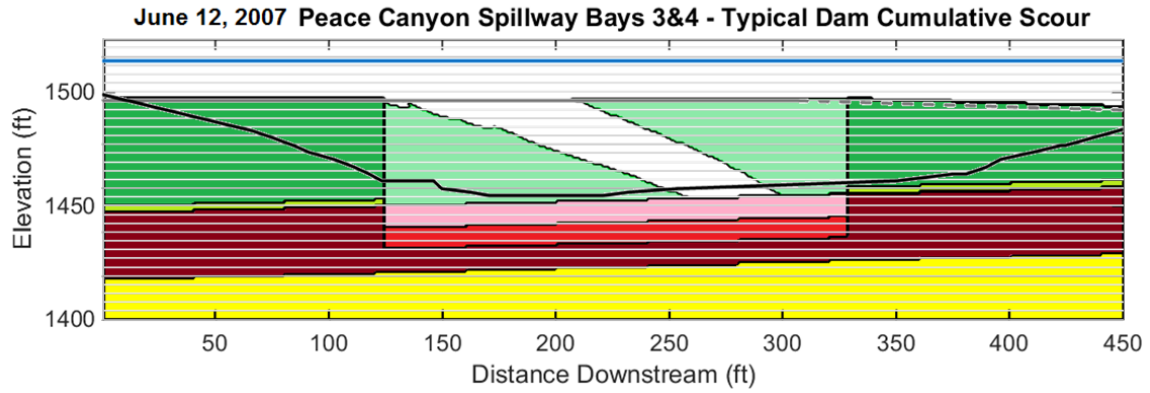

Figure 9.1 PCN-34 final modeled and surveyed plunge pool configuration, based on Peace Canyon Dam June 12, 2007 survey (Hatch Eng. Report No. H326590, 2007).

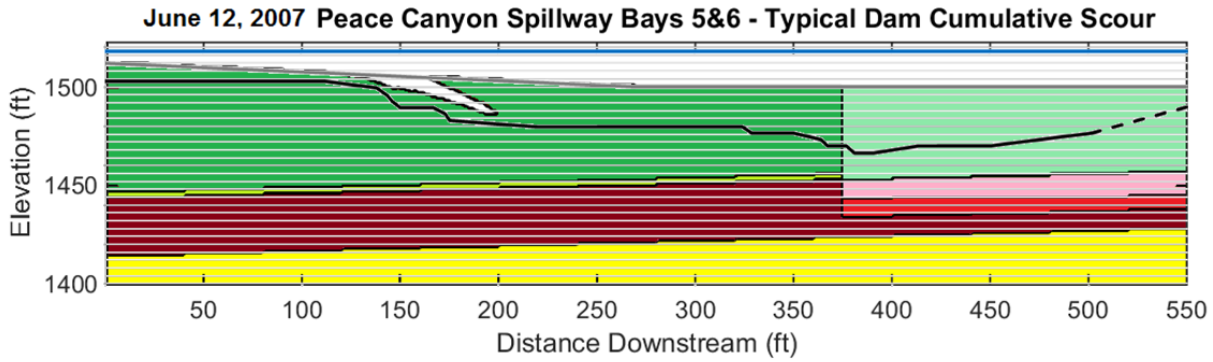

Figure 9.2 PCN-56 final modeled and surveyed plunge pool configuration, based on Peace Canyon Dam June 12, 2007 survey.

In the case of Bays 5 and 6 at Peace Canyon Dam (Figure 9.2) the maximum lateral extent of the simulated scour reaches about 200 ft downstream and closely resembles the surveyed scour depth at that location. When studying the survey plans of the scour hole at Peace Canyon Dam it is concluded that the deeper portion of the plunge pool, at about 400 ft downstream, most likely formed as the result of water flowing from Bays 3 and 4 along the more highly eroded hinge zone. It is unlikely that it resulted from the impinging jets from Bays 5 and 6. As outlined previously, the model developed during this research does not simulate the scour observed more than 200 ft to 300 ft downstream of the spillway flip.

The profile modeled along the W.A.C. Bennett plunge pool, shown in Figure 9.3, also displays good agreement between modeled and surveyed depths from October 2002, as well as overall location of plunge pool scour. Scour at this site is dependent on the location of the more resistant sandstone layer at depth.

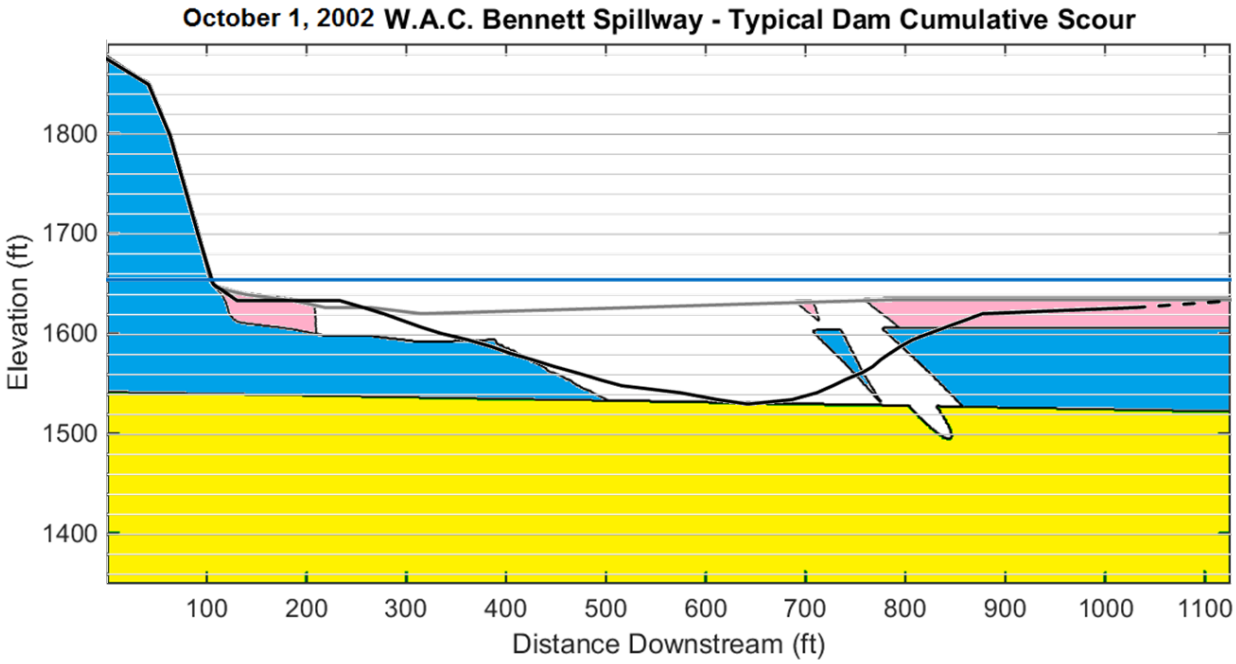

Figure 9.3 WAC-C final modeled and surveyed plunge pool configuration, based on the October 2002 W.A.C. Bennett tailrace survey.

Based on the comparisons in Figure 9.1, Figure 9.2 and Figure 9.3 it is reasonable to conclude that the availability of geologic information, which allowed for more accurate estimates of the spatial distribution of the scour resistance of the rock, coupled with the reliable quantification of the stream power of jets emanating from the flip buckets make it possible to reliably estimate maximum scour depth and the location of the point of maximum scour depth.

In the case of Seven Mile Dam a lesser amount of geologic information was available, and it was not possible to distinguish the variation in scour resistance of the rock in the plunge pool as a function of location within the plunge pool. However, the stream power of the jet projecting from the flip bucket at Seven Mile Dam could be determined using the same theory applied at Peace Canyon and W.A.C. Bennett Dams. Figure 9.4 shows that the maximum scour depth modeled at Seven Mile Dam is deeper than observed, which may be due to underestimating the scour resistance of the rock as a function of location within the plunge pool. It is also noted that the location of the calculated point of maximum scour is closer to the dam than the surveyed location. This is attributed to the fact that the hydraulics within the plunge pool are not dynamically simulated, thereby not accounting for the scour that may occur downstream of the theoretical impingement point of the jet. Although this result is not completely satisfactory, it is noted that the general tendency of the scour hole geometry is similar between what was modeled and observed. Overestimating the scour may, from a practical point of view, be acceptable as it is conservative.

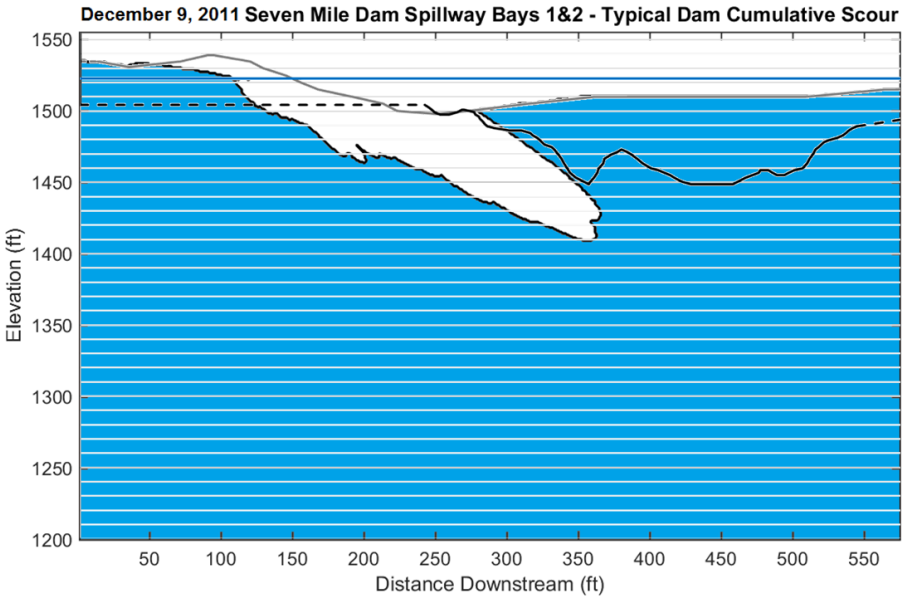

Figure 9.4 SEV-12 final modeled and surveyed plunge pool configuration, based on the December 9, 2011 Seven Mile Dam tailrace survey.

Figure 9.5 illustrates how poor characterization of the geology and inadequate quantification of jet stream power can lead to unsatisfactory results. The big difference between modeled and surveyed scour is likely due to poor geologic characterization, poor quantification of the stream power of the jet, poor quantification of the decay of stream power and an inability to correctly calculate the jet trajectory.

.

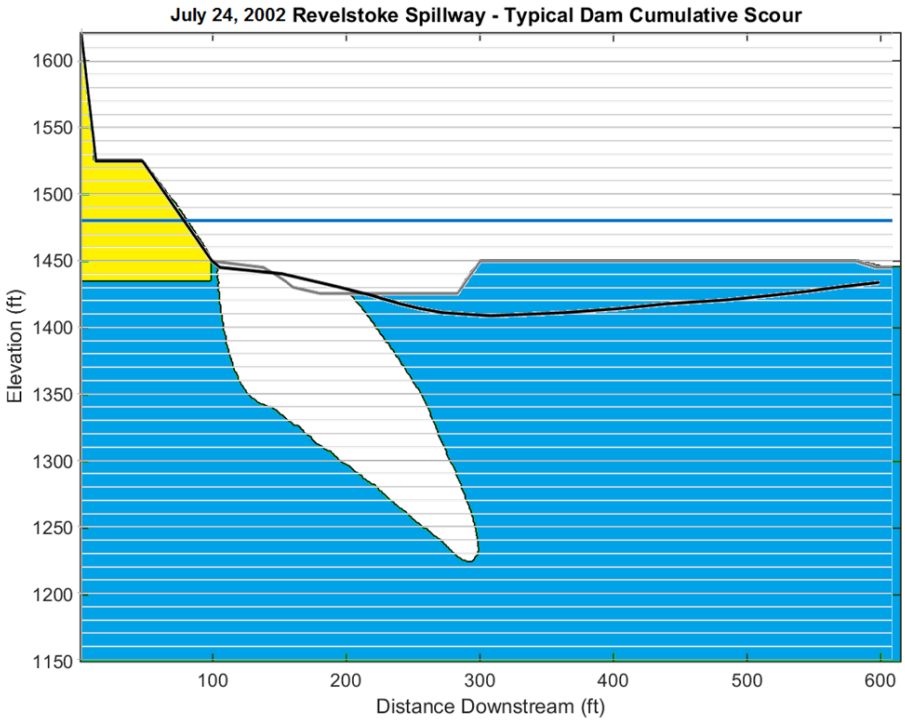

Figure 9.5 REV final modeled and surveyed plunge pool configuration, based on the July 24, 2002 Revelstoke tailrace survey.

In summary, Figure 9.1 to Figure 9.4 illustrate the importance of detailed geologic characterization and correct understanding of how the stream power of flowing water changes as a function of space. Rock core logs taken from plunge pools (or their predicted location) showing strength (UCS), RQD, joint aperture, roughness and alteration are required. Additionally, mapping of joint sets to establish joint persistence, dip angle, and dip direction of discontinuities form part of the information required to quantify the scour resistance of rock. This data is used in Annandale's Erodibility Index Method (Annandale 1995; 2006) to quantify the ability of rock to resist stream power.

The research also emphasizes the importance of quantifying the stream power of flowing water. This may be accomplished by making use of proven hydraulic theory (such as the theory of jets projected from flip buckets (Pfister, 2014). The simplified approach to hydraulic flow prediction used in the model developed during this assessment may be enhance by making use of Three-Dimensional Computational Fluid Dynamics (CFD) software. Such information may help to more accurately predict the shape and lateral extent of scour holes. Executing such hydraulic modeling was beyond the scope of this assessment and may form the basis of future research by others

9.2 Cumulative Energy vs. Depth

The logarithmic nature of the cumulative energy versus the modeled depth, surveyed depth, and difference in depth indicates that the rate of scour decreases over time as each plunge pool develops. Due to this decrease higher magnitude discharge events are required to enact change within the plunge pool, based on data for the dam sites with flip bucket type energy dissipaters. This result is not unexpected and is observed not only in the modeled depths versus cumulative energy, but in the surveyed depths versus cumulative energy as well. In addition, the plot between depth difference and cumulative energy indicates greater variance between modeled and surveyed plunge pool depths with larger cumulative energy inputs; as more energy is absorbed within the plunge pool and underlying rock material, more uncertainty exists within the model.

The comparison between the various depth parameters and cumulative energy introduces a temporal aspect to the analysis. The temporal distribution of the discharge events plays an important role in plunge pool development and merits further study. Scour rate and cumulative energy merit further research to assess the strength, significance, and implications of the relationship between the two.

9.3 Limitations and Sources of Error

This analysis is a two-dimensional simplification of a complex three-dimensional geologic and hydraulic environment. The simplification of such an environment is invariably subject to limitation and error. Three primary types of error were identified over the course of this analysis, including statistical error, sampling error, and methodological error. The full impact of each type of error is not quantifiable within the context of this analysis.

Statistical Error

Statistical error is introduced due to limited sample datasets for EIM input parameters including UCS, RQD, joint roughness, and joint alteration, among others. Limited sample datasets do not necessarily adequately represent the population from which they were taken and larger datasets lead to better overall estimates of rock characteristics. Larger datasets and the subsequently more representative mean and standard deviation values would improve this analysis. Limited datasets also do not reflect changes that occur in characteristic parameters with depth or distance away from structural features, which impacts the spatial distribution of the geomechanical zones used for analysis.

Sampling Error

Sampling error and bias influence results as well. The use of UCS strength laboratory testing, for example, may result in larger model input strength values due to preferential selection of the stronger, more intact pieces of rock core for testing. This leads to overestimates of overall rock mass strength. The combination of UCS strength test results with point load testing and field strength characterization will generate more realistic estimates. Unfortunately point load data and detailed geomechanical rock characterization information is not always available.

Poor drilling or sampling methods may cause core breakage, and subsequent underestimates of RQD values, which will reduce the overall erosive characterization of the rock materials.

Poor logging techniques or the use of different logging methods, standards, and interpretations between loggers and/or drill holes can also complicate the rock mass characterization.

Methodological Error

Methodological error is also introduced during modeling. The model developed for this analysis does not account for variations in discharge over the spillway during 24-hour periods, rather relying on the mean daily discharge values. Pressure fluctuations in the near-bed region due to variability in spillway discharge are likely, but not addressed here.

The model applies stream power in the vertical direction only within the plunge pool and does not account for horizontal loading on plunge pool sidewalls due to acting wall jets. This simplification is anticipated to result in a narrower expression of the scour hole at the rock-water interface than actually experienced. This limitation is considered reasonable due to the limited information on wall jets as well as observations that the most severe hydrodynamic action occurs in the impingement region (Beltaos & Rajartnam, 1973, 1974), which is addressed in this analysis. In nature, steep plunge pool sidewalls may not be expected, depending on the rock mass strength and joint orientation. Natural failures of plunge pool sidewalls and/or overhangs due to slope instability are also not accounted for in this analysis. The invert depth and location, rather, are estimated solely from the characteristics of the impacting jet. Overall plunge pool development, in terms of lateral expansion, is not addressed here.

The equations used here represent a submerged jet plunging through an open, flat bottomed plunge pool. While good as a basis for theory, submerged jets in plunge pools are often influenced by the surrounding topography. This effect can impact the mean and fluctuating pressures, as indicated by Manso's (2006) research on the influence of plunge pool geometry on energy dissipation.

Rectangular jet geometry and energy decay relationships were used for this analysis where possible. More information is available for round jets than rectangular jets, however, and some round jet relationships are used where relationships for rectangular jets have not yet been developed. In addition, most relationships have been developed for the nappe flow case, whereas jets assessed in this analysis are typically generated from flip buckets and exhibit greater jet breakup during free-fall than the nappe flow case. Overall, the understanding of jet hydraulics is still incomplete.

CHAPTER 10

CONCLUSIONS

In conclusion, this analysis indicates that Annandale's Erodibility Index Method provides an accurate assessment of potential plunge pool depth and invert location for spillways with flip bucket type energy dissipaters and relatively dense geologic data.

The best results were obtained from dam sites with a good understanding of the spatial distribution of rock materials, making this information key for good depth and distance predictions. Where geology is complex or poorly understood, every effort should be made to identify trends in EIM input parameters, including increases in rock strength or reductions in fracture aperture or density with depth.

Geologic data density is important and larger datasets tended to produce better statistical relationships in this analysis. UCS strength and RQD, especially, play key roles in this analysis. Joint aperture, roughness, and infilling are also very important, but can be approximated from field observations if required. Joint orientation, in the context of the EIM, is less straightforward and must be assessed on a site by site basis, taking into account which joint sets may be the most detrimental to stability depending on the location within the plunge pool relative to the location of the impinging jet.

Accurate calculation of hydraulic parameters is an integral step in computing realistic scour depths and invert locations. Complex spillway geometries add an additional level of difficulty here. Care should be taken to accurately evaluate these parameters using data from empirical relationships, physical models, and other sources, as available.

Complex plunge pool topography likely plays a role in the amount of energy dissipation that occurs in the plunge pool. Current relationships are based on open, flat bottomed plunge pools when in reality, plunge pool topography can be complex and contribute to energy dissipation. The influence of plunge pool topography requires further assessment for potential inclusion in future versions of this model.

CHAPTER 11

RECOMMENDATIONS

For Practical Application

- Collecting geologic information within the plunge pool should be part of the geologic investigations for future dam sites. Effort should be made to identify the spatial distribution of units within the plunge pool using boreholes, surface mapping, geophysics, and other methods as applicable. Interpolation of existing geologic maps may be appropriate if units are laterally continuous.
- Care should be taken in the calculation of input hydraulic parameters including flow velocity, depth, and issuance angle. Detailed hydraulic numerical models or the use of physical models to accurately assess these parameters is essential.
- This research could be improved by incorporating a Monte Carlo simulation into the program to assess the most probable conditions based on the ranges of the different parameters. Monte Carlo simulations are more applicable for robust datasets in which the sample is more representative of the population. This method is likely to provide a more narrow range of likely scour depths and locations based on the probability of the existence of certain conditions.
- This research should be used in conjunction with other scour-prediction tools, including physical models, and should not be used as the only means of assessing potential scour depth.

For Future Research

- This research would benefit from the inclusion of a larger dataset of dam sites with existing plunge pool surveys, including dam sites with:
    - variable geologic environments,
    - variable spillway structures, and
    - dense available geologic data.
- The research could be improved by incorporating:
    - the influence of plunge pool drawdown,
    - the influence of plunge pool topography, and
    - the influence of spillway terminal structure type on plunge pool scour.
- Energy dissipation calculations within the plunge pool and the radial energy decay that may occur could be adjusted to focus on rectangular jets, which are very common for many dam sites. More recent research by Castillo et al. (2014) on the energy dissipation of rectangular jets in plunge pools that emerged at the conclusion of this analysis should be incorporated in future work.

- The relationship between the temporal distribution of discharge events and plunge pool scour warrants further assessment to relate the cumulative energy absorbed by the plunge pool to plunge pool development.

REFERENCES CITED

Annandale, G.W., 1995, Erodibility: Journal of Hydraulic Research, v. 33, no. 4, p. 471-494.

Annandale, G.W., 2006. Scour Technology; Mechanics and Engineering in Practice, McGraw-Hill: New York, 430 p.

Beltaos, S., and Rajaratnam, N., 1973, Plane turbulent impinging jets: Journal of Hydraulic Research, v. 11, no. 1, p. 29-59.

Beltaos, S., and Rajaratnam, N., 1974, Impinging circular turbulent jets: Journal of Hydraulics Division, v. 100, no. HY10, p. 1313-1328.

Bohrer, J.G., Abt, S.R., Wittler, R.J., 1998, Predicting plunge pool velocity decay of free falling, rectangular jet: Journal of Hydraulic Engineering, v. 124, no. 10, p. 1043-1048.

Bollaert, E.F.R., 2002, Transient water pressures in joints and formation of rock scour due to high-velocity jet impact [PhD Thesis]: Laboratory of Hydraulic Constructions, Ecole Polytechnique Federale de Lausanne, Switzerland. 297 p.

Bollaert, E.F.R., 2004, A comprehensive model to evaluate scour formation in plunge pools: Hydropower and Dams issue 1.

Bollaert, EFR, Munodawafa, M.C., Mazvidza, D.Z., 2013, Kariba Dam plunge pool scour: quasi-3D numerical predictions, *in* Proceedings, International Conference on Scour and Erosion, 6th, Paris: France, Aug 2012.

Bollaert, E.F.R., and Schleiss, A.J., 2003, Scour of rock due to high velocity plunging jets: part I: a state of the art review: Journal of Hydraulic Research [Netherlands], v. 00, no. 0, p. 1-14.

Bollaert, E.F.R., and Schleiss, A.J., 2005, Physically based model for evaluation of rock scour due to high-velocity jet impact: Journal of Hydraulic Engineering, v. 131, no. 3, doi: 10.1061/(ASCE)0733-9429.

Bureau of Reclamation, PROFILE: Water Surface Profile Program for Prismatic Channels Version 1.10: US Bureau of Reclamation, U.S. Department of the Interior, US Bureau of Reclamation, Engineering Monograph No. 42, 1990.

Castillo, L.G., 2006, Aerated jets and pressure fluctuations in plunge pools, *in* Proceedings, International Conference on HydroScience and Engineering, 7th, Philadelphia: Pennsylvania, US, p. 1-23.

Castillo, L.G., 2007, Pressures characterization of undeveloped and developed jets in shallow and deep pool, *in* Proceedings, International Association of Hydraulic Engineering and Research, 32nd Congress, Venice, Italy, p. 1-10.

Castillo, L.G., Carrillo, J.M., and Blázquez, A., 2014. Plunge pool dynamic pressures: a temporal analysis in the nappe flow case: Journal of Hydraulic Research, October 2014.

Coleman, H.W., Wei, C.Y., Lindell, J.E., 1999, Chapter 17 – Hydraulic design of spillways, *in* Mays, L.W. ed. Hydraulic design handbook: McGraw Hill, New York, NY, p. 17.1-17.54.

Ervine, D.A., and Falvey, H.T., 1987, Behavior of turbulent jets in the atmosphere and in plunge pools, *in* Proceedings of the Institution of Civil Engineers, part 2, v. 83, pp. 295.

Ervine, D.A., Falvey, H.T., and Withers, W., 1997, Pressure fluctuations on plunge pool floors: Journal of Hydraulic Research, v.35, p. 295-314.

Falvey, H.T., 1990, Cavitation in chutes and spillways, Engineering Monograph No. 42, US Bureau of Reclamation.

Falvey, H.T., 2014, [Personal Correspondence] 24 Jul 2014.

Hanson, G.J. and Cook, K.R., 2004, Apparatus, test procedures, and analytical methods to measure soil erodibility in situ: Applied Engineering in Agriculture, v. 20, no. 4, pp. 455-462.

Henderson, F.M., 1966, Open Channel Flow, MacMillan, New York, 522 p.

Kachigan, S.K., 1991. Multivariate statistical analysis; a conceptual introduction, Radius Press, New York, NY.

Keaton, J.R., 2013, Estimating erodible rock durability and geotechnical parameters for scour analysis: Environmental & Engineering Geoscience, V. XIX, no. 4, p. 319-343

Kirsten, H.A.D., 1982. A classification system for excavation in natural materials: The Civil Engineer in South Africa [South Africa], July, p. 292-308.

Lewis, T.L, Abt, S.R., Ruff, J.F., Wittler, R.J., and Annandale, G.W., 1996, Erosion at dam foundations: predicting jet velocities, *in* Proceedings, Association of State Dam Safety Officials Annual Conference, Seattle: Washington, p.437-446.

Manso, P.F., 2006. The Influence of pool geometry and induced flow patterns on rock scour by high-velocity plunging jets [PhD Thesis]: Laboratory of Hydraulic Constructions, Ecole Polytechnique Federale de Lausanne, Switzerland, 330 p.

The MathWorks, Inc., 2013, MATLAB: A program for developing computer processing code: version R2013b.

Meyerhoff, G., 1956. Penetration tests and bearing capacity of cohesionless soils. J Soils Mechanics and Foundation Division ASCE, 82(SM1).

Monfette, M., 2004. Comprehensive review of plunge pool performance at four of BC Hydro dam sites and assessment of scour extent [Master's Thesis]: Vancouver, British Columbia, University of British Columbia. 222 p.

Peterka, A.J., 1987, Hydraulic design of stilling basins and energy dissipaters, USBR Engineering Monograph No. 25.

Pfister, M., Hager, W.H., Boes, R.M., 2014. Trajectories and air flow features of ski jump-generated jets. Journal of Hydraulic Research, v. 52, no. 3, pp. 336-346.

Richardson, E.V., 1996. Historical development of bridge scour evaluations, *in* Compendious of Papers ASCE Water Resources Engineering Conferences; 1991-1998, ASCE.

Rhone, T.J.,, 1964, Hydraulic Model Studies of Flaming Gorge Dam Spillway and Outlet Works, USBR Hydraulic Model Study, HYD 531.

Rouse, Hunter, 1950. Engineering hydraulics; proceedings of the fourth Hydraulics Conference, Iowa Institute of Hydraulic Research, 12-15 June 1949., 1039 p.

Schleiss, A.J., 2002, Scour evaluation in space and time – the challenge of dam designers, *in* Rock scour due to falling high-velocity jets, Proceedings of the International Workshop on Rock Scour, Lausanne: Switzerland, p. 3-22.

United States Bureau of Reclamation, 2012, Chapter 15: Erosion of rock and soil *in* Best practices and risk methodology: http://www.usbr.gov/ssle/damsafety/Risk/methodology.html (April 2014).

Wahl, T.L., Frizell, K.H., & Cohen, E.A., 2008, Computing the trajectory of free jets: Journal of Hydraulic Engineering, v. 134, no. 2, pp. 256-260.

Wibowo, J.L., D.E. Yule, and E. Villanueva, "Earth and Rock Surface Spillway Erosion Risk Assessment," Proceedings *in*, 40th U.S. Symposium on Rock Mechanics, Anchorage Alaska, 2005.

BC Hydro Documents

Peace Canyon Dam

BCH Report No. 822 – Appendix A: Site 1 Dam / Engineering Geology of Foundation Bedrock of Dam-Powerhouse-Spillway (Phase A) (by Dolmage Campbell & Associates Ltd.). December 1976.

BCH Report No. 966: Peace River / Site 1 Project / Gravity Dam and Spillway Foundation Report. December 1978.

BCH Report No. 966: Peace River / Site 1 Project / Gravity Dam and Spillway Foundation Report; Appendix A: Geological Assessment of Foundation Conditions (Phase B Structures). December 1978.

BCH Document No. 15472-03: Peace Canyon Project Drill Logs and Geological Data: Drill Hole Data Sheets Summarizing Depths of Significant Geological Features in Drill Holes. 1978.

BCH Document No. 15472-09: Peace Canyon Project Drill Logs and Geological Data: Block S1 Summary Logs and Drill Reports. 1978.

BCH Report No. GEO 9/85: Peace Canyon Project / Memorandum on Plunge Pool Development. July 1985.

BCH Report No. H1742: Peace Canyon Dam / Design Report. December 1987.

BCH Report No. OMSPCN: Peace Canyon Dam Operation, Maintenance and Surveillance Manual for Dam Safety. December 2003.

Hatch Engineering Report No. H326590: BC Hydro Peace Canyon Plunge Pool 2007 Sonar Survey. September 2007.

Seven Mile Dam

BCH Report No. H1743: Seven Mile Dam / Design Report. August 1988.

BCH System Operating Order No. 4P-36: Seven Mile Project. May 1997.

BCH Report No. MEP507: Seven Mile Dam / Deficiency Investigations / Spillway Adequacy for Extreme Floods (by Klohn-Crippen Integ and NHC). March 1999.

BCH Report No. PSE362: Seven Mile Dam / Dam Safety Improvements / Auxiliary Spillway / 1999-2000 Investigation Report. May 2001.

BCH Report No. PSE401: Seven Mile Dam / Dam Safety Improvements / Working Dam Foundation Summary. May 2002.

Revelstoke Project

BCH Report No. RO 0958-12: Columbia River Study / Geologic Report / Revelstoke Dam Sites (by V. Dolmage) October 1957.

BCH Report No. Z0671: Report to IPEC on laboratory Testing of Rock Cores, High Revelstoke Project, B.C.. November 1972.

BCH Report No. RO-0958-11: Revelstoke Project Site Geology (by L. Lane), August 1980.

BCH Report No. H1864: Revelstoke Project / Design Report. February 1988

BCH Local Operating Order No. 3PO3-47: REV-Outlet Works and Spillway Operation (Non Power Water Discharges). March 2000.

BCH Doc. No. RW9304-08: BC Hydro Plunge Pool Geology/ Revelstoke Access Project Drawings (Mike Morgan's Working Files), January 2001.

BCH Factsheet: Revelstoke Generating Station Unit 6 Project, http://www.bchydro.com/content/dam/BCHydro/customer-portal/documents/projects/revelstoke-unit-6/revelstoke-generating-station-unit-6-project-fact-sheet.pdf, June 2014.

W.A.C. Bennett Dam

BCH Report No. 150: First Report of Laboratory Testing on Soil and Rock Samples / Peace River Project (by Ripley and Associates). June 1958.

BCH Report No. 31: Report of Laboratory Testing on Rock Core Samples / Peace River Project (by Ripley and Associates). July 1958.

BCH Report No. N300: Peace River Hydroelectric Project Vol. 2 / Geology (by B.C. and B.B. Power Consultants, Ltd., December 1959.

BCH Report No. N300: Peace River Hydroelectric Project Vol. 3 / Geology / Drill Logs (by B.C. and B.B. Power Consultants, Ltd., December 1959.

V. Dolmage and D.D. Campbell. Geology of the Portage Mountain Damsite, Peace River, B.C.; Transactions, Vol. LXVI, April 1963.

BCH Report No. H2224: Portage Mountain Project / Spillway and Low Level Outlet Works (by H.K. Pratt), September 1967.

BCH Report No. H1756: Portage Mountain Development / Design Report. October 1988.

BCH Report No. E835: Williston lake Probable Maximum Flood. 2012.

APPENDIX A

EIM ROCK PARAMETER TABLES

Table A.1 Mass Strength Number for Rock (M_s)

Hardness	Identification in Profile	Unconfined Compressive Strength (MPa)	Mass Strength Number (M_s)
Very soft rock	Material crumbles under firm (moderate) blows with sharp end of geological pick and can be peeled off with a knife; is too hard to cut tri-axial sample by hand.	Less than 1.7	0.87
		1.7 - 3.3	1.86
Soft rock	Can just be scraped and peeled with a knife; indentations 1mm to 3mm show in the specimen with firm (moderate) blows of the pick point.	3.3 - 6.6	3.95
		6.6 - 13.2	8.39
Hard rock	Cannot be scraped or peeled with a knife; hand-held specimen can be broken with hammer end of geological pick with a single firm (moderate) blow.	13.2 - 26.4	17.7
Very hard rock	Hand-held specimen breaks with hammer end of pick under more than one blow.	26.4 - 53.0	35.0
		53.0 - 106.0	70.0
Extremely hard rock	Specimen requires many blows with geological pick to break through intact material.	Larger than 212.0	280.0

Note: From Kirsten, 1982

Table A.2 Joint Set Number (J_n)

Number of Joint Sets	Joint Set Number (J_n)
Intact, no or few joints/fissures	1.00
One joint/fissure set	1.22
One joint/fissure set plus random	1.50
Two joint/fissure sets	1.83
Two joint/fissure sets plus random	2.24
Three joint/fissure sets	2.73
Three joint/fissure sets plus random	3.34
Four joint/fissure sets	4.09
Multiple joint/fissure sets	5.00

Note: From Kirsten, 1982

Table A.3 Joint Roughness Number (J_r)

Joint Separation	Condition of Joint	Joint Roughness Number (J_r)
Joints/fissures tight or closing during excavation	Stepped joints/fissures	4.0
	Rough or irregular, undulating	3.0
	Smooth undulating	2.0
	Slickensided undulating	1.5
	Rough or irregular, planar	1.5
	Smooth planar	1.0
	Slickensided planar	0.5
Joints/fissures open and remain open during excavation	Joints/fissures either open or containing relatively soft gouge of sufficient thickness to prevent joint/fissure wall contact upon excavation.	1.0
	Shattered or micro-shattered clays	1.0

Note: From Kirsten, 1982

Table A.4 Joint Alteration Number (J_a)

Description of Gouge	Joint Alteration Number (Ja) for Joint Separation (mm)		
	1.0[1]	1.0-5.0[2]	5.0[3]
Tightly healed, hard, non-softening impermeable filling	0.75	-	-
Unaltered joint walls, surface staining only	1.0	-	-
Slightly altered, non-softening, non-cohesive rock mineral or crushed rock filling	2.0	2.0	4.0
Non-softening, slightly clayey non-cohesive rock mineral or crushed rock filling	3.0	6.0	10.0
Non-softening, strongly over-consolidated clay mineral filling, with or without crushed rock	3.0	6.0**	13.0
Softening or low friction clay mineral coatings and small quantities of swelling clays	4.0	8.0	13.0
Softening moderately over-consolidated clay mineral filling, with or without crushed rock	4.0	8.0**	13.0
Shattered or micro-shattered (swelling) clay gouge, with or without crushed rock	5.0	10.0**	18.0

Note: [1]Joint walls effectively in contact; [2]Joint walls come into contact after approximately 100 mm shear; [3]Joint walls do not come into contact at all upon shear; **Also applies when crushed rock occurs in clay gouge without rock wall contact; From Kirsten, 1982.

Table A.5 Relative Ground Structure Number (J_s)

Dip Direction of Closer Spaced Joint Set (degrees)	Dip Angle of Closer Spaced Joint Set (degrees)	Ratio of Joint Spacing[1], r			
		1:1	1:2	1:4	1:8[2]
180/0	90	1.14	1.20	1.24	1.26
In direction of stream flow	89	0.78	0.71	0.65	0.61
	85	0.73	0.66	0.61	0.57
	80	0.67	0.60	0.55	0.52
	70	0.56	0.50	0.46	0.43
	60	0.50	0.46	0.42	0.40
	50	0.49	0.46	0.43	0.41
	40	0.53	0.49	0.46	0.45
	30	0.63	0.59	0.55	0.53
	20	0.84	0.77	0.71	0.67
	10	1.25	1.10	0.98	0.90
	5	1.39	1.23	1.09	1.01
	1	1.50	1.33	1.19	1.10
0/180	0	1.14	1.09	1.05	1.02
Against direction of stream flow	-1	0.78	0.85	0.90	0.94
	-5	0.73	0.79	0.84	0.88
	-10	0.67	0.72	0.78	0.81
	-20	0.56	0.62	0.66	0.69
	-30	0.50	0.55	0.58	0.60
	-40	0.49	0.52	0.55	0.57
	-50	0.53	0.56	0.59	0.61
	-60	0.63	0.68	0.71	0.73
	-70	0.84	0.91	0.97	1.01
	-80	1.25	1.41	1.53	1.61
	-85	1.39	1.55	1.69	1.77
	-89	1.50	1.68	1.82	1.91
180/0	-90	1.14	1.20	1.24	1.26

Notes: [1]For intact material take $J_s = 1.0$; [2]For values of r greater than 8 take J_s as for r=8; From Kirsten, 1982.

APPENDIX B

EIM PROFILE CALCULATION PROGRAM CODE

```
% EIM_ProfileCalc
%
% Program for calculating erosion along a plunge pool profile for spillways
% with rectangular jets
%
% Created by A. Rock, 2014
%
%
% ----------------------------- CONSTANTS --------------------------------

pi = 3.14159265;
g = 32.174; %gravity (ft/s^2)
UW_Wat =  62.30; % unit weight of water @ 70oF (lb/ft^3)

% ------------------------------------------------------------------------
% ----------------------------- USER INPUTS ------------------------------
% ------------------------------------------------------------------------

% -------------------------- Hydraulic Inputs ----------------------------
uiimport('SEV_ProfileCalc_Input.csv');
pause

DamName = ' Seven Mile Dam Spillway Bays 1&2 - High';
DamAbbrev = 'SEV12 - High';

IN_DATE;
IN_TW; % tailwater elevation (ft)
IN_DI; % jet issuance diameter (ft), at flip bucket
IN_VI; % jet issuance vel. at flip bucket (ft/s)
IN_EGL; % jet issuance EGL (ft. elev), at flip bucket lip
IN_N; % Manning's roughness at flip bucket lip
IN_FR; % corrected Froude Number at issuance

% ------------------------ Spillway Parameters --------------------------
theta = 30; % average issuance angle (equal to flip bucket angle) (degrees)
z_bucket = 1554.54; % exact flip bucket elevation (ft)
z_bucket_round = round(z_bucket);
L_bucket = 116; % length of spillway at flip bucket location (ft);
%w_tailrace = 490; % width of tailrace (ft)
R = 60; % flip bucket radius (ft)
phi = atand(0.96513); % spillway face angle (deg)
beta = theta + phi;
lambda = (1 - cosd(beta)) / sind(beta) * (180 / pi);

% Spillway Terminal Structure Type
Type = 'B';
%A = free-falling rectangular jet,
%B = flip-bucket

% ------------------------ Profile Parameters --------------------------
```

```
z_maxhole = 1200; % bottom elevation of imported Karray (ft)
x_max = 575; % maximum horizontal length of profile (ft), measured out from
    % the edge of the flip bucket
x_size = x_max+1;
z_size = z_bucket_round - z_maxhole + 2; % between the tailwater elevation
    % and the the maximum scour hole depth

Karray = csvread('SEV_Karrayin_GMA_High.csv'); % Rock erodibility  matrix
Kdyn = Karray; % dynamic array originally equal to initial conditions prior
% to spillway usage, but is altered with each iteration to used to show
% reduction in elevation due to multiple records of discharge events.

%v = 1000; % plotting contour values
Maxval = 8500; % Maximum EI value, for plotting purposes

% SECTION: Generate Output File ------------------------------------------

CCC = {'Date',  'Di (ft)','Vi (ft/s)','EGL (ft)','Fr', 'TW (ft)', 'Tu',...
    'x_imp (ft)', 'Lj (ft)', 'Lb (ft)', 'H (ft)', 'D_out (ft)',...
    'ai (deg)', 'Qi (cfs)','Pjet (kW)', 'pjet (kW/m^2)',...
    'x_locale_us (ft)', 'x_locale_ds (ft)', 'z_locale (ft)'};

fid1 = fopen(strcat('1_',char(DamAbbrev),'_Results.csv'), 'a');
fprintf(fid1,'%s,%s,%s,%s,%s,%s,%s,%s,%s,%s,%s,%s,%s,%s,%s,%s,%s,%s,%s,%s,%s \r\n',
CCC{:} );
fclose(fid1);

% ------------------------------------------------------------------------
% ------------------------------------------------------------------------
% ------------------------------------------------------------------------



% -------------------------Enter Program Loop -----------------------------

% ENTIRE TIME SERIES LOOP
for kk = 1:length(IN_DATE)

%Provides percent completion, as the model runs
PercentComplete = (kk-1) * 100 / length(IN_DATE)

% sets input variables to specific events
Date = IN_DATE(kk);
Vi = IN_VI(kk);
Di = IN_DI(kk);
z_tw = IN_TW(kk);
Manning = IN_N(kk);
Fri = IN_FR(kk);
EGL = IN_EGL(kk);

% ISSUANCE CONDITIONS ----------------------------------------------------
% TO BE IMPORTED FROM BoR WATER SURFACE PROFILE PROGRAM (V1.10)
Rh = (L_bucket * Di) / (L_bucket + Di + Di); % Hydraulic radius (ft)
Fric = 1.49 * Rh^(1/6) / (Manning * sqrt(8*g)); % Fric = 1/sqrt(f);
Tu = 0.25 / Fric; % turbulence intensity
```

```
hv = Vi * Vi / (2 * g); % jet issuance kinetic energy (ft)
Qi = Vi * Di * L_bucket; %total issuance discharge for spillway(ft3/s)
qi = Vi * Di; % issuance unit discharge (ft^3/s/ft)
Fri_un = Vi / sqrt(Di * g); % uncorrected Froude Number

% FALLING JET ENERGY DISSIPATION
% ------------------------------------------

delz = -(z_bucket - z_tw + (0.5*Di)); %
z = z_bucket; % initialization of vertical distance from flip bucket loc.
x_imp = 0; % initialization of horizontal distance from flip bucket loc.
zm = z_bucket; % initialization of maximum height

% calculate horizontal distance to impact
while z > delz
    x_imp = x_imp + 0.5; % increase horizontal step by 1/2 ft)

    %calculate maximum drop height (ft)
    z = ((x_imp * tand(theta)) - (x_imp * x_imp /(4 * (hv) * ...
        cosd(theta) * cosd(theta))));
end

% Headloss from reservoir to spillway tailwater, assuming constant Vi
% velocity
H = (EGL - z_tw);

% jet trajectory length (ft)
Trajectory = @(x,theta,hv) sqrt(1 + (tand(theta) - ((2*x)/(4* hv * ...
        cosd(theta)*cosd(theta)))).^2);
Lj = integral(@(x)Trajectory(x,theta, hv),0, x_imp);

% plunge pool impingement angle (deg)
ai = atand(tand(theta)-(x_imp / (2 * hv * cosd(theta) * ...
    cosd(theta))))*(-1);

% impact velocity (ft/s)
Vj = sqrt((Vi * Vi) + (2 * g * H));
Vx = Vj * cosd(ai); % x-comp of velocity @ plunge pool impingement(ft/s)

if Type == 'A'
    % jet breakup length (ft) for rectangular jets (Castillo, 2007)
    Lb = 0.85 * Di * Fri_un * Fri_un / (1.07 * Tu * Fri_un * Fri_un)^0.82;
elseif Type =='B'
    %horizontal distance to jet breakup (ft) (Pfister, 2014)
    x_Lb = (76 * Di * (1 + sind(phi)) / (Fri_un * (1 + tand(lambda))^4)) /
...
        cosd(phi);
    Lb = integral(@(x)Trajectory(x,theta, hv),0, x_Lb);
end

% outer jet spread diameter (ft)
D_out = Di + (2 * 0.38 * Tu * Lj);

% diameter of solid core of round jet (Ervine, 1997)
Dj = Di * sqrt(Vi / Vj);
```

```
%Area of jet at impact with plunge pool (ft^2) for rectangular jet
    D_Spread = D_out - Di;% change in jet dia. from issuance to impingement
    L_out = L_bucket + D_Spread; % length of spillway at flip
    % bucket downstream of the two (assumed) identical spillway jets +
    % diameter of jet spread.

    Ajet = L_out * D_out;

% Total Stream Power of plunging jet ------------------------------------
% must be reported in kW & kW/m^2 for comparison with Karray

UW_Wat_m = 9.789; % unit weight of water to kN/m3
Qi_m = Qi * 0.02831685; % convert cfs to cms
H_m = H * 0.3048; % convert ft to m
Ajet_m = Ajet * 0.09290304; % convert ft^2 to m^2

Pjet =UW_Wat_m * Qi_m * H_m; %kW

% Stream Power per unit area
pjet = Pjet / Ajet_m; % kW/m^2

% PLUNGE POOL ENERGY DISSIPATION ----------------------------------------

% Degree of jet development upon plunge pool impingement
% If H < Lb (Lratio < 1), then jet core exists and jet is undeveloped
% If H < Lb (Lratio > 1), then jet is fully developed

Lratio = H / Lb;

% Determine correct Cp calculation input parameters (Castillo, 2006; 2007)
if Lratio <= 0.5
    a1 = 0.98;
    b1 = 0.070;
    Cpless4 = 0.78;
elseif Lratio > 0.5 && Lratio <= 0.6
    a1 = 0.92;
    b1 = 0.079;
    Cpless4 = 0.69;
elseif Lratio > 0.6 && Lratio <= 0.9
    a1 = 0.65;
    b1 = 0.067;
    Cpless4 = 0.50;
elseif Lratio > 0.9 && Lratio <= 1.4
    a1 = 0.65;
    b1 = 0.174;
    Cpless4 = 0.32;
elseif Lratio > 1.4 && Lratio <= 1.95
    a1 = 0.55;
    b1 = 0.225;
    Cpless4 = 0.22;
elseif Lratio > 1.95 && Lratio <=2.3
    a1 = 0.50;
    b1 = 0.250;
    Cpless4 = 0.18;
```

```
else
    a1 = 0.50;
    b1 = 0.40;
    Cpless4 = 0.1;
end

% Determine correct C'pa calculation input parameters (Castillo, 2006;2007)

if Lratio <= 1.4
    a2 = 0.0003;
    a3 = -0.0104;
    a4 = 0.0900;
    a5 = 0.0830;
elseif Lratio > 1.4 && Lratio <= 2.0
    a2 = 0.0003;
    a3 = -0.0094;
    a4 = 0.0745;
    a5 = 0.0500;
elseif Lratio > 2.0
    a2 = 0.0002;
    a3 = -0.0061;
    a4 = 0.0475;
    a5 = 0.010;
end

if Lratio <= 1.4
    b2 = 5.30;
    b3 = -1.405;
elseif Lratio > 1.4 && Lratio <= 2.0
    b2 = 3.14;
    b3 = -1.422;
elseif Lratio > 2.0
    b2 = 1.50;
    b3 = -1.500;
end

% Preallocate arrays
Cparray = zeros(z_size,2);
Cpparray = zeros(z_size,2);
Yarray = zeros(z_size-1,1);
Xarray = zeros(z_size-1,1);

Cparray(:,1) = Karray(:,1); % set first column of each array = elev value
Cpparray(:,1) = Karray(:,1); % set first column of each array = elev value

z_air = z_bucket_round - z_tw; % portion of matrix above water level

for k = 2:z_size % loop increasing vertical depth in plunge pool
    z = k-2;
     if z < z_air
         Cparray(k,2) = 0;
         Cpparray(k,2) = 0;
     else
         j = z-z_air;
         x = j / tand(ai); % calculate horz distance from pt of impingement
```

```
        Lpp = j / sind(ai); % calculate flow depth (at an angle) (ft)

        z_pp = z_tw - z; % calculate elevation within plunge pool (ft)
        x_pp = x_imp + x; % calculate horizontal distance from flip
            % bucket (ft)
        Xarray(k-1) = round(x_pp); % round horz distance for array indexing
        % (columns)
        Y = Lpp; % Plunge pool depth (ft)

        % Calculate mean dynamic pressure coefficient along jet trajectory
        if Y/D_out <= 4
            Cp = Cpless4; % When dimensionless plunge pool depth <= 4
        else
            Cp = a1 * exp(-b1*(Y/D_out)); % When dpp depth is > 4
        end

        % Calculate fluctuating dynamic pressure coefficient along jet
        % trajectory
        if Y/D_out < 14
            Cpp = (a2*(Y/D_out)^3)+(a3*(Y/D_out)^2)+(a4*(Y/D_out))+ a5;
        else
            Cpp = b2 * (Y/D_out)^b3;
        end

        % Store Cp and Cpp values in arrays, by elevation
        Cparray(k,2) = Cp;
        Cpparray(k,2) = Cpp;
        Yarray(k-1) = Y;
    end
end

% Preallocate Cp radial decay matrix
    cpr = zeros(z_size,x_size);
    cpr(:,1) = Karray(:,1);
    cpr(1,:) = Karray(1,:);

% Preallocate Cp_prime radial decay matrix
    cppr = zeros(z_size,x_size);
    cppr(:,1) = Karray(:,1);
    cppr(1,:) = Karray(1,:);

% Calculate radial decay of pressure coefficients ---------------------
    for j = 2:z_size
        if j-2 <= z_air
            cppr(j,2:end) = 0;
            cppr(j,2:end) = 0;
        else
            %Calculate maximum submerged jet radius
            rmax = (0.5 * D_out) + (0.25 * Yarray(j-1));
            %area of influence is 1.6rmax (Bollaert, 2002)
            rmaxmax = round(1.6*rmax);

        % If undeveloped upon entry, the length of the jet within the
        % plunge pool:
        Ljet = Dj / (2 * tand(8));
```

```
        for r = 0:rmaxmax
            % For Undeveloped Jets:
            if Lratio < 1 && Lpp < Ljet && r<= (0.5 * rmax)
                Cpprr = 1;
                Cprr = exp((-6)*(r/rmax)^2);

            elseif Lratio < 1 && Lpp < Ljet && r > (0.5 * rmax)
                Cpprr = exp((-3)*((r / rmax) - 0.5)^2);
                Cprr = exp((-6)*(r/rmax)^2);

            elseif Lratio < 1 && Lpp >= Ljet
                Cpprr = exp((-3)*(r/rmax)^2);
                Cprr = exp((-3)*(r/rmax)^2);

                % For Developed Jets:
            elseif Lratio >= 1
                Cpprr = exp((-3)*(r/rmax)^2);
                Cprr = exp((-3)*(r/rmax)^2);
            end

            x_rmin = Xarray(j-1) - r; % min horizontal distance, r (ft)
            x_rmax = Xarray(j-1) + r; % max horizontal distance, r (ft)

            cpr(j,x_rmax+1) = Cprr;
            cppr(j,x_rmax+1) = Cpprr;

            if x_rmin >=0 %prevents issues with negative indices due when
                    % jet is within close proximity to flip buckets
            cpr(j,x_rmin+1) = Cprr;
            cppr(j,x_rmin+1) = Cpprr;
            end
        end
        end
    end

%---- TOTAL STREAM POWER CALCULATION ---------------------------------------
    % Calculate stream power at each node when jet is airborne(kW/m^2);

    SParray = zeros(z_size,x_size);
    SParray(:,1) = Karray(:,1);
    SParray(1,:) = Karray(1,:);

% For plunging jet:
    for x_plunge = 1:0.25:x_imp
        z_plunge = ((x_plunge * tand(theta_j)) - (x_plunge * x_plunge /...
            (4*hv * cosd(theta_j) * cosd(theta_j))));
        z_plunge = round(z_bucket + z_plunge + (0.5 * Di));

         for iii = 2:z_size
            if z_tw == SParray(iii,1) % match elevation of plunging jet
                    % to SParray elevation
                hug = iii + 1;
            end
         end
```

```
          for kkkk = 2: hug
             if z_plunge == SParray(kkkk,1) % match elevation of
                         % plunging jet to SParray elevation

             % Calculate trajectory length for plunging jet at x_plunge,
             % z_plunge
              Lj_plunge = integral(@(x)Trajectory(x,theta_j, hv),0, x_plunge);

              % Calculate radius of spread at x_plunge, z_plunge
              R_plunge = Di + (2 * 0.38 * Tu * Lj_plunge);

              % Calculate area of  plunging jet at x_plunge, z_plunge(m^2)
              A_plunge = (2 * R_plunge)*(L_bucket +(2 * R_plunge))*
0.09290304;

              % Calculate stream power of plunging jet ( in metric units)
              H_plunge = (EGL - z_plunge) * 0.3048;
              p_plunge =  UW_Wat_m * Qi_m * H_plunge / A_plunge; %kW/m^2

              % Set outer bounds of jet as centerline of trajectory +/-
              % radius of jet spread
              x_p_min = round(x_plunge - R_plunge); % min horz. distance(ft)
              x_p_max = round(x_plunge + R_plunge); % max horz. distance(ft)

              % prevents issues with negative indices when jet is within
              % close proximity to flip buckets
                  if x_p_min > 0
                      for jjj = x_p_min:x_p_max
                          SParray(kkkk,jjj) = p_plunge;
                      end
                  end
              end
          end
      end

% For submerged jet:
      for ii = hug:z_size
          for jj = 2:x_size
            SParray(ii,jj) = pjet * ((Cparray(ii,2)*cpr(ii,jj)) + ...
                (Cpparray(ii,2)* cppr(ii,jj)));
          end
      end

%---- PROBABILITY OF FAILURE CALCULATION ---------------------------------
      % Calculate probability of failure at each node based on Wibowo (2005);
      % column 1 of matrix is reserved for elevation reference (ft); row 1 of
      % matrix is reserved for horizontal distance (ft) from flip bucket.

      PEarray = zeros(z_size,x_size);
      PEarray(:,1) = Karray(:,1);
      PEarray(1,:) = Karray(1,:);

      for ii = 2:z_size
          for jj = 2:x_size
```

```
            PEarray(ii,jj) = 1 / (1 + exp(-(-1.859-(7.029 * ...
                log(Kdyn(ii,jj)))+(9.798 * log(SParray(ii,jj))))));
            if isnan(PEarray(ii,jj))
                PEarray(ii,jj) = 1; % prevents NAN values from appearing
                    % below water level, but above rock surface.
            end
        end
    end

% Check for erosion barriers (ie. lower SP near surface prevent propogation
% of erosion downward, where SP values may be higher or erosive capacity
% may be lower)

PErows = ones(z_size,1);
    for ii = 2:z_size
            SP_max = SParray(ii,2); % set initial 'max' value to the first
                % element in row
            SPmax_i = ii;
            SPmax_j = 2;

            for jj = 2:x_size
                if SParray(ii,jj) > SP_max
                    SP_max = SParray(ii,jj);
                    SPmax_i = ii;
                    SPmax_j = jj;
                end
                K_bound = Kdyn(SPmax_i,SPmax_j);
            end

        % Calculate greatest probability of removal of material in each row
        PErows(ii) = 1 / (1 + exp(-(-1.859-(7.029 * log(K_bound))+...
            (9.798 * log(SP_max)))));

        if isnan(PErows(ii))
           PErows(ii) = 1;
        end
    end

    PE = PErows(2);
    PE_bound = 1;

    while PE > 0.5
        PE = PErows(PE_bound);
        PE_bound = PE_bound + 1; % Probability of removal of material
            % below this point is zero
    end


% --- ROCK REMOVAL ------------------------------------------------------

    for ii = 2:z_size
        for jj = 2:x_max
            % if probability of removal is >= 50%
            if ii < PE_bound && PEarray(ii,jj) >= 0.50
                % then "remove" rock and set K value = 0 kW/m^2
```

```
                Kdyn(ii,jj) = 0;
            % Otherwise,leave existing value
            else Kdyn(ii,jj) = Kdyn(ii,jj);
            end
        end
    end

    csvwrite(strcat(DamAbbrev,'_',char(Date),'_Kdyn.csv'),Kdyn);

 % Identify elevation of plunge pool invert (ft)
 z_locale=Kdyn(2,1);
    for ii = 1:z_size-1
        C = min(Kdyn(ii,:));
        D = min(Kdyn(ii+1,:));
        if C == 0 && D > 0
           z_locale = Kdyn(ii,1);
           z_ind = ii;
        end
    end

 % Identify upstream and downstream extent of invert (ft)
    x_locale_us = Kdyn(1,2);
    x_locale_ds = Kdyn(1,2);
    for jj = 1:x_size-1
        if Kdyn(z_ind,jj+1) == 0 && Kdyn(z_ind,jj) > 0
            x_locale_us = Kdyn(1,jj);
            x_ind_us = jj;
        end

        if Kdyn(z_ind,jj) == 0 && Kdyn(z_ind, jj+1) > 0
            x_locale_ds = Kdyn(1,jj);
            x_ind_ds = jj;
        end
    end

% SECTION: Generate Output File ----------------------------------------

SD = [Di ,Vi, EGL, Fri, z_tw, Tu, x_imp, Lj, Lb, H,...
    D_out, ai, Qi,Pjet, pjet, x_locale_us, x_locale_ds,z_locale];

SDd = num2cell(SD);
CCC = [Date,SDd];

fid1 = fopen(strcat('1_',char(DamAbbrev),'_Results.csv'), 'a');
    fprintf(fid1, '%s,%d,%d,%d,%d,%d,%d,%d,%d,%d,%d,%d,%d,%d,%d,%d,%d,%d,%d,
\r\n', CCC{:});
fclose(fid1);

% -------------------------- PLOTTING ----------------------------------

        contourf(Kdyn(1,2:end),Kdyn(2:end,1),Kdyn(2:end,2:end))
        hold on;
        xlabel('Distance Downstream (ft)')
        ylabel('Elevation (ft)')
        caxis([0,Maxval])
```

```
        colormap([1 1 1; 0.5 0.5 0.5])
        %contourf(SParray(1,2:end),SParray(2:end,1),SParray(2:end,2:end))
        %colormap(gcf, [1 1 1; 1 0.25 0.25])
        %alpha(0.5)
        axis([0 x_max z_maxhole z_bucket_round])
        axis equal
        axis tight
        title(strcat(char(Date),char(DamName),' Dam Cumulative Scour'));

saveas(gcf,strcat(char(Date),'_',char(DamAbbrev),'_CumulativeScour','.tif'));
        hold off;
end
```

APPENDIX C

BC HYDRO EXISTING PLUNGE POOL SURVEYS

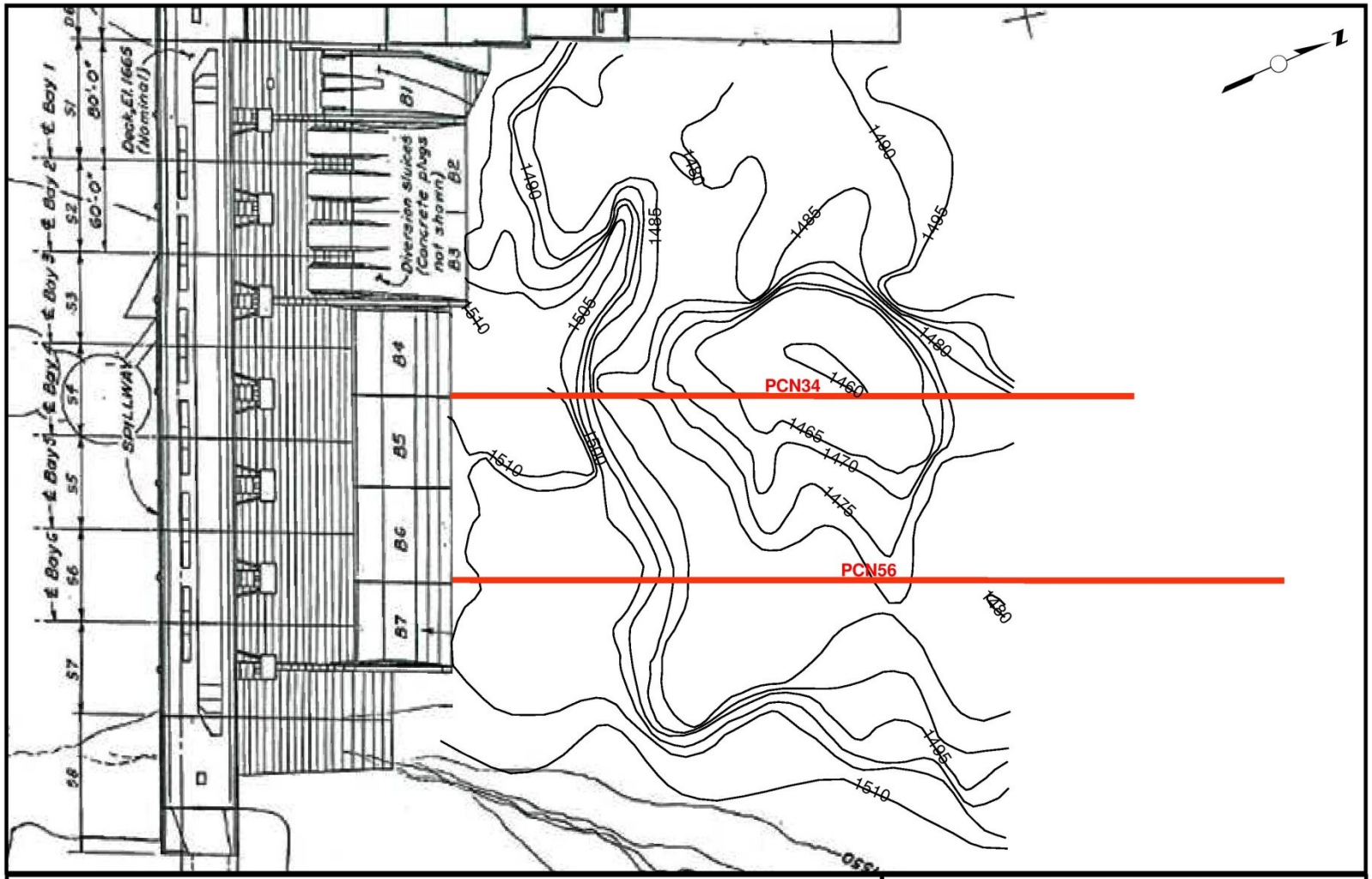

Coordinate System: NAD 1927 UTM Zone 12N
Projection: Transverse Mercator
Datum: North American 1927
False Easting: 500,000.0000
False Northing: 0.0000
Central Meridian: -111.0000
Scale Factor: 0.9996
Latitude Of Origin: 0.0000
Units: Meter
Dam Plan from BC Hydro Dwg. 1007-C14-U4707, Dec. 1987

0 25 50 100 150 200 Feet

Legend

Cross Section Locations

Plunge Pool Contours - 5ft. Interval

Peace Canyon Dam
Plunge Pool Topography

April 15, 1980

From BC Hydro Dwg. 007-C14-X8423

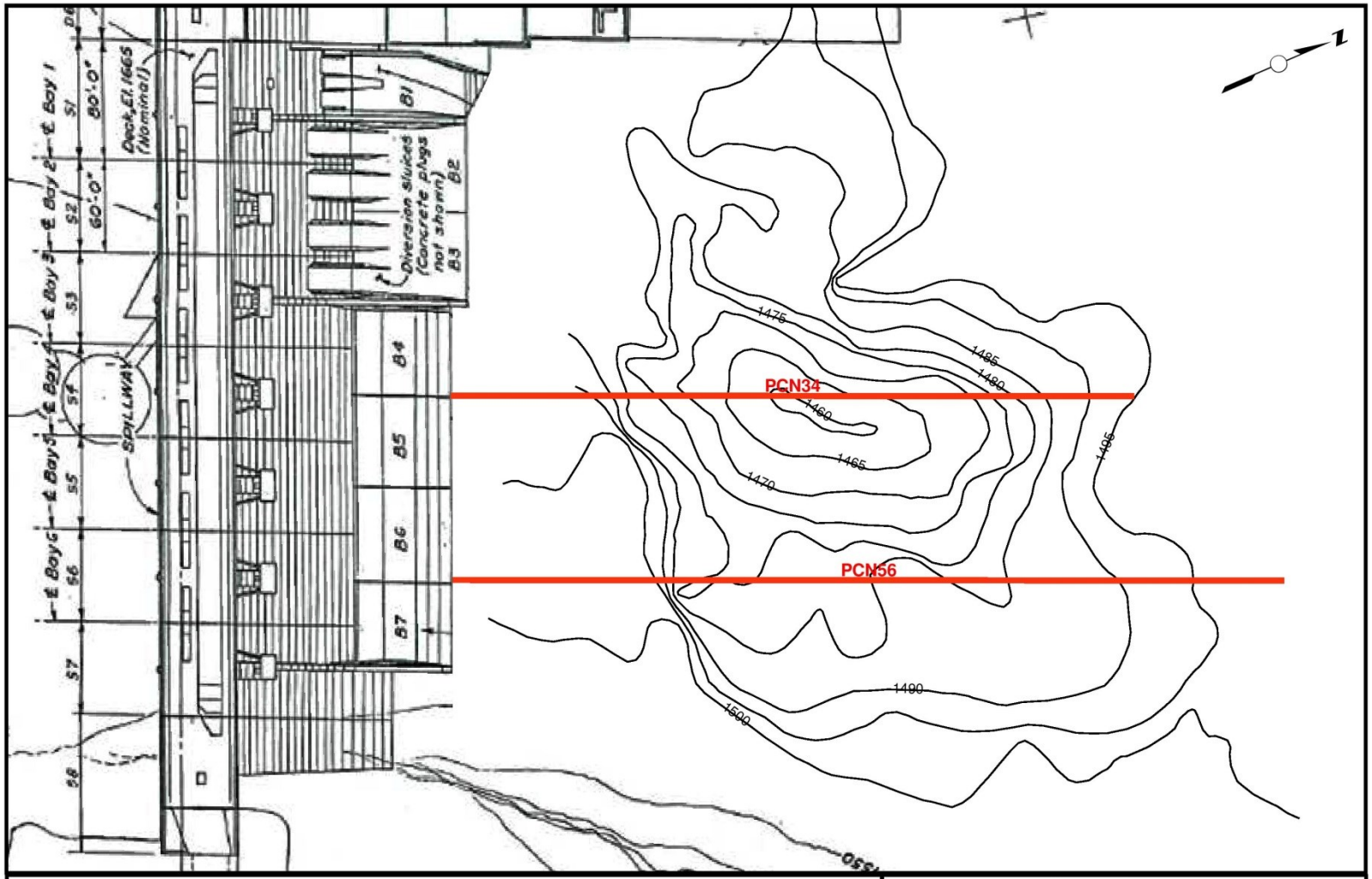

Coordinate System: NAD 1927 UTM Zone 12N
Projection: Transverse Mercator
Datum: North American 1927
False Easting: 500,000.0000
False Northing: 0.0000
Central Meridian: -111.0000
Scale Factor: 0.9996
Latitude Of Origin: 0.0000
Units: Meter
Dam Plan from BC Hydro Dwg. 1007-C14-U4707, Dec. 1987

0 25 50 100 150 200 Feet

Legend

Cross Section Locations

Plunge Pool Contours - 5 ft. Interval

Peace Canyon Dam
Plunge Pool Topography

September 5, 1981

From BC Hydro Dwg. 007-C14-U8440

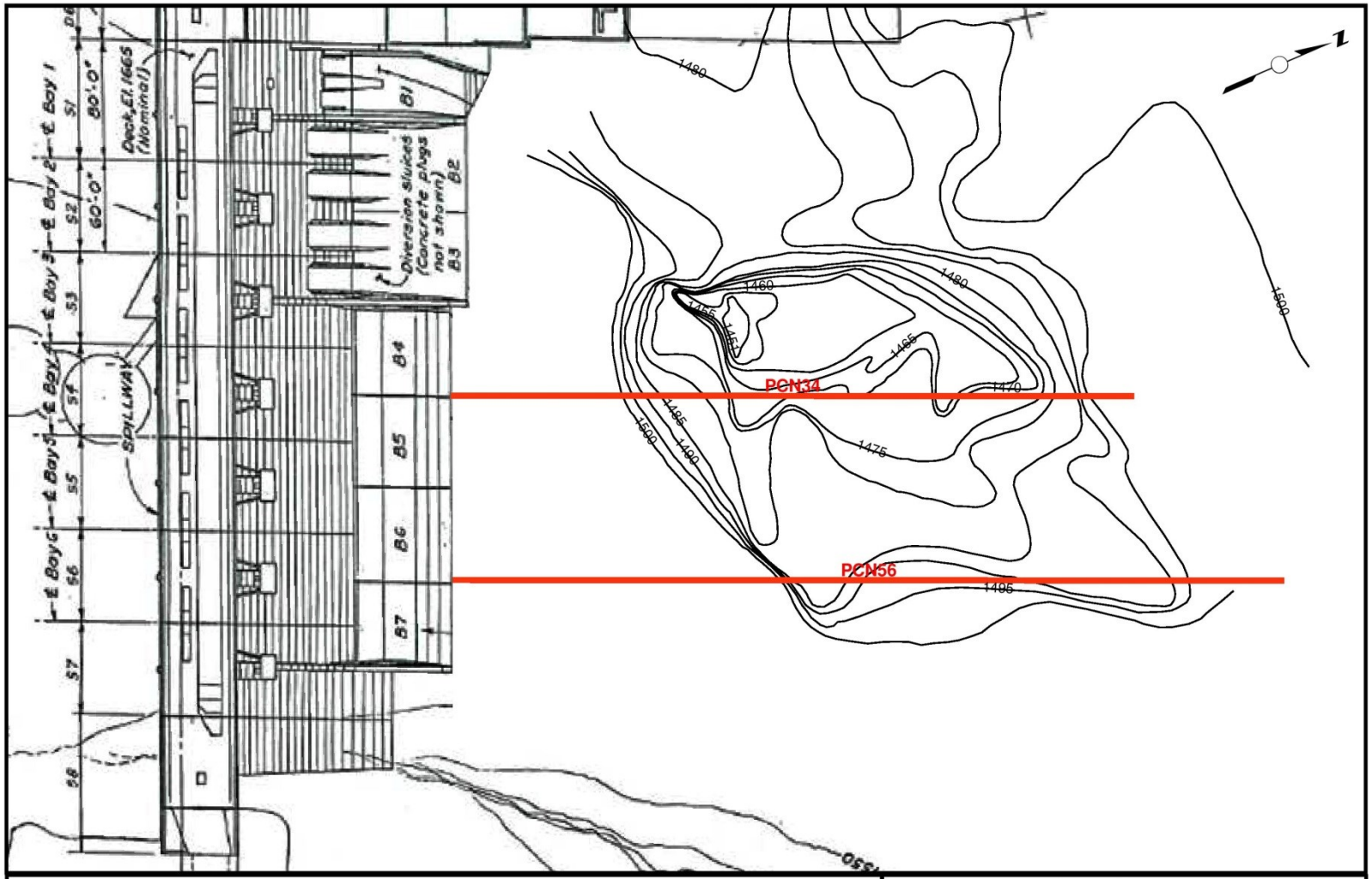

Coordinate System: NAD 1927 UTM Zone 12N
Projection: Transverse Mercator
Datum: North American 1927
False Easting: 500,000.0000
False Northing: 0.0000
Central Meridian: -111.0000
Scale Factor: 0.9996
Latitude Of Origin: 0.0000
Units: Meter
Dam Plan from BC Hydro Dwg. 1007-C14-U4707, Dec. 1987

0 25 50 100 150 200 Feet

Legend

Cross Section Locations

Plunge Pool Contours - 5 ft. Interval

Peace Canyon Dam
Plunge Pool Topography

April 1983

From BC Hydro Dwg. 007-C14-D4471

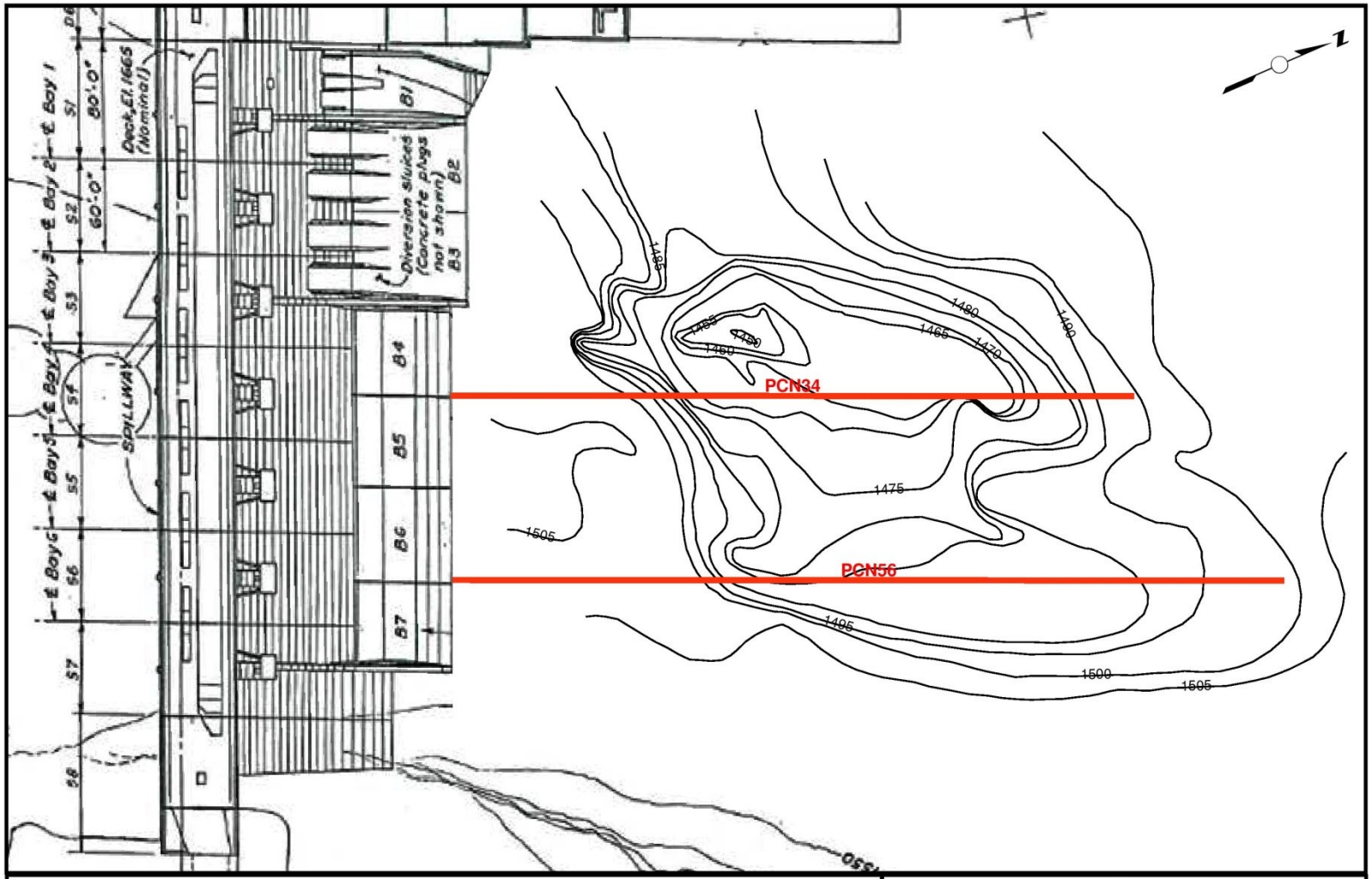

Coordinate System: NAD 1927 UTM Zone 12N
Projection: Transverse Mercator
Datum: North American 1927
False Easting: 500,000.0000
False Northing: 0.0000
Central Meridian: -111.0000
Scale Factor: 0.9996
Latitude Of Origin: 0.0000
Units: Meter
Dam Plan from BC Hydro Dwg. 1007-C14-U4707, Dec. 1987

0 25 50 100 150 200 Feet

Legend

Cross Section Locations

Plunge Pool Contours - 5 ft. Interval

Peace Canyon Dam
Plunge Pool Topography

October 1983

From BC Hydro Dwg. 007-C14-D4472

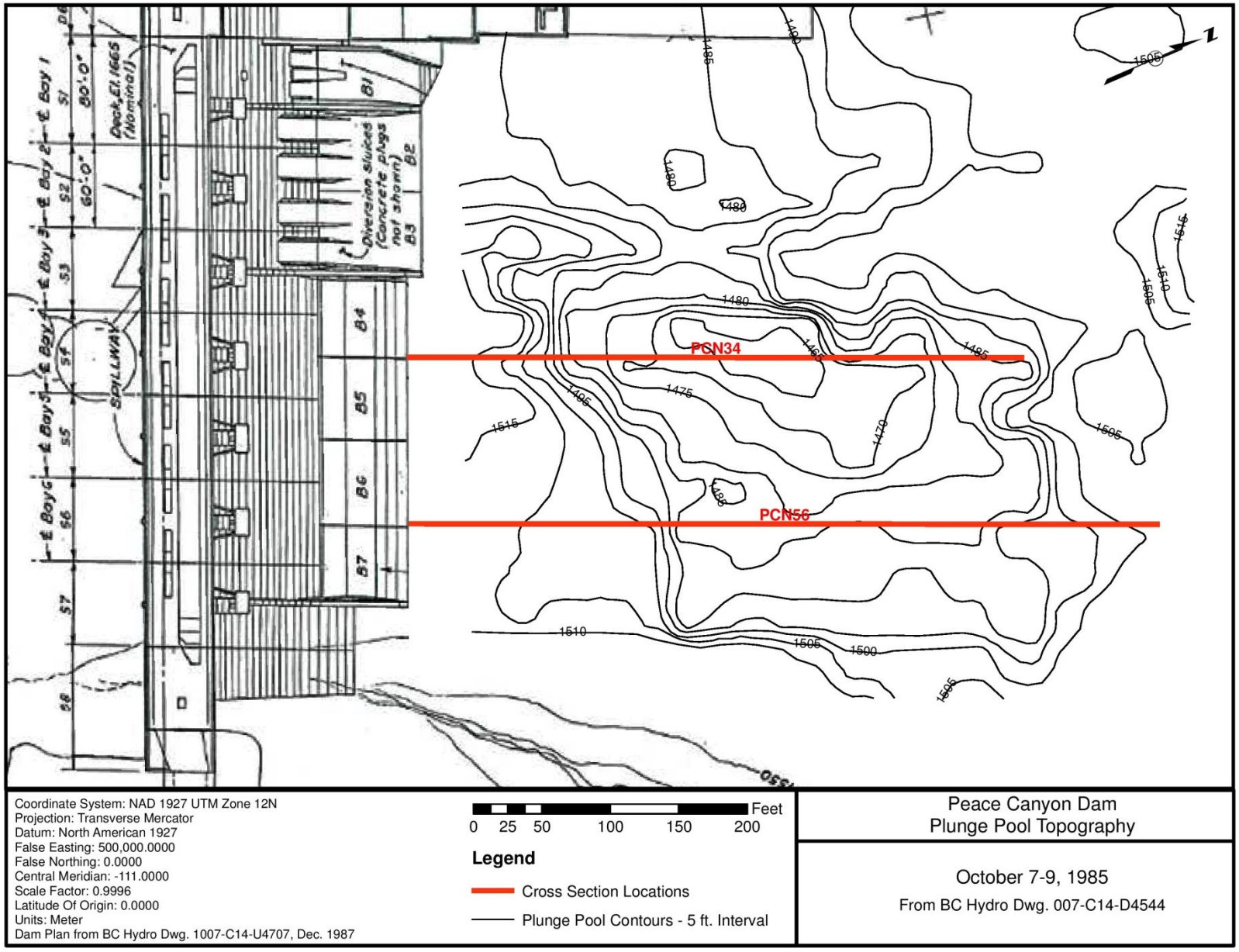
PCN34
PCN56
Deck El. 1665 (Nominal)
Diversion sluices (Concrete plugs not shown)
SPILLWAY
1480
1485
1490
1505
1515
1510
1500
1475
1470
1495
1550
Coordinate System: NAD 1927 UTM Zone 12N
Projection: Transverse Mercator
Datum: North American 1927
False Easting: 500,000.0000
False Northing: 0.0000
Central Meridian: -111.0000
Scale Factor: 0.9996
Latitude Of Origin: 0.0000
Units: Meter
Dam Plan from BC Hydro Dwg. 1007-C14-U4707, Dec. 1987
Feet
0 25 50 100 150 200
Legend
Cross Section Locations
Plunge Pool Contours - 5 ft. Interval
Peace Canyon Dam
Plunge Pool Topography
October 7-9, 1985
From BC Hydro Dwg. 007-C14-D4544

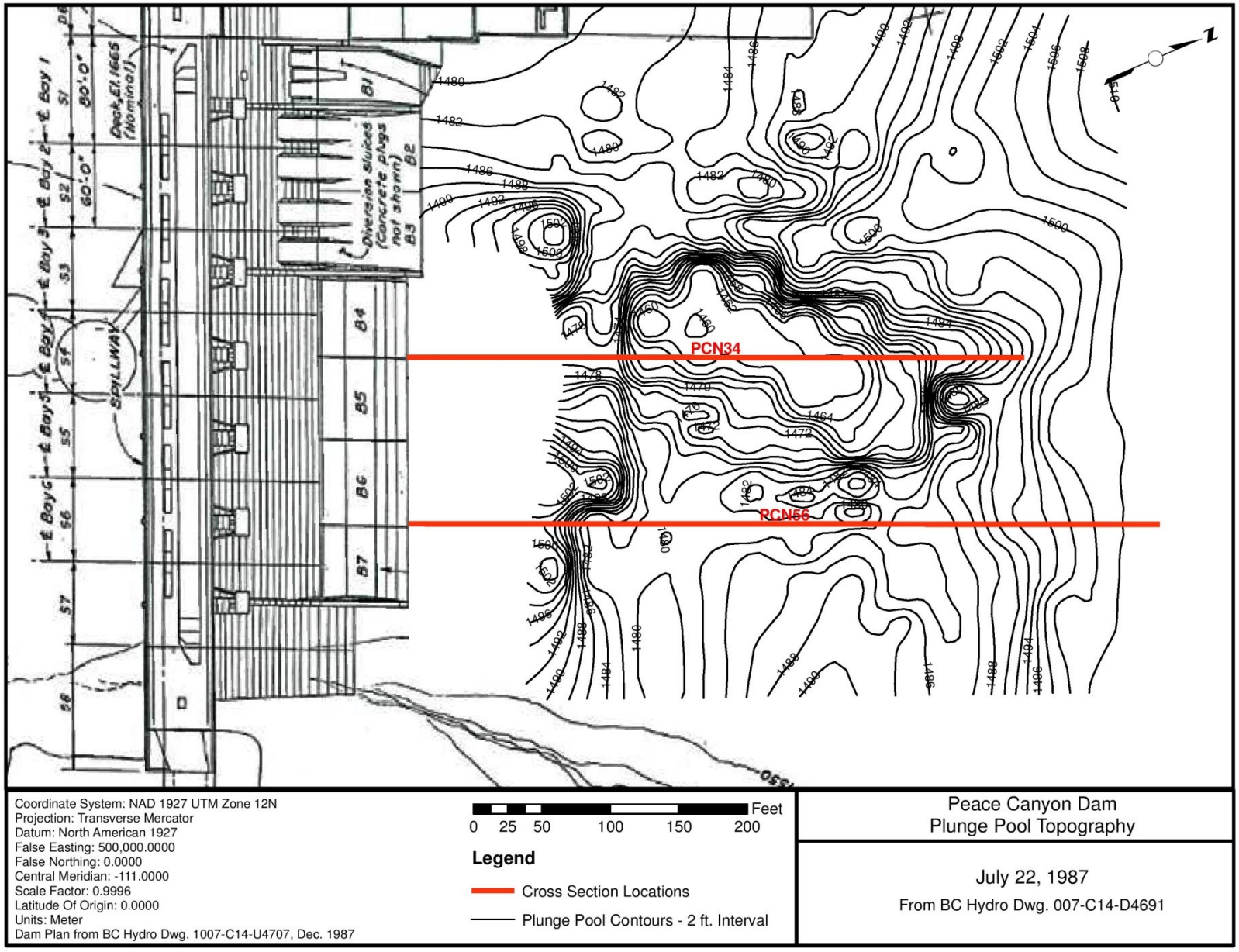
PCN34
PCN56
Deck El. 1665 (Nominal)
Diversion sluices (Concrete plugs not shown)
SPILLWAY
Bay 1
Bay 2
Bay 3
Bay 4
Bay 5
Bay 6
Coordinate System: NAD 1927 UTM Zone 12N
Projection: Transverse Mercator
Datum: North American 1927
False Easting: 500,000.0000
False Northing: 0.0000
Central Meridian: -111.0000
Scale Factor: 0.9996
Latitude Of Origin: 0.0000
Units: Meter
Dam Plan from BC Hydro Dwg. 1007-C14-U4707, Dec. 1987
0 25 50 100 150 200 Feet
Legend
Cross Section Locations
Plunge Pool Contours - 2 ft. Interval
Peace Canyon Dam
Plunge Pool Topography
July 22, 1987
From BC Hydro Dwg. 007-C14-D4691

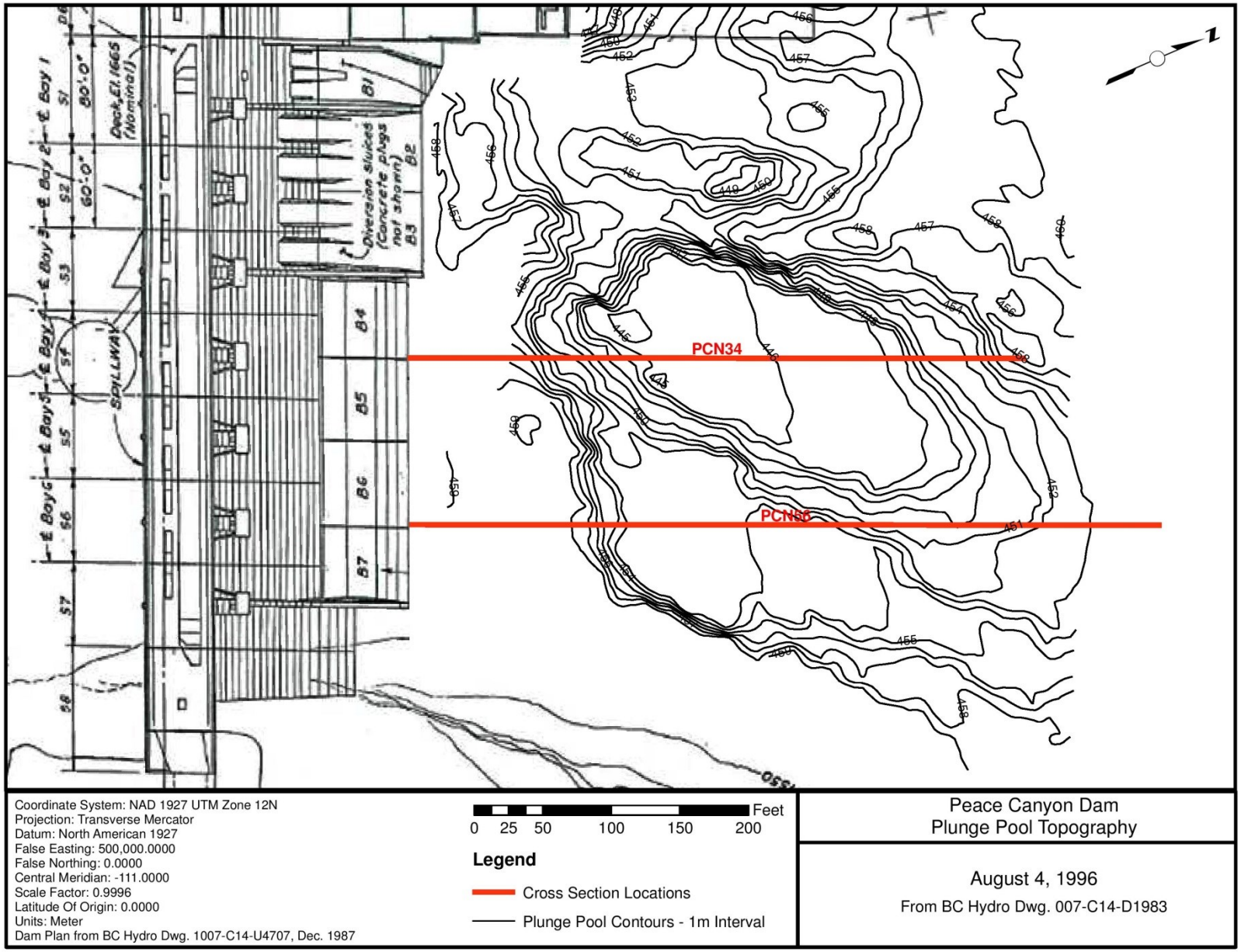
PCN34
PCN56
Deck El. 1665 (Nominal)
Diversion sluices (Concrete plugs not shown)
SPILLWAY
Bay 1
Bay 2
Bay 3
Bay 4
Bay 5
Bay 6
Coordinate System: NAD 1927 UTM Zone 12N
Projection: Transverse Mercator
Datum: North American 1927
False Easting: 500,000.0000
False Northing: 0.0000
Central Meridian: -111.0000
Scale Factor: 0.9996
Latitude Of Origin: 0.0000
Units: Meter
Dam Plan from BC Hydro Dwg. 1007-C14-U4707, Dec. 1987
Feet
0 25 50 100 150 200
Legend
Cross Section Locations
Plunge Pool Contours - 1m Interval
Peace Canyon Dam
Plunge Pool Topography
August 4, 1996
From BC Hydro Dwg. 007-C14-D1983

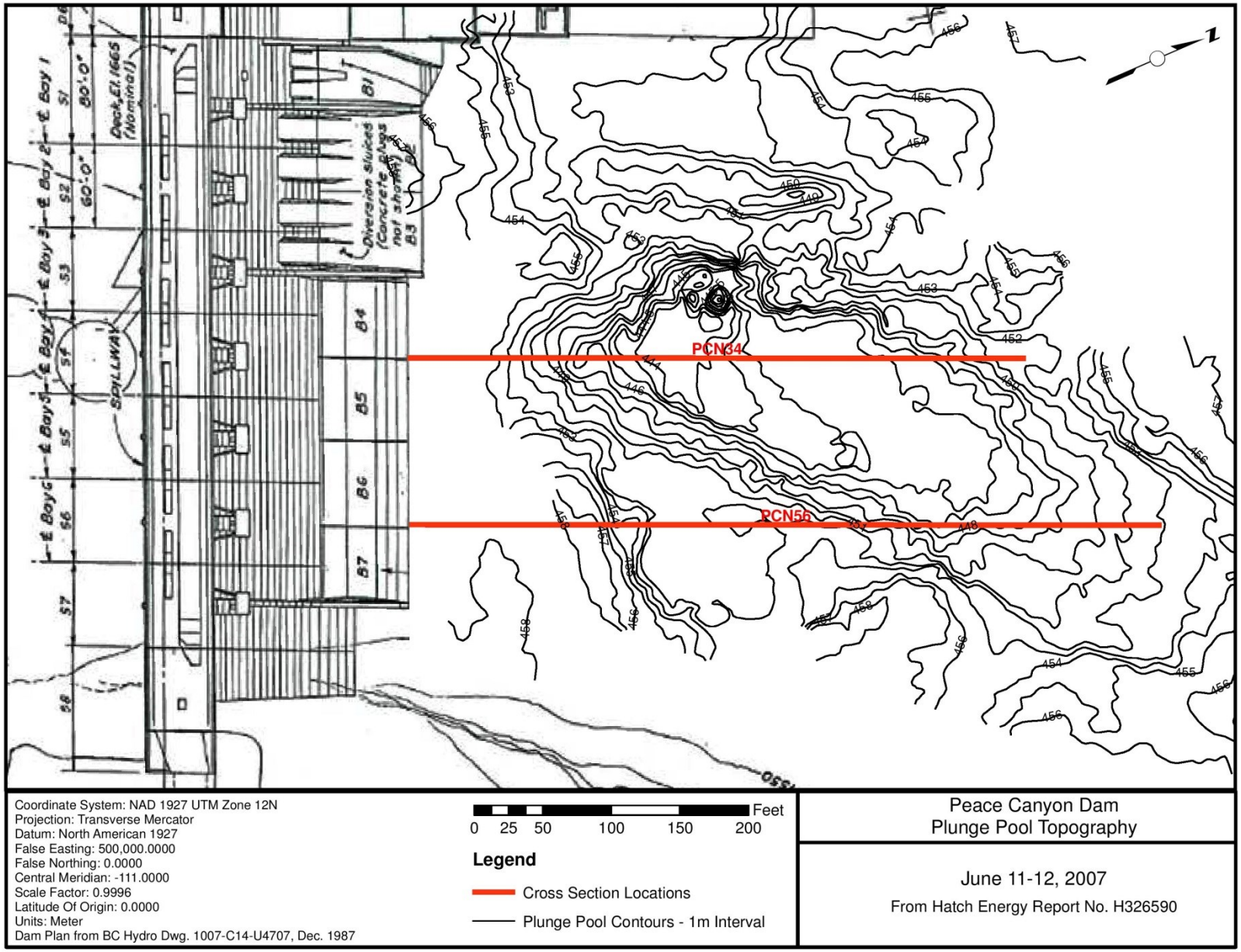
PCN34
PCN56
Deck El. 1665 (Nominal)
Diversion sluices (Concrete plugs not shown)
Spillway
Coordinate System: NAD 1927 UTM Zone 12N
Projection: Transverse Mercator
Datum: North American 1927
False Easting: 500,000.0000
False Northing: 0.0000
Central Meridian: -111.0000
Scale Factor: 0.9996
Latitude Of Origin: 0.0000
Units: Meter
Dam Plan from BC Hydro Dwg. 1007-C14-U4707, Dec. 1987
Feet
0 25 50 100 150 200
Legend
Cross Section Locations
Plunge Pool Contours - 1m Interval
Peace Canyon Dam
Plunge Pool Topography
June 11-12, 2007
From Hatch Energy Report No. H326590

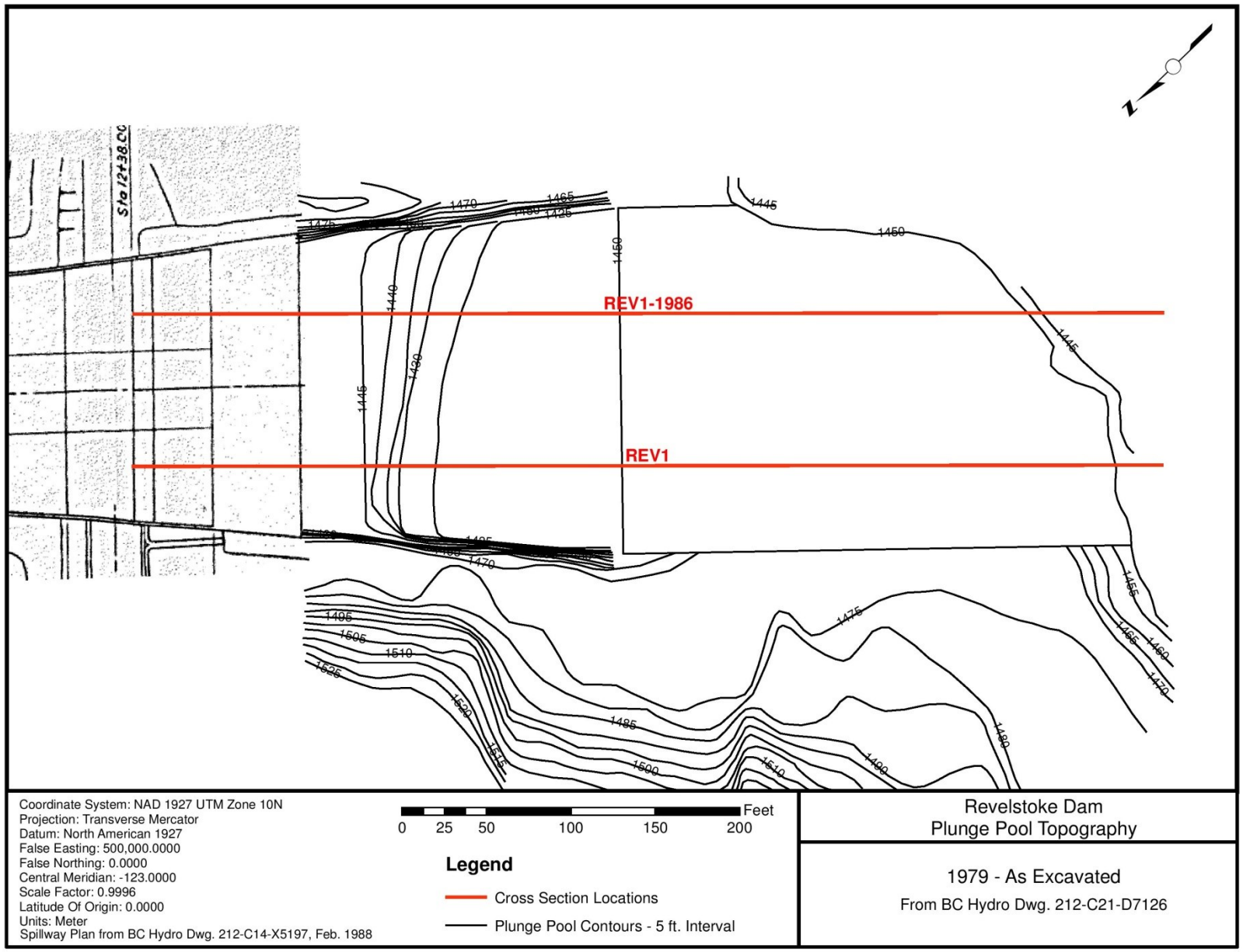
Sta 12+38.00
REV1-1986
REV1
1445
1450
1440
1430
1445
1470
1475
1495
1505
1510
1515
1520
1485
1500
1490
1510
1455
1465
1460
1470
Coordinate System: NAD 1927 UTM Zone 10N
Projection: Transverse Mercator
Datum: North American 1927
False Easting: 500,000.0000
False Northing: 0.0000
Central Meridian: -123.0000
Scale Factor: 0.9996
Latitude Of Origin: 0.0000
Units: Meter
Spillway Plan from BC Hydro Dwg. 212-C14-X5197, Feb. 1988
0 25 50 100 150 200 Feet
Legend
Cross Section Locations
Plunge Pool Contours - 5 ft. Interval
Revelstoke Dam
Plunge Pool Topography
1979 - As Excavated
From BC Hydro Dwg. 212-C21-D7126

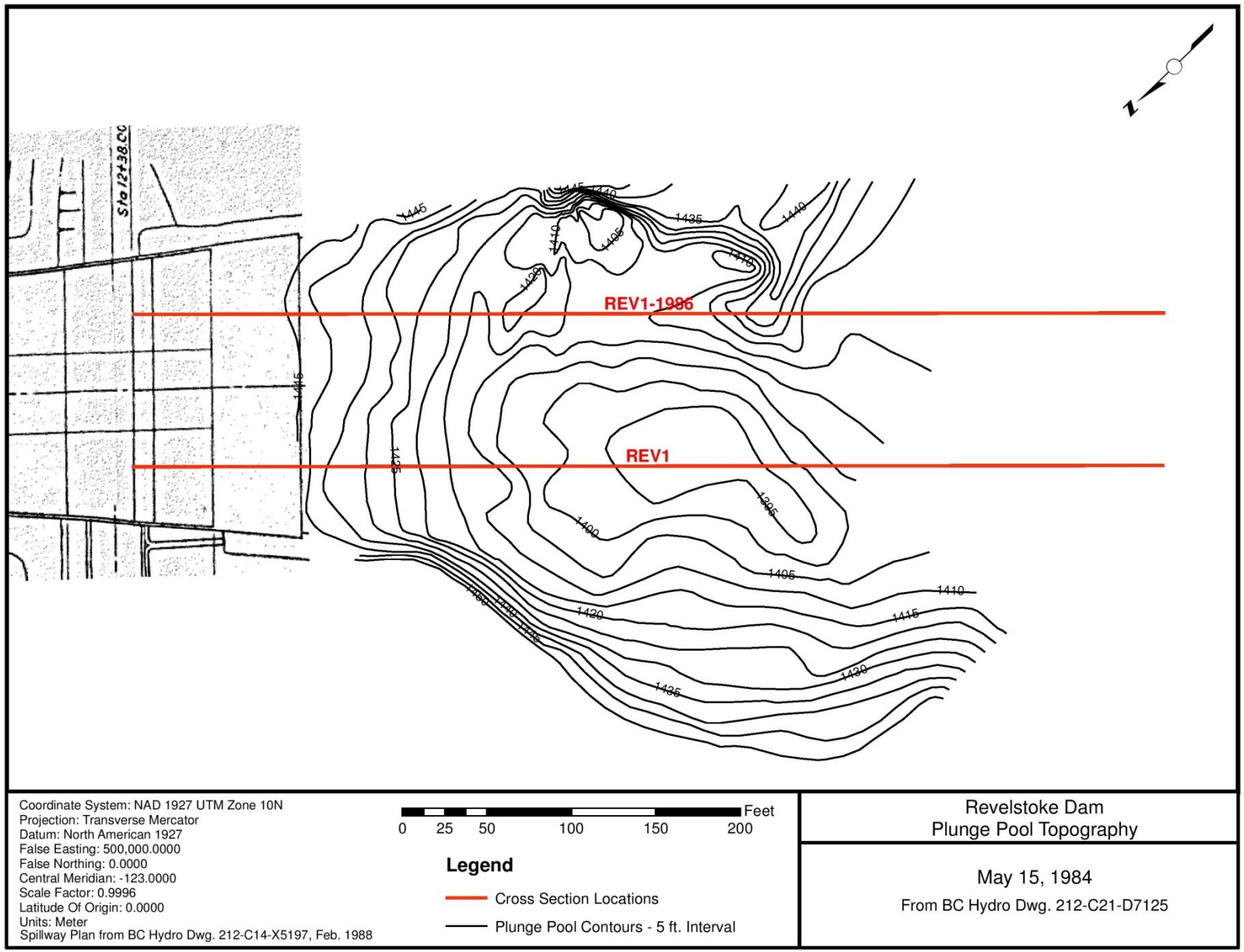
Sta 12+38.00
REV1-1986
REV1
1445
1440
1435
1430
1425
1420
1415
1410
1405
1400
1395
Coordinate System: NAD 1927 UTM Zone 10N
Projection: Transverse Mercator
Datum: North American 1927
False Easting: 500,000.0000
False Northing: 0.0000
Central Meridian: -123.0000
Scale Factor: 0.9996
Latitude Of Origin: 0.0000
Units: Meter
Spillway Plan from BC Hydro Dwg. 212-C14-X5197, Feb. 1988
Feet
0 25 50 100 150 200
Legend
Cross Section Locations
Plunge Pool Contours - 5 ft. Interval
Revelstoke Dam
Plunge Pool Topography
May 15, 1984
From BC Hydro Dwg. 212-C21-D7125

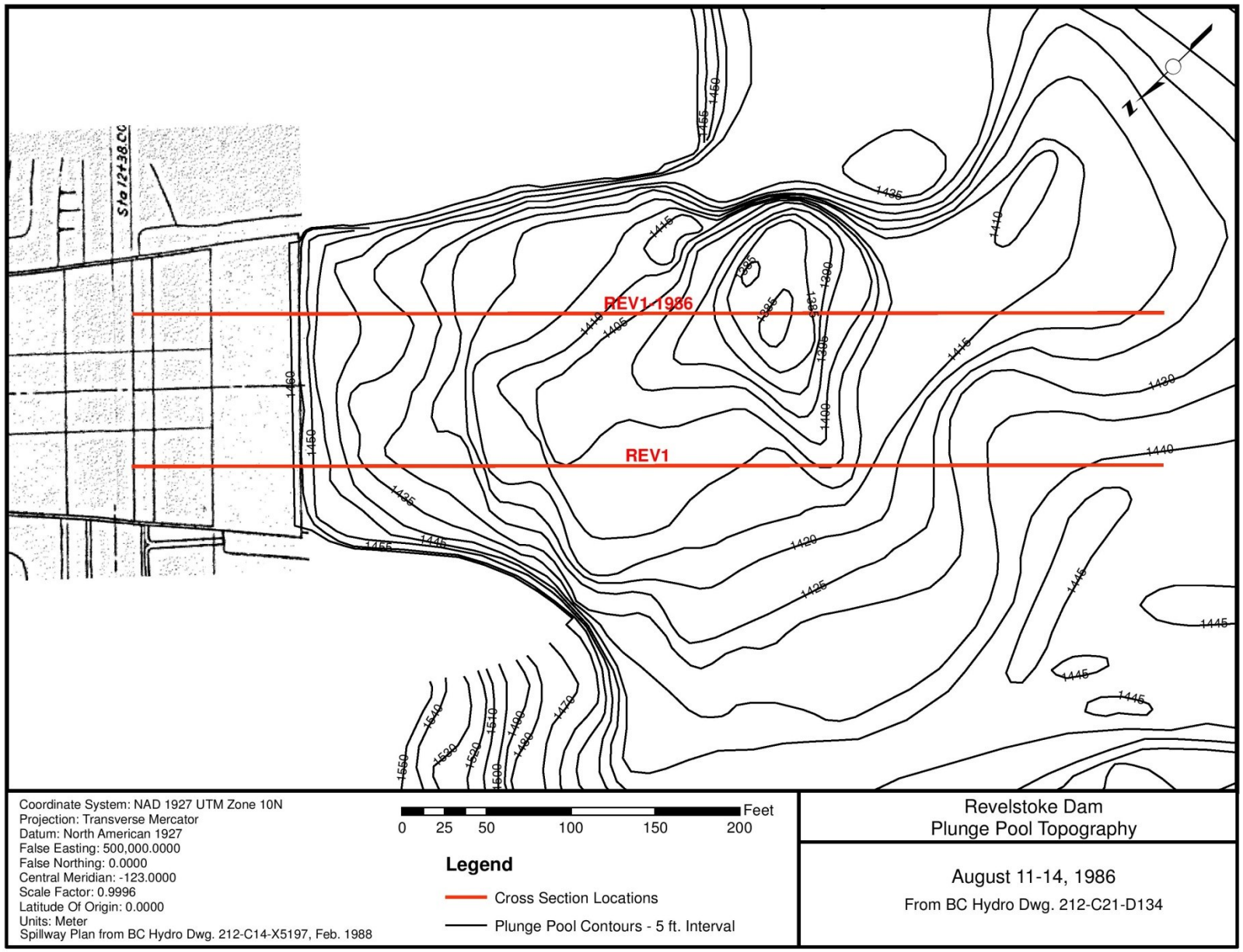

Coordinate System: NAD 1927 UTM Zone 10N
Projection: Transverse Mercator
Datum: North American 1927
False Easting: 500,000.0000
False Northing: 0.0000
Central Meridian: -123.0000
Scale Factor: 0.9996
Latitude Of Origin: 0.0000
Units: Meter
Spillway Plan from BC Hydro Dwg. 212-C14-X5197, Feb. 1988

0 25 50 100 150 200 Feet

Legend

Cross Section Locations

Plunge Pool Contours - 5 ft. Interval

Revelstoke Dam
Plunge Pool Topography

August 11-14, 1986

From BC Hydro Dwg. 212-C21-D134

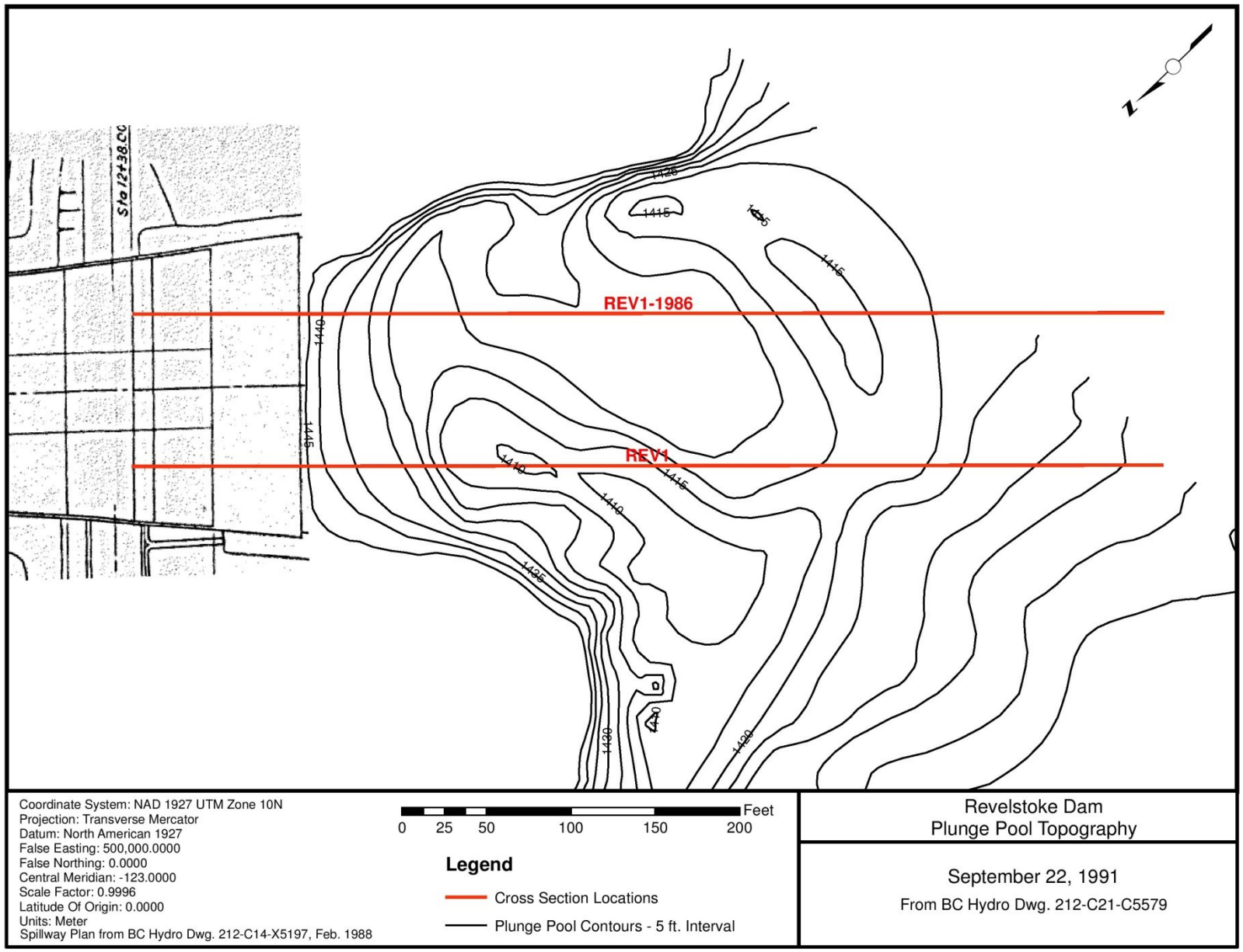
Sta 12+38.00
REV1-1986
REV1
1415
1410
1420
1425
1430
1435
1440
Coordinate System: NAD 1927 UTM Zone 10N
Projection: Transverse Mercator
Datum: North American 1927
False Easting: 500,000.0000
False Northing: 0.0000
Central Meridian: -123.0000
Scale Factor: 0.9996
Latitude Of Origin: 0.0000
Units: Meter
Spillway Plan from BC Hydro Dwg. 212-C14-X5197, Feb. 1988
0 25 50 100 150 200 Feet
Legend
Cross Section Locations
Plunge Pool Contours - 5 ft. Interval
Revelstoke Dam
Plunge Pool Topography
September 22, 1991
From BC Hydro Dwg. 212-C21-C5579

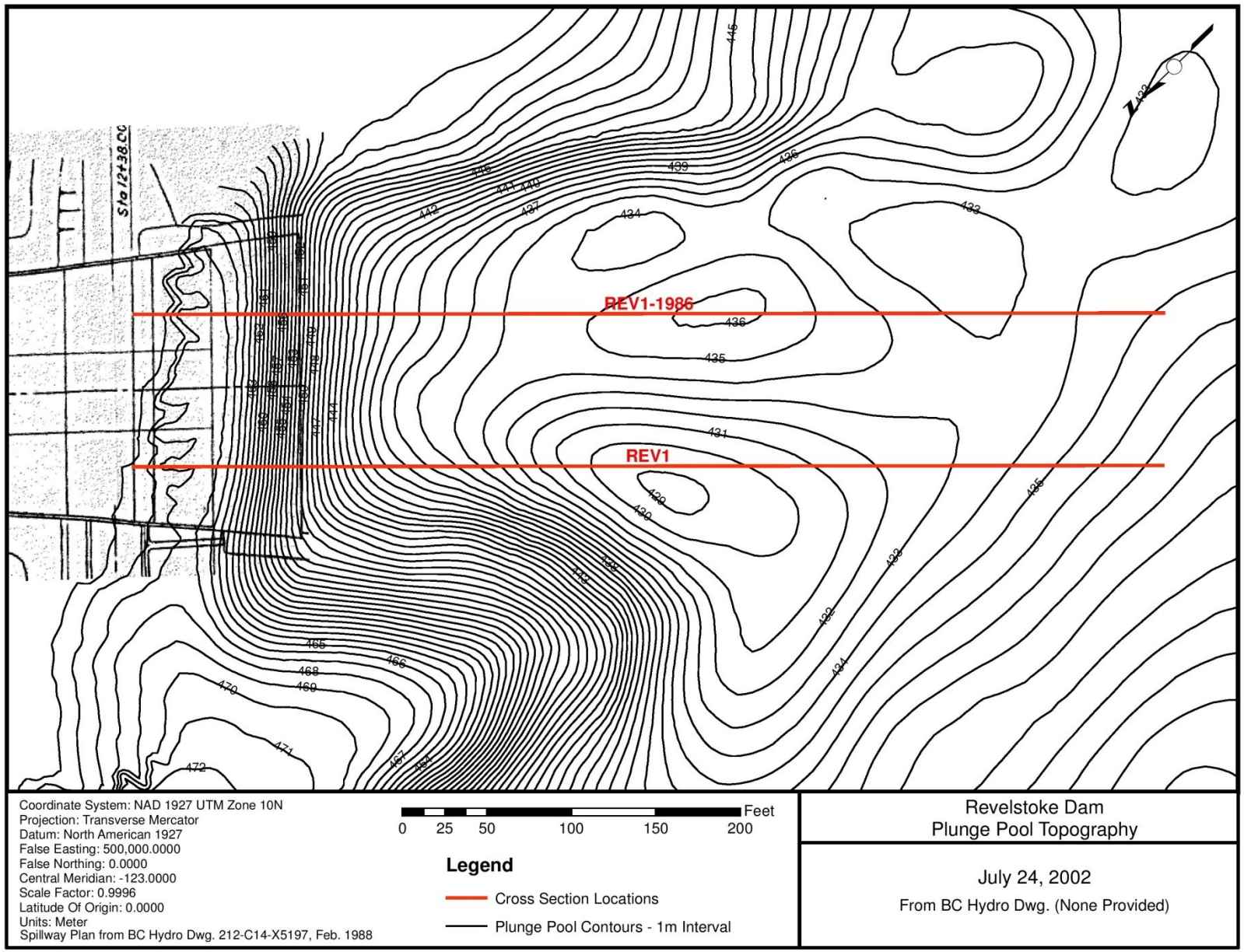
REV1-1986
REV1
Coordinate System: NAD 1927 UTM Zone 10N
Projection: Transverse Mercator
Datum: North American 1927
False Easting: 500,000.0000
False Northing: 0.0000
Central Meridian: -123.0000
Scale Factor: 0.9996
Latitude Of Origin: 0.0000
Units: Meter
Spillway Plan from BC Hydro Dwg. 212-C14-X5197, Feb. 1988
Feet
0 25 50 100 150 200
Legend
Cross Section Locations
Plunge Pool Contours - 1m Interval
Revelstoke Dam
Plunge Pool Topography
July 24, 2002
From BC Hydro Dwg. (None Provided)

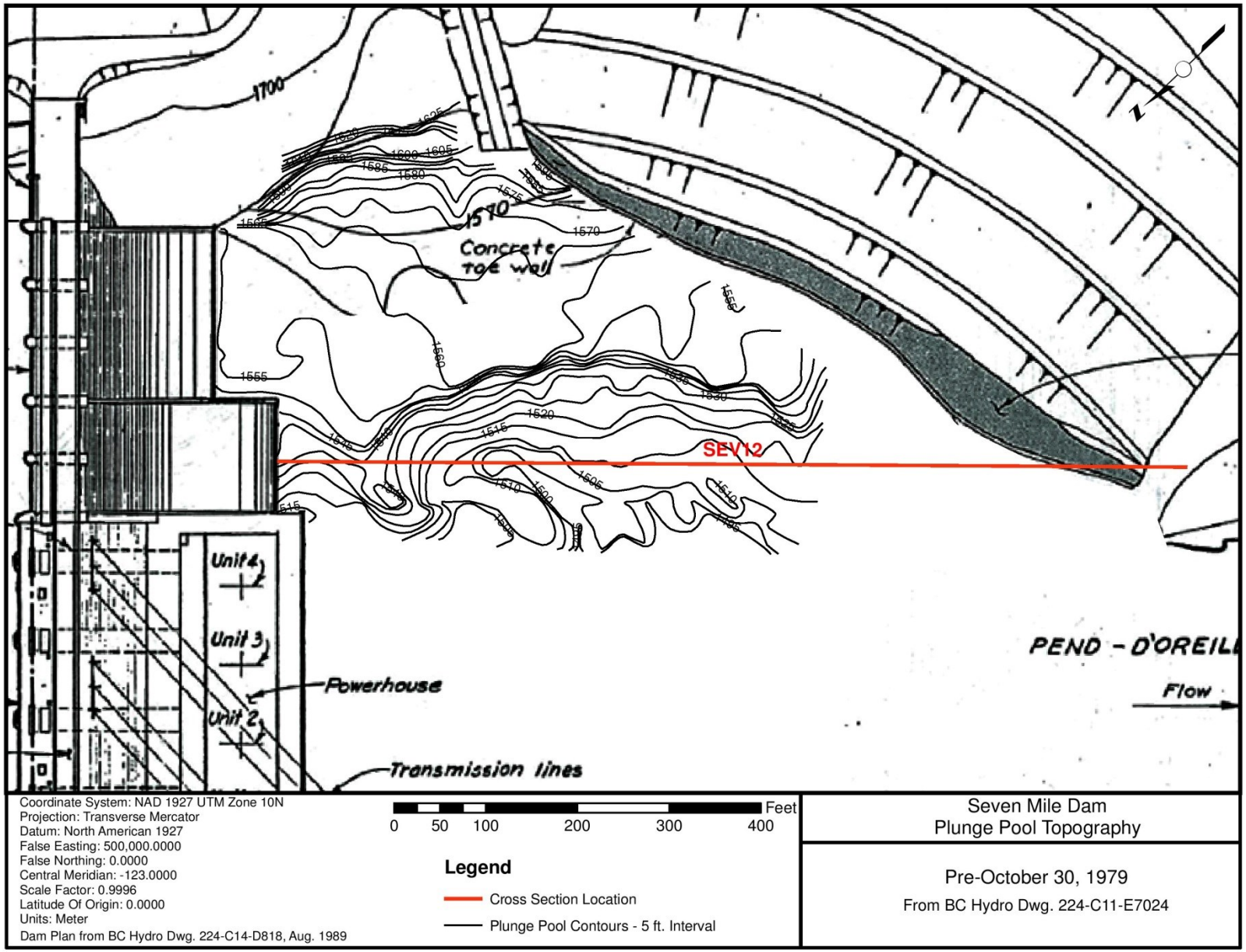

Coordinate System: NAD 1927 UTM Zone 10N
Projection: Transverse Mercator
Datum: North American 1927
False Easting: 500,000.0000
False Northing: 0.0000
Central Meridian: -123.0000
Scale Factor: 0.9996
Latitude Of Origin: 0.0000
Units: Meter
Dam Plan from BC Hydro Dwg. 224-C14-D818, Aug. 1989

0 50 100 200 300 400 Feet

Legend

Cross Section Location

Plunge Pool Contours - 5 ft. Interval

Seven Mile Dam
Plunge Pool Topography

Pre-October 30, 1979

From BC Hydro Dwg. 224-C11-E7024

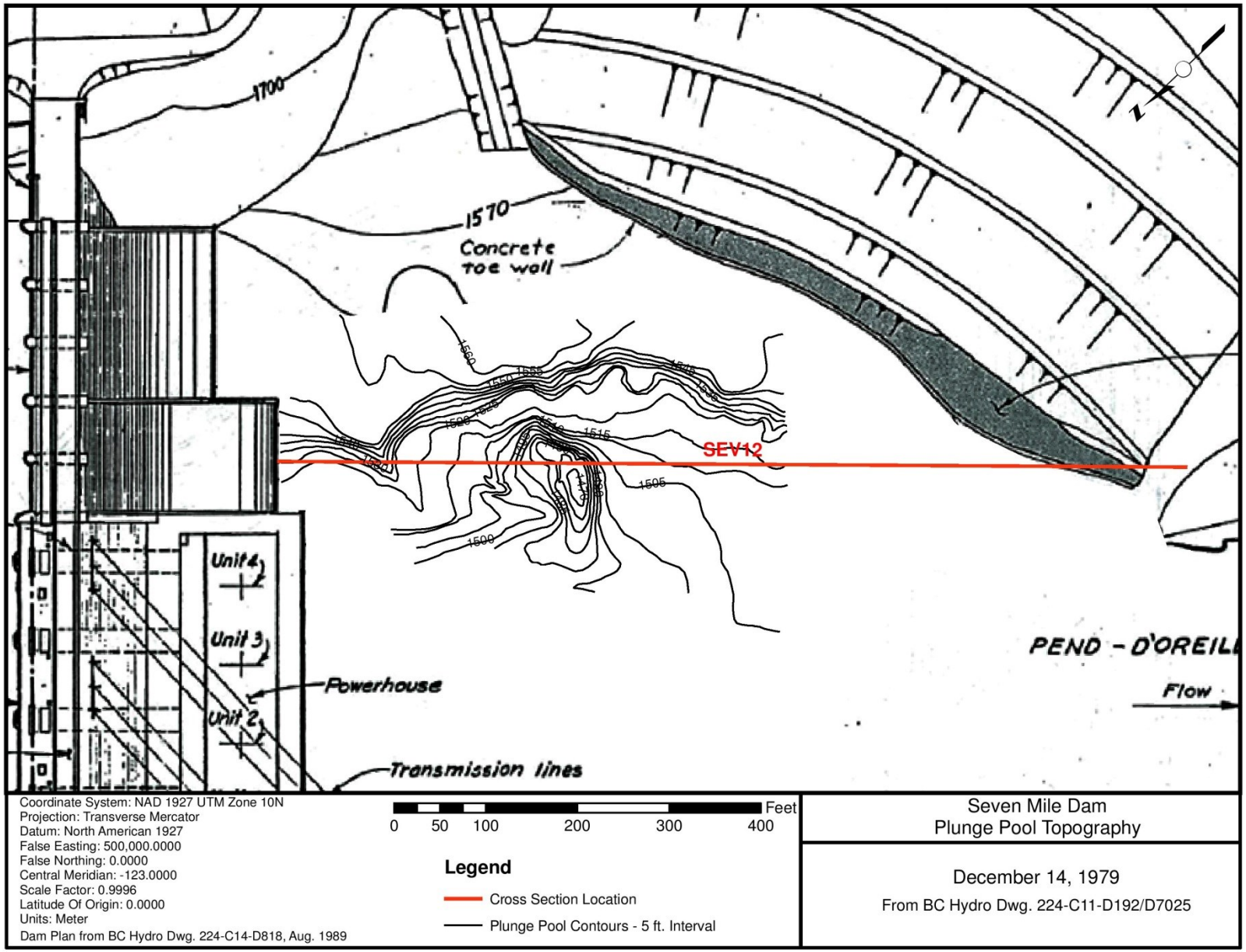

Coordinate System: NAD 1927 UTM Zone 10N
Projection: Transverse Mercator
Datum: North American 1927
False Easting: 500,000.0000
False Northing: 0.0000
Central Meridian: -123.0000
Scale Factor: 0.9996
Latitude Of Origin: 0.0000
Units: Meter
Dam Plan from BC Hydro Dwg. 224-C14-D818, Aug. 1989

0 50 100 200 300 400 Feet

Legend

Cross Section Location

Plunge Pool Contours - 5 ft. Interval

Seven Mile Dam
Plunge Pool Topography

December 14, 1979

From BC Hydro Dwg. 224-C11-D192/D7025

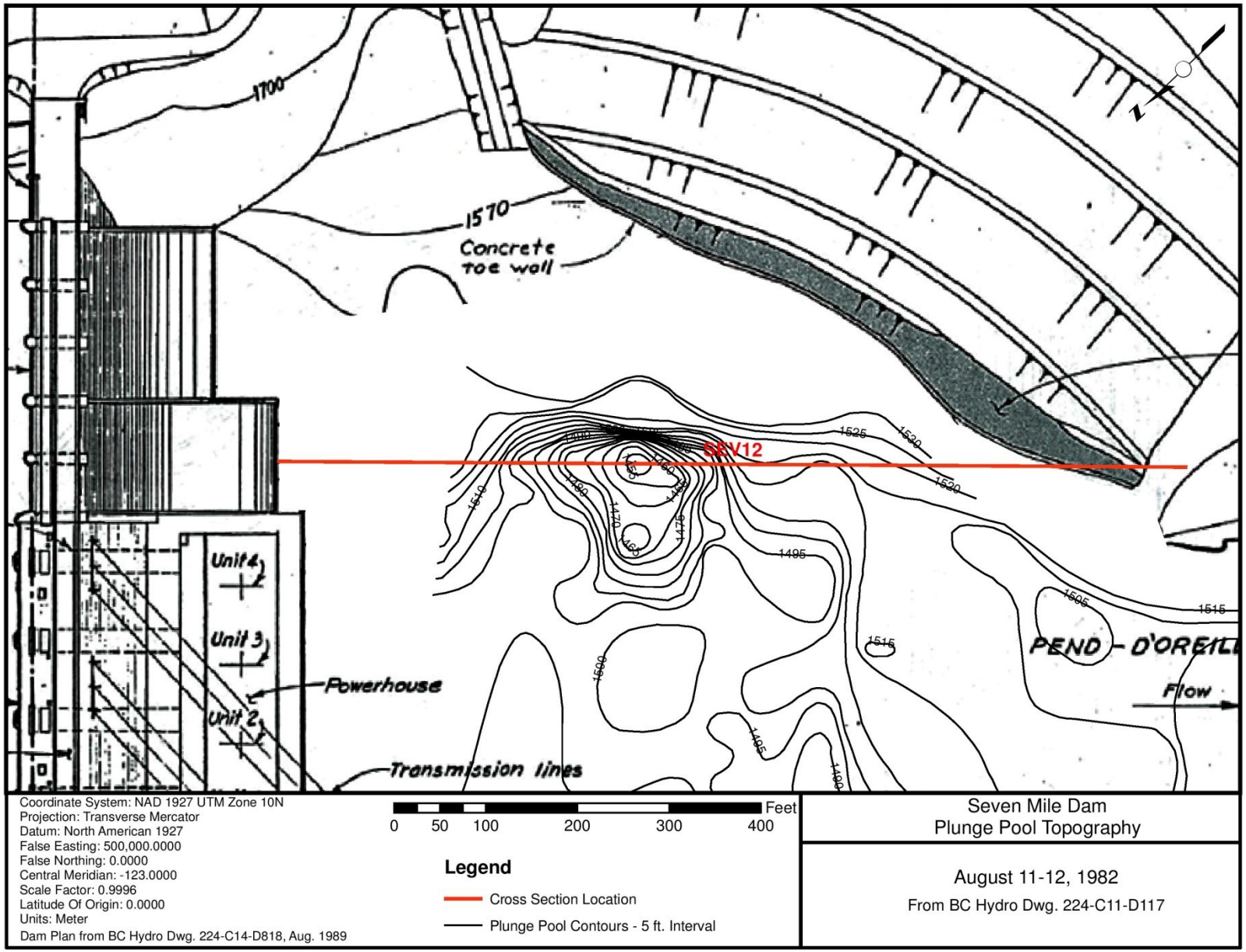
1700
1570
Concrete toe wall
SEV12
1525
1530
1520
1510
1495
1515
1505
1500
1490
Unit 4
Unit 3
Unit 2
Powerhouse
Transmission lines
PEND - D'OREILL
Flow
N
Coordinate System: NAD 1927 UTM Zone 10N
Projection: Transverse Mercator
Datum: North American 1927
False Easting: 500,000.0000
False Northing: 0.0000
Central Meridian: -123.0000
Scale Factor: 0.9996
Latitude Of Origin: 0.0000
Units: Meter
Dam Plan from BC Hydro Dwg. 224-C14-D818, Aug. 1989
0 50 100 200 300 400 Feet
Legend
Cross Section Location
Plunge Pool Contours - 5 ft. Interval
Seven Mile Dam
Plunge Pool Topography
August 11-12, 1982
From BC Hydro Dwg. 224-C11-D117

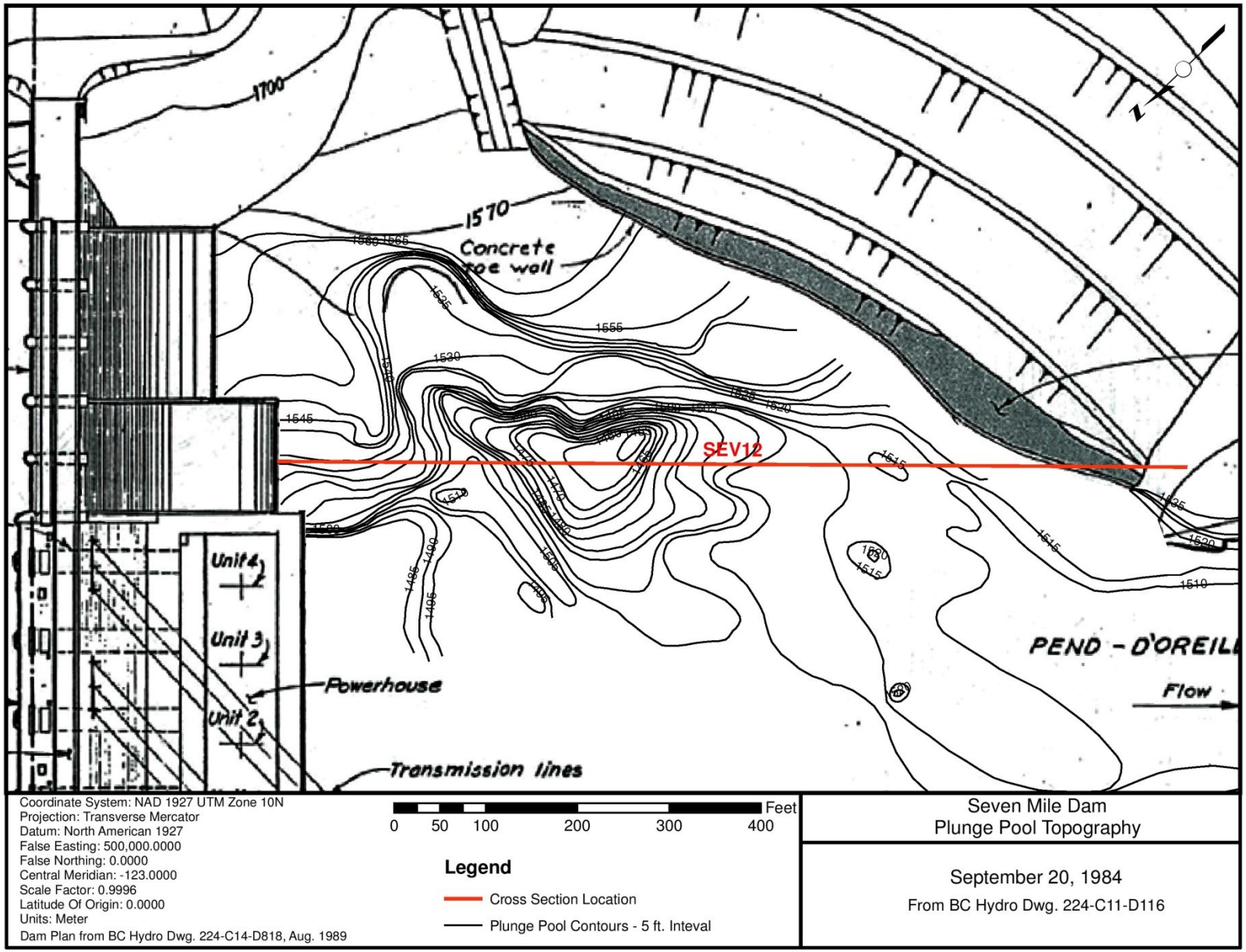
1700
1570
Concrete toe wall
1555
1545
1520
SEV12
1515
1510
Unit 4
Unit 3
Unit 2
Powerhouse
Transmission lines
PEND - D'OREIL
Flow
N
Coordinate System: NAD 1927 UTM Zone 10N
Projection: Transverse Mercator
Datum: North American 1927
False Easting: 500,000.0000
False Northing: 0.0000
Central Meridian: -123.0000
Scale Factor: 0.9996
Latitude Of Origin: 0.0000
Units: Meter
Dam Plan from BC Hydro Dwg. 224-C14-D818, Aug. 1989
0 50 100 200 300 400 Feet
Legend
Cross Section Location
Plunge Pool Contours - 5 ft. Inteval
Seven Mile Dam
Plunge Pool Topography
September 20, 1984
From BC Hydro Dwg. 224-C11-D116

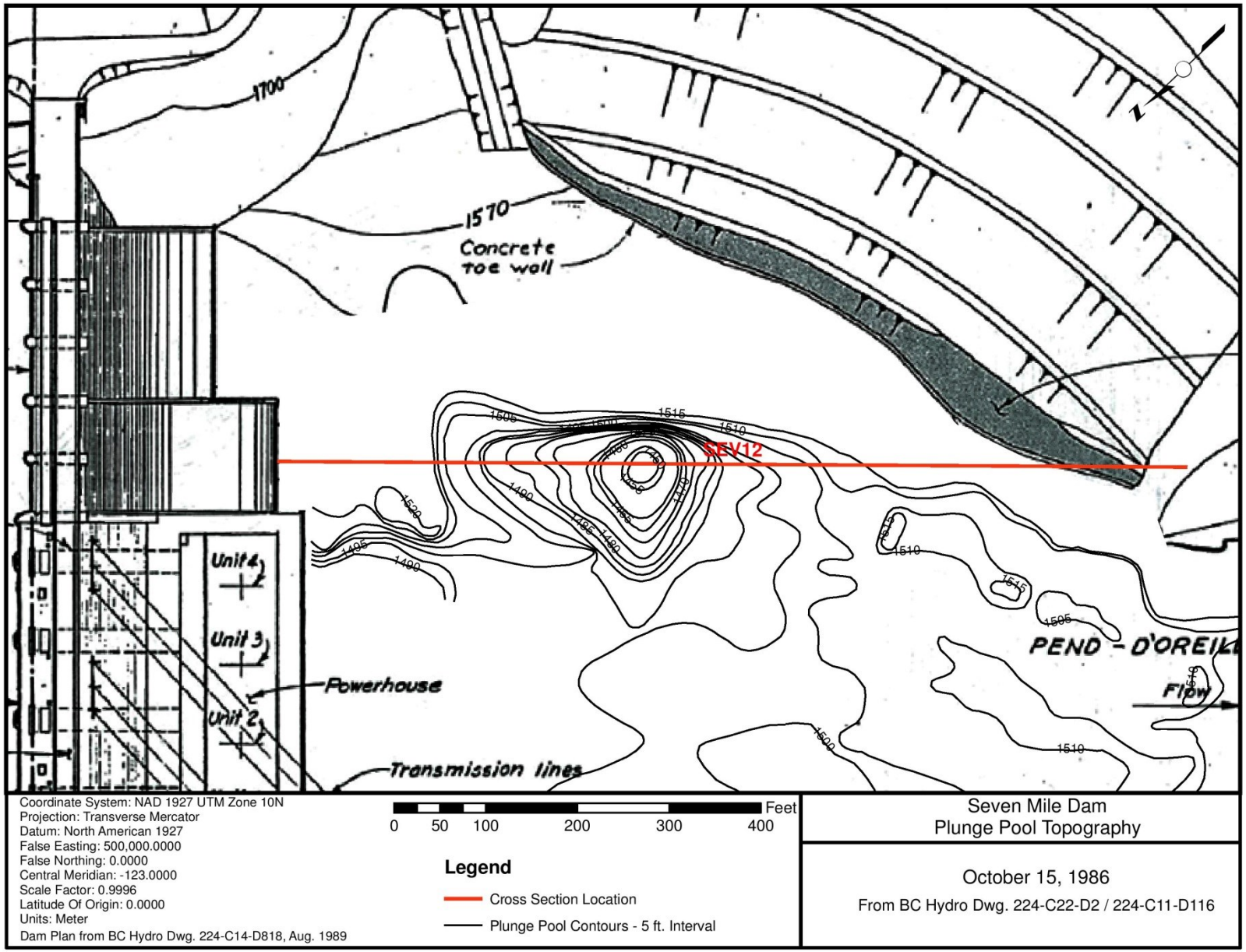
1700
1570
Concrete toe wall
SEV12
Unit 4
Unit 3
Unit 2
Powerhouse
Transmission lines
PEND - D'OREIL
Flow
Coordinate System: NAD 1927 UTM Zone 10N
Projection: Transverse Mercator
Datum: North American 1927
False Easting: 500,000.0000
False Northing: 0.0000
Central Meridian: -123.0000
Scale Factor: 0.9996
Latitude Of Origin: 0.0000
Units: Meter
Dam Plan from BC Hydro Dwg. 224-C14-D818, Aug. 1989
0 50 100 200 300 400 Feet
Legend
Cross Section Location
Plunge Pool Contours - 5 ft. Interval
Seven Mile Dam
Plunge Pool Topography
October 15, 1986
From BC Hydro Dwg. 224-C22-D2 / 224-C11-D116

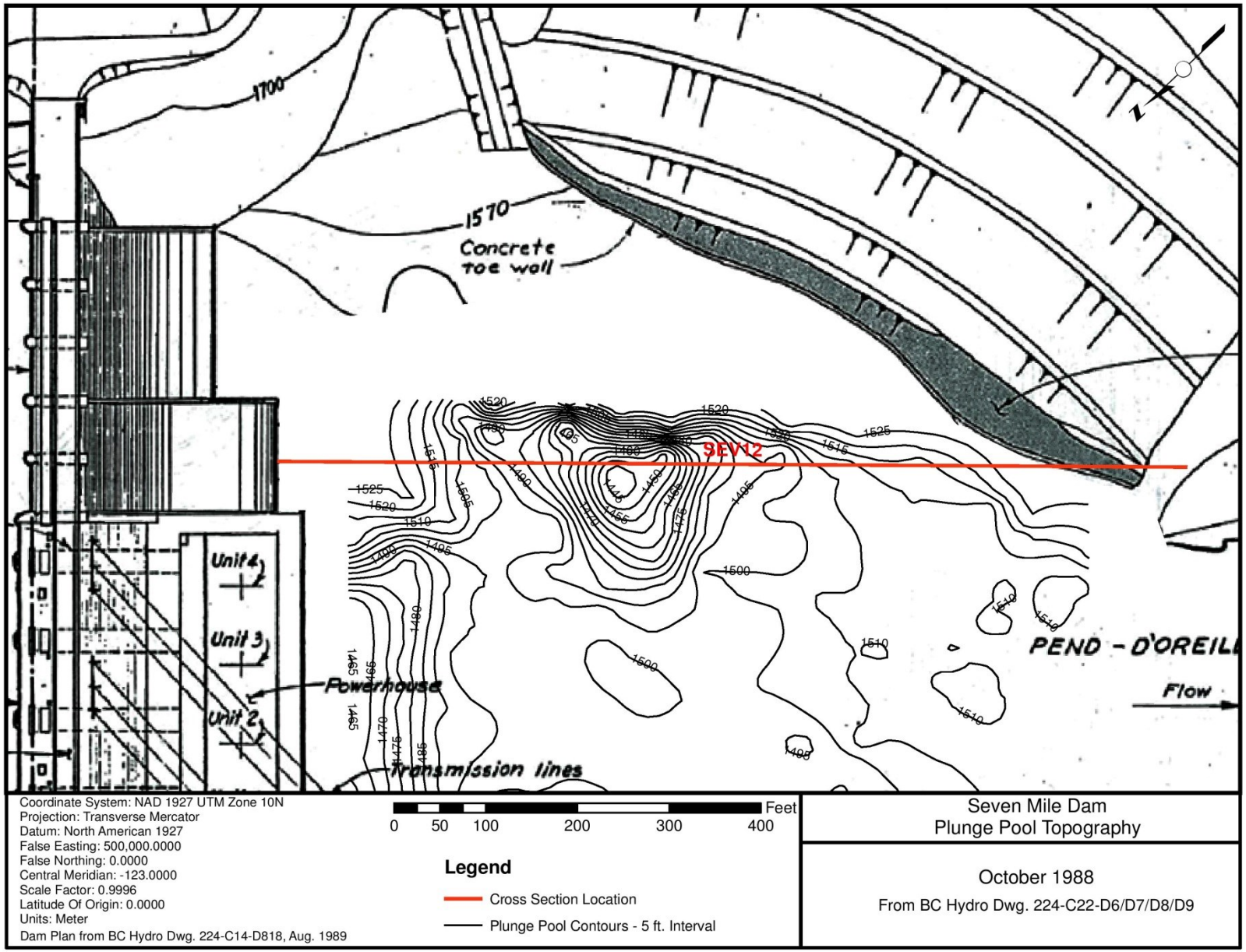

Coordinate System: NAD 1927 UTM Zone 10N
Projection: Transverse Mercator
Datum: North American 1927
False Easting: 500,000.0000
False Northing: 0.0000
Central Meridian: -123.0000
Scale Factor: 0.9996
Latitude Of Origin: 0.0000
Units: Meter
Dam Plan from BC Hydro Dwg. 224-C14-D818, Aug. 1989

0 50 100 200 300 400 Feet

Legend

Cross Section Location

Plunge Pool Contours - 5 ft. Interval

Seven Mile Dam
Plunge Pool Topography

October 1988

From BC Hydro Dwg. 224-C22-D6/D7/D8/D9

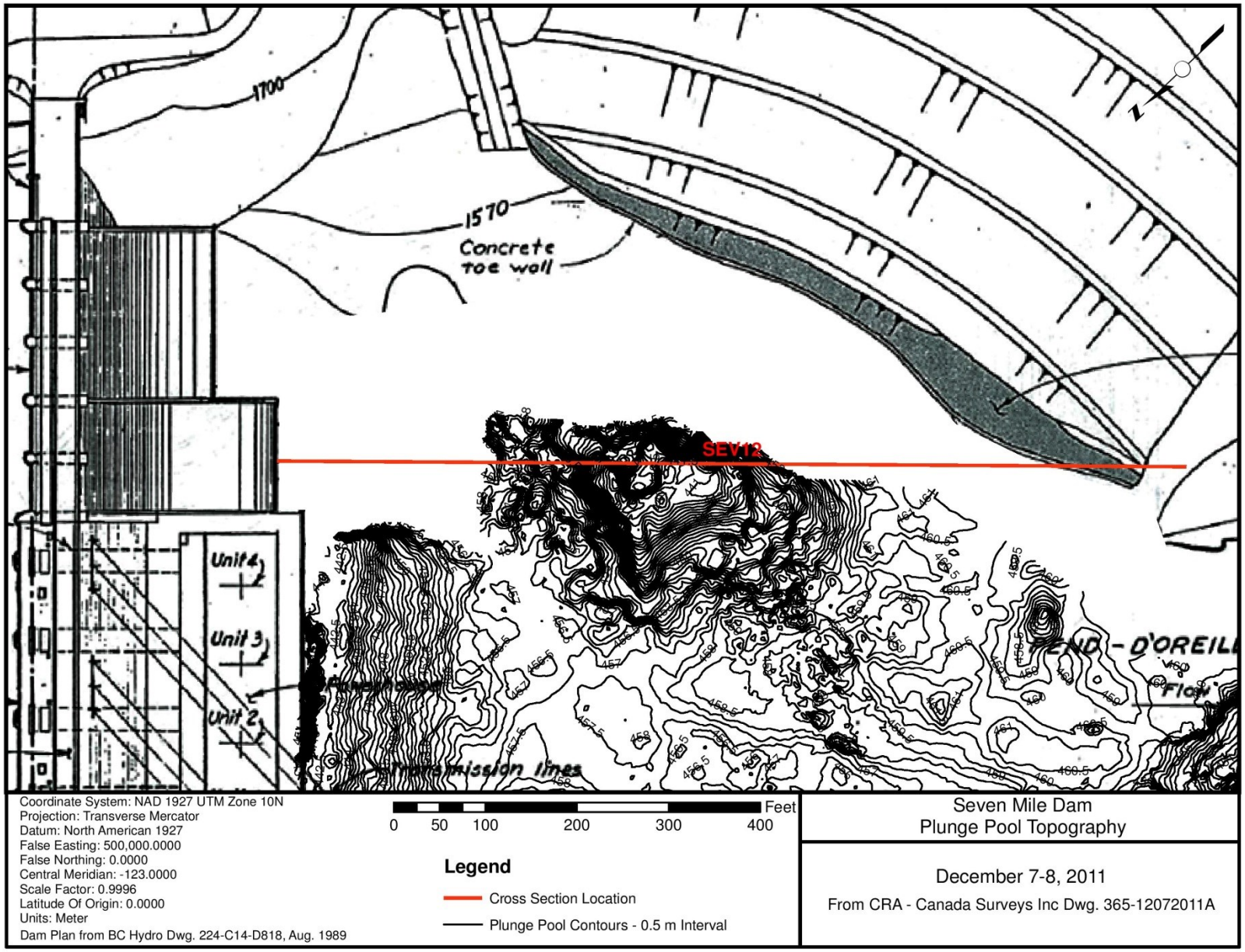
1700
1570
Concrete
toe wall
SEV12
Unit 4
Unit 3
Unit 2
Transmission lines
Flow
Coordinate System: NAD 1927 UTM Zone 10N
Projection: Transverse Mercator
Datum: North American 1927
False Easting: 500,000.0000
False Northing: 0.0000
Central Meridian: -123.0000
Scale Factor: 0.9996
Latitude Of Origin: 0.0000
Units: Meter
Dam Plan from BC Hydro Dwg. 224-C14-D818, Aug. 1989
Feet
0 50 100 200 300 400
Legend
Cross Section Location
Plunge Pool Contours - 0.5 m Interval
Seven Mile Dam
Plunge Pool Topography
December 7-8, 2011
From CRA - Canada Surveys Inc Dwg. 365-12072011A

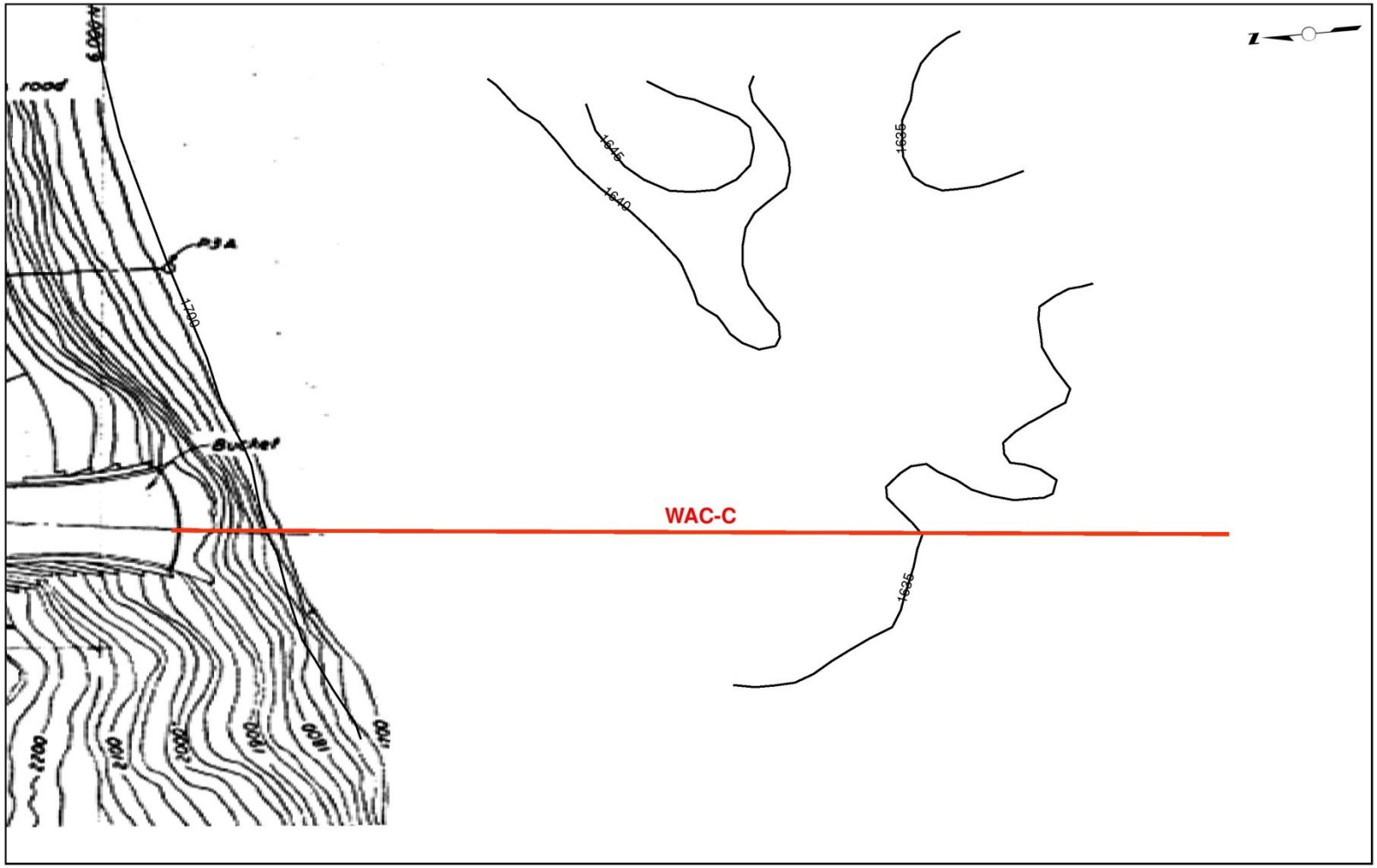

Coordinate System: NAD 1927 UTM Zone 11N
Projection: Transverse Mercator
Datum: North American 1927
False Easting: 500,000.0000
False Northing: 0.0000
Central Meridian: -117.0000
Scale Factor: 0.9996
Latitude Of Origin: 0.0000
Units: Meter
Spillway Plan from BC Hydro Dwg. 1006-C14-C293, Jul. 1973

Feet
0 40 80 160 240 320

Legend

Cross Section Location

Plunge Pool Contours - 5 ft. Interval

W.A.C. Bennett Dam
Plunge Pool Topography

June 1969

From BC Hydro Dwg. 1006-C14-B1262

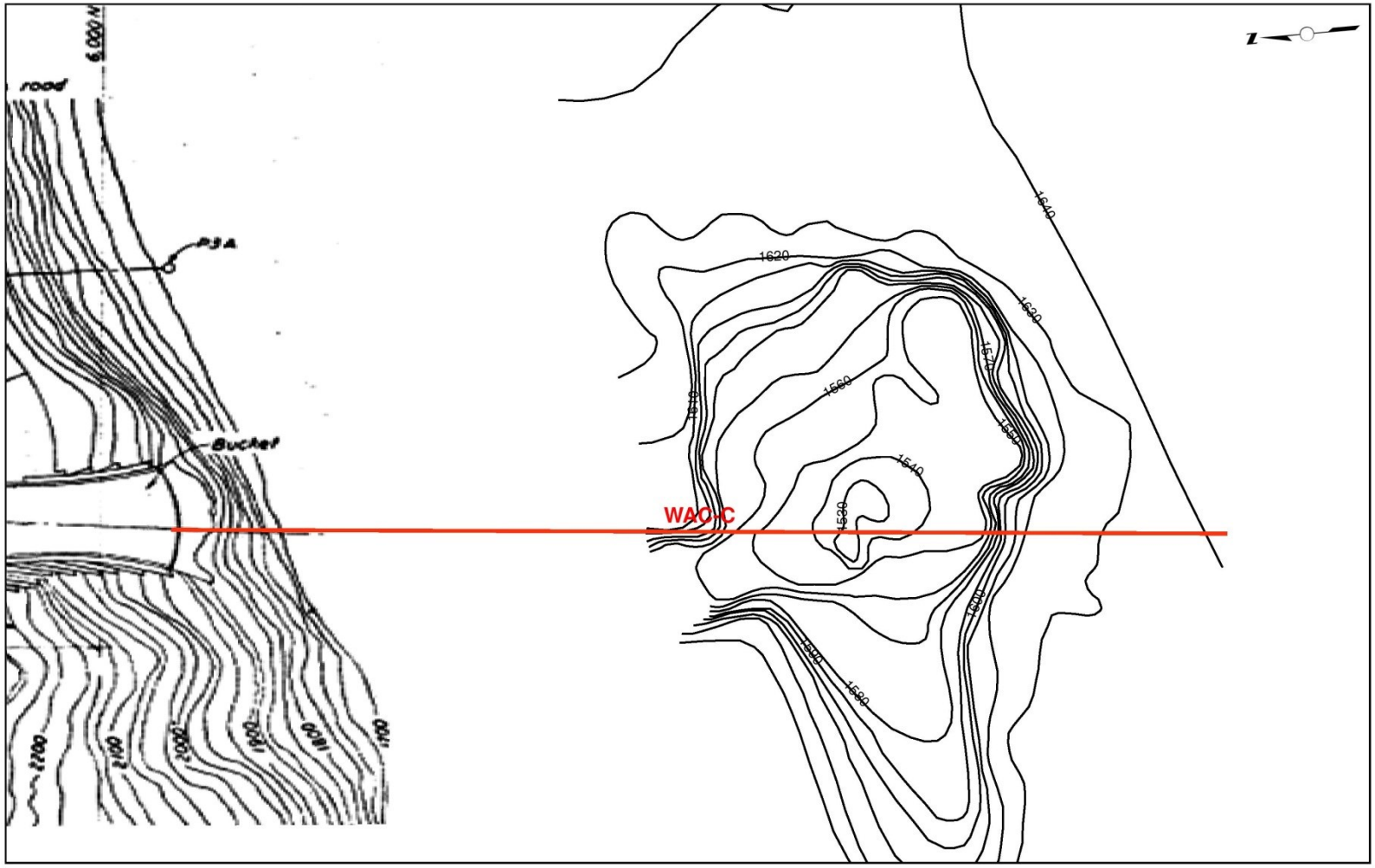

Coordinate System: NAD 1927 UTM Zone 11N
Projection: Transverse Mercator
Datum: North American 1927
False Easting: 500,000.0000
False Northing: 0.0000
Central Meridian: -117.0000
Scale Factor: 0.9996
Latitude Of Origin: 0.0000
Units: Meter
Spillway Plan from BC Hydro Dwg. 1006-C14-C293, Jul. 1973

0 40 80 160 240 320 Feet

Legend

Cross Section Location

Plunge Pool Contours - 5 ft. Interval

W.A.C. Bennett Dam
Plunge Pool Topography

May 15-16, 1973

From BC Hydro Dwg. 1006-C14-B1262

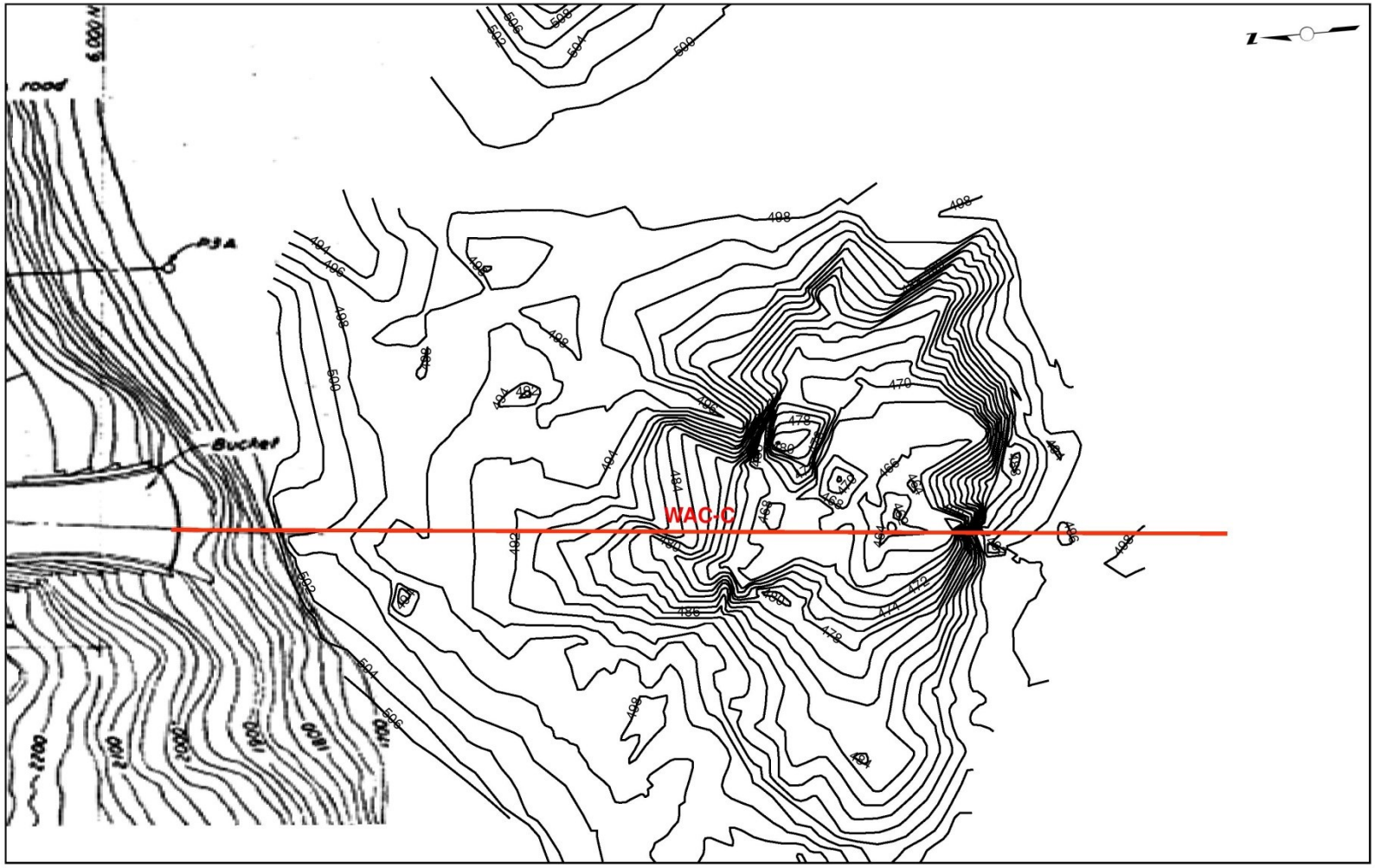

Coordinate System: NAD 1927 UTM Zone 11N
Projection: Transverse Mercator
Datum: North American 1927
False Easting: 500,000.0000
False Northing: 0.0000
Central Meridian: -117.0000
Scale Factor: 0.9996
Latitude Of Origin: 0.0000
Units: Meter
Spillway Plan from BC Hydro Dwg. 1006-C14-C293, Jul. 1973

0 40 80 160 240 320 Feet

Legend

Cross Section Location

Plunge Pool Contours - 2 m Interval

W.A.C. Bennett Dam
Plunge Pool Topography

August 4, 1996

From BC Hydro Dwg. 1006-C11-D1107

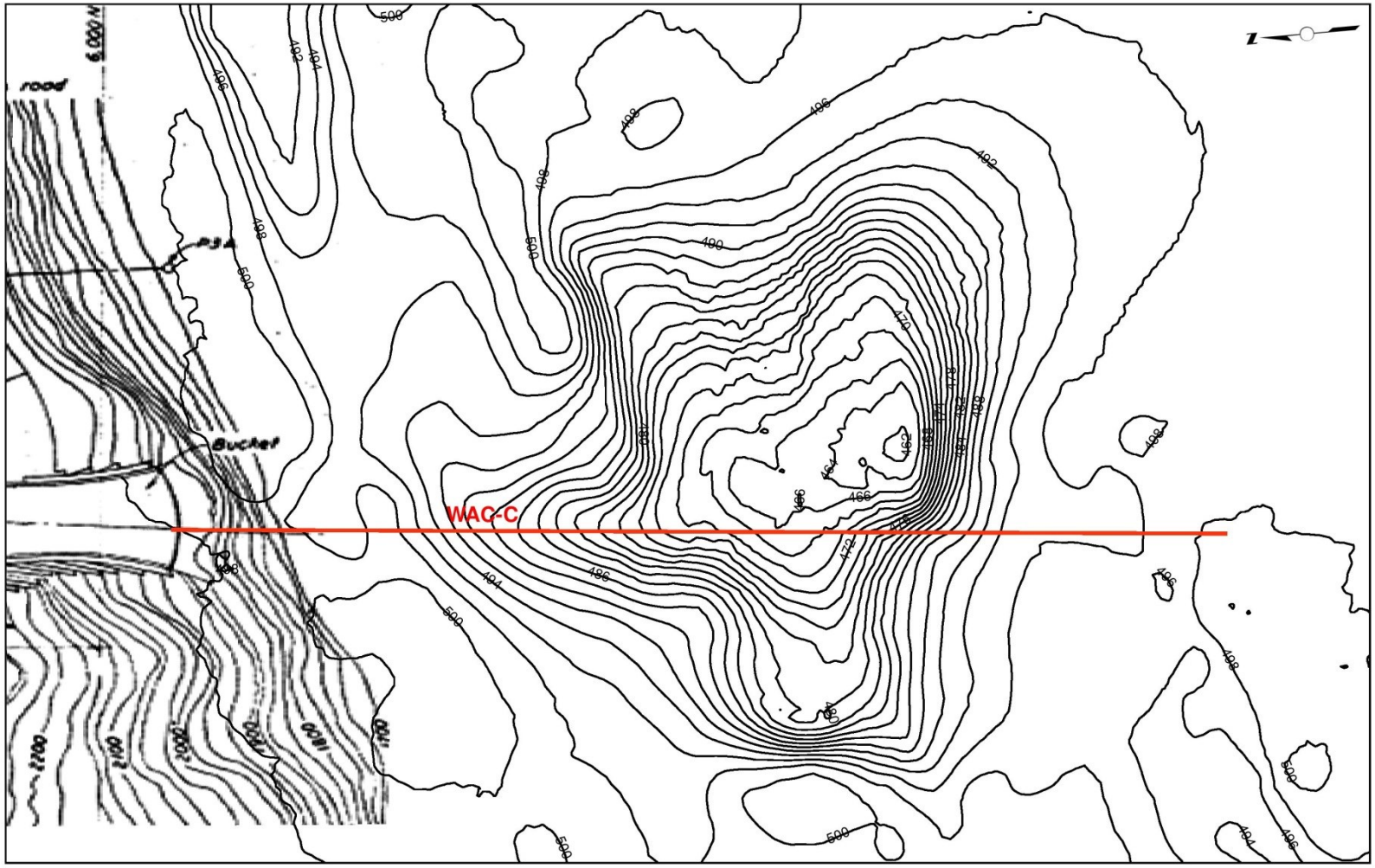

Coordinate System: NAD 1927 UTM Zone 11N
Projection: Transverse Mercator
Datum: North American 1927
False Easting: 500,000.0000
False Northing: 0.0000
Central Meridian: -117.0000
Scale Factor: 0.9996
Latitude Of Origin: 0.0000
Units: Meter
Spillway Plan from BC Hydro Dwg. 1006-C14-C293, Jul. 1973

0 40 80 160 240 320 Feet

Legend

Cross Section Location

Plunge Pool Contours - 2 m Interval

W.A.C. Bennett Dam
Plunge Pool Topography

October 2002

From BC Hydro Dwg. (None Provided)

APPENDIX D

NUMERICAL MODEL RESULTS – ELECTRONIC FILES

Included in this appendix are *EIM_ProfileCalc* program output files for each modeled cross-section. Each file included here contains four sheets: 1) Explanation of variables, 2) model results for 'Low' EIM values, 3) model results for 'Mean' EIM values, and 4) model results for 'High' EIM values. Each row is associated with a date of discharge represents the input values for, and the output values from, the program.

Model Output Files	Files containing tabular data for each modeled cross section, with model input and output values.
PCN34-ModelOutput.xlsx	Contains tabulated data of modeled results for cross section PCN-34 from Peace Canyon Dam
PCN56-ModelOutput.xlsx	Contains tabulated data of modeled results for cross section PCN-56 from Peace Canyon Dam
SEV12-ModelOutput.xlsx	Contains tabulated data of modeled results for cross section SEV-12 from Seven Mile Dam
REV-ModelOutput.xlsx	Contains tabulated data of modeled results for cross section REV-1 from Revelstoke Dam
WAC-ModelOutput.xlsx	Contains tabulated data of modeled results for cross section WAC-C from W.A.C. Bennett Dam

APPENDIX E

MODELED PROFILES

Appendix E.1 Peace Canyon Dam Profile PCN-34 – Low Erodibility Index

See Section 7.1.3 for explanation of geomechanical zones

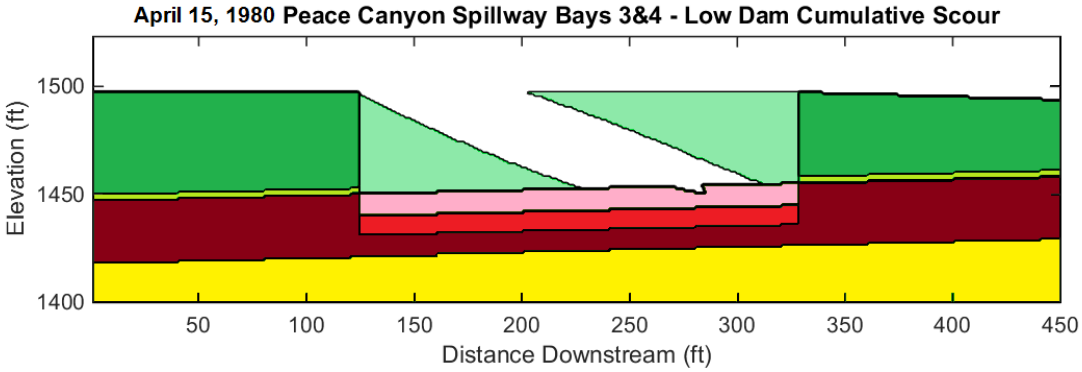

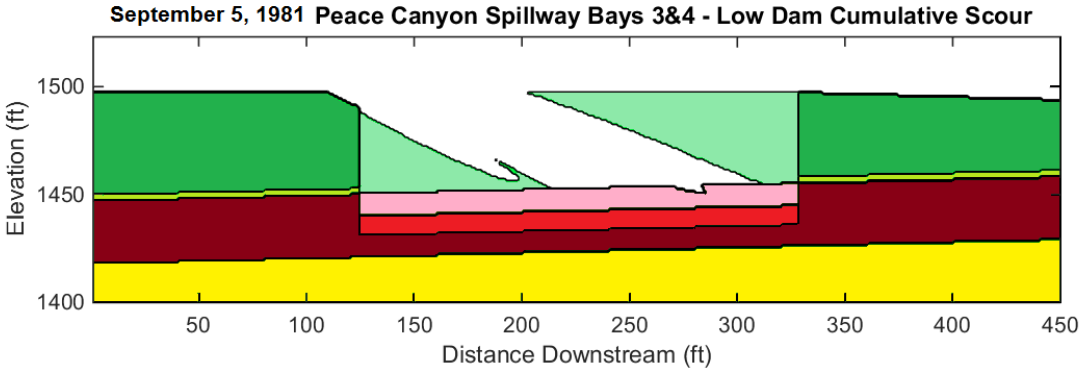

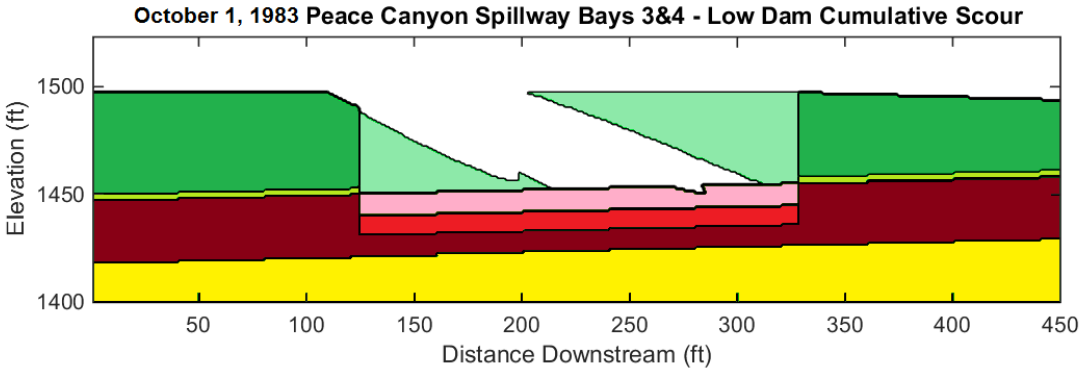

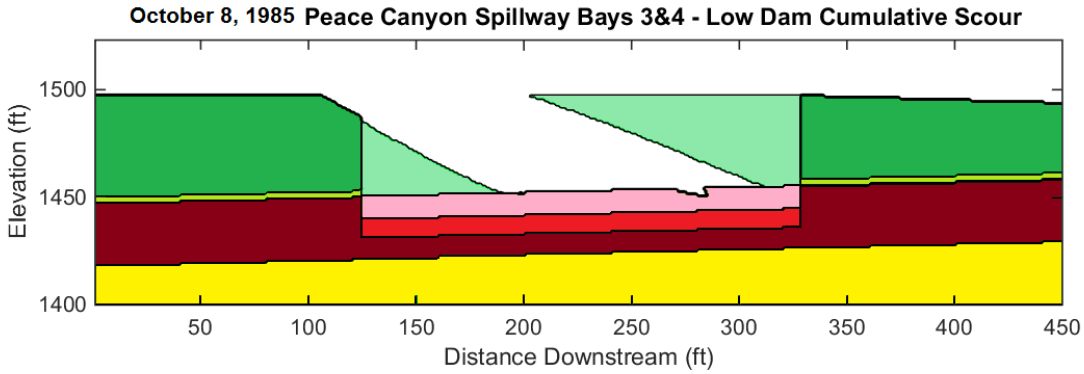
October 8, 1985 Peace Canyon Spillway Bays 3&4 - Low Dam Cumulative Scour
Elevation (ft)
1500
1450
1400
50
100
150
200
250
300
350
400
450
Distance Downstream (ft)

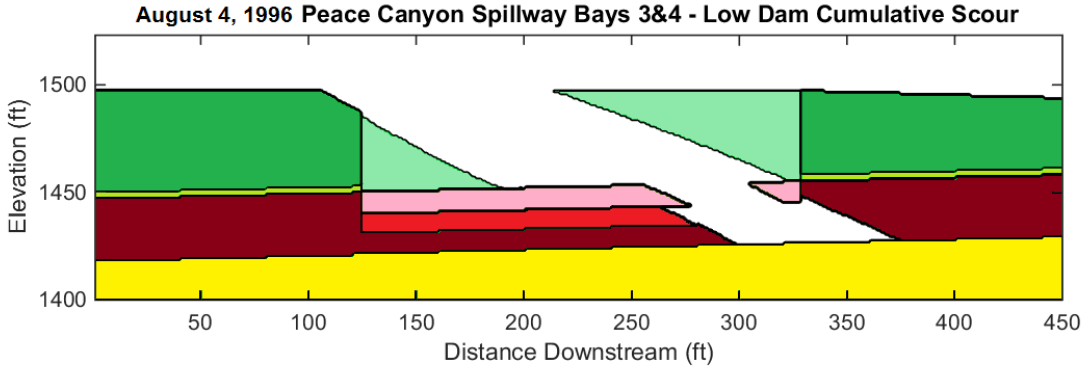
August 4, 1996 Peace Canyon Spillway Bays 3&4 - Low Dam Cumulative Scour
Elevation (ft)
1500
1450
1400
50
100
150
200
250
300
350
400
450
Distance Downstream (ft)

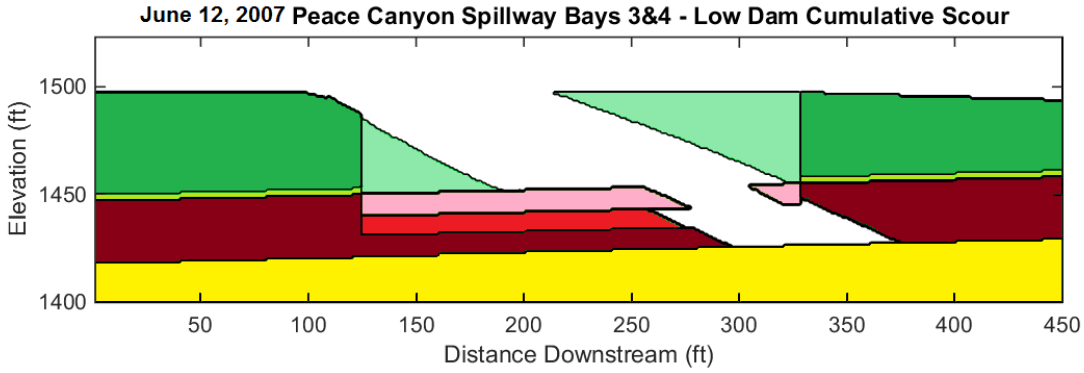
June 12, 2007 Peace Canyon Spillway Bays 3&4 - Low Dam Cumulative Scour
Elevation (ft)
1500
1450
1400
50
100
150
200
250
300
350
400
450
Distance Downstream (ft)

Appendix E.1 Peace Canyon Dam Profile PCN-34 – Mean Erodibility Index

See Section 7.1.3 for explanation of geomechanical zones

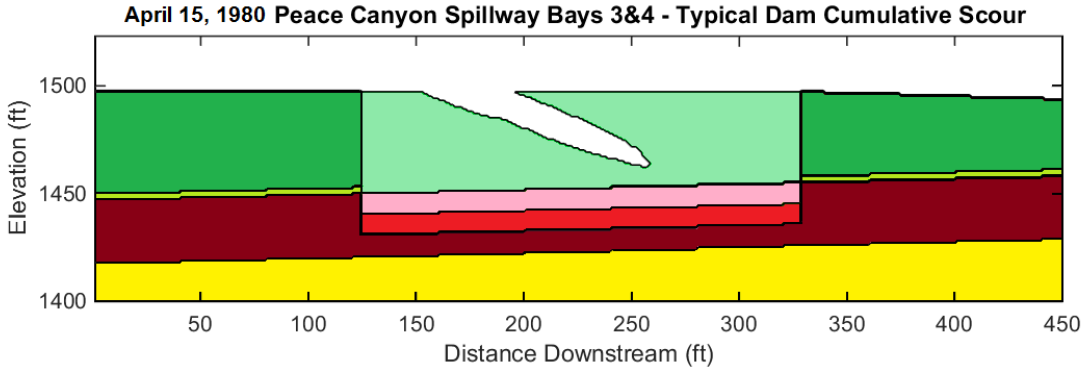

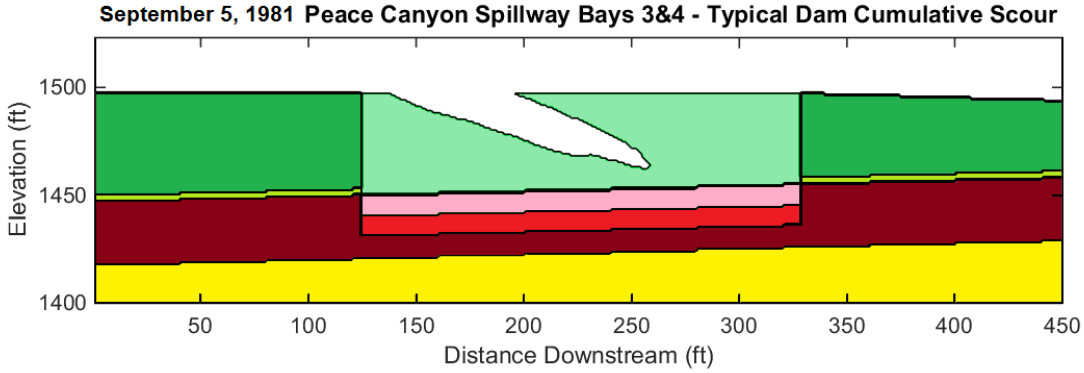

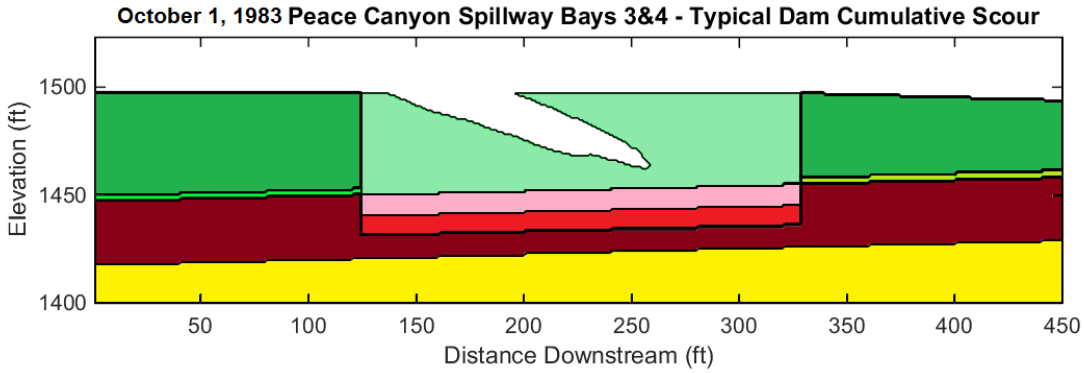

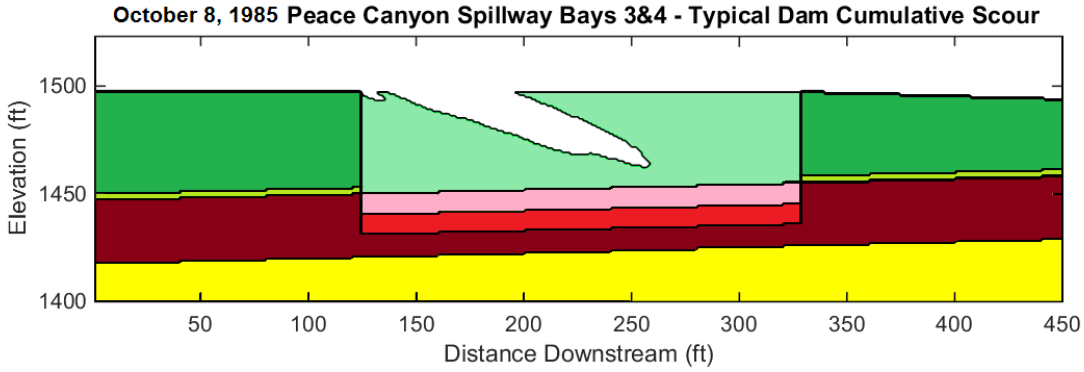
October 8, 1985 Peace Canyon Spillway Bays 3&4 - Typical Dam Cumulative Scour
Elevation (ft)
1500
1450
1400
50
100
150
200
250
300
350
400
450
Distance Downstream (ft)

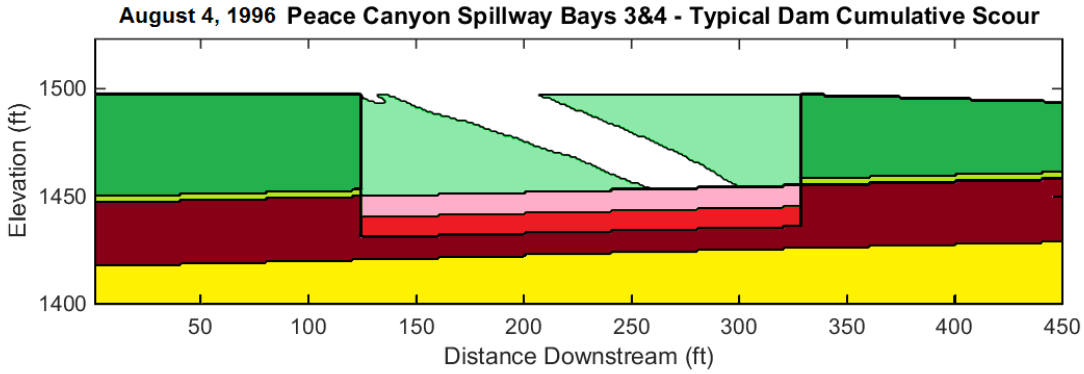
August 4, 1996 Peace Canyon Spillway Bays 3&4 - Typical Dam Cumulative Scour
Elevation (ft)
1500
1450
1400
50
100
150
200
250
300
350
400
450
Distance Downstream (ft)

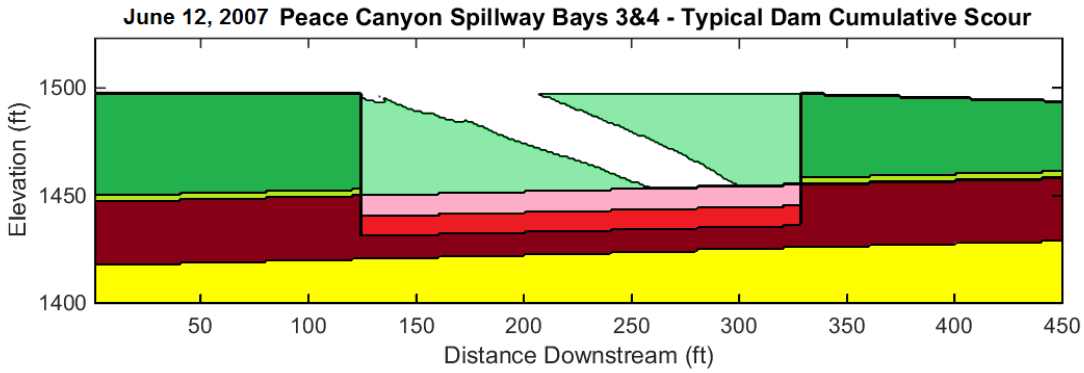
June 12, 2007 Peace Canyon Spillway Bays 3&4 - Typical Dam Cumulative Scour
Elevation (ft)
1500
1450
1400
50
100
150
200
250
300
350
400
450
Distance Downstream (ft)

Appendix E.1 Peace Canyon Dam Profile PCN-34 – High Erodibility Index

See Section 7.1.3 for explanation of geomechanical zones

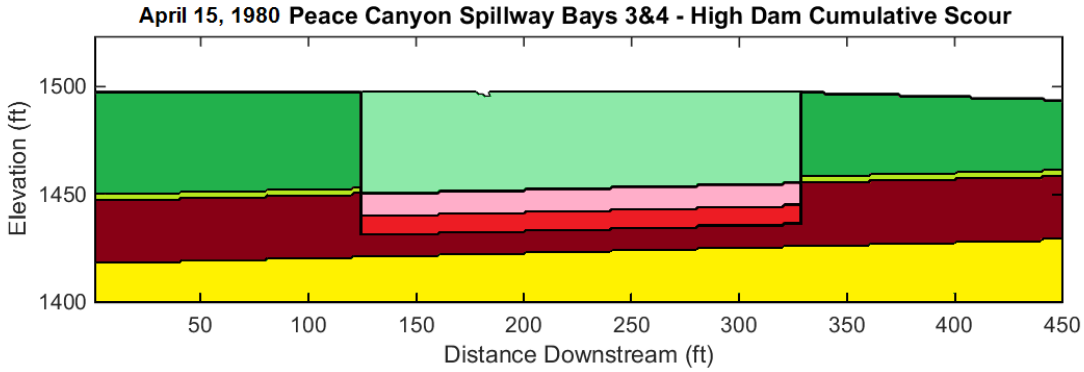

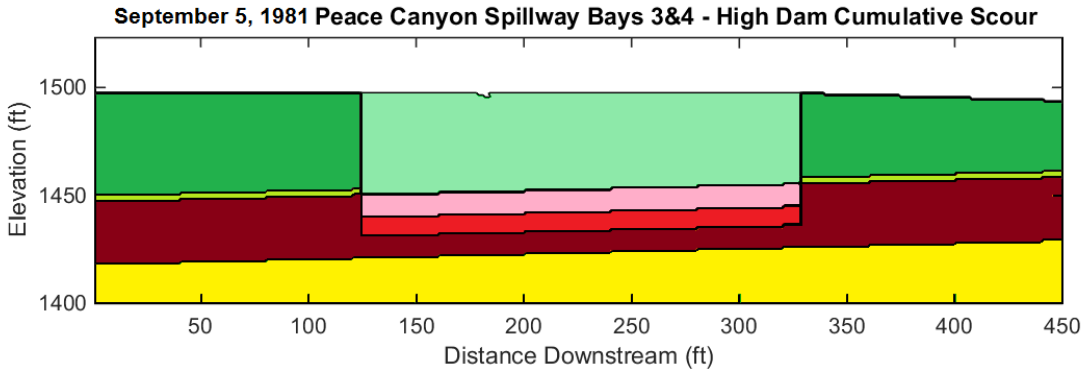

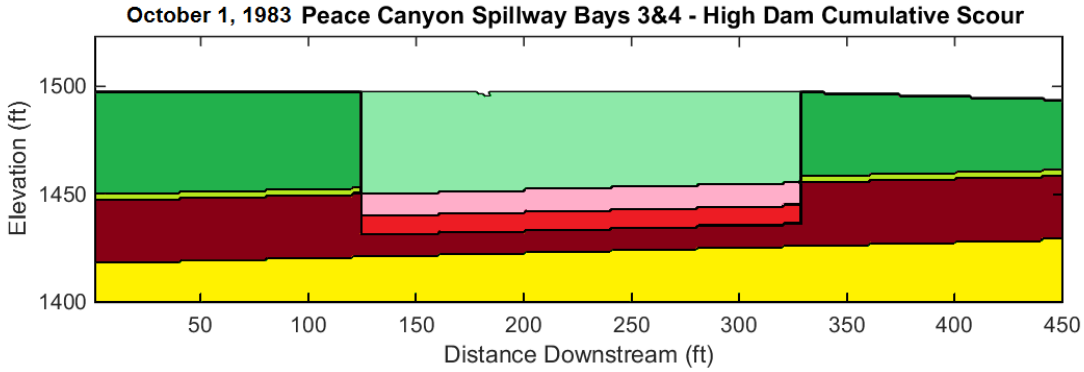

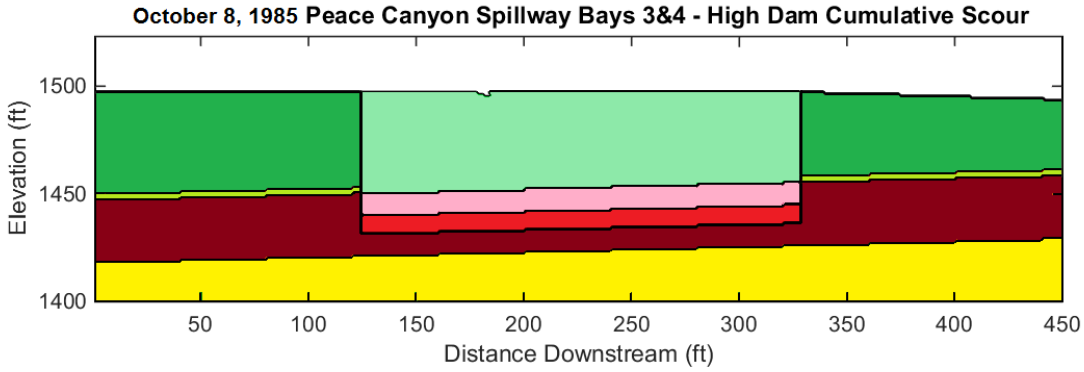
October 8, 1985 Peace Canyon Spillway Bays 3&4 - High Dam Cumulative Scour
Elevation (ft)
1500
1450
1400
50
100
150
200
250
300
350
400
450
Distance Downstream (ft)

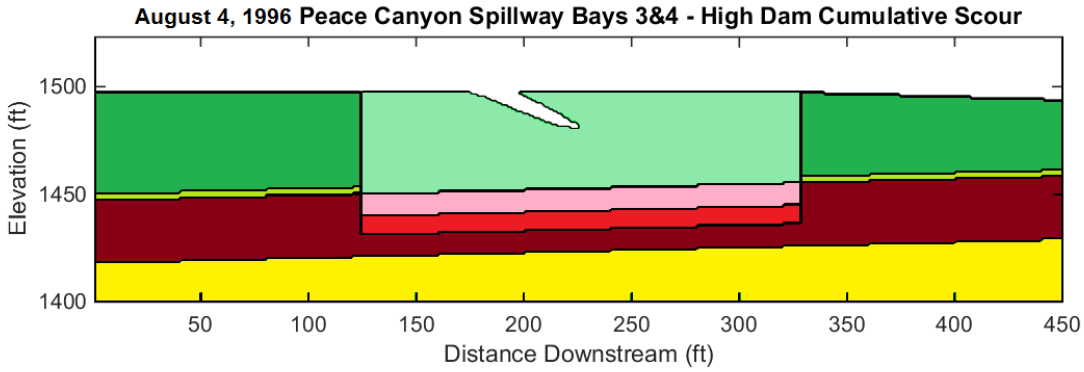
August 4, 1996 Peace Canyon Spillway Bays 3&4 - High Dam Cumulative Scour
Elevation (ft)
1500
1450
1400
50
100
150
200
250
300
350
400
450
Distance Downstream (ft)

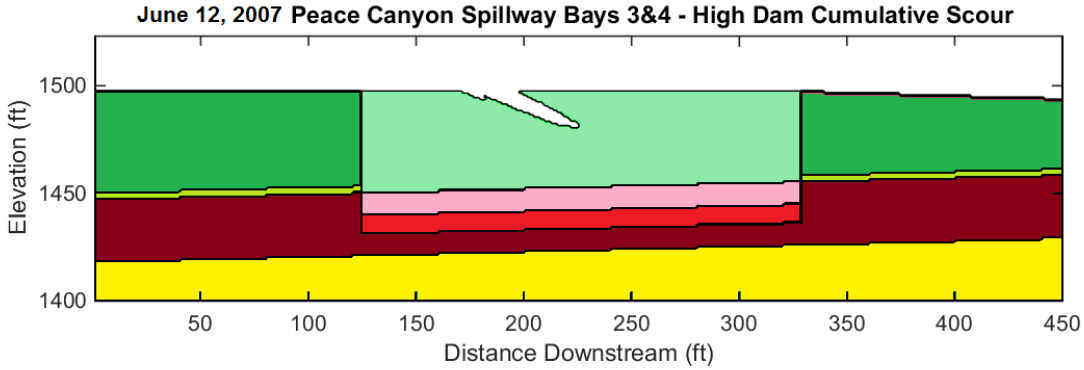
June 12, 2007 Peace Canyon Spillway Bays 3&4 - High Dam Cumulative Scour
Elevation (ft)
1500
1450
1400
50
100
150
200
250
300
350
400
450
Distance Downstream (ft)

Appendix E.2 Peace Canyon Dam Profile PCN-56 – Low Erodibility Index

See Section 7.1.3 for explanation of geomechanical zones

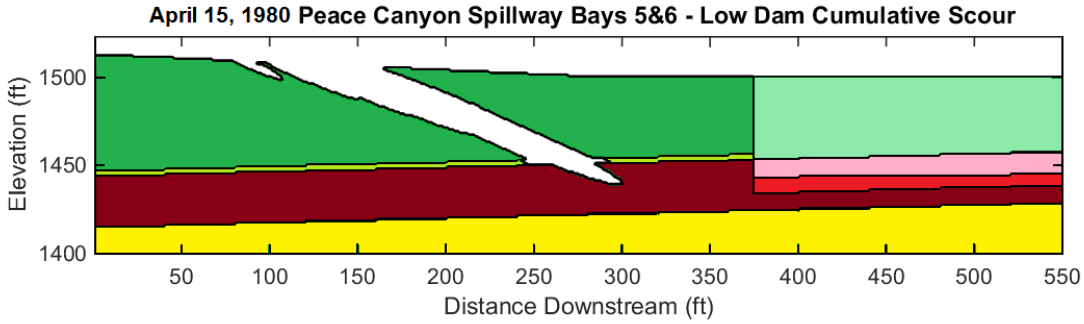

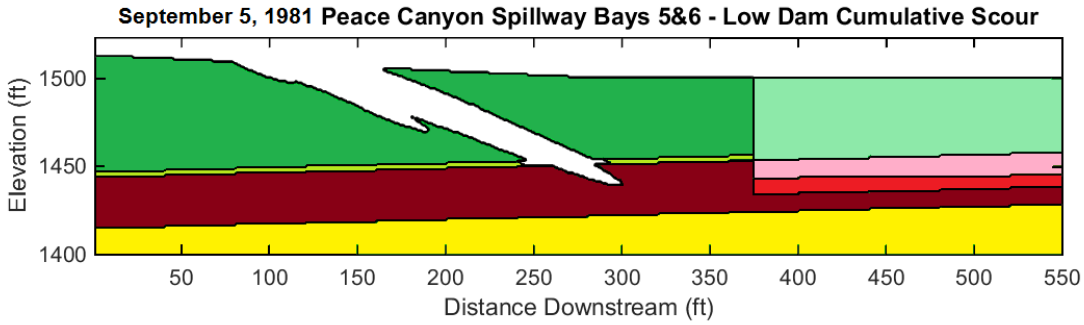

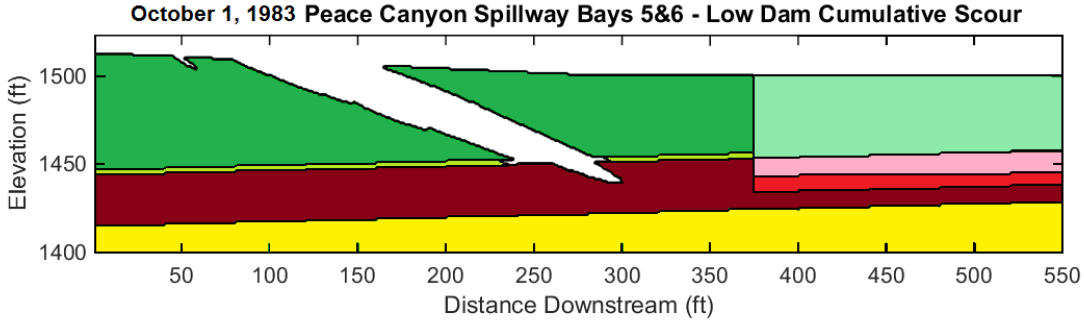

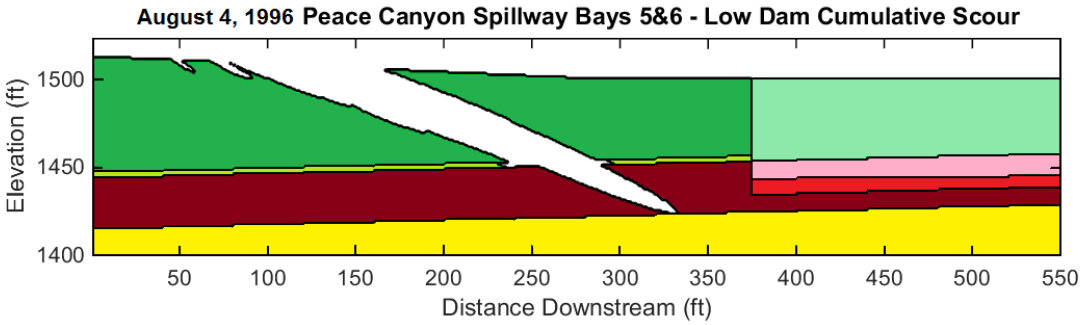
August 4, 1996 Peace Canyon Spillway Bays 5&6 - Low Dam Cumulative Scour
Elevation (ft)
1500
1450
1400
50
100
150
200
250
300
350
400
450
500
550
Distance Downstream (ft)

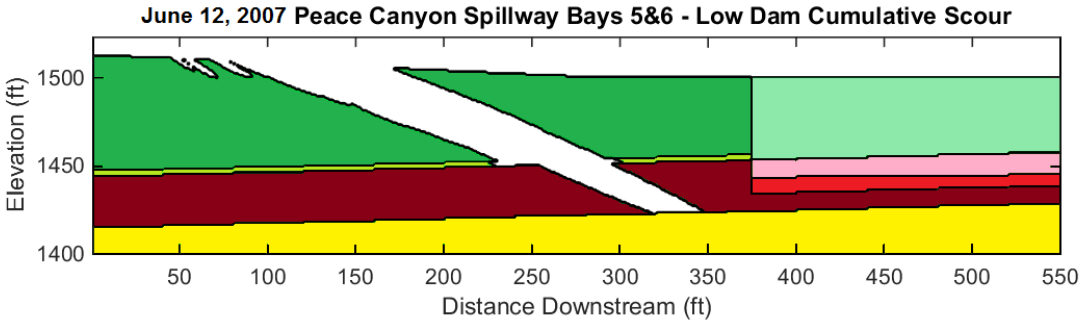
June 12, 2007 Peace Canyon Spillway Bays 5&6 - Low Dam Cumulative Scour
Elevation (ft)
1500
1450
1400
50
100
150
200
250
300
350
400
450
500
550
Distance Downstream (ft)

Appendix E.2 Peace Canyon Dam Profile PCN-56 – Mean Erodibility Index

See Section 7.1.3 for explanation of geomechanical zones

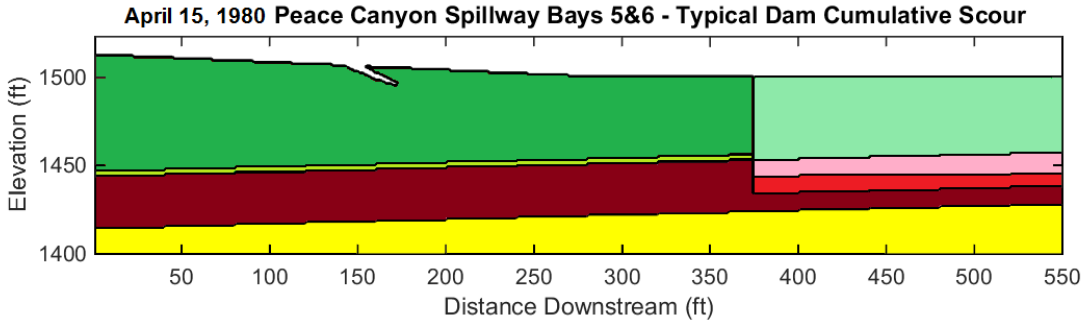

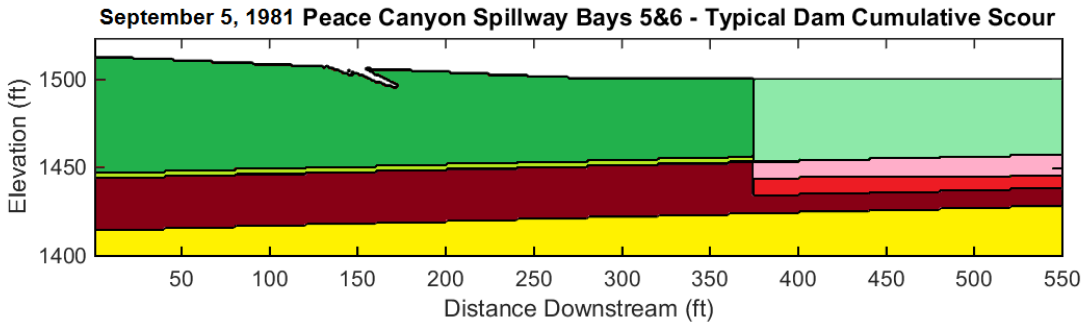

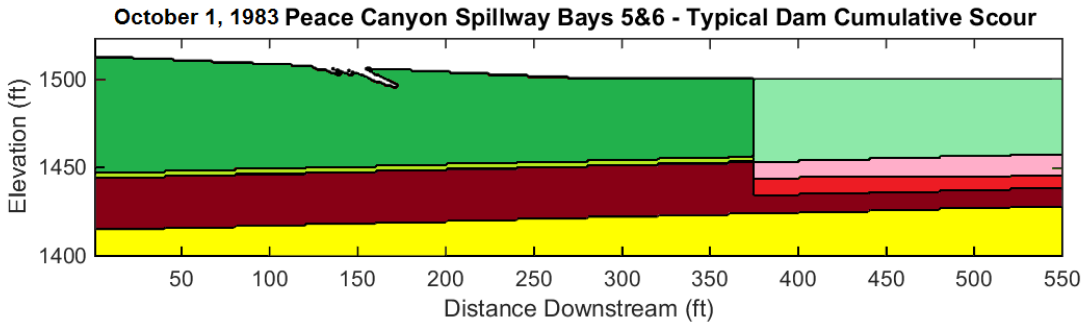

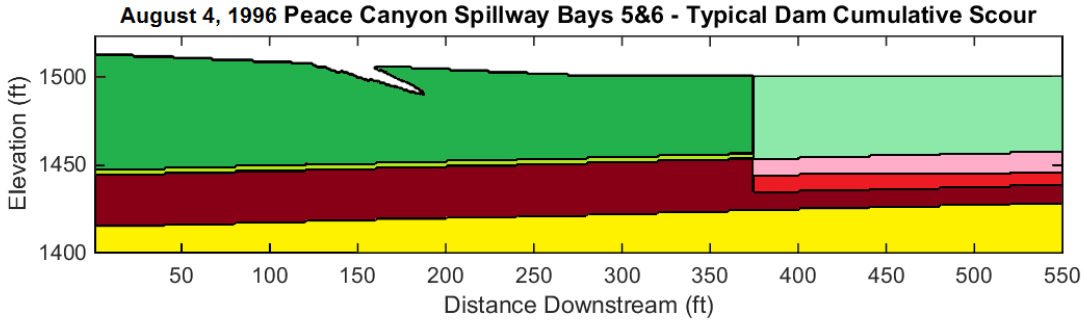
August 4, 1996 Peace Canyon Spillway Bays 5&6 - Typical Dam Cumulative Scour
Elevation (ft)
1500
1450
1400
50
100
150
200
250
300
350
400
450
500
550
Distance Downstream (ft)

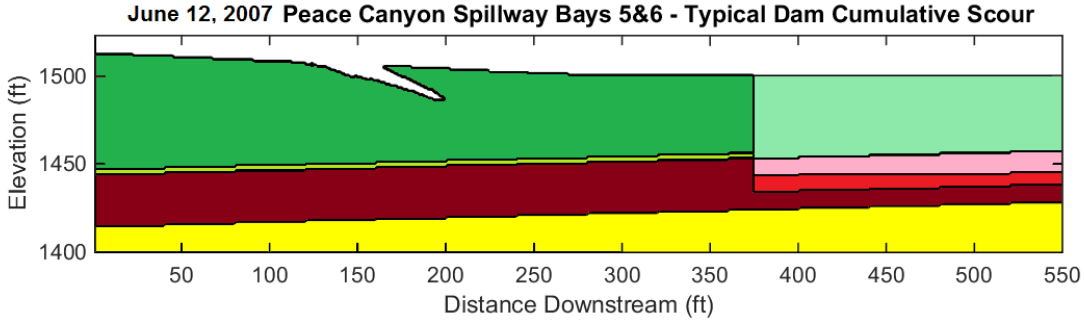
June 12, 2007 Peace Canyon Spillway Bays 5&6 - Typical Dam Cumulative Scour
Elevation (ft)
1500
1450
1400
50
100
150
200
250
300
350
400
450
500
550
Distance Downstream (ft)

Appendix E.2 Peace Canyon Dam Profile PCN-56 – High Erodibility Index

See Section 7.1.3 for explanation of geomechanical zones

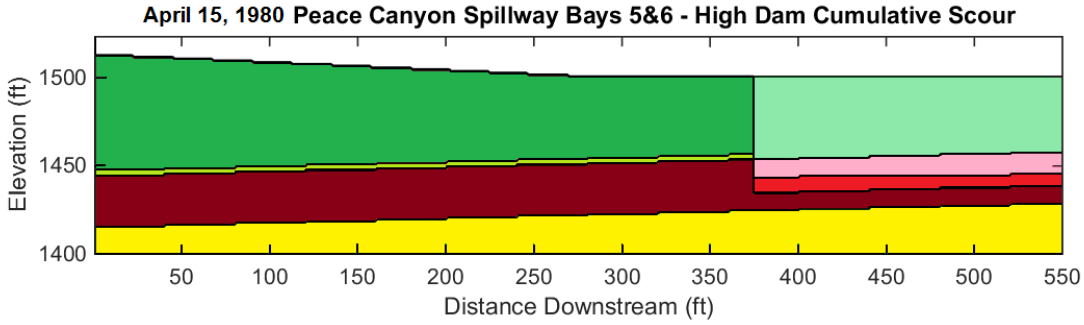

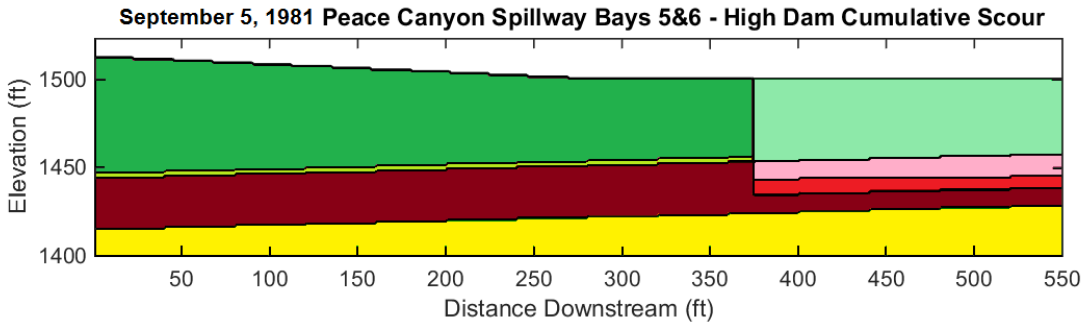

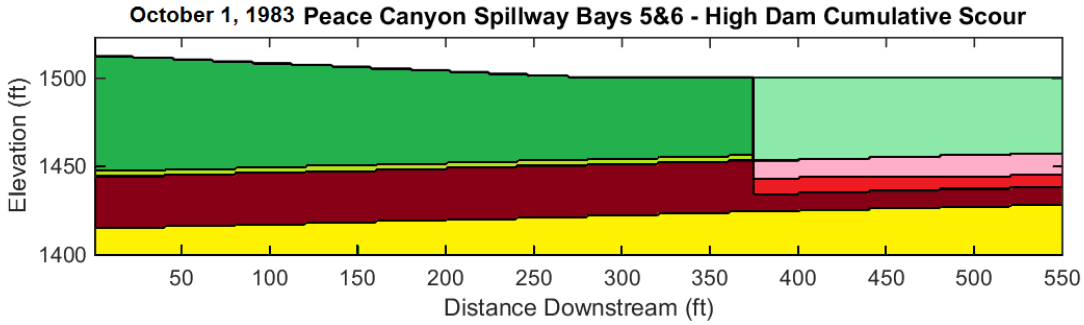

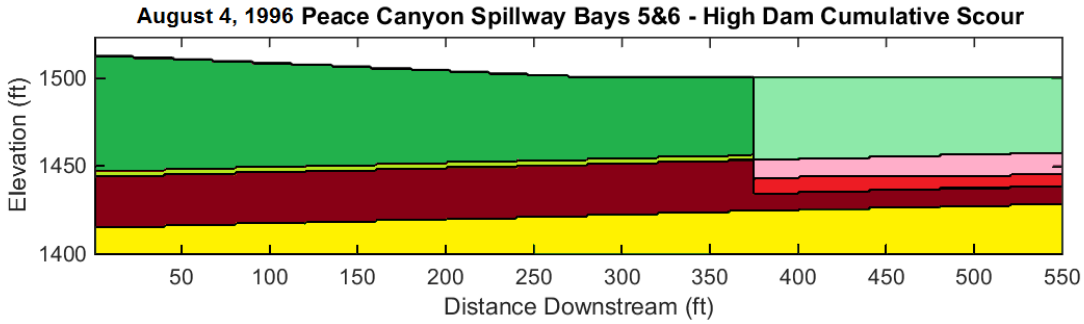
August 4, 1996 Peace Canyon Spillway Bays 5&6 - High Dam Cumulative Scour
Elevation (ft)
1500
1450
1400
50
100
150
200
250
300
350
400
450
500
550
Distance Downstream (ft)

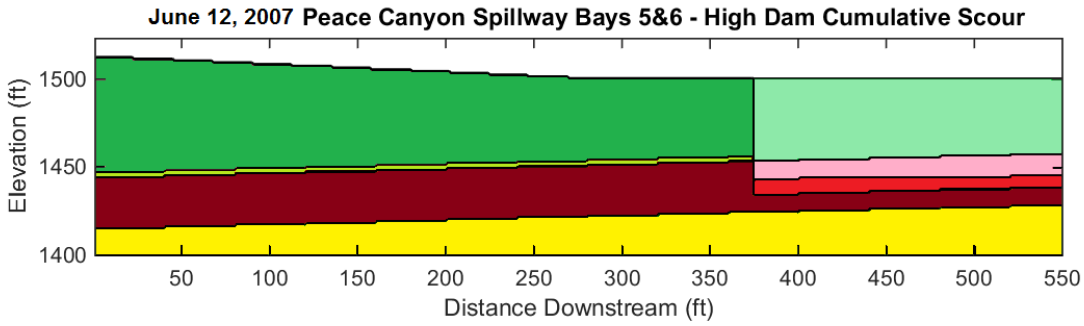
June 12, 2007 Peace Canyon Spillway Bays 5&6 - High Dam Cumulative Scour
Elevation (ft)
1500
1450
1400
50
100
150
200
250
300
350
400
450
500
550
Distance Downstream (ft)

Appendix E.3 Seven Mile Dam Profile SEV-12 – Low Erodibility Index

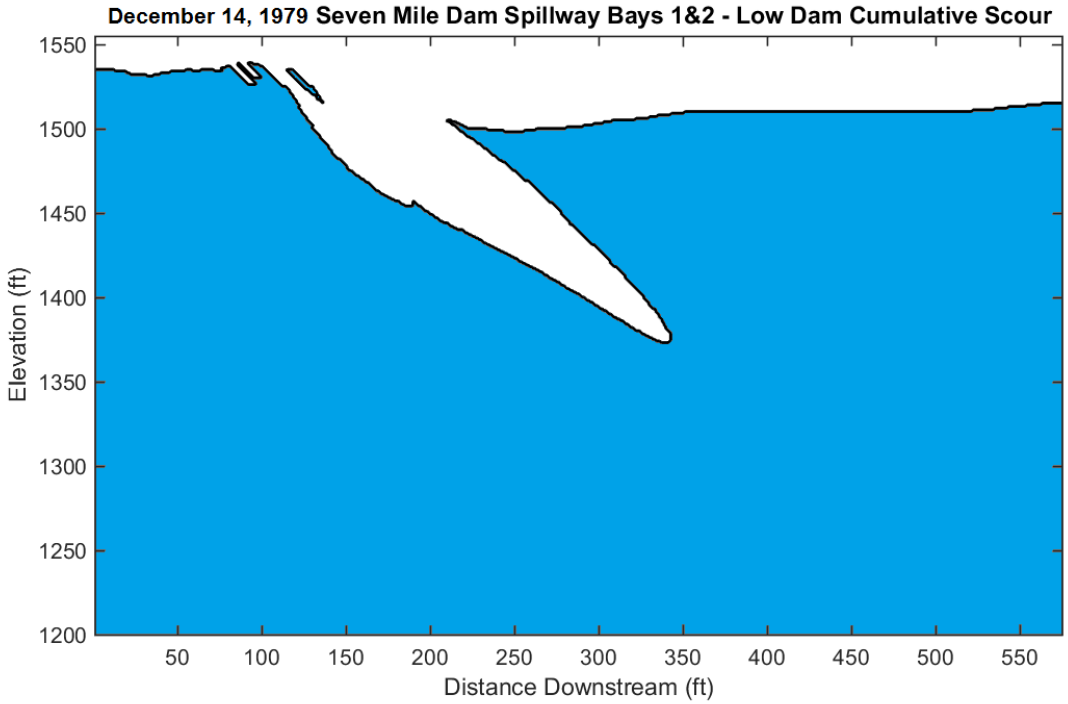

Appendix E.3 Seven Mile Dam Profile SEV-12 – Mean Erodibility Index

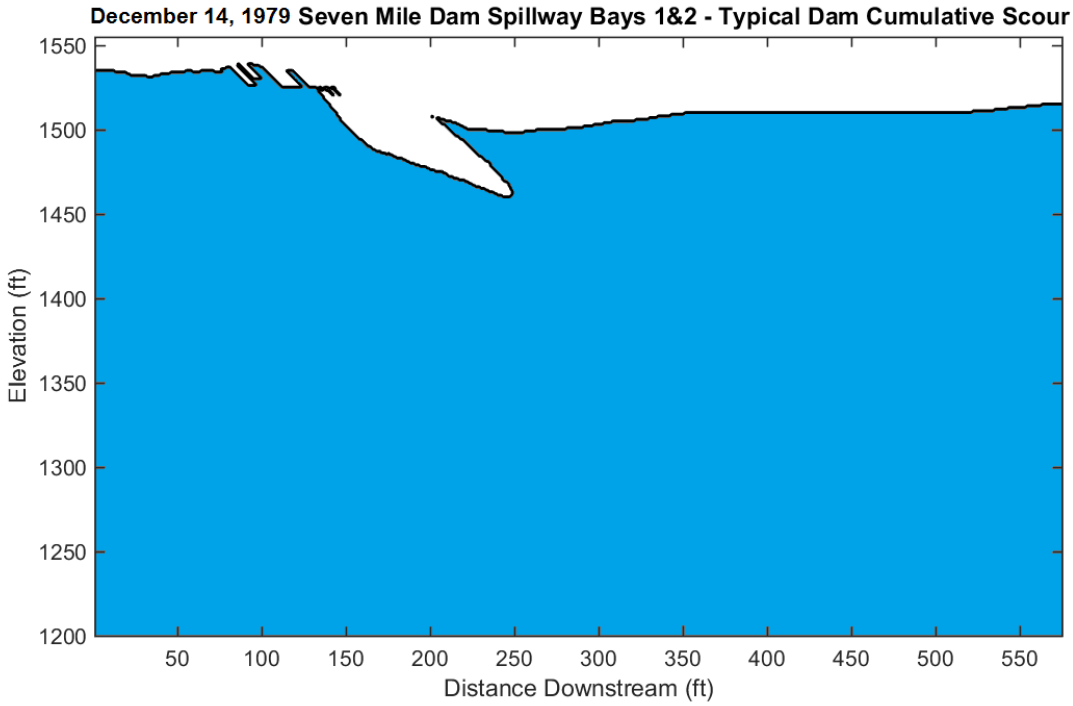

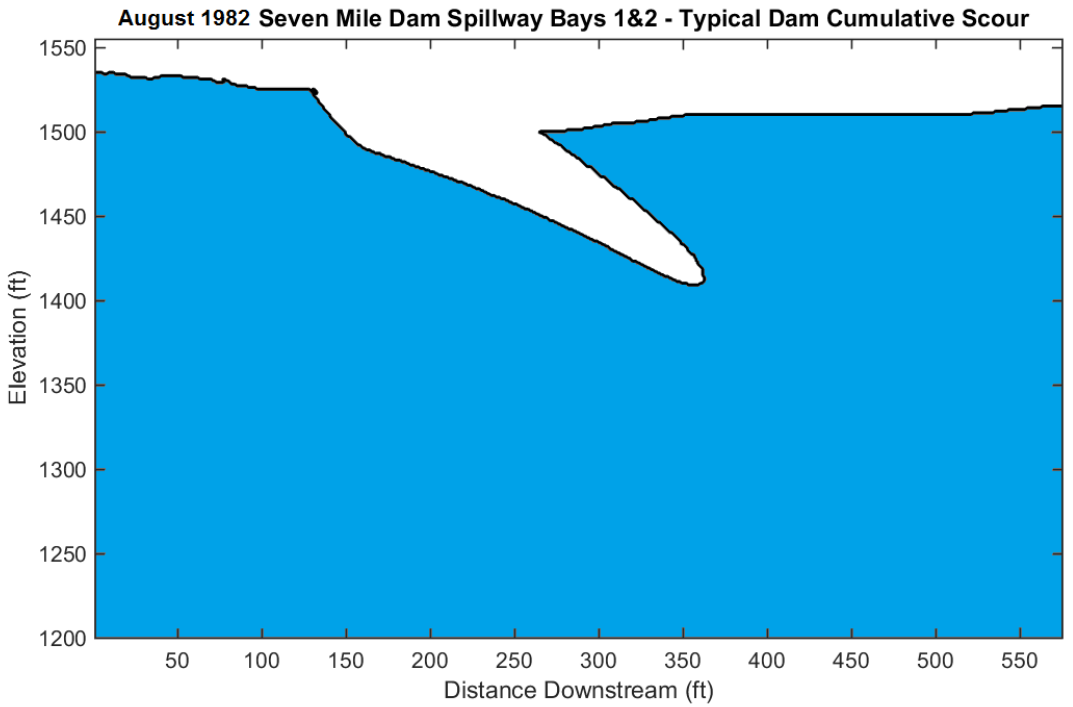

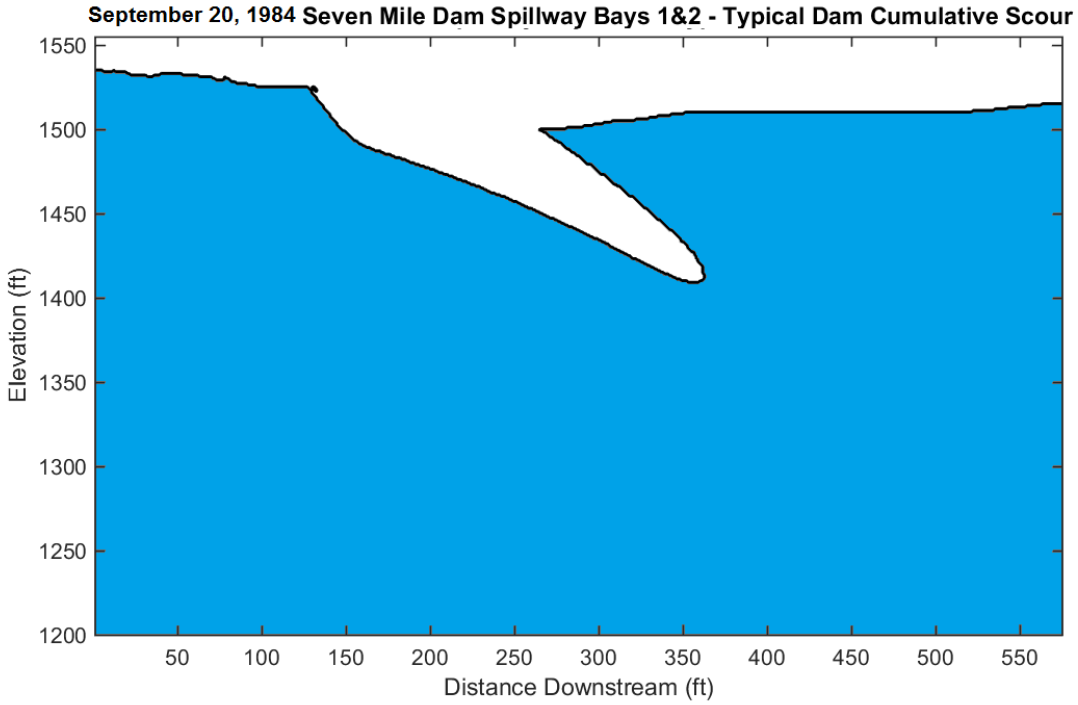
September 20, 1984 Seven Mile Dam Spillway Bays 1&2 - Typical Dam Cumulative Scour
Elevation (ft)
1550
1500
1450
1400
1350
1300
1250
1200
50
100
150
200
250
300
350
400
450
500
550
Distance Downstream (ft)

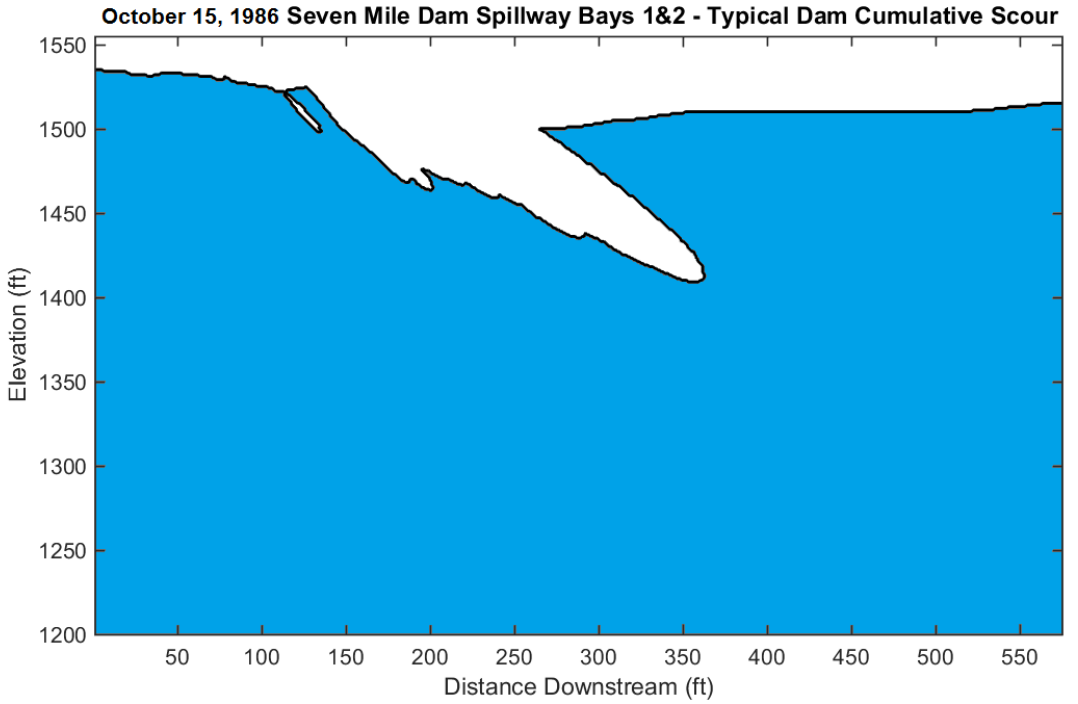
October 15, 1986 Seven Mile Dam Spillway Bays 1&2 - Typical Dam Cumulative Scour
Elevation (ft)
1550
1500
1450
1400
1350
1300
1250
1200
50
100
150
200
250
300
350
400
450
500
550
Distance Downstream (ft)

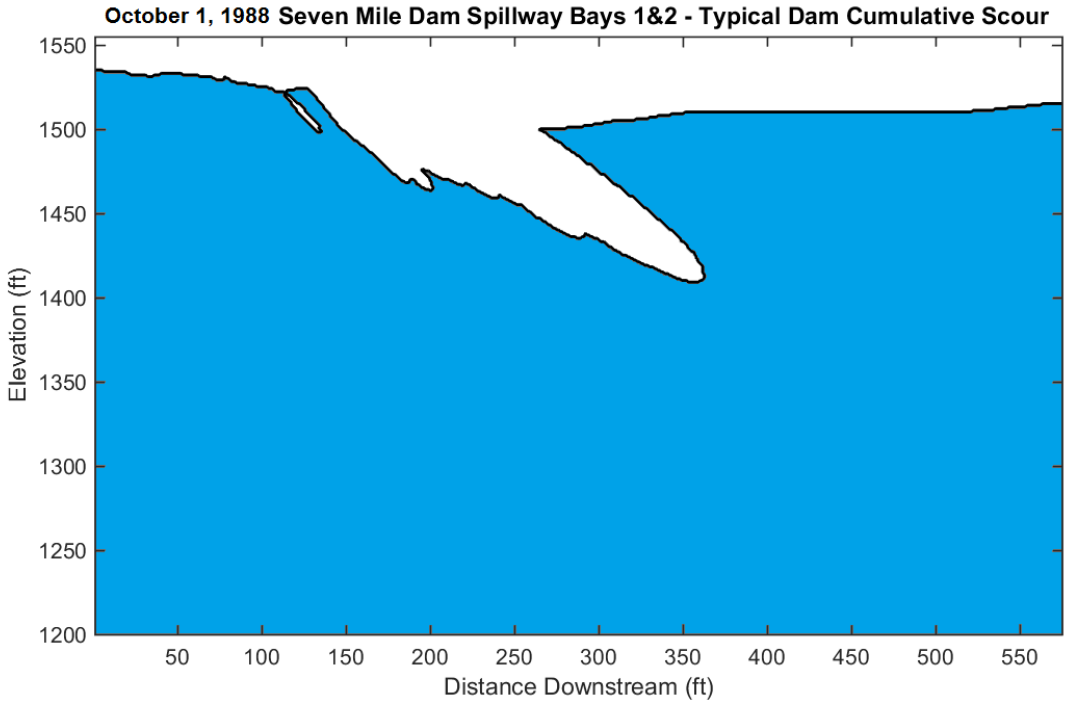
October 1, 1988 Seven Mile Dam Spillway Bays 1&2 - Typical Dam Cumulative Scour
Elevation (ft)
1550
1500
1450
1400
1350
1300
1250
1200
50
100
150
200
250
300
350
400
450
500
550
Distance Downstream (ft)

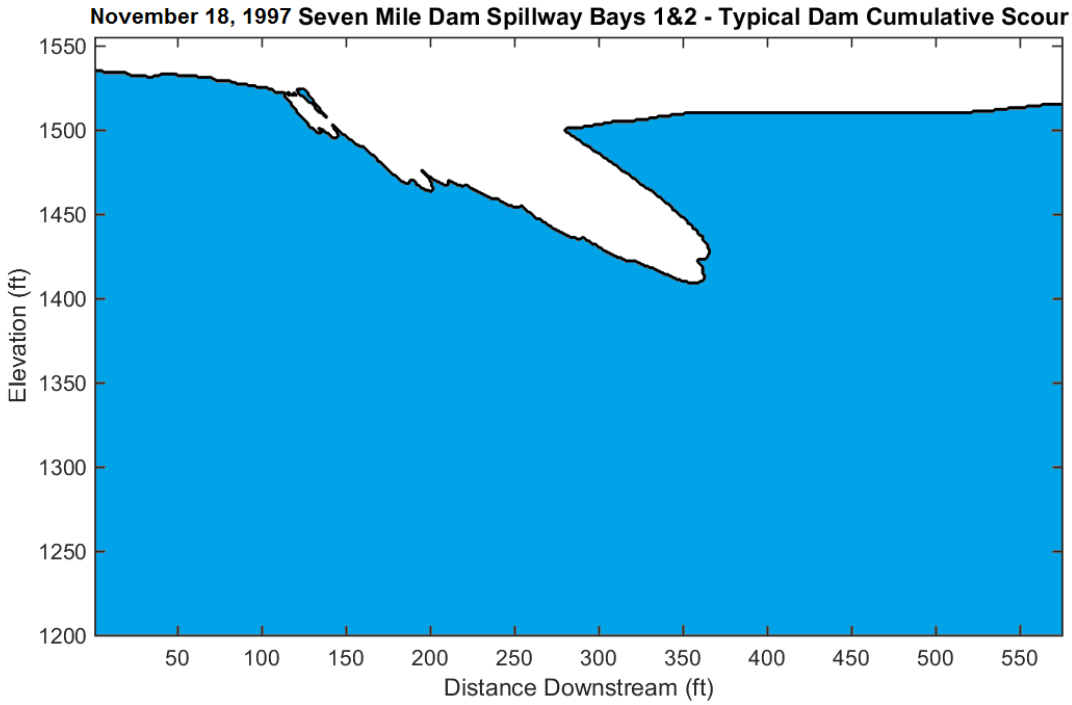
November 18, 1997 Seven Mile Dam Spillway Bays 1&2 - Typical Dam Cumulative Scour
Elevation (ft)
1550
1500
1450
1400
1350
1300
1250
1200
50
100
150
200
250
300
350
400
450
500
550
Distance Downstream (ft)

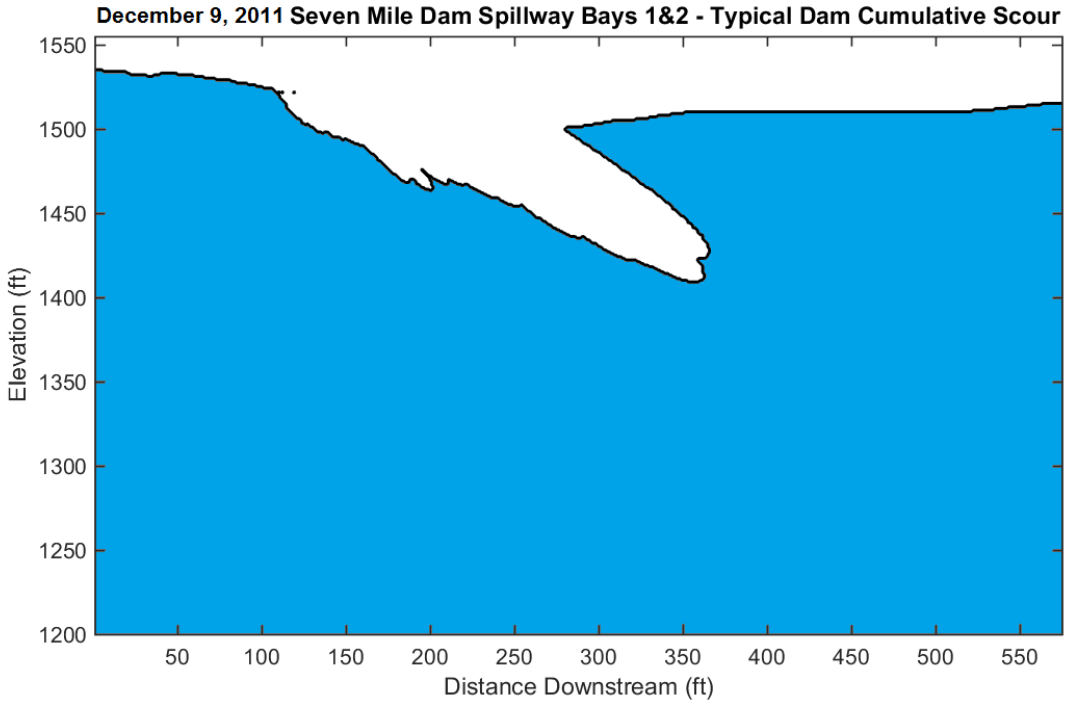
December 9, 2011 Seven Mile Dam Spillway Bays 1&2 - Typical Dam Cumulative Scour
Elevation (ft)
1550
1500
1450
1400
1350
1300
1250
1200
50
100
150
200
250
300
350
400
450
500
550
Distance Downstream (ft)

Appendix E.3 Seven Mile Dam Profile SEV-12 – High Erodibility Index

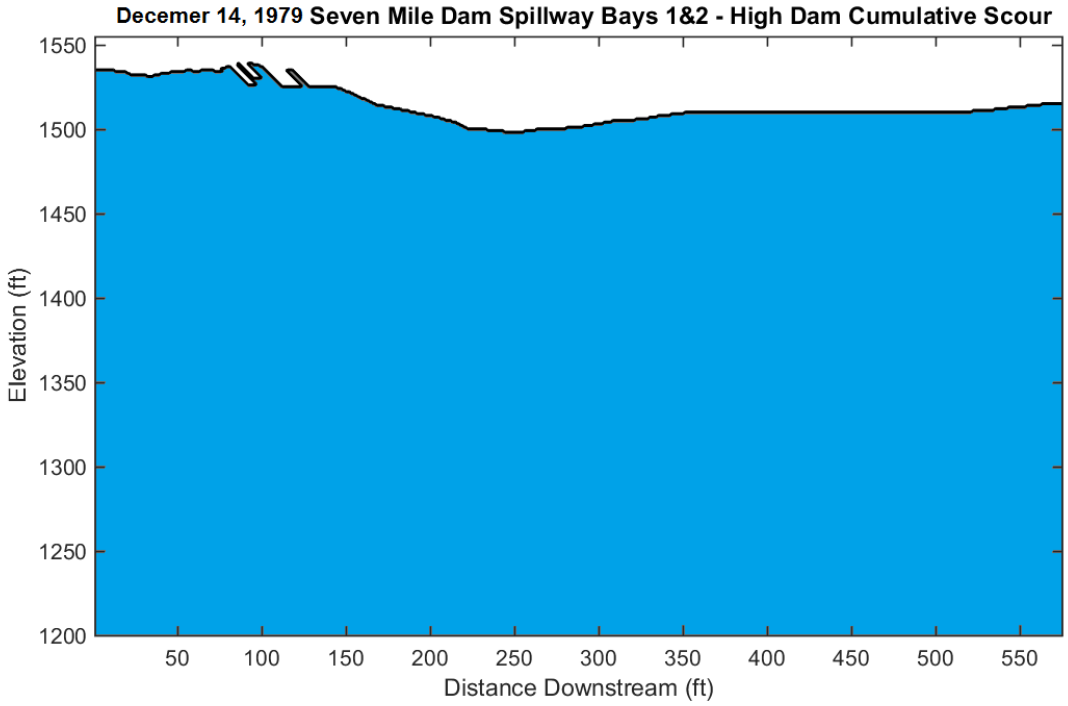

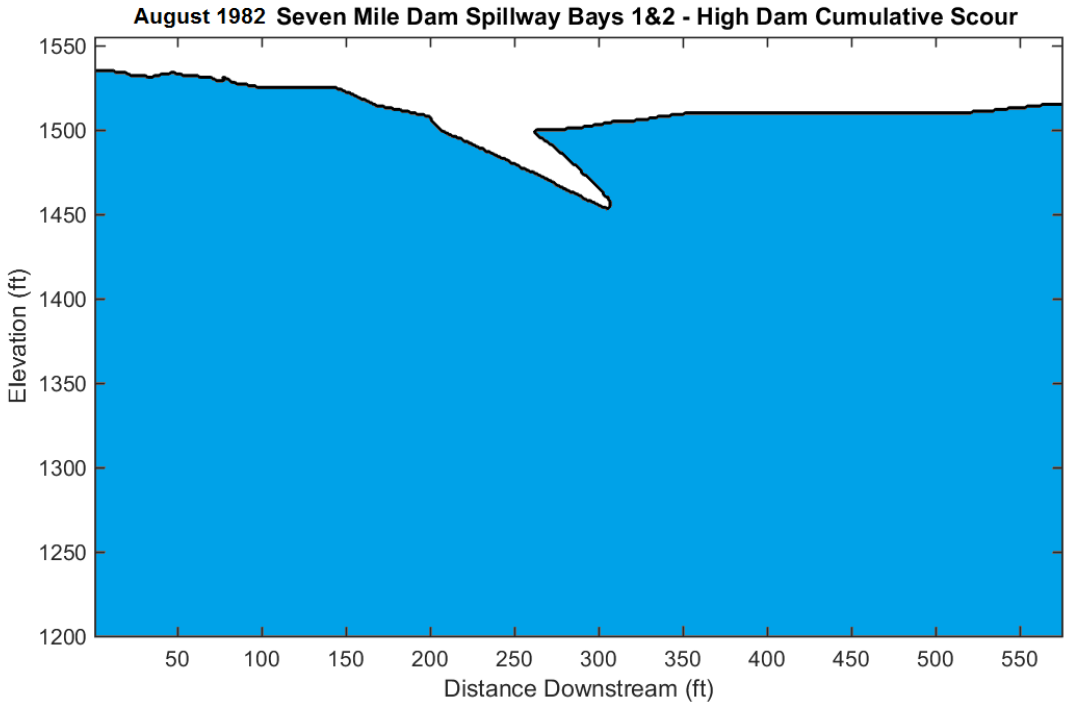

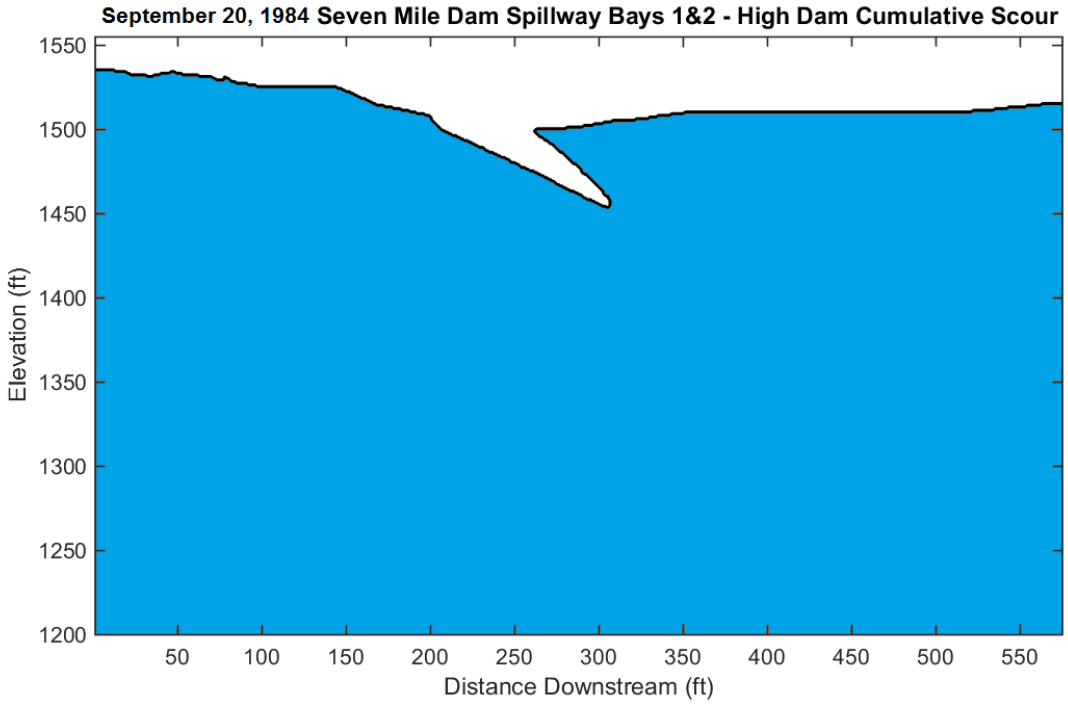
September 20, 1984 Seven Mile Dam Spillway Bays 1&2 - High Dam Cumulative Scour
Elevation (ft)
1550
1500
1450
1400
1350
1300
1250
1200
50
100
150
200
250
300
350
400
450
500
550
Distance Downstream (ft)

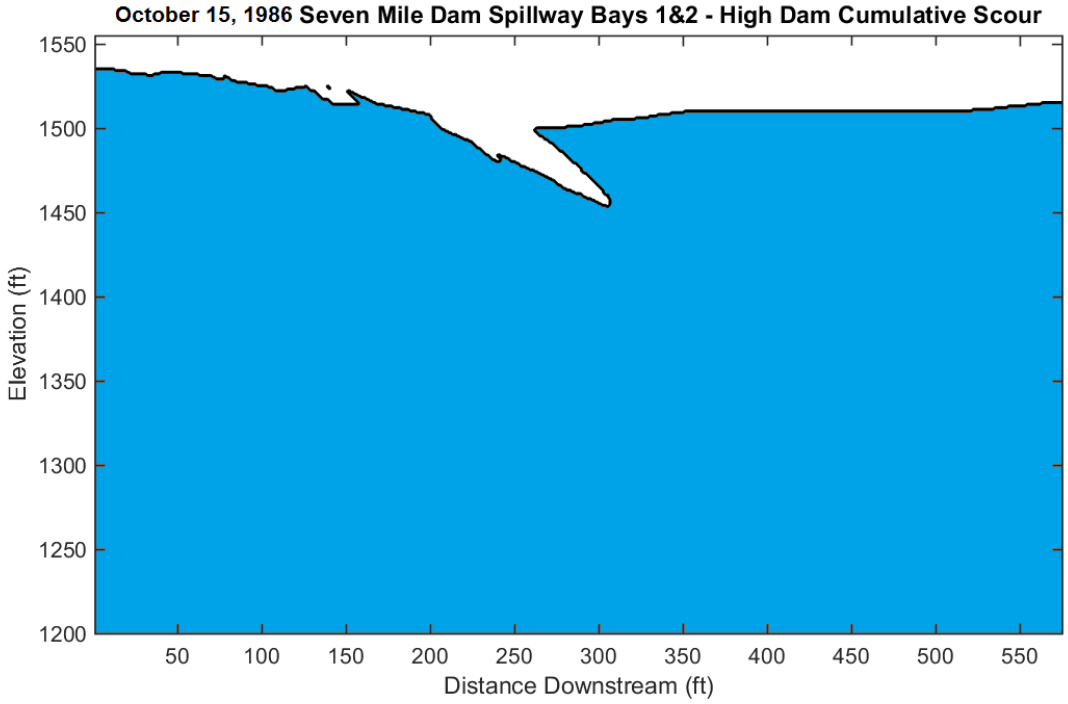
October 15, 1986 Seven Mile Dam Spillway Bays 1&2 - High Dam Cumulative Scour
Elevation (ft)
1550
1500
1450
1400
1350
1300
1250
1200
50
100
150
200
250
300
350
400
450
500
550
Distance Downstream (ft)

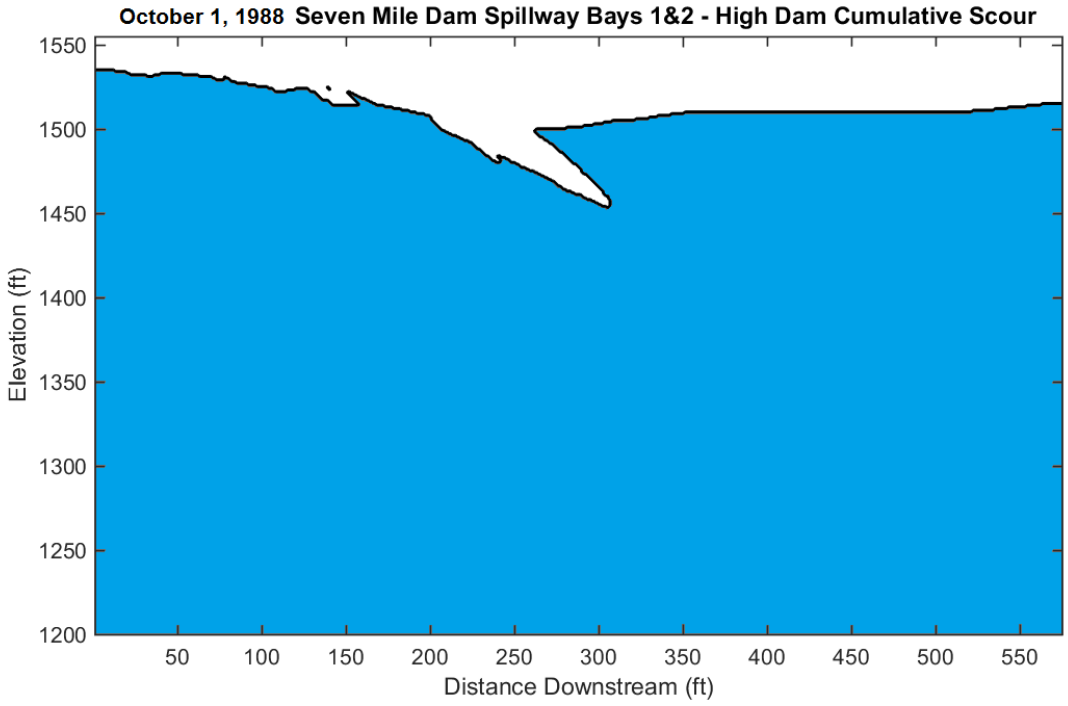
October 1, 1988 Seven Mile Dam Spillway Bays 1&2 - High Dam Cumulative Scour
Elevation (ft)
1550
1500
1450
1400
1350
1300
1250
1200
50
100
150
200
250
300
350
400
450
500
550
Distance Downstream (ft)

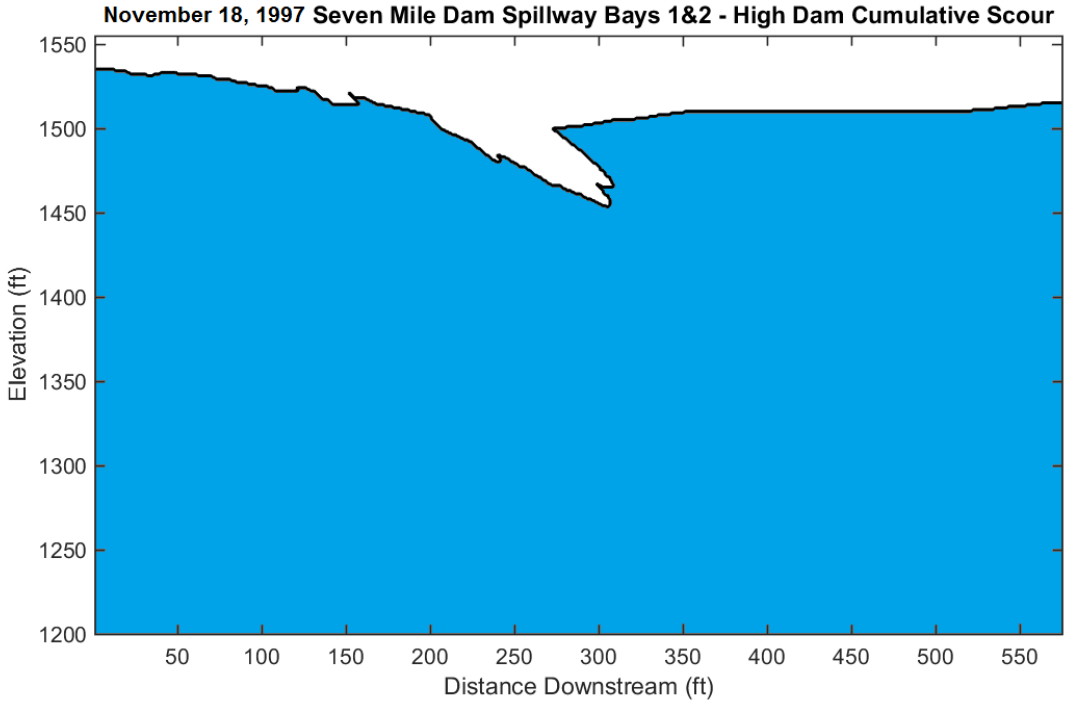
November 18, 1997 Seven Mile Dam Spillway Bays 1&2 - High Dam Cumulative Scour
Elevation (ft)
1550
1500
1450
1400
1350
1300
1250
1200
50
100
150
200
250
300
350
400
450
500
550
Distance Downstream (ft)

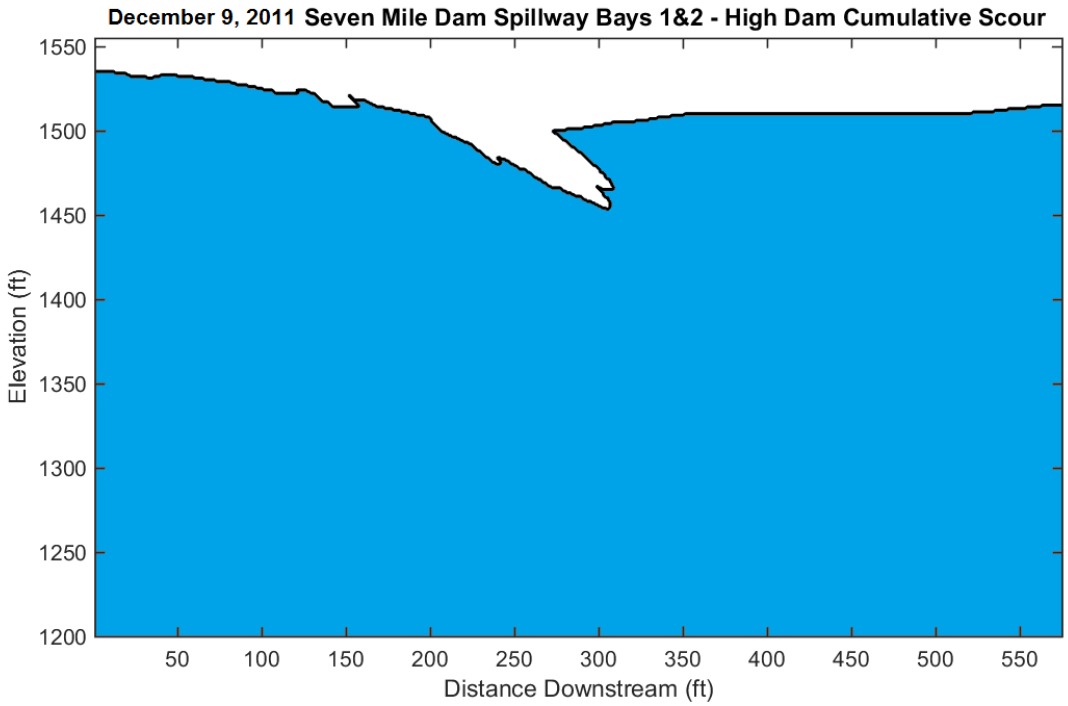
December 9, 2011 Seven Mile Dam Spillway Bays 1&2 - High Dam Cumulative Scour
Elevation (ft)
1550
1500
1450
1400
1350
1300
1250
1200
50
100
150
200
250
300
350
400
450
500
550
Distance Downstream (ft)

Appendix E.4 Revelstoke Dam Profile REV-1 – Low Erodibility Index

Scour immediately exceeded lower bound of modeled profile; no profiles available.

Appendix E.4 Revelstoke Dam Profile REV-1 – Mean Erodibility Index

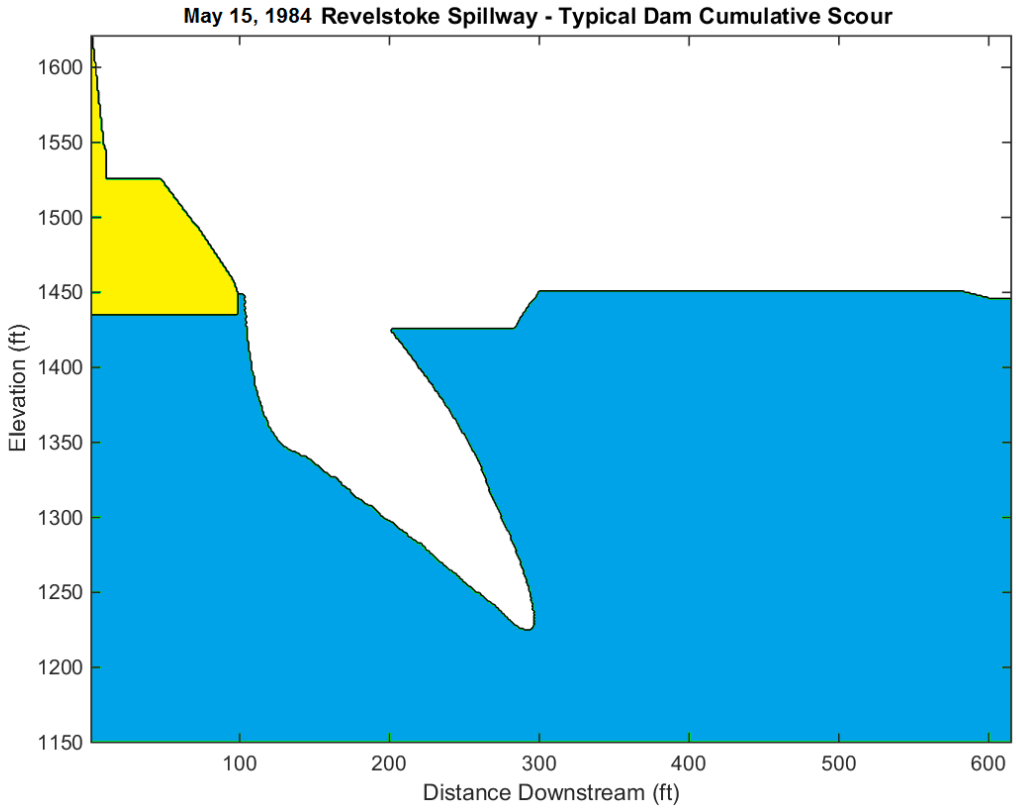

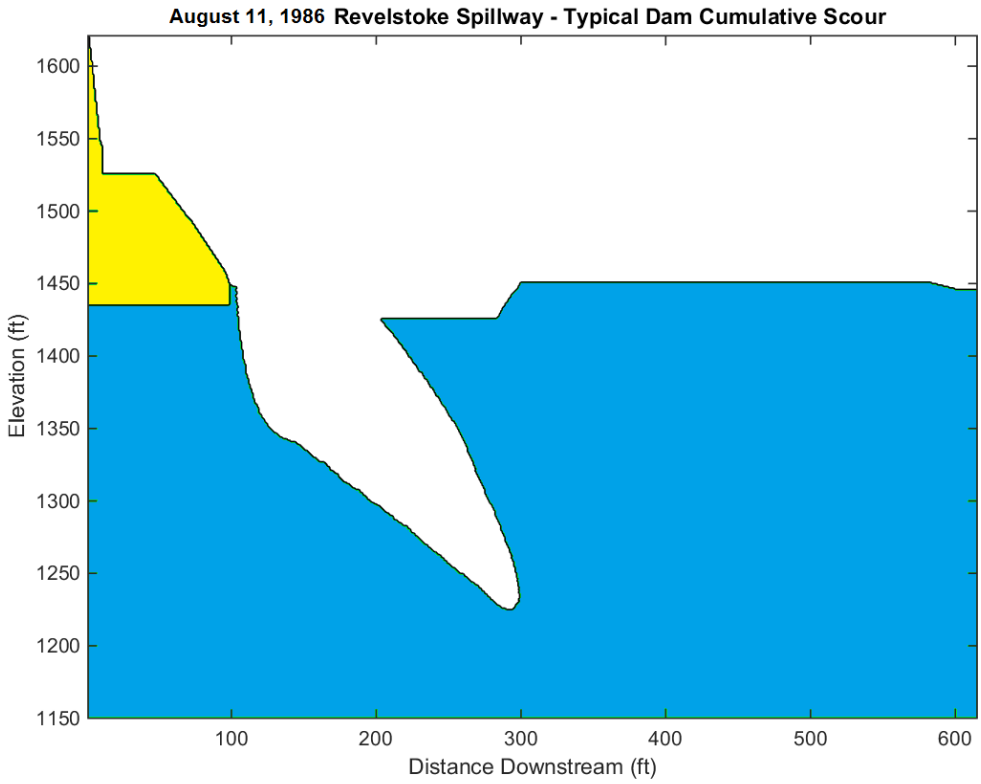
August 11, 1986 Revelstoke Spillway - Typical Dam Cumulative Scour
Elevation (ft)
1600
1550
1500
1450
1400
1350
1300
1250
1200
1150
100
200
300
400
500
600
Distance Downstream (ft)

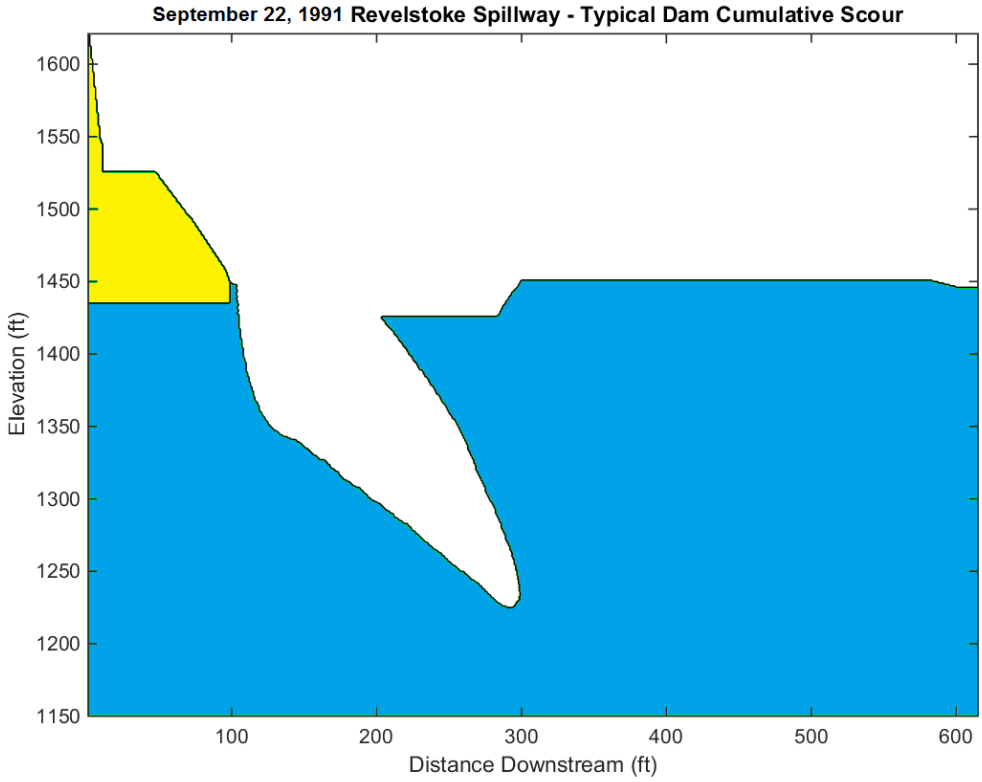
September 22, 1991 Revelstoke Spillway - Typical Dam Cumulative Scour
Elevation (ft)
1600
1550
1500
1450
1400
1350
1300
1250
1200
1150
100
200
300
400
500
600
Distance Downstream (ft)

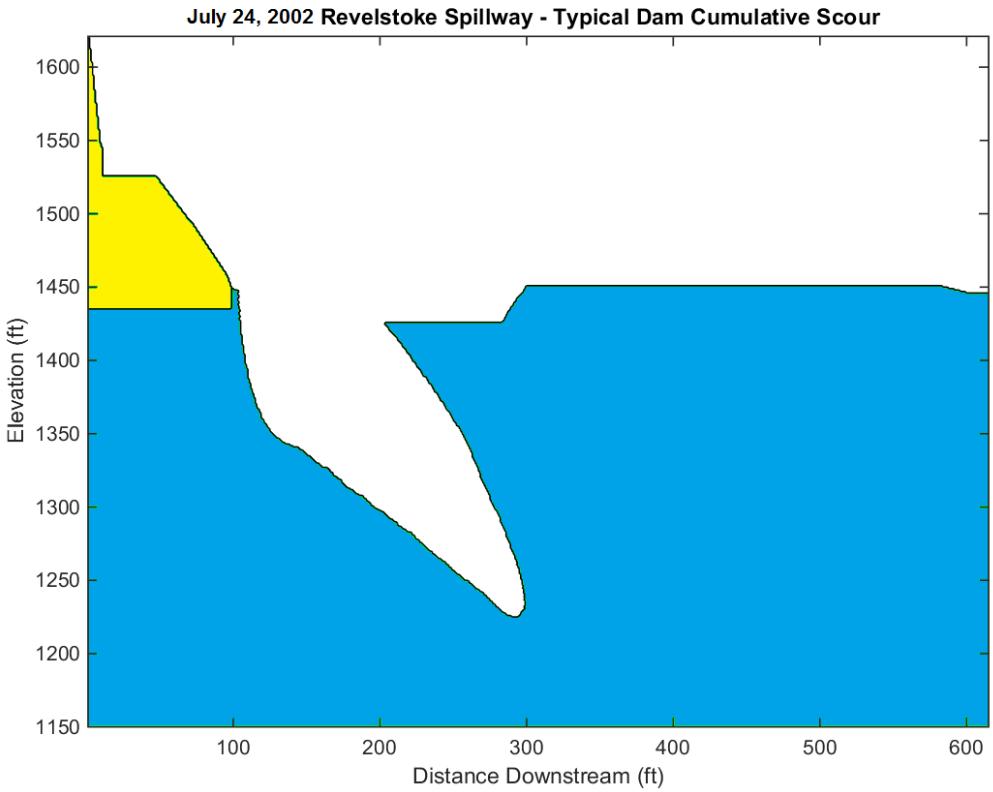
July 24, 2002 Revelstoke Spillway - Typical Dam Cumulative Scour
Elevation (ft)
1600
1550
1500
1450
1400
1350
1300
1250
1200
1150
100
200
300
400
500
600
Distance Downstream (ft)

Appendix E.4 Revelstoke Dam Profile REV-1 – High Erodibility Index

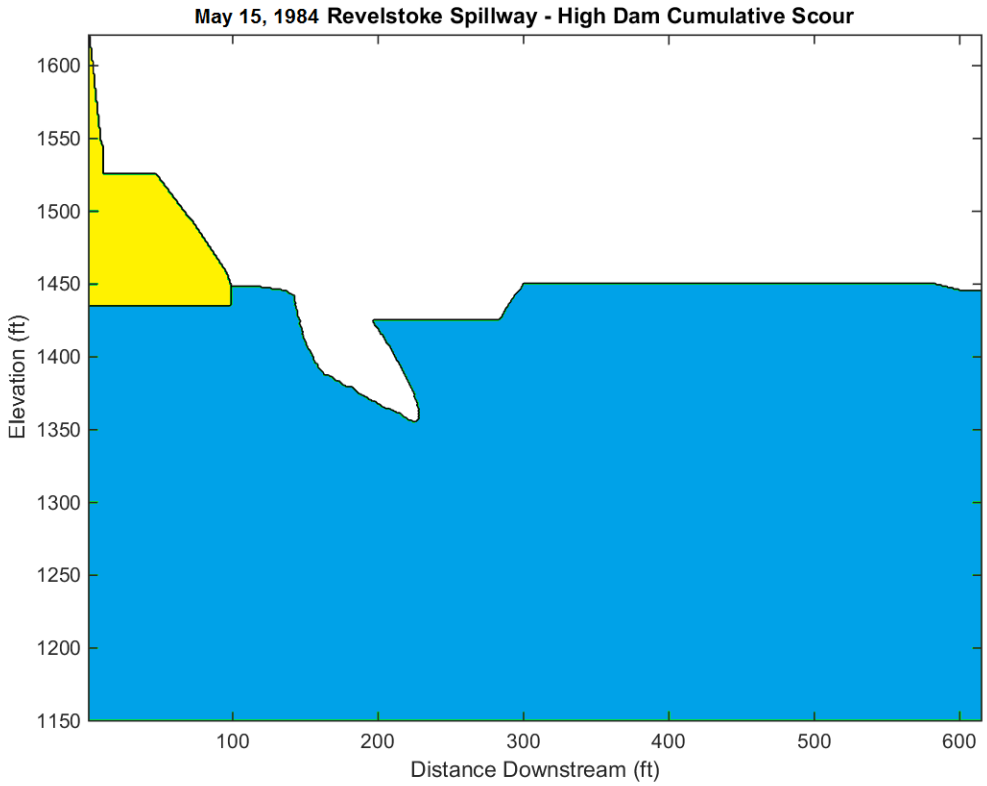

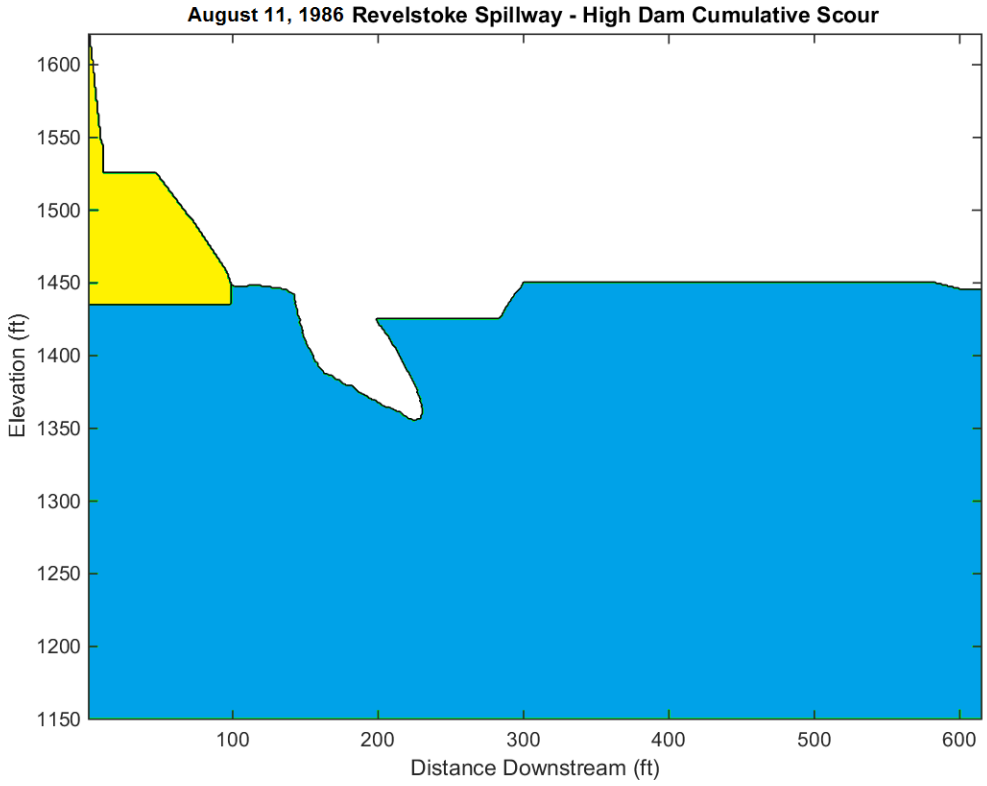

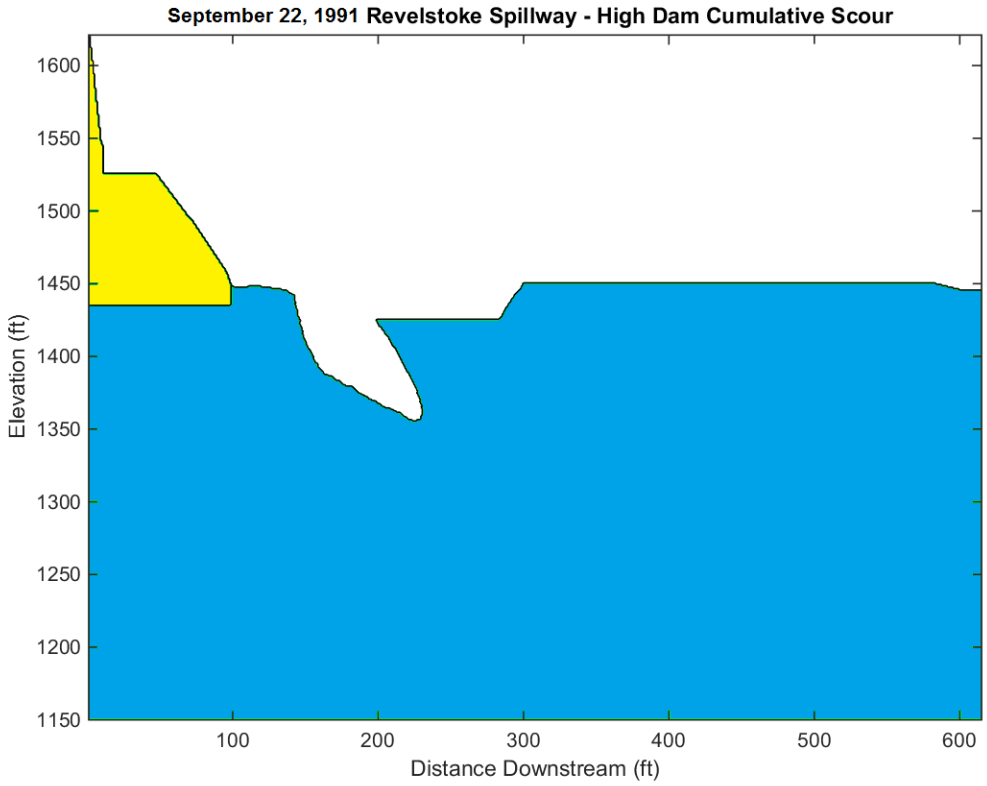
September 22, 1991 Revelstoke Spillway - High Dam Cumulative Scour
Elevation (ft)
1600
1550
1500
1450
1400
1350
1300
1250
1200
1150
100
200
300
400
500
600
Distance Downstream (ft)

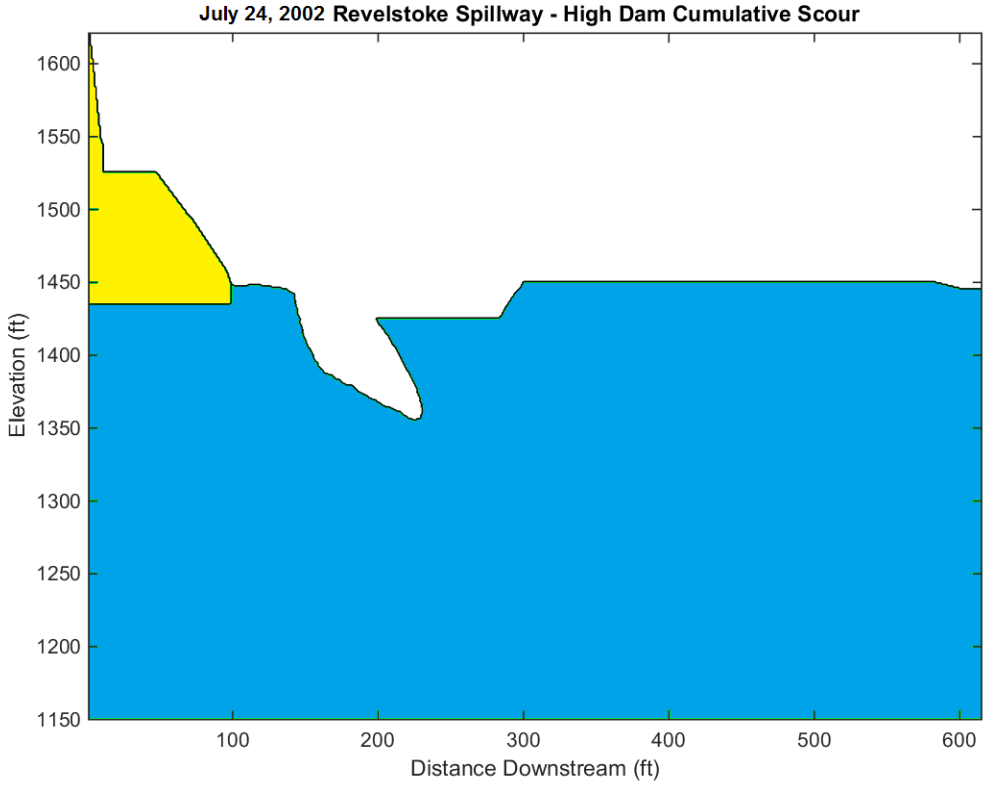
July 24, 2002 Revelstoke Spillway - High Dam Cumulative Scour
Elevation (ft)
1600
1550
1500
1450
1400
1350
1300
1250
1200
1150
100
200
300
400
500
600
Distance Downstream (ft)

Appendix E.5 W.A.C. Bennett Dam Profile WAC-C – Low Erodibility Index

See Section 0 for explanation of geomechanical zones

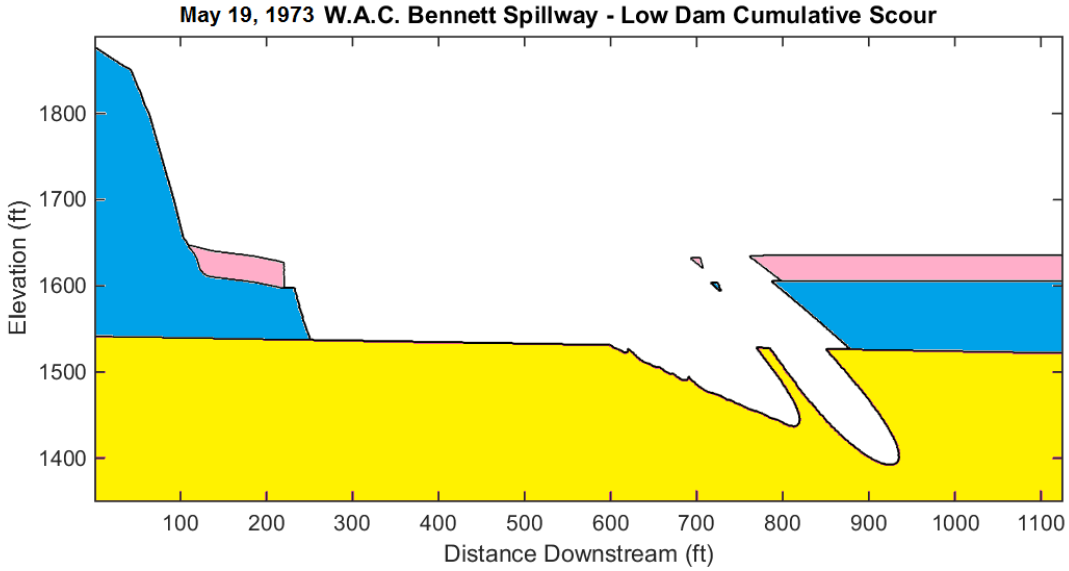

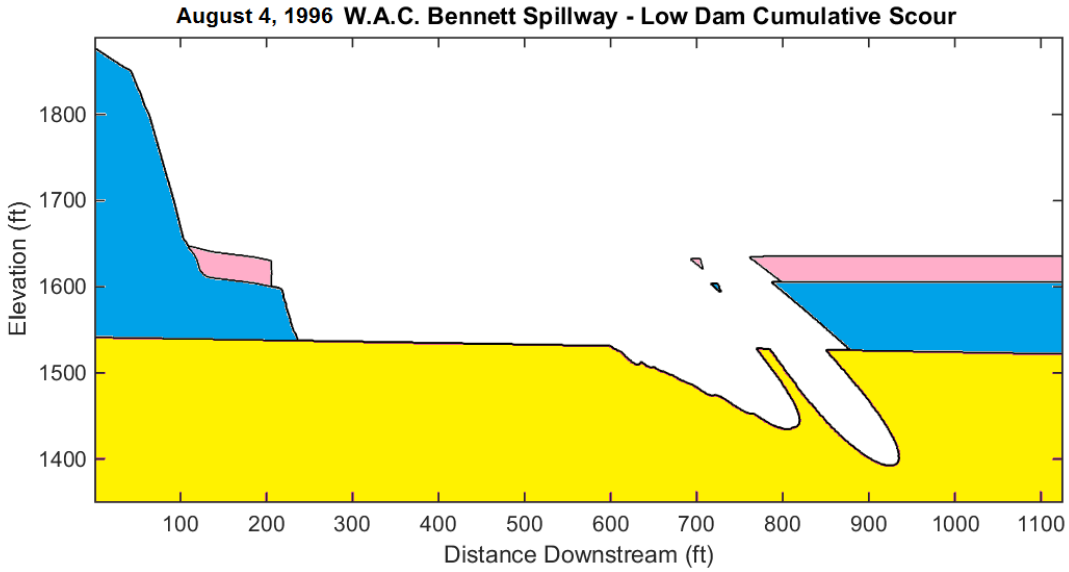

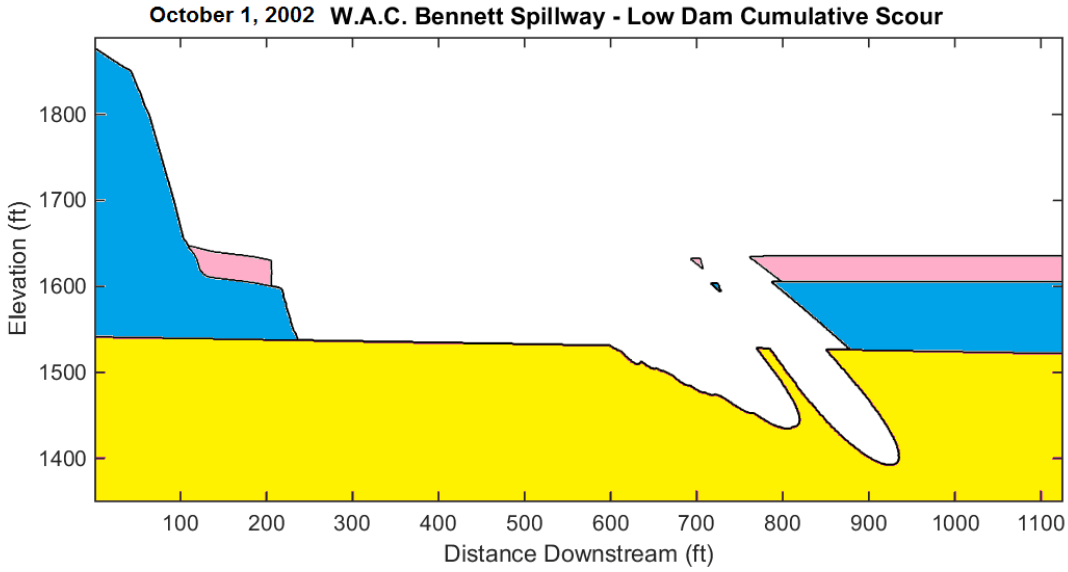
October 1, 2002 W.A.C. Bennett Spillway - Low Dam Cumulative Scour
Elevation (ft)
1800
1700
1600
1500
1400
100
200
300
400
500
600
700
800
900
1000
1100
Distance Downstream (ft)

Appendix E.5 W.A.C. Bennett Dam Profile WAC-C – Mean Erodibility Index

See Section 0 for explanation of geomechanical zones

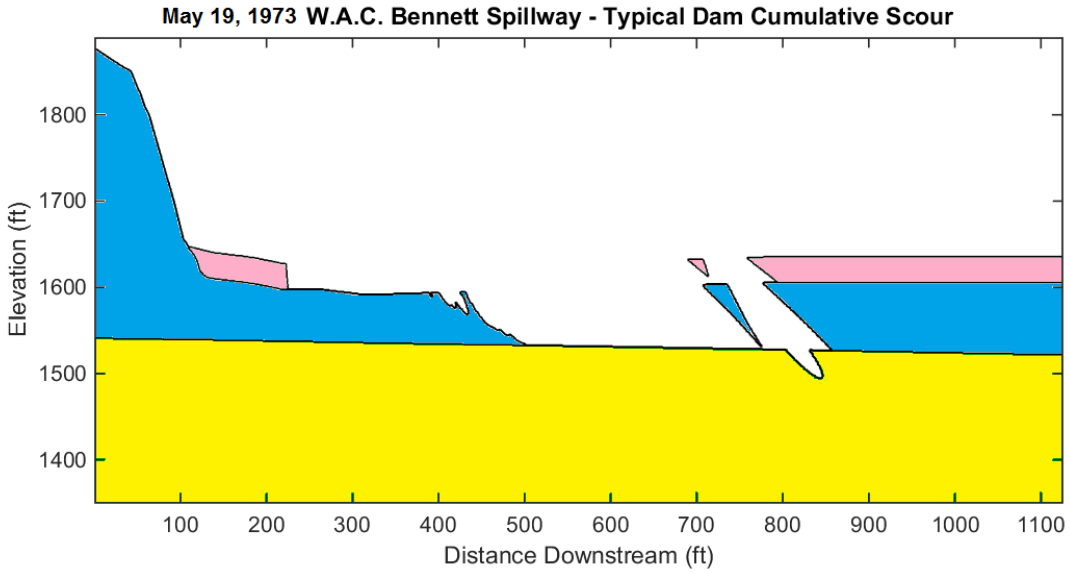

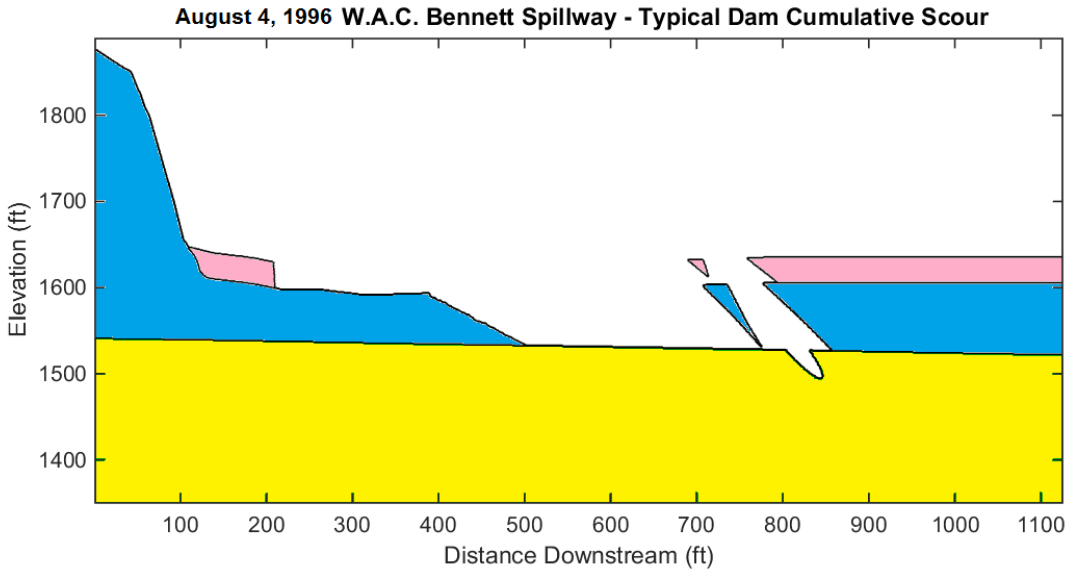

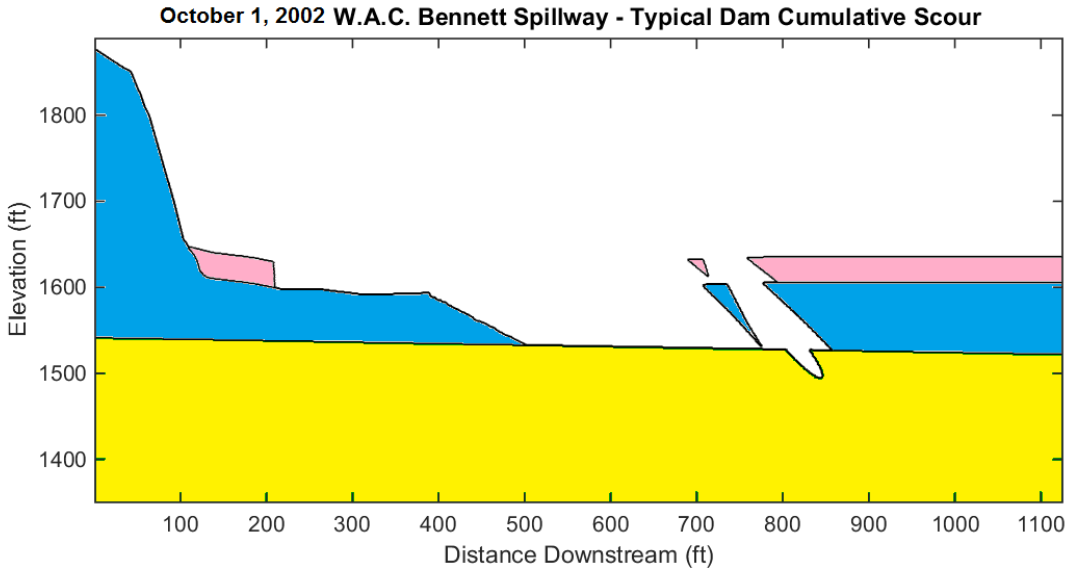
October 1, 2002 W.A.C. Bennett Spillway - Typical Dam Cumulative Scour
Elevation (ft)
1800
1700
1600
1500
1400
100
200
300
400
500
600
700
800
900
1000
1100
Distance Downstream (ft)

Appendix E.5 W.A.C. Bennett Dam Profile WAC-C – High Erodibility Index

See Section 0 for explanation of geomechanical zones

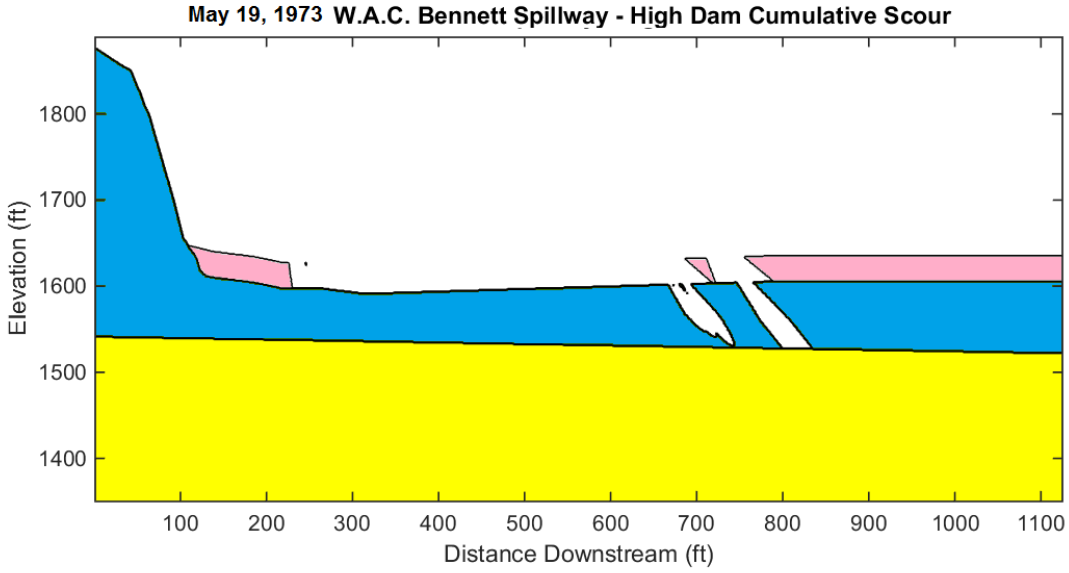

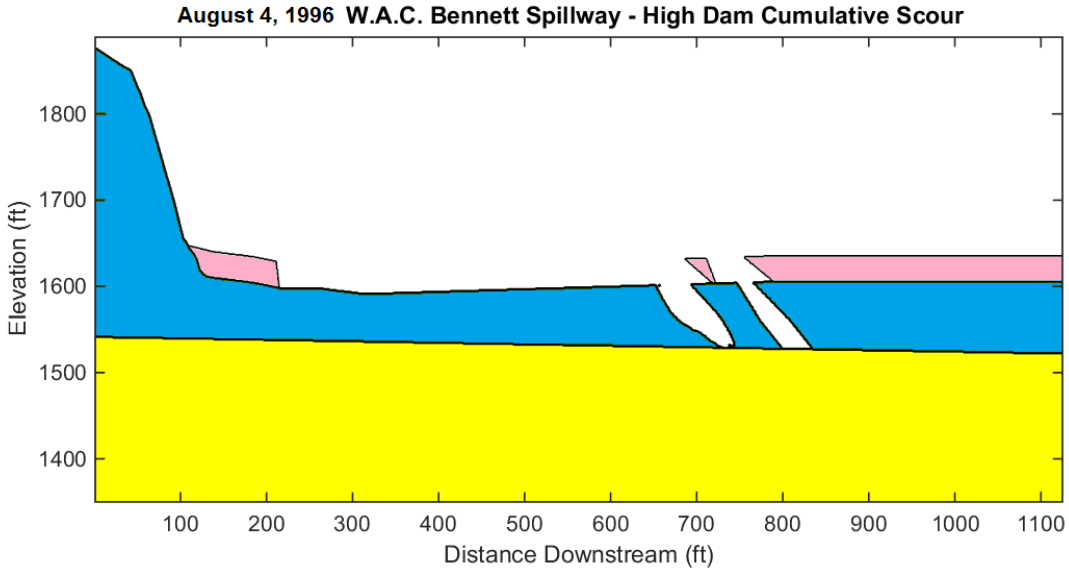

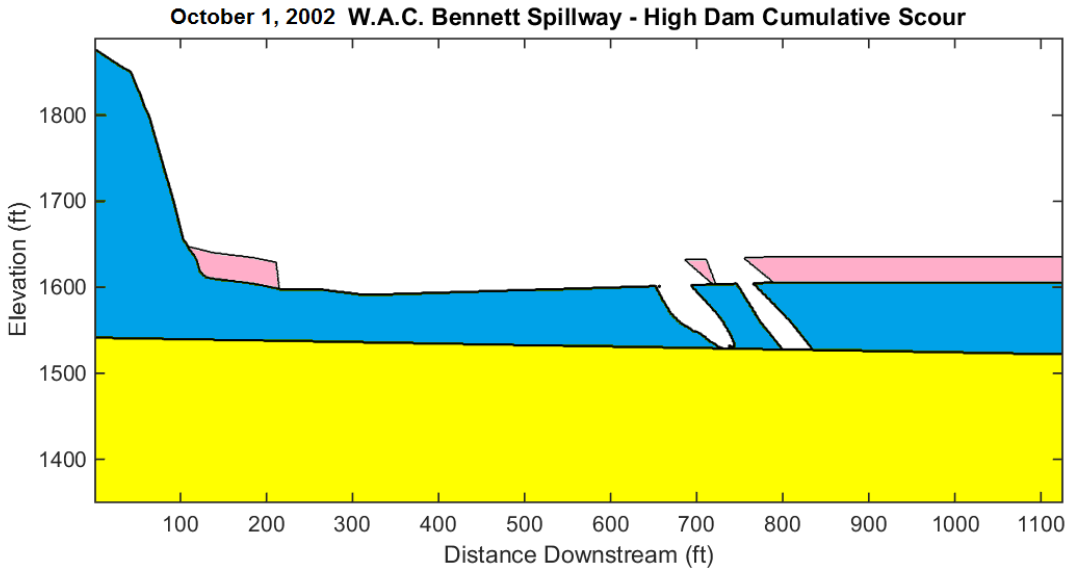
October 1, 2002 W.A.C. Bennett Spillway - High Dam Cumulative Scour
Elevation (ft)
1800
1700
1600
1500
1400
100
200
300
400
500
600
700
800
900
1000
1100
Distance Downstream (ft)